



GluN3A expression in oligodendrocyte progenitor cells controls activity-dependent myelin plasticity

Doctoral thesis presented by

Alice Staffa

Thesis director: *Dr. Isabel Pérez-Otaño*

- 2024 -

Instituto de Neurociencias (CSIC-UMH)
Programa de Doctorado en Neurociencias
Universidad Miguel Hernández de Elche





This Doctoral Thesis, entitled “**GluN3A expression in oligodendrocyte progenitor cells controls activity-dependent myelin plasticity**”, is presented under the conventional thesis form with the following quality indicator::

Staffa, A., Chatterjee, M., Diaz-Tahoces, A., Leroy, F., Perez-Otaño, I. Monitoring Fine and Associative Motor Learning in Mice Using the Erasmus Ladder. J. Vis. Exp. (202), e65958, (2023).



Dr. Isabel Pérez-Otaño, Director of the doctoral thesis entitled “**GluN3A expression in oligodendrocyte progenitor cells controls activity-dependent myelin plasticity**”,

CERTIFIES:

That Ms. Alice Staffa has carried out under my supervisión the work entitled “**GluN3A expression in oligodendrocyte progenitor cells controls activity-dependent myelin plasticity**” in accordance with the terms and conditions defined un her Research Plan and in accordance with the Codeo f Good Practice of the University Miguel Hernández of Elche, satisfactorily fulfilling the objectives foreseen for its public defense as a doctroal thesis.

I sign for appropriate purposes, at Sant Joan d’Alancant, 28th of May of 2024

Thesis Director

Dr. Isabel Pérez-Otaño



Dr. Maria Cruz Morenilla Palao, Coordinator of the Neuroscience PhD programme at the Institute of Neuroscience in Alicante, a joint center of the Miguel Hernández University (UMH) and the Spanish National Research Council (CSIC),

INFORMS:

That Ms. Alice Staffa has carried out under the supervision of our PhD programme the work entitled “**GluN3A expression in oligodendrocyte progenitor cells controls activity-dependent myelin plasticity**” in accordance with the terms and conditions defined in her Research Plan and in accordance with the Code of Good Practice of the University Miguel Hernández of Elche, satisfactorily fulfilling the objectives foreseen for its public defense as a doctoral thesis.

I sign for appropriate purposes, at Sant Joan d’Alacant, 28th of May of 2024

Coordinator of the PhD programme in Neuroscience

Dr. Maria Cruz Morenilla Palao



To whom it may concern,

The present PhD thesis has been funded by the following research agencies: FPI fellowship to Alice Staffa (BES-2017-08200) and grants to Isabel Pérez-Otaño from the Agencia Española de Investigación (SAF2016-80895-R and PID2019-111112RB-I00), Prometeo Excellence Program, Generalitat Valenciana (2019/020; CIPROM2022/8).

A microscopic image of cells, likely neurons, showing green and red fluorescence. The green fluorescence highlights the cell bodies and their processes, while the red fluorescence highlights specific organelles or structures within the cells. The background is dark, making the fluorescent cells stand out.

1. TABLE OF CONTENTS

1. TABLE OF CONTENTS	13
2. SUMMARY / RESUMEN	19
3. ABBREVIATIONS	23
4. INTRODUCTION	27
4.1. Oligodendroglia and myelination in the central nervous system (CNS)	27
4.1.1 Oligodendrocyte progenitor cells (OPCs)	28
4.1.2 OPC proliferation and differentiation	31
4.1.3 Myelination	33
4.1.4 Activity-dependent myelination	36
4.1.4.1 Physical exercise	39
4.1.4.2 Motor skill learning	41
4.1.4.3 Sensory experience	42
4.1.4.4 Social experience	44
4.1.4.5 Memory and cognition	45
4.2. Neuron-oligodendroglial interactions	49
4.2.1 Neuron-secreted factors in neuron-oligodendroglial interactions	51
4.2.2 Neurotransmitters in neuron-oligodendroglial interactions	53
4.2.2.1 AMPA receptors in oligodendroglia	54
4.2.2.2 NMDA receptors (NMDARs) in oligodendroglia	55
4.3. GluN3A-containing NMDA receptors (GluN3A-NMDARs)	59
4.3.1 Properties and expression pattern of GluN3A-NMDARs	59
4.3.2 GluN3A cell-type specific expression	62
4.3.3 GluN3A in the oligodendroglial lineage	62

4.4. Demyelination and remyelination in aging and disease	66
4.4.1 Demyelination and remyelination processes	66
4.4.2 Multiple sclerosis (MS) and experimental animal models	66
4.4.3 Myelin loss in other neurodegenerative diseases	68
4.4.4 Why does remyelination fail in MS? Intrinsic and extrinsic factors	68
5. OBJECTIVES	73
6. MATERIALS AND METHODS	79
6.1. Experimental animals	79
6.1.1 Mouse lines	79
6.1.2 Mouse genotyping	81
6.2. Transcriptomic analysis	82
6.3. Histological analysis	84
6.3.1 Fluorescent in situ hybridization (FISH)	85
6.3.2 Immunofluorescence (IF)	85
6. 4. Electron microscopy (EM)	87
6.5. Western blotting	89
6.6. Paradigms for stimulation of activity-dependent plasticity	90
6.6.1 Chemogenetic stimulation of neuronal activity <i>in vivo</i> (DREADDs)	90
6.6.2 Chronic physical exercise (Treadmill)	90
6.6.3 Motor learning (Erasmus Ladder)	91
6.7. Cell proliferation assay	93
6.8. Lysolecithin-induced focal demyelination	93
6.9. Electrophysiology	94

6.10. Image acquisition, processing and analysis	95
6.11. Statistical analysis	95
7. RESULTS	99
7.1. GluN3A is expressed in postnatal and young adult OPCs	99
7.1.1 Transcriptomic analyses demonstrate <i>Grin3a</i> mRNA expression in OPCs	99
7.1.2 Localization of <i>Grin3a</i> mRNA and GluN3A protein in OPCs	102
7.1.3 Electron microscopy confirms the localization of GluN3A protein in OPC processes that surround unmyelinated axons	103
7.1.4 Electrophysiological evidence for functional GluN3A receptors in OPCs	104
7.2. Accelerated expression of markers of OPC differentiation and myelination in postnatal <i>Grin3a</i> ^{-/-} mice	106
7.2.1 Markers of OPC differentiation and myelination are upregulated in <i>Grin3a</i> ^{-/-} mice during a critical window of postnatal development	106
7.2.2 Accelerated OPC differentiation and myelination in <i>Grin3a</i> ^{-/-} mice	109
7.2.3 Preferential myelination of large caliber axons in <i>Grin3a</i> ^{-/-} mice	115
7.3. Loss of activity-dependent OPC plasticity in <i>Grin3a</i> ^{-/-} mice	117
7.4. Characterization of Cre-driver mouse lines for specific GluN3A deletion in oligodendroglial cells	120
7.5. Loss of activity-dependent OPC plasticity in <i>Sox10-Cre</i> ^{+/-} ; <i>Grin3a</i> ^{fl/fl} mice	122
7.5.1 Loss of OPC plasticity in response to chemogenetic activation of callosal axons activity in <i>Sox10-Cre</i> ^{+/-} ; <i>Grin3a</i> ^{fl/fl}	122
7.5.2 Loss of OPC plasticity in response to natural stimulation of neuronal activity with chronic physical exercise in <i>Sox10-Cre</i> ^{+/-} ; <i>Grin3a</i> ^{fl/fl}	124
7.5.3 A novel paradigm to study myelin plasticity and different aspects of motor learning using the Erasmus Ladder	127

7.6. Molecular properties of plastic GluN3A-expressing OPCs	131
7.7. Preliminary insights into GluN3A role in remyelination	132
8. DISCUSSION	137
9. CONCLUSIONS / CONCLUSIONES	147
10. BIBLIOGRAPHY	151
11. ANNEX	175
12. ACKNOWLEDGMENTS / AGRADECIMIENTOS	195

The background of the entire page is an abstract, high-contrast image. It features a dense network of thin, green, fiber-like structures that resemble neural or biological pathways. Overlaid on these are several thicker, more prominent lines in a vibrant red or orange hue. These red lines crisscross the frame, some appearing as straight paths while others are more jagged or curved. The overall effect is one of complex, interconnectedness against a solid black background.

2. SUMMARY / RESUMEN

Work over the last decade demonstrates that the myelin sheaths enwrapping axons, classically seen as static insulators, are highly dynamic and respond to axonal activity and experience. This phenomenon, called “myelin plasticity”, goes beyond postnatal stages into adulthood and plays a key role in remodeling neuronal circuits to support adaptive behavior or functional recovery upon injury. Here we show that NMDA receptors containing GluN3A subunits (GluN3A-NMDARs), key players in synaptic plasticity, are expressed by postnatal and young adult oligodendrocyte progenitor cells (OPCs) and are essentially required for activity-dependent myelin plasticity. Specifically, we find that genetic removal of GluN3A from young brains accelerates the differentiation of OPCs into mature oligodendrocytes (mOLs) in a variety of brain areas during a critical time window of postnatal development, driving an upregulation of multiple markers of OL differentiation and myelination. The phenomenon is not related to time-courses or region-specific patterns of neuronal activity and resembles gene expression programs typical of aged OPCs, pointing towards loss of activity-dependent myelination driven by absence of GluN3A expression. We confirmed this with functional assays in OPC-restricted GluN3A knockouts where OPCs-lacking GluN3A failed to differentiate in response to chemo-genetic stimulation of callosal axons or natural triggers of myelin plasticity like chronic physical exercise. In line with these findings, the regenerative capacity of OPCs declines with aging and correlates with a significant down-regulation of GluN3A expression that predicts limits in plasticity. Our study opens an opportunity to better understand neuron-glia communication and develop strategies to re-express GluN3A to boost myelin plasticity during aging and neurodegenerative diseases.

El trabajo realizado durante la última década demuestra que las vainas de mielina que envuelven los axones, clásicamente consideradas como aislantes estáticos, son altamente dinámicas y responden a la actividad y experiencia axonal. Este fenómeno, llamado "plasticidad mielínica", va más allá de las etapas posnatales hasta la edad adulta y desempeña un papel clave en la remodelación de los circuitos neuronales para apoyar el comportamiento adaptativo o la recuperación funcional tras una lesión. Aquí mostramos que los receptores NMDA que contienen subunidades GluN3A (GluN3A-NMDAR), actores clave en la plasticidad sináptica, se expresan en células progenitoras de oligodendrocitos (OPC) durante la etapa postnatal y en jóvenes adultos y son necesarios para la plasticidad mielínica dependiente de la actividad axonal. Específicamente, encontramos que la eliminación genética de GluN3A de cerebros jóvenes acelera la diferenciación de OPC en oligodendrocitos maduros (mOL) en una variedad de áreas del cerebro durante una ventana de tiempo crítica del desarrollo posnatal, impulsando una mayor expresión de múltiples marcadores de diferenciación y mielinización de OL. El fenómeno parece no estar relacionado con el curso del tiempo o con patrones de actividad neuronal específicos de una región y se asemeja a los programas de expresión genética típicos de las OPC envejecidas. Los ensayos funcionales con ratones con delección específica de GluN3A en OPC mostraron además que las OPC que carecen de GluN3A no logran diferenciarse en respuesta a la estimulación quimiogénica de los axones callosos o desencadenantes naturales de la plasticidad mielínica, como el ejercicio físico crónico. Es importante destacar que la capacidad regenerativa de las OPC disminuye con el envejecimiento, lo que se correlaciona con una importante regulación negativa de la expresión de GluN3A y predice límites en la plasticidad. Nuestro estudio abre una oportunidad para comprender mejor la comunicación entre neurona y glía y desarrollar estrategias para reexpresar GluN3A con el objetivo de aumentar la plasticidad mielínica que disminuye durante el envejecimiento y las enfermedades neurodegenerativas.



3. ABBREVIATIONS

Abbreviations

ACC
AD
AIS
AMPA
AMPA
ANOVA
AP
AU
Bcas1
BDNF
BLA
BrdU
BSA
CC
CNO
CNS
CPZ
CS
CSPG
DAPI
DNQX
Dpi
DREADD
DRG
EAE
EdU
EM
Ennp6
Erbb3
ESC
EYFP
FISH
GABA
GFP
GluN3A-NMDAR
GM
Gpr17
I.P.
Iba1
IF
iPSC
ISH
IUE
Ko

Full description

Anterior Cingulate Cortex
Alzheimer's Disease
Axon Initial Segment
 α -amino-3-hydroxy-5-methyl-4-isoxazolepropionic acid
AMPA Receptor
Analysis of variance
Action Potential
Arbitrary Units
Brain enriched myelin associated protein 1
Brain-Derived Neurotrophic Factor
Basolateral Amygdala
5-bromo-2-deoxyuridine
Bovine Albumin Serum
Corpus Callosum
Clozapine-N-Oxide
Central Nervous System
Cuprizone
Conditioned Stimulus
Chondroitin Sulfate ProteoGlycan
4',6-diamidino-2-phenylindole
6,7-dinitroquinoxaline-2,3-dione
Days Post Injection
Designer Receptor Exclusively Activated by Designer Drug
Dorsal Root Ganglion
Experimental Autoimmune Encephalomyelitis
5-ethynyl-2'-deoxyuridine
Electron Microscopy
Ectonucleotide pyrophosphatase/phosphodiesterase 6
Receptor tyrosine-protein kinase 3
Embryonic Stem Cell
Enhanced Yellow Fluorescent Protein
Fluorescent In-Situ Hybridization
Gamma-aminobutyric acid
Green Fluorescent Protein
GluN3A-containing NMDA Receptor
Grey Matter
G-Protein-coupled Receptor 17
Intraperitoneal
Allograft Inflammatory Factor 1 (AIF1)
Immunofluorescence
Induced Pluripotent Stem Cell
In-Situ Hybridization
In Utero Electroporation
Knockout

Kv1	Voltage-gated potassium 1
LPC	Lysophosphatidylcholine or Lysolecithin
M1	Primary Motor Cortex
M2	Secondary Motor Cortex
Mag	Myelin Associated Glycoprotein
Mbp	Myelin Basic Protein
Mobp	Myelin associated Oligodendrocyte Basic Protein
mOL	Mature Oligodendrocyte
(m)PFC	(Medial) Prefrontal Cortex
MRI	Magnetic Resonance Imaging
mRNA-seq	Messenger RNA-sequencing
MS	Multiple Sclerosis
mTOR	Mechanistic Target of Rapamycin kinase
MTX	Methotrexate
Myrf	Myelin regulatory factor
Nav	Voltage-gated sodium
NFOL	Newly-Formed Oligodendrocyte
NG2	Neuron-Glial antigen 2
NMDA	N-methyl D-aspartate
NMDAR	NMDA Receptor
NRG1	Neuregulin 1
OL	Oligodendrocyte
OPC	Oligodendrocyte Progenitor Cell
PB(S)	Phosphate-Buffered (Saline)
PDGFR α	Platelet-Derived Growth Factor Receptor alpha
PFA	Paraformaldehyde
Plp1	Proteolipid Protein 1
PNS	Peripheral Nervous System
PSD	Postsynaptic densities
PV	Parvalbumin
RNA-seq	RNA-sequencing
scRNA-seq	Single-Cell RNA-sequencing
scWM	Subcortical White Matter
SEM	Standard Error Mean
SS1	Primary Somatosensory Cortex
SVZ	Subventricular Zone
Tcf4	Transcription factor 4
TrkB	Tropomyosin Receptor Kinase B
TTX	Tetrodotoxin
US	Unconditioned Stimulus
V1	Primary Visual cortex
WM	White Matter
Wt	Wild-type



4. INTRODUCTION

4.1. Oligodendroglia and myelination in the central nervous system (CNS)

Myelination, the formation of lipid wraps around axons, is a tightly controlled process that over development and adulthood allows efficient and fast conduction of action potentials (APs). Oligodendrocytes are the myelin-forming cells in the central nervous system (CNS) and spinal cord, while Schwann cells do this function in peripheral nerves. They originate from oligodendrocyte progenitor cells (OPCs) which proliferate, migrate and express characteristic genes to differentiate and adopt a mature phenotype at their final destination, or remain in an immature state to sustain the basal turnover and plasticity of myelin (Miller, 1996; Hughes et al., 2013; Young et al., 2013); or exert other less-known non-myelinating functions.

Oligodendrocytes were first described by Robertson in 1899. In 1921, Pío del Río Hortega named these cells oligodendrocytes (OLs), after differentiating them from microglia and astrocytes using new staining techniques such as silver carbonate. Del Río Hortega published a meticulous review of his discoveries on the morphology and functionality of oligodendroglial cells in 1928. He was able to visualize OLs with their thin processes connected to myelin sheaths. His stainings showed that OLs are enriched in the white matter (WM) but also found in the grey matter (GM), and are mostly localized intrafascicularly, sometimes also perineuronally or perivascularly (Del Río Hortega, 1928; Pérez-Cerdá et al., 2015; **Figure 1**). Yet the demonstration that oligodendroglia are the cells that produce and maintain the myelin sheaths that insulate CNS axons had to wait for the introduction of immunohistochemical and electron microscopy techniques in the 1960s (Geren, 1954; Bunge et al., 1962).

The prevailing view since the discovery of myelination in the peripheral nervous system (PNS) (Vesalius, 1543 and Van Leeuwenhoek, 1719) has been that the only function of myelin-forming cells is to enable maximum conduction velocity, reducing axonal energy consumption and ensuring axonal integrity (Ranvier, 1871; Huxley and Stämpfli, 1949). However, a number of observations have challenged this notion transforming the view of myelin from a static, inactive insulator factor into a dynamic player that shapes changes in adult brain circuits in response to learning. Increasing evidence supports a role for activity-dependent changes in OPCs and myelin-forming OLs that

influence neuronal circuit function (see 4.1.4) and for a metabolic role in supporting neurons on demand via their myelin sheaths (Griffiths et al., 1998; Funfschilling et al., 2012; Saab et al., 2016).

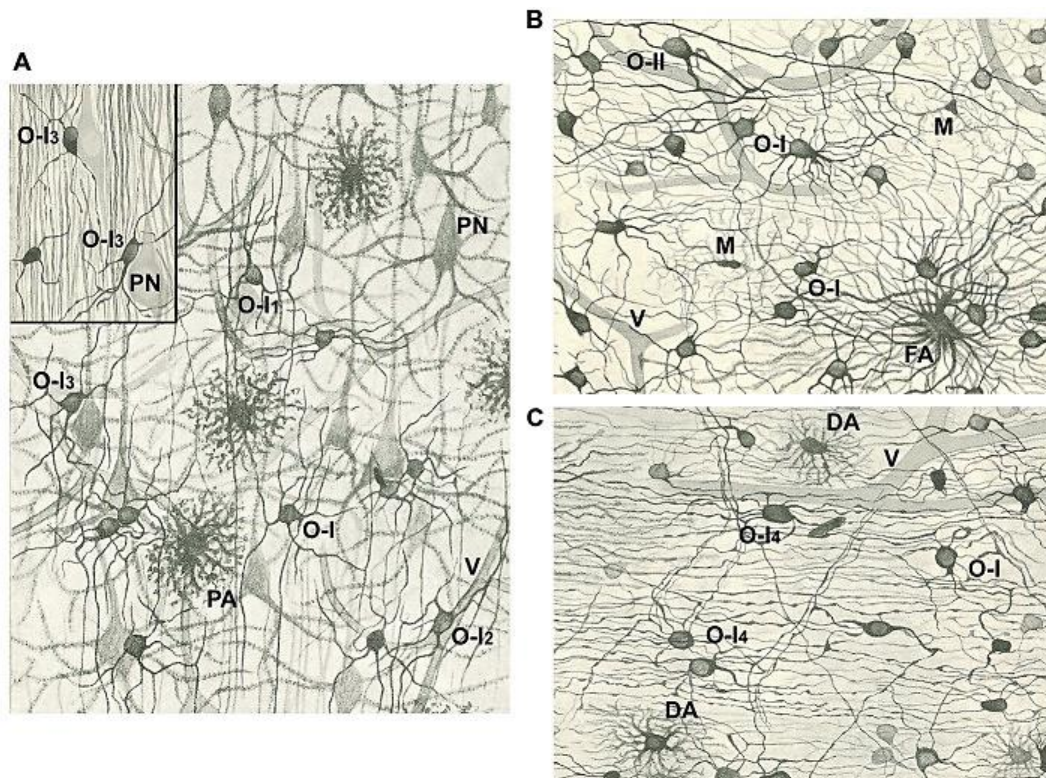


Figure 1. Drawings of the cerebral cortex (A) and white matter (B, C) stained with the Golgi-Hortega silver carbonate method (inset in A). (A) Pyramidal neurons (PN), protoplasmic astrocytes (PA), vessels (V), and type I oligodendrocytes (OLs; O-I) with many processes. Some OLs have processes oriented in the direction of projecting axons (O-I1), while others have a perivascular (O-I2) or perineuronal (O-I3; see inset) localization. (B) Note a fibrous astrocyte (FA), some OLs of the first type (O-I) and one of the second type (O-II), as well as microglia cells (M). (C) See type I OLs similar to those in (A, B) (O-I) or with long processes that follow axons (O-I4), and two dwarf astrocytes (DA). Vessels (V) are also present in (B, C). Modified from Del Río Hortega 1928 in the review of Pérez-Cerdá et al., 2015.

4.1.1. Oligodendrocyte progenitor cells (OPCs)

Three sequential waves of OPCs populate the mouse cerebral cortex early on in a ventro-dorsal temporal progression. OPCs originate from the subventricular zone (SVZ) or the medial ganglionic eminence in a first ventral wave at embryonic day (E) 12.5 (Warf et al., 1991; Rowitch and Kriegstein, 2010). Gradually, the stream of OPC generation moves dorsally with OPCs produced in a second wave from the lateral and caudal ganglionic eminences by E15.5. At birth (E21/P0), a

third wave of OPCs arises from the dorsal SVZ and migrates into the cortex (Kessaris et al., 2006). These waves drive an overproduction of progenitors which compete for space and survival factors provided by astrocytes and axons, leading to the death of a majority of OPCs generated during the first cortical wave (Kessaris et al., 2006; Barres et al., 1992; Trapp et al., 1997; Barres and Raff, 1999). The same happens to 40% of interneurons that share common embryonic origin with the first-OPCs and undergo programmed cell death during the first two postnatal weeks (Ordaz et al., 2019).

OPCs (also known as NG2 glia or polydendrocytes) are the major dividing cell population in the CNS and comprise 3–9% of the total cell population (Dawson et al., 2003). They are distributed ubiquitously throughout the CNS and can be identified by the expression of three cell surface molecules, the chondroitin sulfate proteoglycan NG2 (or CSPG4), the platelet-derived growth factor receptor alpha (PDGFR α) and A2B5 (**Figure 2-3**). OPCs maintain unique territories through self-avoidance, and loss of OPCs because of differentiation, death, or ablation triggers the rapid migration and proliferation of adjacent cells to restore their density and maintain homeostasis (Hughes et al., 2013). The life-long ability for self-renewal makes them unique in the CNS and they are considered as stem cells despite not having a specific niche.

Whether OPCs are a heterogeneous cell population has been historically controversial. Initial studies suggested that despite heterogeneity of OLs, OPC populations are transcriptionally homogenous in the developing and adult brain (single-cell RNA-sequencing data from Marques et al., 2018; Hilscher et al., 2022). Morphologically, OPCs in GM are characterized by their symmetrically oriented processes that extend radially from the soma. By contrast, OPCs in the WM have a more elongated, bipolar morphology, with their longer axes parallel to the axons (Chittajallu et al., 2004). Physiologically, OPCs proliferate and differentiate more rapidly in the WM than in the GM (Dimou et al., 2008; Vigano et al., 2013). The slower kinetics of OL generation in GM has also been demonstrated in the human cortex (Yeung et al., 2014). In addition, OPCs cycle less intensely with age and their differentiation rate declines progressively into adult life (Psachoulia et al., 2009; Spitzer et al., 2019). However, and surprisingly, OPCs in both WM and GM depolarize in response to vesicular release of glutamate and gamma-aminobutyric acid (GABA) from neurons and responses are thought to be mediated by synapse-

like contacts (Bergles et al., 2000, 2010). The presence of synaptic inputs onto OPCs initially appeared to be ubiquitous, although the magnitude of synaptic input seems to vary among OPCs in different niches or in different states. Indeed, two distinct types of morphologically identical OPCs in rat CNS WM have been reported but: one expresses voltage-gated sodium and potassium channels, generates “action potentials” when depolarized and senses its environment by receiving excitatory and inhibitory synaptic input from axons; the other lacks action potentials and synaptic input. The first ones are preferentially damaged by ischemia (Káradóttir et al., 2008). Differences have also been found in the responses of dorsal and ventral OPC to demyelination, age-related functional decline and DNA damage (Crawford et al., 2016; Boda et al., 2022). In line with these findings, OPCs have been found to be functionally more heterogeneous than previously expected with their electrophysiological properties and molecular signature varying both between brain regions and with age (Spizter et al., 2019; de la Fuente et al., 2020; Beiter et al., 2022; see 4.2.2). Thus, OPCs might have a broader heterogeneity of functions than anticipated. Although mature patterns of myelination are largely established within the first three postnatal weeks in rodents or first two years after birth in humans, OPCs continue to represent about 3-4% of cells in adult GM and 8-9% of cells in the adult WM suggesting roles beyond oligodendrogenesis and myelination. For instance, a growing number of studies show that OPCs promote angiogenesis (Yuen et al., 2014; Chavali et al., 2020), glial scar formation (Bradbury et al., 2019), axon remodeling (Xiao et al., 2022; Buchanan et al., 2022) and antigen presentation (Falcao et al., 2018; Kirby et al., 2019) in both the healthy and diseased brain functions.

Human OPCs have been harder to study because of ethical and technical limitations. However, incorporation of additional approaches is now opening new perspectives. Generation and isolation of OPCs from engineered embryonic stem cells (ESCs) or human pluripotent stem cells (human iPSC-derived OPCs) using a chemically defined growth factor-rich medium can now be used to assess the biology of human OLs *in vitro*, and investigate to what extent findings from rodent OPCs can be translated to humans. Single-cell RNA-sequencing (scRNA-seq) on human ESC-derived reporter cells purified at various time points after the initiation of differentiation, have revealed molecular diversity and developmental heterogeneity of human OPCs (Chamling et al.,

2021). They identified sub-populations of OPCs defined by their developmental stage and commitment to either the OL or astrocyte lineages as well as a sub-population with enriched cytokine response signaling. This heterogeneity has been also described using human post-mortem WM samples from the brain, cerebellum and spinal cord (Seeker et al., 2023). Human iPSC-derived OPCs can be also potentially used for transplantation in disease context in a manner largely – though perhaps not completely - free of rejection risk (Wang et al., 2013). Advances in human brain organoids also provide an opportunity to study human OL function in health and disease under conditions that more closely mimic the *in vivo* 3D make-up of the brain (Velasco et al., 2019; Shaker et al., 2021). A combination of these two techniques was developed to create a human stem cell-derived organoid model of widespread and compact myelination (James et al., 2021). Nevertheless, a long list of limitations persists and further investigation needed.

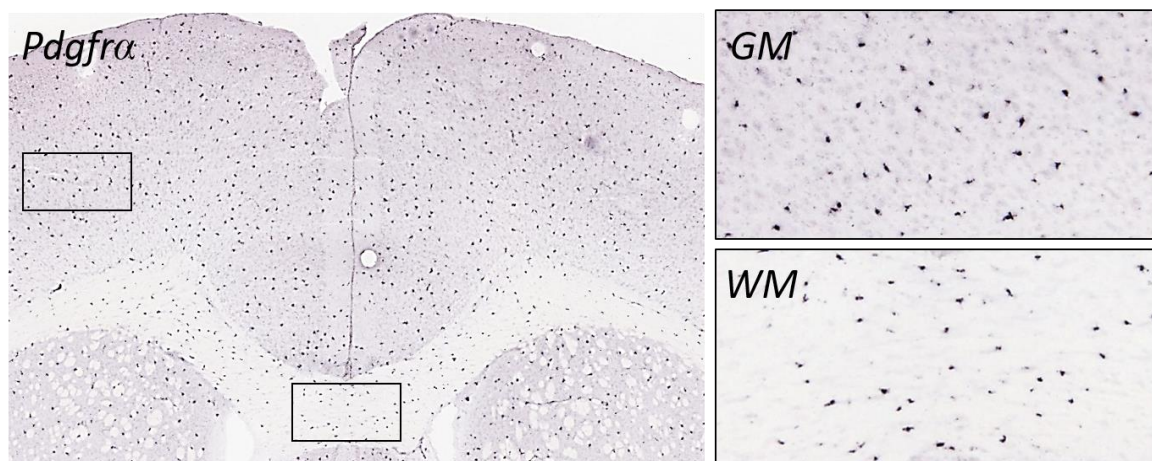


Figure 2. PDGFR α in situ hybridization in P56 brain from Allen Brain Atlas. PDGFR α -positive OPCs are abundant and uniformly distributed in the adult mouse brain (left panel), both in WM and GM regions (right panels).

4.1.2 OPC proliferation and differentiation

Cell cycle progression (also referred to as cell proliferation) is characterized by *de novo* DNA synthesis during the S-phase and can be studied using fate mapping techniques where injection of DNA intercalating agents like 5-bromo-2-deoxyuridine (BrdU) or 5-ethynyl-2'-deoxyuridine (EdU) is followed by detection with antibodies or click chemistry. Using these methods, OPC proliferation and differentiation has been shown to follow a complex sequence of events that

require specific transcriptional programs. During the postnatal period of OPC proliferation and rapid OL production that precedes and accompanies myelination, many recently divided OPCs give rise to two differentiated OLs. In the mature CNS most OPC divisions are self-renewing and generate either one OL and a replacement OPC, or two OPCs, like stem cells (Zhu et al., 2011). Rapid downregulation of OPC markers and upregulation of molecules associated with lineage progression contributes to generate early sister OPC asymmetry. Analyses during aging and upon exposure to physiological (i.e., increased motor activity) and pathological (i.e., trauma or demyelination) stimuli showed that both intrinsic and environmental factors influence the fraction of symmetric and asymmetric OPC pairs and the phenotype of the OPC progeny as soon as cells exit mitosis (Boda et al., 2015).

Postmitotic OPCs enter a newly-formed pre-myelinating OL stage (NFOL) where they remain for roughly 2 days, according to Barres and Raff, 1999. During this short window of time, NFOLs either find an axon to enwrap or undergo programmed cell death (Barres et al., 1992; Sun et al., 2018; Hill et al., 2018; Hughes et al., 2018). They are characterized by a radial morphology and express genes such as G-protein-coupled receptor 17 (*Gpr17*), brain enriched myelin associated protein 1 (*Bcas1*), transcription factor 4 (*Tcf4*, also known as *Tcf12*) and ectonucleotide pyrophosphatase/phosphodiesterase 6 (*Enpp6*). OPCs that progress through the critical survival checkpoint generate new myelinating mature OLs (mOLs) and undergo a dramatic morphological change as they form myelin sheaths around axons. At the transcriptional level, there is a major upregulation of genes such as proteolipid protein 1 (*Plp1*), myelin associated oligodendrocyte basic protein (*Mobp*), myelin associated glycoprotein (*Mag*) and myelin basic protein (*Mbp*) accompanied by down-regulation of early gene markers (**Figure 3**).

Thus, the differentiation of OPCs into myelinating OLs is a multistep process tightly controlled by the spatiotemporal activation and repression of specific growth and transcription factors. Transcription factors and epigenetic mechanisms (DNA methylation, histone modifications, and microRNAs, reviewed by Emery and Lu, 2015 and Tian et al., 2019) have been implicated in orchestrating OPC proliferation vs differentiation. For instance, the myelin regulatory factor (*Myrf*), discovered by Emery et al., 2009, is a key transcription factor essentially required for

functional activation of myelin gene expression and a valuable *Myrf*-knockout mouse model has been created and extensively used in recent work to study adult oligodendrogenesis and *de novo* myelination impact on plasticity, behavior and disease (see 4.1.4).

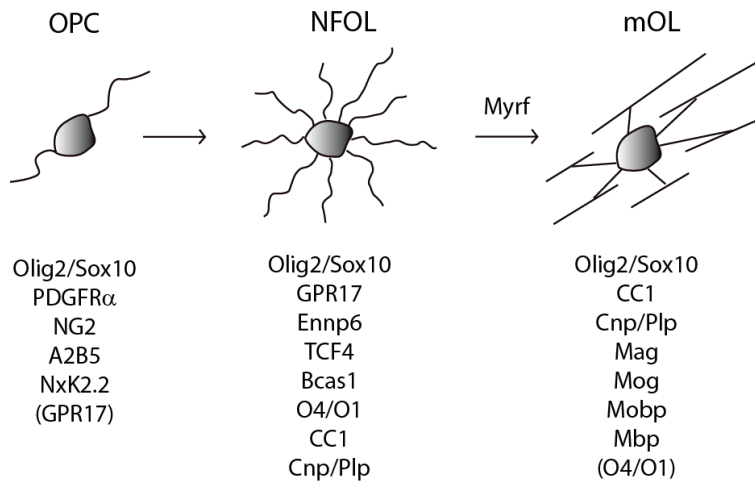


Figure 3. Stage specific-OL morphology and markers. OPC lineage progression is defined by dramatic morphological changes and sequential down-regulation and up-regulation of proteins encoded by specific genes and transcription factors that mediate state transitions.

Of note, while in the early postnatal period OPCs throughout the mouse brain exhibit similar transcriptional phenotypes, scRNA-seq analysis identified 13 distinct OL populations, 12 of which represent a continuum from *Pdgfr α* -positive OPCs to distinct mOLs, 6 different populations enriched in specific regions of the juvenile and adult mouse brain (postnatal day P10-P60) (Marques et al., 2016 & 2018; Hilsher et al., 2022). Given the initial similarities, it is likely that the local microenvironment, which OPCs are exposed to during differentiation, regulates acquisition of this diversity. Human mOLs exhibit a comparable transcriptional heterogeneity that correlates with different CNS regions as well as factors such as sex and age (Seeker et al., 2023). This heterogeneity is altered in disease contexts such as multiple sclerosis (Jäkel et al., 2019).

4.1.3 Myelination

Vertebrate myelination is an evolutionary advancement essential for motor, sensory and higher order cognitive functions. In humans, it begins before birth with OPC proliferation, migration and maturation into myelin-forming OLs within the caudal brain stem and progresses rostrally to the forebrain. But the most rapid and dramatic period of CNS myelination takes place during the first two years of postnatal life. During this critical period, myelin is laid down in virtually all WM

tracts, starting during the first 3 months of life in the midbrain and cerebellum and ending with occipital cortical regions and prefrontal cortex (GM), higher order cognitive areas where myelination continues into adulthood (Jakovcevski & Zecevic, 2005). In rodents, myelination follows a similar timescale and pattern (Van Tilborg et al., 2018, **Figure 4**).

Axons from both excitatory and inhibitory neurons can be myelinated. Some OLs seem to myelinate axons of both excitatory and inhibitory neurons equally while other OLs display a bias in the choice of either inhibitory or excitatory axons (Zonouzi et al., 2019). Importantly, not all brain axons are myelinated. It is possible to find unmyelinated thinner axons as well as intermittently myelinated axons, mainly in the cortex, that are thought to represent an evolutionary strategy to modulate long-distance communication and provide a substrate for circuit plasticity and higher order brain functions (Tomassy et al., 2014; Bacmeister et al., 2022; Munyeshyaka and Douglas Fields, 2022). Intermittent myelination has been proposed to be particularly important in the synchronization of high-frequency spike-timing, the provision of metabolic support by OLs to the axon, or the creation of neuron-OPC synapses along the unmyelinated segments that would not be possible in a fully myelinated axon (Micheva et al., 2016; Tomassy et al., 2014). However, the functional significance of intermittent myelination patterns must be deferred until histological and electrophysiological measurements reveal the distribution of ion channels in the unmyelinated segments (Munyeshyaka and Douglas Fields 2022).

The myelin sheath is a multilamellar spiral, protective layer made of lipids and protein that enwraps neuronal axons. Differently from Schwann cells, a single OL can extend processes that myelinate several axons at the same time, and multiple OLs can myelinate different segments of the same axon with different myelin sheaths. Therefore, myelinated axons are organized into a series of specialized domains with distinct molecular compositions and functions: the axon initial segment (AIS), internodes (anatomical term for myelin sheath segments), juxtaparanodes, paranodes and nodes of Ranvier (Susuki, 2013; **Figure 5**).

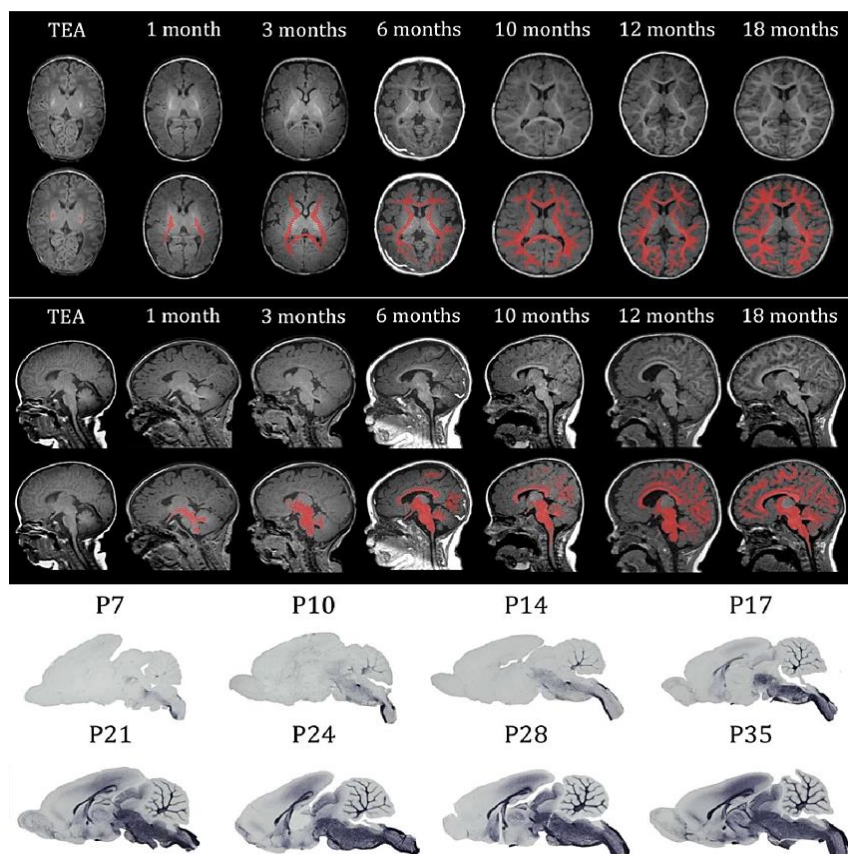


Figure 4. Overview of myelination throughout development from term-equivalent age (TEA) to 18 months in human infants and from P7 to P35 in rats. The upper panel shows transverse sections of magnetic resonance imaging scans at different ages; in the lower sections the myelinated WM is manually colorized (red). The middle panel shows the sagittal sections. The lower panel shows sagittal sections of rat brains at different ages, stained for MBP, a myelin marker. The general spatiotemporal pattern of myelination in humans shows high resemblance with that of rodents. Image selected from Van Tilborg et al., 2018.

The AIS is a thin unmyelinated part of the axon (10-60 μm in length) located between the axon hillock, site in the soma where membrane potentials arising from multiple synaptic inputs are summated before being transmitted to the axon, and the beginning of the first myelinated segment (Peters et al., 1968; Kole and Stuart, 2012). The nodes of Ranvier are periodic gaps in the insulating myelin sheaths that allow the fast saltatory conduction of action potentials and share a common molecular organization with the AIS (Susuki et al., 2013; Rasband and Peles, 2015). At the AIS, voltage-gated sodium (Nav) channels accumulate to initiate the AP, whereas at the nodes they are responsible for AP propagation. At the flanking paranodes, axonal contactin associated protein (Caspr) and glial neurofilament (NF)155 form a tripartite cell adhesion molecular complex that mediates the assembly of the junction between the myelin sheath and the axon. Juxtaparanodes flank paranodes and are enriched in voltage-gated potassium 1 (Kv1) channels. AIS and node composition, length and localization will determine the neuron's spiking properties.

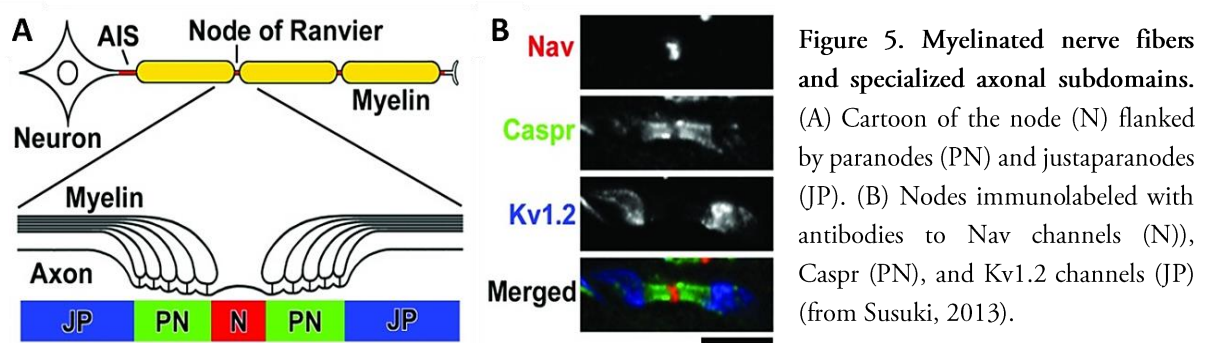


Figure 5. Myelinated nerve fibers and specialized axonal subdomains. (A) Cartoon of the node (N) flanked by paranodes (PN) and juxtaparanodes (JP). (B) Nodes immunolabeled with antibodies to Nav channels (N), Caspr (PN), and Kv1.2 channels (JP) (from Susuki, 2013).

The phenomenon by which new myelin sheaths are generated around axons demyelinated by a lesion or an insult in the adult CNS is called remyelination. While sharing similarities with developmental myelination, it unfolds in a completely distinct context, rendering it a unique phenomenon (refer to Chapter 4).

4.1.4 Activity-dependent myelination

Traditional models of developmental myelination proposed an innate program of robust OPC expansion during postnatal development, followed by widespread differentiation and myelination of target axons in a uniform pattern. OLs possess an intrinsic capacity to myelinate any correctly sized fiber: OLs can myelinate paraformaldehyde-fixed axons and polymer filaments of appropriate diameter and form internodes and myelin sheaths of thickness that is proportional to the diameter of filaments (Bechler et al., 2015; Lee et al., 2012; Redmond et al., 2016). However, *in vivo* they have a remarkable capacity to myelinate only specific axons or parts of axons. The discovery that the cell-intrinsic capacity for myelination can be modulated by environmental cues gave rise to the idea that there is a second, **distinct mode of adaptive or experience-dependent, activity-dependent myelination** (see 4.1.4.1 to 4.1.4.5).

Gyllenstein and Malmfors (1963) were the first to introduce the intriguing idea that neuronal activity could influence oligodendroglia dynamics in experiments where dark-rearing inhibited developmental myelination in the mouse optic nerve. The finding was supported by a later study showing that premature eye-opening accelerates myelin formation (Tauber et al., 1980). Initially sparse evidence for the exciting notion that axonal electrical activity and different types of environmental experience can regulate myelination has now been significantly advanced by recent

work investigating multiple aspects of the myelination process aided by magnetic resonance imaging (MRI) in humans or sophisticated genetic and powerful imaging tools in rodents (Yalçın and Monje, 2021; **Figure 6**). To date, remodeling of nodes of Ranvier, internodes and myelin sheaths in the juvenile and adult brain has been described during sensorimotor experience and learning (see summary **Table 1**), chronic stress (Koskinen et al., 2023), aging and diseases such as multiple sclerosis (Hinman et al., 2006; Howell et al., 2006; Fu et al., 2011).

However, the co-existence or consecutive activation of these two modes of myelination (activity independent and activity dependent) during development and adulthood and the underlying cell biological and molecular mechanisms are yet poorly understood and remains to be explored.

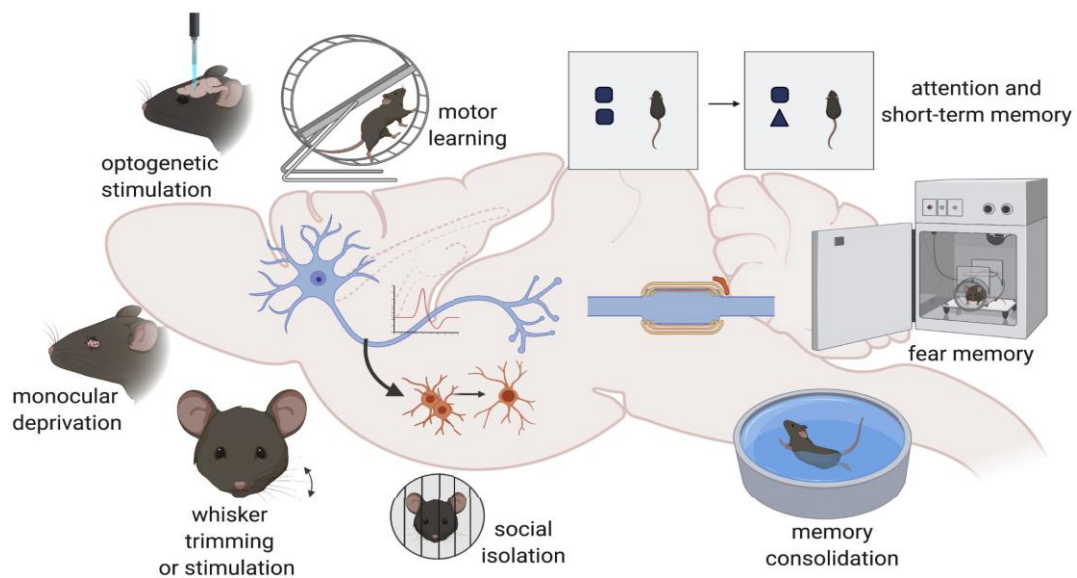


Figure 6. Myelin plasticity is activated in response to neuronal activity and learning. Cartoon of motor, sensory, social and cognitive (learning) paradigms that have been shown to induce and essentially require oligodendrogenesis and myelin plasticity for neural circuit and behavioral adaptation (from Yalçın and Monje, 2021).

In principle, myelination can modulate information flow in neural circuits through several potential mechanisms, including: 1) *de novo* myelination of unmyelinated axons or unmyelinated segments of partially myelinated axons, 2) myelin replacement, where an old sheath is replaced by one or more new sheaths, 3) thickening or thinning of existing sheaths, 4) lengthening or shortening of existing sheaths, and 5) myelin retraction, where sheaths are removed and not replaced (Kaller et al., 2017; **Figure 7**). Additionally, adjustment of node of Ranvier length has also been suggested as another potential mechanism for tuning the arrival time of information in

the CNS (Arancibia-Cárcamo et al., 2017). These adaptive changes can be driven by newly-formed OPCs that proliferate and differentiate (or directly differentiate) into OLs response to neuronal activity, or by pre-existing OLs (Hughes et al., 2018; Yang et al., 2020) over different time scales. *In vivo*, enhancing neuronal activity pharmacologically in the optic nerve (Demerens et al., 1996), or with optogenetic (Gibson et al., 2014) or chemogenetic stimulation (Mitew et al., 2018) of cortical neurons in adult motor or somatosensory cortex triggers an increase in OPC proliferation, differentiation, and myelination in the stimulated brain areas. Conversely, decreasing neuronal activity by pharmacological or chemogenetic manipulations (Demerens et al., 1996; Mitew et al., 2018) decreases OPC differentiation and/or myelination in mice. Neuronal activity also promotes OL survival *in vitro* (Gary et al., 2012) and *in vivo* via a glutamate-to- α -amino-3-hydroxy-5-methyl-4-isoxazolepropionic acid (AMPA) receptors signaling (Kougioumtzidou et al., 2017) although the mechanisms are unclear.

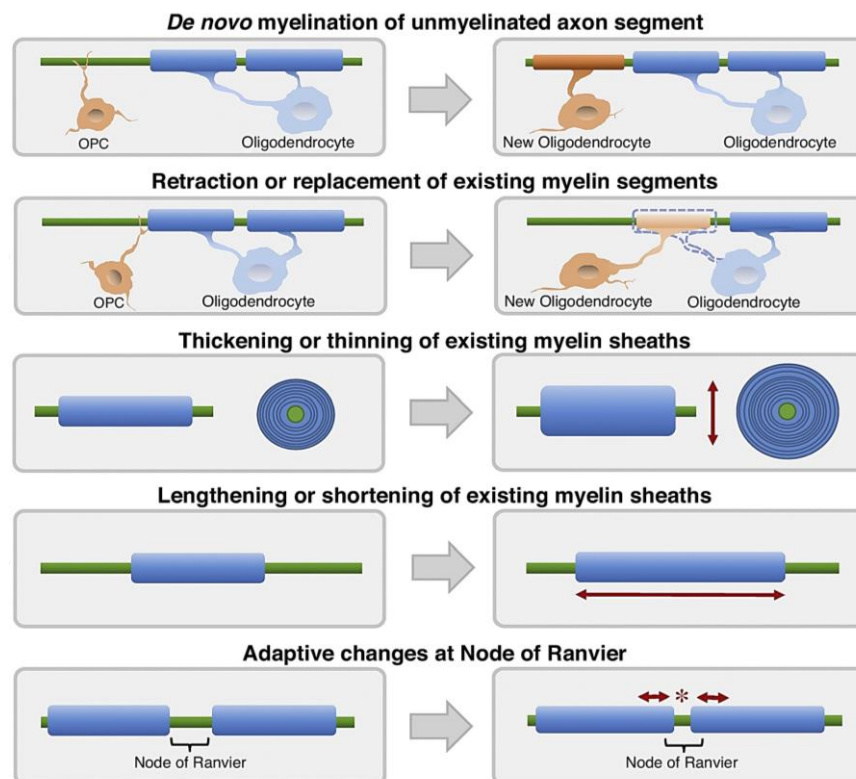


Figure 7. Different cellular processes may lead to dynamic changes in myelination during adulthood. Cartoon of the different mechanisms by which newly-formed or pre-existing OLs can drive myelin plasticity. Image adapted from Kaller et al., 2017.

As a result, activity-dependent myelination can fine-tune neural network dynamics and selectively promote conduction in specific neural circuits and axonal subpopulations. However, aberrant neuronal activity that occurs in disorders with recurrent seizures such as epilepsy, could promote “maladaptive” myelination and has been shown to contribute to the pathogenesis. For instance, Knowles and colleagues (2022) found network-specific increased oligodendrogenesis and myelination after the onset of absence seizures in two distinct rodent models of generalized epilepsy. Structural alterations included increased callosal myelin sheath thickness and number of myelinated axons. Increased myelination did not occur when seizures were pharmacologically prevented, and seizures and epilepsy progression did not progress when activity-regulated myelination was genetically or pharmacologically blocked. Thus, myelin plasticity may become maladaptive in some contexts. More myelin is not necessarily better, and seizure-related increases in axonal myelination beyond a healthy optimum could disrupt the normal circuit function, for example by interfering with fine oscillatory synchrony between brain regions that supports vital cognitive processes.

4.1.4.1 Physical exercise

Physical activity and an active lifestyle have a beneficial effect on myelin content in humans (4 cross-sectional and 4 longitudinal MRI-based studies reviewed in Kujawa et al., 2023). Myelin expansion can be induced in humans throughout the entire lifespan by intensive aerobic exercise (1 hour per day for 6 months, average age of individuals=65 years, Colmenares et al., 2021), providing preliminary evidence for experience-induced plasticity even in the aging WM.

In rodents, the impact of physical exercise [as opposed to motor learning (see 4.1.4.2)] on adaptive myelination in the adult healthy brain is more ambiguous and contradictory. Voluntary physical exercise on a running wheel has been reported to stimulate OPC cell cycle exit resulting in an increased differentiation and decreased proliferation (Simon et al., 2011; Boda et al., 2014), but consequences on myelination and behavior were not assessed. Other studies showed that long-lasting voluntary wheel running promotes both proliferation and differentiation of newly-formed OPCs and thus enhances the myelination in a brain region-dependent manner in adult mice (Zheng et al., 2019, Eugenin von Bernhardt and Dimou, 2022). Conversely, Alvarez-Saavedra et

al., 2016 and Mandolesi et al., 2019 studies are not indicative of adaptive myelination as voluntary running on a wheel slightly increased OPC numbers with no subsequent increase in OLs and myelin.

At least one study evaluated the effect of forced physical activity on adaptive myelination in young mice. Chen and colleagues (2019) subjected 4-week-old mice to a 1-hour daily treadmill run for three consecutive weeks. Following the exercise paradigm, increases in proliferating OPCs and new mOLs as well as higher MBP intensity were detected in the corpus callosum; myelin in these regions had increased thickness as measured by electron microscopy. The treadmill-enhanced myelination was dependent on the activation of the mechanistic target of rapamycin kinase (mTOR). This was evidenced by the fact that intraperitoneal injection of the mTOR inhibitor rapamycin, administered every three days throughout the 21-day training paradigm, prevented both activity-dependent oligodendrogenesis and enhanced myelination. Yet more studies are needed to confirm this finding (see **Results** here).

While in the healthy brain the effect of physical exercise on myelination is still not clear, its benefits against chronic stress (Tang et al., 2021; Yan et al., 2023) and demyelination (Jensen et al., 2018; Mandolesi et al., 2019) find more general consensus. Physical exercise (running on a regular wheel) enhanced oligodendrogenesis and remyelination in the lysolecithin model of toxin-induced demyelination (Jensen et al., 2018) and in the cuprizone model of demyelination (Mandolesi et al., 2019) (see 4.4.2). However, in these contexts it is difficult to discriminate between a direct or indirect role as exercise can firstly reduce inflammation and in turn improve remyelination. Indeed, some studies have addressed the immunomodulatory and neuroprotective effects of exercise in multiple sclerosis (MS) animal models such as Experimental Autoimmune Encephalomyelitis (EAE) mice (see 4.4). Exercise was shown to reduce 1) the immune-specific response of antigen presenting cells against myelin epitopes, 2) the activation and infiltration of T and B cells in the brain, 3) the production of inflammatory cytokines, 4) the astrogliosis and microgliosis; and to increase neurotrophins which can restore neuronal functioning (Souza et al., 2017; Einstein et al., 2018; Bernardes et al., 2013; Xie et al., 2019; Klaren et al., 2016; Pryor et al., 2015).

4.1.4.2 Motor skill learning

We learn new motor skills throughout life, and this ability allows us to adapt to new environments and compensate for injury. Recent evidence suggests that myelination may be dynamically regulated by, and required for, motor learning. Structural changes in human WM occur when learning complex tasks, such as playing the piano (Bengtsson et al., 2005) or learning how to juggle (Scholz et al., 2009). Experiments in adult mice combining diffusion MRI fractional anisotropy (as in human studies) and immunohistochemistry have shown that motor learning (single-pellet reaching task) leads to WM structural changes which correlate with increased myelin density (Sampaio-Baptista et al., 2013).

Much of the work implicating oligodendroglial cells in motor skill learning and memory (see 4.1.4.5) was made possible by the identification of *Myrf*, a transcription factor required for OPC differentiation, and generation of a *Myrf* knockout line with targeted deletion in OPCs using the PDGFR α promoter (*PDGFR α -CreERT2;Myrf^{flox}*). OPC-targeted *Myrf* deletion prevents oligodendrogenesis in adulthood blocking OPC differentiation into myelin-forming OLs without disturbing the preexisting OLs (Emery et al., 2009; McKenzie et al., 2014; Xiao et al., 2016), and was used to demonstrate the necessity of new myelin formation for motor skill learning. Running on a complex wheel with irregularly spaced rungs for 12 days triggered a transient increase in OPC proliferation after 2 days that was followed by increased OPC differentiation by 11 days in the corpus callosum of wild-type (Wt) mice (McKenzie et al., 2014). After 3 weeks of running, there were ~50% more EdU⁺/CC1⁺ OLs in runners than non-runners. A deficiency in new OL generation during this complex learning task prevented *Myrf* knockout mice from mastering the skill. Mutant mice learned over days but the daily average and maximum running speeds were significantly lower compared to controls. Oligodendrogenesis seemed to be mainly involved in the acquisition of the motor skill, as *Myrf* deletion after learning the skill did not affect mice performance when re-introduced in the complex wheel later on (ability to recall a pre-learned skill). Some years later, the same laboratory analyzed at higher temporal resolution the time-course of learning and contribution of oligodendrogenesis. Quite unexpectedly, the performance of the two groups diverged very early, within 2-3 hours after being introduced to the wheel. Immature OLs, labeled with Enpp6, were increased within 2.5 hours of introduction to the complex wheel in the

corpus callosum, and within 4 hours the increase was also detectable in the motor cortex (Xiao et al., 2016). The rapid early phase of OL production presumably involves direct differentiation of OPCs that were paused in the G1-phase of the cell cycle, with no previous proliferation needed. This scenario could potentially cause a temporary decrease in local OPC density that leads to the increased proliferation and differentiation of the remaining OPCs observed in the long term (>10 days), as a compensatory mechanism. This study suggests that OL differentiation is required at a very early stage of motor skill learning, close to the point when synaptic changes occur (Xu et al., 2009). They can be complementary mechanisms underlying learning and memory.

More recently, Bacmeister and colleagues (2020; 2022) applied longitudinal *in vivo* two-photon imaging of individual OLs, myelin sheaths and neuronal axons combined with labeling of learning-activated neurons in mice to study how the pattern of intermittent myelination was altered specifically on individual cortical axons involved in learning a novel forelimb reaching task. Myelin and nodal plasticity were observed in distinct phases of learning: 1) decreased oligodendrogenesis and myelin sheath retraction (increased “nodal” distance) during the first phases of learning and 2) increased oligodendrogenesis and myelin sheath addition (decreased “nodal” distance) immediately post-learning. Computational modeling suggested that motor learning-induced myelin plasticity initially slows oligodendrogenesis. Subsequent increases in the magnitude and timing of nodal and myelin dynamics and axonal conduction speed correlated with improved behavioral performance during motor learning. These results support the notion that a transient “suppressed OPC differentiation state” allows later selection of task-related axons by OLs. Motor learning can also promote oligodendrogenesis and myelin remodeling by pre-existing OLs in a timing-dependent manner during remyelination (Bacmeister et al., 2020).

4.1.4.3 Sensory experience

Deprivation experiments show that experience-dependent myelin plasticity operates as well in visual and somatosensory systems. Binocular enucleation during a specific critical period (postnatal week 4) transiently increases OPC proliferation in the subcortical WM (scWM) of primary visual cortex (V1) without altering the number of mOLs measured several days later (Shin and Kawai, 2021). Monocular deprivation in adult rats decreases myelin markers in the V1-related hemisphere,

whereas the opposite is observed in the non-deprived hemisphere (Murphy et al., 2020). Myelin adaptation to visual deprivation is neuron-specific: myelination of cortical projection neurons remains unchanged, while the myelin profiles of inhibitory parvalbumin (PV) neurons remodel with redistribution of ion channels at the nodes of Ranvier (Yang et al., 2020). This again suggested that myelin plasticity is part of the reconfiguration process that adjusts and fine-tunes neural circuits to change sensory experience. Etxeberria and colleagues (2016) demonstrated that long-term monocular deprivation in mice increases oligodendrogenesis in the retino-geniculate pathway but shortens myelin internode lengths and increases the number of nodes of Ranvier, significantly reducing conduction velocity in the optic nerve.

During formation of the mouse barrel cortex in the somatosensory cortex (the area responding to whisker activity), OPCs receive glutamatergic synapses from thalamocortical fibers and accumulate along septa separating the barrels that represent specific whiskers. Cauterization of whiskers from birth increases OPC proliferation in the barrel fields by P6 (Mangin et al., 2012) and reduces myelinated axon density at P60 in the barrel cortex (Barrera et al., 2013). Whisker trimming also increases the rate of apoptosis of newly-generated OPCs and overall reduces the total number of differentiated OLs, pointing to the initial increase in OPC proliferation as a homeostatic response to a reduction of mOLs. Thus, a critical time window between OPC cell division and differentiation seems to determine OPC survival as a function of changes in the microenvironment and neuronal activity (Hill et al., 2014).

Sensory enhancement can also reshape myelin during adulthood. Three weeks of exposure to a sensory-enriched environment that enhances whisker stimulation and exploration increases oligodendrogenesis and myelination of the barrel cortex (Hughes et al., 2018). However, longitudinal *in vivo* two-photon imaging shows that only a fraction of the differentiated OLs achieves stable integration while the rest die, resembling the developmental critical window. Remarkably, once integrated, OLs remain particularly stable throughout life (Hughes et al., 2018; Tripathi et al., 2017; Yeung et al., 2014).

4.1.4.4 Social experience

Social experience modulates myelin profiles in relevant anatomical regions. An influential study showed that people raised in orphanages with severe social deprivation display altered myelination in limbic WM tracts. The structural changes are associated with long-lasting cognitive impairment (Chugani et al., 2001; Eluvathingal et al., 2006). Inspired by these human imaging and neuropsychological studies, a critical period for myelination was identified in the early juvenile period following weaning in mice (Makinodan et al., 2012). Mice that were socially isolated just after weaning (P21) showed decreased sociability and working memory, along with thinner myelin, shorter and fewer internodes, and reduced length of mOL processes in the medial prefrontal cortex (mPFC). Importantly, the myelin deficits caused by social isolation were not reversed by social re-integration at P35. Prolonged periods of social isolation in adult mice also reduced myelin thickness in the mPFC and caused social withdrawal (Liu et al., 2012). However, the defects could be reversed by social re-integration, indicating that experience-dependent myelin plasticity of adulthood differs from the juvenile period as is the case with other forms of brain plasticity.

Little is known about the molecular mechanisms that mediate social experience driven changes in mPFC myelination. Neuregulin1 (NRG1)/receptor tyrosine-protein kinase3 (ErbB3) signaling has been implicated (Makinodan et al., 2012; Roy et al., 2007). For instance, ErbB3 deletion from OLs mimics the effects of social isolation, causing decreased sociability and thinner myelin sheaths. Reduced expression of type III NRG1 in mPFC neurons during social isolation can cause reduced OL ErbB3 signaling, leading to defects in myelination (Makinodan et al., 2012). Another line of evidence links blood vessels to myelin plasticity in mPFC via vasoactive peptide endothelin signaling (Swire et al., 2019).

Recently, chronic social stress has also been linked to myelin remodeling. In adult mice, a 15-day chronic social stress leads to increased aversion responsiveness and altered OL/myelin-related transcript expression within mPFC and amygdala network (Poggi et al., 2022).

4.1.4.5 Memory and cognition

A question in the field was whether myelination is triggered only by sensorimotor learning, or is a response common to other types of learning and cognitive processes. Human studies have reported changes in WM following reading (Carreiras et al., 2009), learning a second language (Schlegel et al., 2012) or working memory training (Takeuchi et al., 2010; Vestergaard et al., 2011), suggesting that modifications in myelin also occur during cognitive learning.

Mice studies are starting to support this concept. For instance, fear learning induces proliferation and subsequent differentiation of OPCs in the mPFC, a key brain area for long-term adaptations, over several weeks, increasing the number of myelinated axons (Pan et al., 2020). The basolateral amygdala (BLA) also exhibits an initial increase in OPC proliferation, but the new OPCs fail to survive and differentiate into mOLs over the following weeks. No changes were observed in other regions involved such as the anterior cingulate cortex (ACC) or hippocampus, concordant with observations that different neuronal types differentially exhibit activity-regulated myelin changes (Gibson et al., 2014; Yang et al., 2020). Remote (30 days after conditioning) but not recent (24 hours) fear memory recall was impaired in *Myrf*-knockout mice (Pan et al., 2020), suggesting that oligodendrogenesis is required exclusively for fear memory consolidation.

Similar findings were reported by Steadman and colleagues (2020) using the Morris water maze as a spatial learning paradigm. Over the course of training, adult Wt mice found the hidden platform with decreasing latency. Analysis of EdU⁺ cells revealed that oligodendrogenesis and *de novo* myelination increased during training in some but not all task-related brain regions analyzed. Across the 4 training days, OPC-specific *Myrf* lacking mice required progressively less time to locate the platform, like age-matched control mice, indicating robust short-term learning. However, in the probe test 24 hours later they searched the platform less selectively than controls. Interestingly, oligodendrogenesis continued during the post-training consolidation period in the absence of additional training as shown using Edu injection immediately after training. Its disruption in *Myrf*-knockouts specifically impaired remote memory tested 28 days later and oscillatory coupling of hippocampal sharp wave ripples and cortical spindles were impaired.

Apart from fear and spatial memory, Shimizu and colleagues (2023) recently reported a role of oligodendrogenesis in spatial working memory. Working memory operates in short-time scales to maintain and update task-relevant information despite interference from competing inputs and is a crucial cognitive process for reasoning and decision-making. Using T-maze and radial arm maze protocols, they showed that working memory training stimulates and requires OPC proliferation and differentiation, with performance of individual mice strongly correlated with the numbers of OPCs and OLs generated during training. Yet unexpectedly, they were unable to find any correlation between mouse performance and bulk neuronal activity in task-related brain areas such as the ACC.

Type Of Activity	Myelin Changes	Brain Region	Species Model/Age	References
Optogenetic stimulation of neuronal activity	Increased OPC proliferation and differentiation; increased myelin thickness	M2, scWM	Adult Wt mouse <i>in vivo</i>	Gibson et al., 2014
Chemogenetic stimulation of neuronal activity (DREADDs)	Increased OPC proliferation, differentiation with myelination of active axons	CC	Adult Wt mouse <i>in vivo</i>	Mitew et al., 2018
Voluntary physical exercise (wheel)	Higher MBP protein expression with increased myelinated axons and myelin thickness; increased OPC proliferation and differentiation	M1	Adult Wt mouse <i>in vivo</i>	Zheng et al., 2019; Eugenin von Bernhardt and Dimou, 2022
Forced physical exercise (treadmill)	m-TOR-dependent increase in newly-formed OPCs and mOLs	CC	Adult Wt mouse <i>in vivo</i>	Chen et al., 2019
Motor learning (single-pellet reaching task)	Transiently suppressed oligodendrogenesis and increased myelin retraction (node length) over learning; increased oligodendrogenesis, OPC	M1	Adult Wtmouse <i>in vivo</i> ; Lysolecithin	Bacmeister et al., 2020, 2022

	differentiation and addition of new myelin sheaths to fill the gaps		demyelination model	
Motor learning (complex wheel)	Early increase in OPC proliferation and differentiation	CC, M1	Adult Wt and <i>Myrf</i> ^{-/-} mouse <i>in vivo</i>	Chen et al., 2019
Sensory deprivation (whisker cauterization)	Increased OPC proliferation but reduced axon density	S1	Postnatal and adult Wt mouse <i>in vivo</i>	Mangin et al., 2012; Barrera et al., 2013
Sensory deprivation (whisker trimming)	Increased apoptosis of newly-generated OPCs and overall decrease in differentiated OLs	S1	Postnatal Wt mouse <i>in vivo</i>	Hill et al., 2014
Sensory deprivation (dark rearing)	Inhibition of developmental myelination	Optic nerve	Postnatal Wt mouse <i>in vivo</i>	Gyllenstein and Malmfors (1963)
Sensory deprivation (binocular enucleation)	Transient increase in OPC proliferation without effect on differentiation	V1, scWM	Postnatal Wt mouse <i>in vivo</i>	Shin and Kawai, 2021
Sensory deprivation (monocular enucleation)	Decreased MBP in the deprived-hemisphere and myelin remodeling with ion channel redistribution at nodes of Ranvier; Increased oligodendrogenesis but shorter myelin internode length and increased number of paranodes	V1; Optic nerve	Adult Wt rat <i>in vivo</i>	Murphy et al., 2020; Yang et al., 2020; Etzeberria et al., 2016
Sensory enrichment (enriched environment)	Increased oligodendrogenesis and myelination; remodeling of pre-existing myelin sheaths	S1, CC	Adult and postnatal Wt mouse <i>in vivo</i>	Hughes et al., 2018; Goldstein et al., 2021; Nicholson et al., 2020

Social isolation	Thinner myelin, shorter and fewer internodes and reduced length of mOL processes (NRG1/ErbB3 dependent)	mPFC	Postnatal and adult Wt mouse <i>in vivo</i>	Makinodan et al., 2012
Fear learning (fear conditioning)	Increased OPC proliferation, differentiation and number of myelinated axons Inhibition of myelin formation impairs remote fear memory	mPFC	Adult Wt and <i>Myrf</i> -Ko mouse <i>in vivo</i>	Pan et al., 2020
Spatial learning (Morris Water Maze)	Oligodendrogenesis and de novo myelination increased during training and post-training. Inhibition of myelin formation impairs memory consolidation	ACC, RSC, CC/Cing	Adult Wt and <i>Myrf</i> -Ko mouse <i>in vivo</i>	Steadman et al., 2020
Spatial working memory (T-maze; Radial Maze)	Increased OPC proliferation and differentiation in myelin-forming OLs	CC, ACC	Adult Wt and <i>Myrf</i> -Ko mouse <i>in vivo</i>	Shimizu et al., 2023

Table 1. Summary of key studies describing activity or experience-dependent changes in oligodendroglia and myelin in rodents.

4.2. Neuron-oligodendroglial interactions

The mechanisms that regulate the interaction between neurons and oligodendroglial cells, especially in the context of myelin plasticity, are still poorly understood as most genetic manipulations to date have used the *Myrf*-knockout mouse model that blocks OPC differentiation and myelination non-selectively. A growing body of literature highlights that mechanisms for neuron-to-OPC communication engage bona-fide synapses between axons and OPCs, non-synaptic vesicle exocytosis, or paracrine signaling via mediators secreted by neurons.

Axon-OPC synapses: More than twenty years ago, Bergles and colleagues (2000) discovered functional synaptic contacts between neurons and NG2⁺ OPCs (**Figure 8**). Evidence of excitatory (Bergles et al., 2000) and inhibitory (Lin and Bergles, 2004) synaptic input onto OPCs was reported in GM (e.g. in the hippocampus, cerebellum and cochlear nucleus, Bergles et al., 2000; Mangin et al., 2008; Lin et al., 2005; Müller et al., 2009), and in WM (Kukley et al., 2007; Etxeberria et al., 2010). The properties of axon-OPC synapses encompassed essential features of neuron-to-neuron synapses: fast activation, quantal responses, presynaptic inhibition, and both facilitation and depression. Further, presynaptic vesicle machinery accumulates on axons under their myelin sheaths. And, synaptic adhesion proteins and postsynaptic organizers including the PSD-95 scaffold are expressed in OPCs and down-regulated upon OPC differentiation (Li et al., 2024; Hughes and Appel, 2019). Finally, OPCs express functional neurotransmitter receptors for both glutamate and GABA (see 4.2.2) and respond physiologically to presynaptic release of these neurotransmitters. Recently, tracing approaches have begun to reveal the connectivity between neurons and OPCs across brain regions (Mount et al., 2019) and time-lapse *in vivo* imaging studies in the developing zebrafish spinal cord have significantly contributed to our understanding of these fascinating contacts and underlying mechanisms (Li et al., 2022; Hines et al., 2015; Marisca et al., 2020; Hughes and Appel., 2019).

What is the functional significance of neuron-OPC synapses? Why are they disassembled upon OPC differentiation? Since OPCs do not appear to fire action potentials and transmit electrical signals to other cells, information derived from neuronal activity is likely to instruct functions specific to these progenitors: proliferation, differentiation and activity-dependent myelination (see

4.1.4) as well as synapse refinement and neural circuit remodeling. On one hand, using zebrafish Hines and colleagues (2015) showed that activity-dependent vesicle secretion stabilizes myelin sheaths formed on selected axons, and Almeida and colleagues (2021) described how axonal vesicular fusion was enriched in hotspots in heminodal non-myelinated domains into which sheaths grew at the onset of myelination. On the other hand, consistent with the idea that OPCs have a unique and separate role in neural circuit remodeling, two studies provided evidence that OPCs phagocytose synapses in the developing and mature mouse visual cortex (Auguste et al., 2022; Xiao et al., 2022; Buchanan et al., 2022). The question is: are some OPCs specialized in engulfing synapses while others are not? To address this, Auguste and colleagues (2022) developed a high-throughput flow cytometry approach to profile the amount of presynaptic material in over 25,000 OPCs. The analysis revealed that about 20% of OPCs do not contain synaptic material, 75% contain a moderate number of synaptic material, and 5% of OPCs are ‘heavy engulferers’ that phagocytose a large number of synapses.

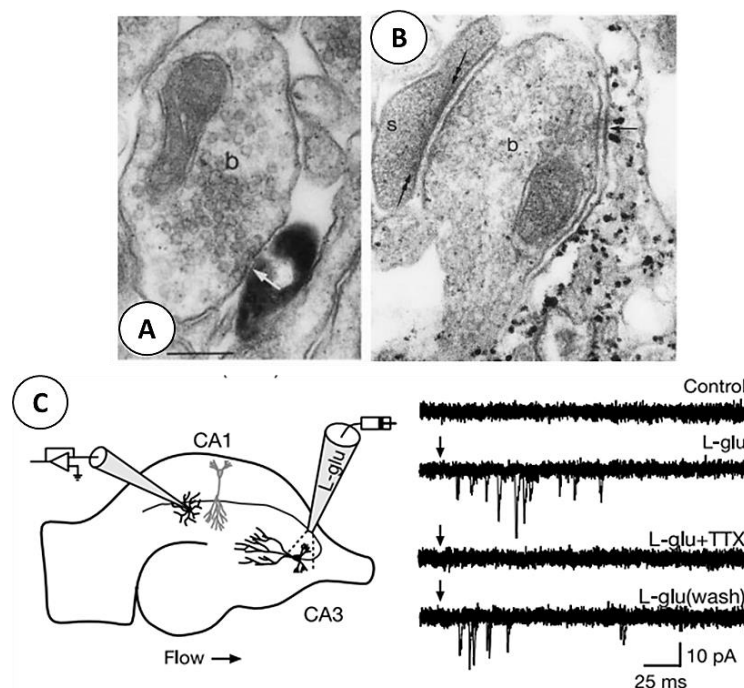


Figure 8. Axon-OPC synapses. (A) Electron microscopy images showing a process of a biocytin labeled OPC receiving a synapse from a neuronal button (b). (B) Silver-intensified gold reaction of an OPC process revealing the thinner postsynaptic membrane specialization (arrows) as compared with the postsynaptic density (between double arrows) of a spine (s) innervated by the same button (b). (C) Puffer application of L-glutamate (200mM, 50 ms; down arrow) onto CA3 pyramidal neurons eliciting bursts of inward currents in OPCs blocked by TTX (1mM). Adapted from Bergles et al., 2000.

Axon-OPC communication via non-synaptic neurotransmitter release. Neuron-to-OPC communication at non-synaptic sites has also been described to promote preferential myelination of electrically active axons *in vitro*. Glutamate release from synaptic vesicles that accumulate in varicosities (or “hot-spots”) along axons of mouse dorsal root ganglion (DRG) neurons triggers local rises in cytoplasmic calcium in OPC processes. Release happens at non-synaptic axo-glial junctions and promotes local synthesis of MBP in the myelin sheath through Fyn kinase-dependent signaling (Wake et al., 2011).

Axon-myelin signaling. During the differentiation process, OPCs undergo intense structural changes and the processes generate a large amount of membrane around axons to create the myelin sheath. The level of expression of the majority of glutamate receptor subunits has been shown to be reduced in mOLs compared to OPCs (see 4.2.2) and to be locally restricted to OPC processes and growing myelin sheaths (Karadottir et al., 2005; Piña-Crespo et al., 2010; Micu et al., 2016). The unique electrical properties of mOLs, characterized by high resting potassium-dependent conductance and very low impedance (Kukley et al., 2010), pose challenges in achieving adequate voltage control over the distal parts of myelin sheaths during whole-cell patch-clamp recordings. Despite these challenges, evidence points to glutamate release beneath the myelin sheath as a mode of neuron-to-mOL communication (Micu et al., 2016). Additionally, glutamate receptor responses have been implicated in calcium accumulation within myelin, especially during chemical ischemia (Micu et al., 2006; Doyle et al., 2018). However, this mechanism differs from classical synaptic release and can be explained also by non-vesicular glutamate release along the axons via reverse glutamate uptake.

Finally, apart from neurotransmitters, neurons secrete factors that are important for oligodendroglial cell survival and dynamics upon activity stimulation (see below).

4.2.1 Neuron-secreted factors in neuron-oligodendroglial interactions

While in the PNS, axonal expression of type III NRG1 is sufficient to instruct Schwann cells to myelinate axons (Michailov et al., 2004; Taveggia et al., 2005), not such molecular mediator has been identified in CNS myelination, suggesting that multiple signals might exist. Nevertheless,

numerous neuron-secreted factors have been identified as critical players in interactions between neurons and oligodendroglia and shown to influence the process of myelination.

A key player is brain-derived neurotrophic factor (BDNF), a microenvironmental cue regulated by neuronal activity whose effects are mediated through tropomyosin receptor kinase B (TrkB) receptors in OPCs (Geraghty et al., 2019; Vondran et al., 2010). BDNF plays a role in both developmental myelination and activity-regulated myelin plasticity. In development, heterozygous loss resulting in ~40% decreased BDNF protein reduces OPC numbers and decreases myelin-associated protein levels without changing OL numbers (Vondran et al., 2010).

In line with these findings, conditional *TrkB* deletion in mature OLs using the MBP promoter does not change OL numbers but reduces myelin sheath thickness in the CNS (Wong et al., 2013). OPC-specific deletion of *TrkB* entirely abrogates activity-dependent myelination of cortical projection neuron axons (Geraghty et al., 2019). Mechanistically, Lundgaard and colleagues (2013) showed that BDNF increases OPC responses to glutamate by enhancing N-methyl D-aspartate (NMDA) receptor function and switching OPCs to an activity-dependent mode. NRG1 also activates this switch, suggesting that multiple factors may impact OPC responses to similar neurotransmitter signals (see 4.2.2.2 and 4.3.3). These data, combined with the finding that social isolation leads to decreased NRG1/ErbB3 signaling in OLs and PFC hypomyelination (Makinodan et al., 2012; see 4.1.4.4) support a mechanism whereby neuronal, activity-dependent release of growth factors gates responses of oligodendroglia to neurotransmitter release. A related line of research suggests an additional contribution of microglia to this regulation (Gibson et al., 2019; Geraghty et al., 2019). In a mouse model of chemotherapy-related cognitive impairment using methotrexate (MTX), activated microglia reduce BDNF expression and impair activity-dependent OPC proliferation, differentiation, and myelination. Mice that lack TrkB in OPCs (*Pdgfra*-creER^{T2};*TrkB*^{fl/fl}) or are defective in BDNF transcription (BDNF^{TMKI} mice with knock-in mutations in calcium regulatory element binding sites in the *Bdnf* promoter) exhibit impaired activity-dependent myelination in premotor circuits accompanied by deficits in a novel object recognition test. Conversely, stimulating TrkB signaling rescued cognitive function after MTX exposure. Depleting microglia through pharmacological colony-stimulating factor 1 (CSF1)

receptor blockade restored neuronal BDNF expression, reversed the myelin deficits and rescued cognitive performance (Geraghty et al., 2019; Gibson et al., 2019). These findings underscore a sensitive balance between interactions of glial cell types in the brain and how glial dysregulation can exert persistent impairments on neurological function.

Along with the described implication of NRG1 and BDNF, Osso and colleagues (2021) identified the neuropeptide dynorphin as a mediator of activity-dependent myelination following stress. Forced swim stress induces striatal dynorphin release by unmyelinated axons which activates kappa opioid receptor (the endogenous dynorphin receptor) expression in OPCs, resulting in increased OPC differentiation and myelination of neighboring axons. Neurotrophin 3, ciliary neurotrophic factor (CNTF) and PDGF have also been shown to be crucial for OPC survival and proliferation *in vitro* (Barres et al., 1993). Finally, many other factors, including Jagged1, neural cell adhesion molecules (NCAMs; such as L1-CAM, PSA-NCAM, TAG-1), Lingo1, Fractalkine, Laminin- α 2, and certain cadherins regulate axon-oligodendroglia interactions at the various stages of axon selection and myelination during development and beyond (reviewed in Almeida, 2018).

4.2.2 Neurotransmitters in neuron-oligodendroglial interactions

Glutamate and GABA release from activated axons likely serves as a triggering mechanism for activity-dependent myelination. As mentioned, OPCs receive synaptic inputs from both glutamate and GABA neurons and express a variety of ionotropic glutamate (kainate, AMPA, NMDA) and GABA receptors (Bergles et al., 2000; Karadottir et al., 2005, 2008; Micu et al., 2006; Kukley et al., 2007; Ziskin et al., 2007; Lundgaard et al., 2013; Gautier et al., 2015; Spitzer et al., 2019; Mount et al., 2019) that allow them to sense and respond to neuronal activity. Nevertheless, the roles of these receptors in oligodendroglia is still the subject of controversy. Below we review current evidence for the involvement of the two major families of glutamate receptors, AMPA-type and NMDA-type, which mediate fast excitatory synaptic transmission and plasticity in neurons in the CNS.

4.2.2.1 AMPA receptors in oligodendroglia

Electrophysiological studies demonstrate the expression of AMPA-type glutamate receptors (AMPA receptors) in oligodendroglial cells, principally OPCs (Kukley et al., 2007; Ziskin et al., 2007). Double in situ hybridization (ISH) for *Pdgfra* and AMPA receptor subunits (*Gria1-4*) followed by Olig2 immunolabelling in the developing scWM show GluA2, 3 and 4 subunits in a majority of OPCs, with almost absence of GluA1 (Kougioumtzidou et al., 2017). Of note, the edited GluA2 form – with Arg in position 583 - renders GluA2-containing AMPA receptors Ca²⁺-impermeable. Both calcium permeable (GluA2-lacking) and impermeable AMPA receptors (Maldonado and Angulo, 2015; Chen et al., 2018) are expressed by OPCs, allowing OPCs to respond to synaptic input with membrane depolarization and local calcium influx.

Functionally, studies in isolated OPC cultures or organotypic cerebellar slices showed that AMPAR activation inhibits OPC proliferation while AMPAR block with the antagonist 6,7-dinitroquinoxaline-2,3-dione (DNQX) promotes proliferation and differentiation (Gallo et al., 1996; Yuan et al., 1998; Fannon et al., 2015). The *in vitro* data support an anti-proliferative role of AMPARs, but paradoxically, AMPAR block decreased myelination suggesting that full-differentiation did not occur (Fannon et al., 2015). In addition, genetic mouse studies showed minimal and opposite effects of OPC-selective deletion of AMPA receptor subunits (GluA2-3-4) in OPC proliferation or differentiation *in vivo*, i.e. only a small decrease on the number and survival of newly differentiating OLs (Kougioumtzidou et al., 2017). Importantly for interpretation, these experiments were performed in the absence of experimental modulation of neuronal activity, which could lead to missing activity-dependent roles for these receptors. Indeed, blocking neuronal activity, axon vesicular release or AMPA receptors in toxin-induced focal demyelinated lesions results in impaired remyelination (Gautier et al., 2015).

To clarify these issues, Chen and colleagues (2018) chose an alternative approach: to increase the Ca²⁺-permeability of AMPA receptors in OPCs using retroviral injections of GluA2 variants in the mouse corpus callosum. Experiments were conducted during the 2nd-3rd postnatal week, when OPC differentiation and myelination rates are high. Expression of unedited GluA2 increased AMPAR currents and Ca²⁺ permeability, leading to OPC proliferation but reduced differentiation.

The finding suggested that that Ca^{2+} -permeability of AMPARs might be involved in regulating the choice between proliferation and differentiation in OPCs. And indeed, differentiating OPCs have been shown to have a lower Ca^{2+} -permeability than immature cycling OPCs (Zonouzi et al., 2011).

4.2.2.2 NMDA receptors (NMDARs) in oligodendroglia

WM oligodendroglia was initially reported to lack NMDARs (Berger et al., 1992; Patneau et al., 1994), the classical mediator of glutamate toxicity, and it was thus believed that an excess of glutamate damages OPCs by acting on calcium-permeable AMPA/kainate receptors (Gautier et al., 2015) or by depriving cells of antioxidant protection (Oka et al., 1993). However, a series of breakthrough studies (Karadottir et al., 2005; Salter and Fern, 2005; Micu et al., 2006; see also Burzomato et al., 2010) reported for the first time oligodendroglial expression of NMDARs. Karadottir et al. (2005) provided a detailed description of NMDA-evoked currents in postnatal OPCs and mOLs mediated by receptors which are blocked only weakly by Mg^{2+} and likely contained NR1, NR2C and NR3 NMDAR subunits. Application of NMDA ($60\mu\text{M}$) evoked an inward current in corpus callosum and cerebellum oligodendroglia, which was comparable in size (at -63mV in 0mM Mg^{2+}) to currents evoked by AMPA ($20\mu\text{M}$) or kainate ($30\mu\text{M}$). The NMDA currents were blocked by the competitive NMDA receptor antagonist D-AP5 but unaffected by antagonists of AMPA/KA, mGluR, GABAA, or glycine receptors. While AMPA receptors mainly clustered on the soma, NMDARs were present in the OL myelinating processes (Salter and Fern, 2005) and were activated by ischemia. The authors suggested that NMDARs mediate, at least in part, the inward current generated in OLs in response to the kind of energy deprivation that occurs in periventricular leukomalacia, stroke, and after ischemia in spinal cord injury. Parallel studies showed that NMDAR activation during ischemia causes Ca^{2+} accumulation in myelin (Micu et al., 2006) with rapid loss of oligodendroglial process (Salter and Fern, 2005) and myelin decomposition that can be prevented by NMDAR inhibitors (Micu et al., 2006). Notably, the higher glutamate affinity of NMDARs, relative to AMPA receptors, makes them more likely to be activated in neurodegenerative disorders which involve a prolonged but small rise of extracellular glutamate concentration, as may occur in MS.

Yet similarly to AMPA receptors, genetic deletion of the obligatory NMDAR subunit GluN1 appeared to have no discernible impact on OPC density, proliferation nor developmental oligodendrogenesis and myelination *in vivo* (de Biase et al., 2011; Guo et al., 2012). The only change observed by de Biase and colleagues (2011) was enhanced surface expression of calcium-permeable AMPA receptors. In contrast to these results, Li and colleagues (2013) reported a role of NMDARs in regulating OPC differentiation and remyelination potential *in vitro*. In cultured rat OPCs, NMDA stimulation regulated myelin proteins expression and increased the complexity of process branching and extension during OPC differentiation. Pharmacological NMDAR antagonism or GluN1 knockdown by RNA interference in OPCs prevented the differentiation induced by NMDA. The pro-differentiation effect of NMDA was linked to activation of mTOR and was blocked by the mTOR inhibitor rapamycin, suggesting an mTOR-dependent mechanism. Furthermore, NMDA increased numbers of myelin segments in DRG-OPC cocultures. In line with these results, Li and colleagues (2013) provided *in vivo* evidence for NMDAR role in remyelination. This is demonstrated by the delayed remyelination observed in the cuprizone model, examined through *in vivo* immunofluorescence and electron microscopy, when treated with the NMDAR antagonist MK801.

Further evidence for NMDARs in OPCs has emerged in the last few years. Spitzer and colleagues (2019) conducted electrophysiological recordings of fluorescently labeled OPCs in NG2-EYFP (enhanced yellow fluorescent protein) knock-in mice. The most prominent age-related changes were in Nav channels (which determine OPC excitability) and NMDAR densities. Both peaked during the first/second postnatal week (P6-P16, **Figure 9**) when OPCs start to differentiate into myelinating OLs. However, while Nav density remains high in the adult and aged brain (**Figure 9A and 9B**), NMDAR density gradually decreases with age correlating with a reduction in OPC proliferation and myelination potential (note the dramatic decrease after P200, **Figure 9C and 9D**). Parallel RNA-seq of OPCs isolated by PDGFR α magnetic activated cell sorting was used to correlate electrophysiological currents in OPCs with gene expression. Age-related changes in Nav and NMDAR densities in OPCs were associated with changes in their molecular signature: at P12 OPCs mainly express genes of proliferation, early differentiation and transcription that decreases with age and concomitant upregulation of pro-quiescence and inflammatory genes. In terms of

subunit composition, gene expression of Nav (α subunits *Scn3a* and *Scn7a*, and β auxiliary subunits *Scn1b*, *Scn3b*, and *Scn4b*) and NMDAR subunits (*Grin1*, *Grin2a*, *Grin2c*, and *Grin3a*) significantly increased from embryonic to postnatal OPCs and subsequently remained constant to old age, with the exception of *Scn3b* and *Grin3a*, that were still present in adult but almost completely disappeared in aged mice (see **Results** section).

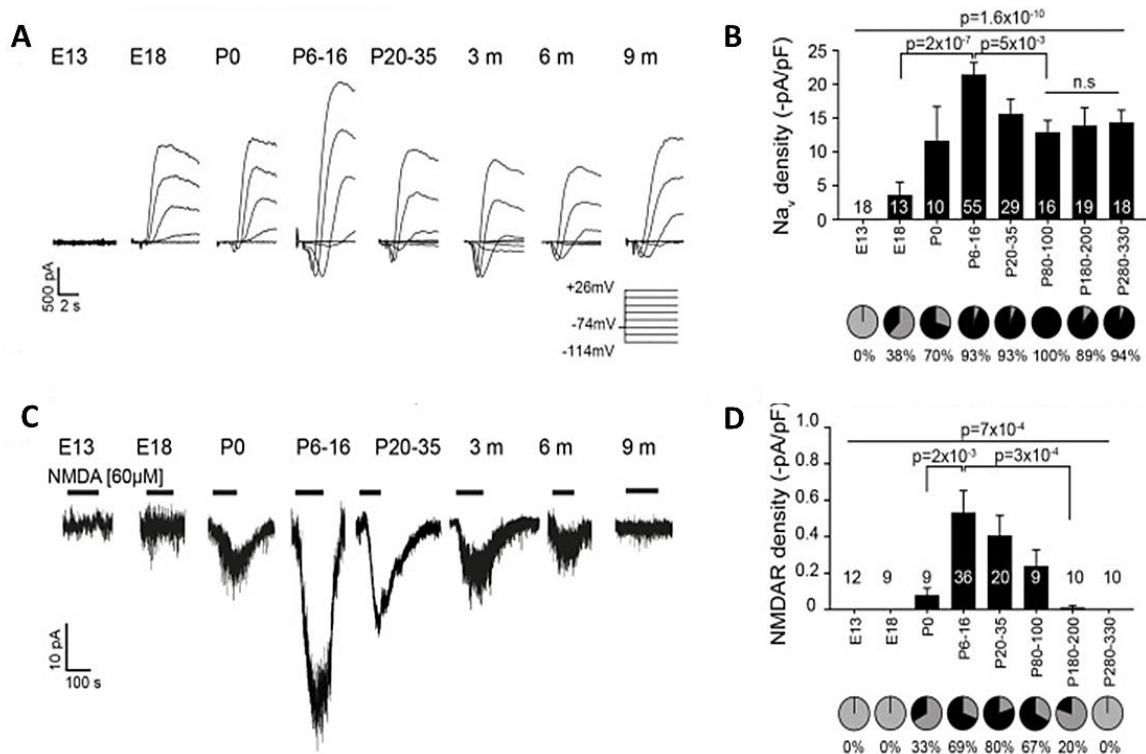


Figure 9. OPCs acquire functional ion channels at different developmental time points. (A) Leak-subtracted traces of Nav currents in response to 20-mV steps from a holding potential of -74 mV (inset, voltage pulses from -114 to +26 mV) in OPCs from E13 to 9-month-old-mice. (B) Nav densities significantly differ between age groups, with a peak at P6-16, at the time when myelination is at its highest rate. (C) NMDA (60 μ M)-evoked currents in OPCs from E13 to 9-month-old-mice. (D) Both current density and proportion of OPCs with detectable currents peaked during P6-P35, at the time when myelination is at its highest rate, and declined until becoming undetectable. Figure adapted from Spitzer et al., 2019.

Recently, a newly identified metabolic role for NMDARs in oligodendroglia has been described. OLs take up glucose using the cell surface-expressed glucose transporter 1 (GLUT1) and then convert glucose into lactate through glycolysis. Saab and colleagues (2016) described that OL NMDARs regulate GLUT1 surface expression, glucose uptake and axonal energy metabolism upon activity-dependent glutamate release *in vitro*. This is also important in disease contexts. For

instance, studies of early stages of the EAE model of MS have shown that axonal damage can start well before axons become demyelinated, suggesting loss of OL metabolic support as a very early event in the pathogenesis (Nikić et al., 2011).

4.3. GluN3A-containing NMDA receptors (GluN3A-NMDARs)

NMDARs are heterotetrameric assemblies of two mandatory GluN1 subunits and combinations of GluN2 (A-D) and GluN3 (A-B) subunits (Monyer et al., 1992; Schorge and Colquhoun, 2003); in older terminology GluNs are referred to as NRs. Combinatorial subunit composition confers specific biophysical properties and protein interactions and yields multiple receptor subtypes with distinct single-channel conductance, Mg^{2+} blockade, and Ca^{2+} permeability as well as unique trafficking, localization and signaling (Lau and Zukin, 2007; Paoletti et al., 2013). GluN1/2A or 2B NMDARs are historically defined as the mediators of brain plasticity because of their high calcium permeability and signaling properties that convert neuronal activity patterns into long-term changes in synapse structure (Monyer et al., 1994). During critical periods of postnatal development, a switch from juvenile (containing GluN2B or GluN3A) to mature (containing GluN2A) NMDAR subtypes is thought to gate the maturation and stabilization of excitatory synapses and formation of precise neural circuits (Paoletti et al., 2013; Hansen et al., 2017). Current data pinpoints the relevance of non-conventional GluN3A-containing NMDARs (from now on GluN3A-NMDARs) as gate-keepers of synaptic plasticity and stabilization during postnatal development. More recent work suggest that they maintain juvenile plasticity modes into adulthood in specific brain areas and in non-neuronal populations (Perez-Otaño et al., 2016; Crawley et al., 2022).

4.3.1 Properties and expression pattern of GluN3A-NMDARs

Non-conventional GluN3A subunits can assemble into two types of receptor complexes: i) tri-heteromeric receptors (GluN1/2/3A, or non-conventional GluN3A-NMDARs) that respond to glutamate and NMDA but exhibit smaller single-channel conductance, lower Ca^{2+} permeability, lower open probability (but longer open times) and relative insensitivity to Mg^{2+} block compared to classical GluN1/GluN2 NMDARs; or ii) di-heteromeric (GluN1/3A) receptors that do not bind glutamate and function as excitatory glycine receptors (**Figure 10**) (Burzomato et al., 2010; Das et al., 1998; Perez-Otaño et al., 2001, Roberts et al., 2009; Sasaki et al., 2002; Tong et al., 2008). Along with distinct biophysical properties, a second characteristic of non-conventional

GluN3A-NMDARs is a decreased concentration at postsynaptic densities (PSDs) of excitatory synapses relative to GluN1/2 postsynaptic NMDARs. Electron microscopy and biochemical fractionation studies show that GluN3A, while present in PSDs, predominates at perisynaptic or extrasynaptic locations, suggesting specialized functions such as sensing specific patterns of glutamate release or glycine or dominant-negative effects on classical NMDAR signaling (see below modulation by GluN3A of mTOR signaling). Immunogold electron microscopy studies have also reported GluN3A at presynaptic locations next to astrocytes (Larsen et al., 2011; Savtchouk et al., 2019).

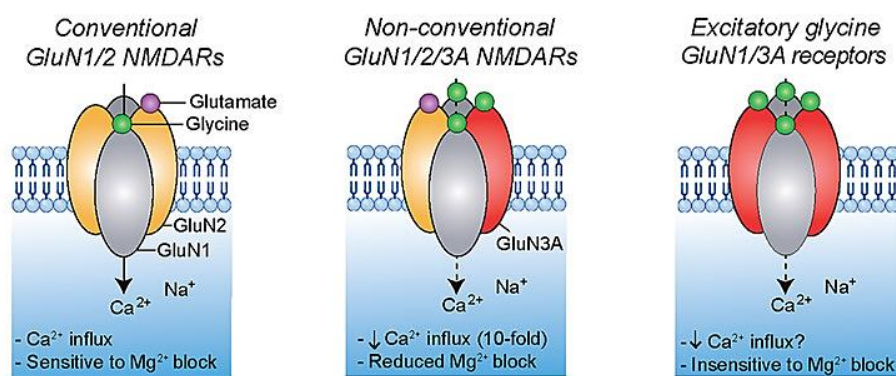


Figure 10. Unique properties of GluN3A-containing receptors. Cation permeabilities of classical NMDARs and different types of GluN3A-containing complexes. Note that the calcium permeability and Mg^{2+} sensitivity of both non-conventional GluN1/2/3A triheteromers and excitatory glycine GluN1/3A diheteromers are lower than conventional GluN1/2 receptors (from Crawley et al., 2021).

GluN3A is highly expressed during postnatal critical periods of experience-dependent plasticity (peak at P8-P12) and expression drops dramatically in most brain regions as synapse stabilization and maturation occur (Perez-Otaño et al., 2006; Wong et al., 2002). Recent work from our lab (Murillo et al., 2021) revealed that beyond postnatal periods, significant GluN3A levels are retained into adulthood in selected brain regions such as the amygdala, medial habenula, association cortices, and high-order thalamic nuclei. These findings confirmed and expanded another study that found *Grin3a* expression in adult mouse brain to be one of the strongest correlates with a hierarchical gradient of functional integration across the neocortex - from primary sensory to transmodal association cortices, established using the MRI T1w/T2w ratio, marker of myelin content and cytoarchitecture (Fulcher et al., 2019). Low T1w/T2w ratios and high *Grin3a* expression were typical of less differentiated association and transmodal cortical areas with strong

needs for plasticity and functional integration throughout life such as the claustrum, rhinal, insular or prefrontal cortex, in adult mouse brain. Similar correlation was observed in human brains.

Functionally, molecular manipulations in mice showed that prolonging GluN3A expression beyond its natural time window inhibits synapse plasticity and maturation and promoted pruning, whereas GluN3A deletion accelerated synapse maturation and stabilization (Henson et al., 2012, Kehoe et al., 2014; Roberts et al., 2009; reviewed in Pérez-Otaño et al., 2016, see **Figure 11**). These and many other *in vitro* and *in vivo* experiments support the hypothesis that GluN3A-NMDARs act as a “brake” to prevent the premature strengthening and stabilization of synapses and keep plasticity high until the arrival of sensory activity. Properly-timed and activity dependent removal of GluN3A-NMDARs then would allow their replacement by conventional NMDARs that in turn will drive the maturation of active synapses. Another hypothesis is that GluN3A-NMDARs act as a “tagging” mechanism to label weak and inactive synapses, which will promote the retraction, and final elimination of the spine and synapse (Henson et al., 2010).

Of mysterious function long since their discovery in 2001 (Perez-Otaño et al., 2001; Chatterton et al., 2002), functional di-heteromeric GluN1/GluN3A receptors have now been described in juvenile hippocampal (Grand et al., 2018) and adult medial habenula neurons (Otsu et al., 2019). Electrophysiological recordings suggest that, rather than gating plasticity as GluN1/2/3 complexes, they modulate neuronal excitability by acting at dendritic localization as sensors of endogenous glycine levels (Bossi et al., 2022).

From a signaling point of view, metabotropic interactions with the postsynaptic scaffold GIT1 allow GluN3A to control local mTOR complex 1 (MTORC1) or actin cytoskeleton activity (Fiuza et al, 2013; Conde-Dusman et al., 2021). For instance, enhancing GluN3A expression in cortical neurons disrupts GIT1/mTORC1 complexes and prevents (BDNF) activity-dependent synaptic mTOR activation. Conversely, GluN3A removal enables complex formation, potentiates mTOR-dependent protein synthesis and facilitates the consolidation of associative and spatial memories in mice. The regulation of protein synthesis by GluN3A via mTOR signaling suggest a putative mechanism of action of GluN3A-NMDARs expressed by other cell types, such as OPCs.

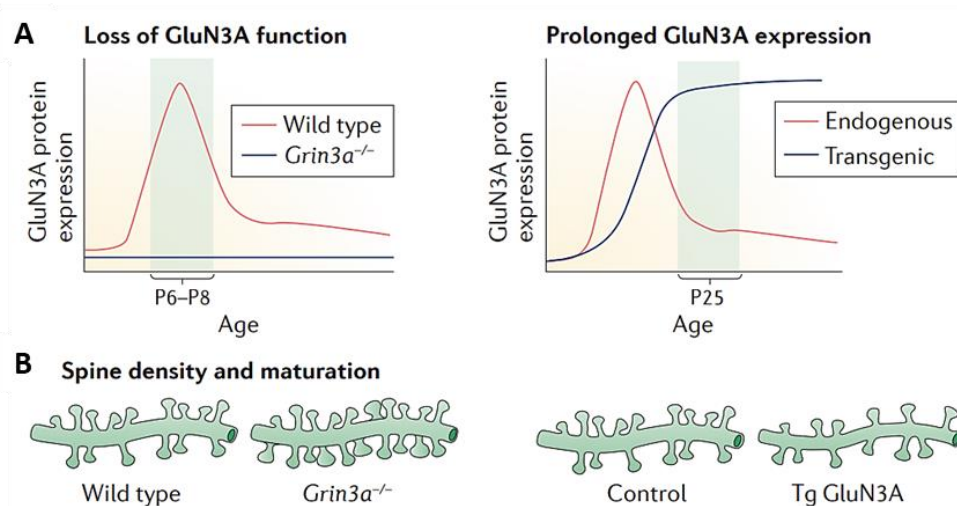


Figure 11. Roles of GluN3A-NMDARs in synapse maturation and pruning. (a) Loss and gain of GluN3A expression (encoded by the *Grin3a* gene) in constitutive *Grin3a*^{-/-} and transgenic mice where green fluorescent protein (GFP)-GluN3A was overexpressed under the control of the calcium/calmodulin-dependent protein kinase type 2a (*Camk2a*) promoter (Tet-On system) (Roberts et al 2009). P6-P8, peak of endogenous GluN3A expression; P25, plateau of transgenic GluN3A expression. (b) Cerebrocortical neurons from P18 *Grin3a*^{-/-} mice had increased density of dendritic spines with large heads, indicative of a mature morphology. Conversely, dendritic spine density and size were reduced in transgenic mice in which GluN3A expression was prolonged (Tg GluN3A). Adapted from Pérez-Otaño et al., 2016.

4.3.2 GluN3A cell-type specific expression

GluN3A is expressed in both excitatory and inhibitory neurons in mice and humans. *Grin3a* mRNA has been detected in mouse somatostatin interneurons at high levels, in excitatory pyramidal neurons of primary cortices, hippocampus, basolateral amygdala and prefrontal cortex and retinal ganglion cells among others (Pachernegg et al., 2012; Pfeffer et al., 2013; Murillo et al 2021). It is however unclear which complexes are functionally assembled, and which roles they fulfill in specific cellular populations beyond the synapse refinement hypothesis. Recent studies using RNA-seq or other approaches indicate that GluN3A is expressed in other cell types such as enteric neurons in the gut (Osorio et al., 2023) and in non-neuronal cells, most prominently oligodendroglia (see 4.3.3 and this study).

4.3.3 GluN3A in the oligodendroglial lineage

As mentioned above, Karadottir and colleagues (2005) were able to record small NMDA-evoked currents in both OPCs and mOLs. Changing from Mg^{2+} -free to 2mM Mg^{2+} superfusion solution decreased NMDA-current by 3 to 5-fold (**Figure 12A and 12C**). The 3 to 5-fold reduction was much lesser than the measured in neurons, or in studies of recombinant GluN1/2 NMDARs expressed in HEK293 cells or oocytes (60-fold for receptors containing GluN1 and GluN2A or 2B subunits; 20-fold for receptors comprising GluN1 and GluN2C or 2D), but comparable to recombinant receptors comprising GluN1, GluN2A or 2C and GluN3A subunits (**Figure 12B**, Karadottir et al., 2005; Burzomato et al., 2010). The weak Mg^{2+} -block, together with antibody labeling (**Figure 12D**) and co-immunoprecipitation (IP) data (**Figure 12E**) suggested that the NMDARs in OLs are composed of GluN1, GluN2C and GluN3 subunits (Káradóttir et al., 2005; Saltern and Fern, 2005; Burzomato et al., 2010).

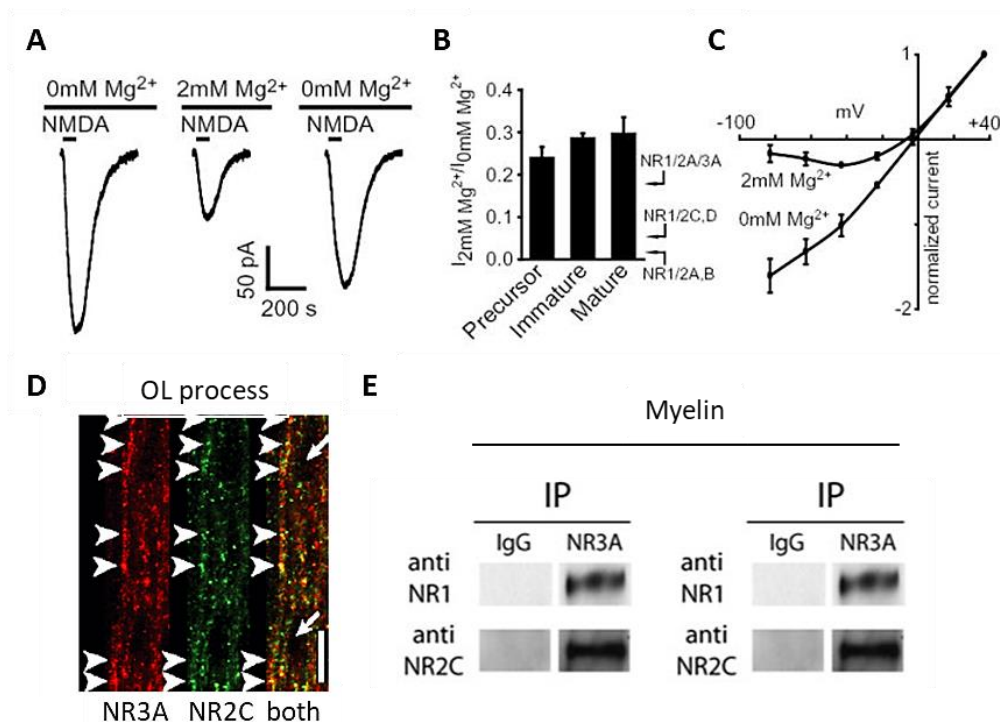


Figure 12. NMDA evoked currents in oligodendroglia exhibit GluN3A-NMDAR-like properties. (A) NMDA response in 0mM, 2mM and 0mM Mg^{2+} conditions. (B) Fraction of NMDA-evoked current remaining in 2mM Mg^{2+} , in 4 OPCs, 6 immature and 9 mature cerebellar OLs. Arrows: values from Kuner and Schoepfer, 1996 for NR1/2A,B or NR1/2C,D, and Sasaki et al., 2002 for NR1/2A/3A receptors. (C) Normalized I-V relationship for NMDA-evoked current in 0mM (2 precursors) and 2mM Mg^{2+} (3 different precursors). (D) Colocalization (yellow) of NR3 (red) and NR2C subunit (green) labeling in cerebellar OL processes. (E) Western blot showing IP of myelin preparation using antibody to NR2C probed with antibodies to NR3A and NR1 (left) or antibody to NR3A probed with antibodies to NR1 and NR2C (right). Adapted from Káradóttir et al., 2005; Saltern and Fern, 2005; Burzomato et al., 2010.

The findings were received with controversy in the community. Years later, mouse DNA-microarray, bulk and scRNA-seq analysis provided independent evidence for the presence of *Grin3a* mRNA, albeit restricted to OPCs rather than in both OPCs and OLs as previously reported (Cahoy et al., 2008; Zhang et al., 2014; Marques et al., 2016, 2018; Spitzer et al., 2019; Neumann et al., 2019; Falcao et al., 2018;) (see **Results**). To date transcriptomic analysis of human tissue has been able to detect *Grin3a* expression only in inhibitory interneurons and some excitatory neurons, but not in oligodendroglia lineage cells (La Manno et al., 2016; Jäkel et al., 2019). This might be related to the comparatively smaller size of these cells compared to neurons and lower gene expression levels that pose sensitivity challenges for human RNA-seq experiments and analysis. Nevertheless, immunoblotting and immunostaining have detected GluN3A expression in the WM of the developing and young adult human brain (Jantzie et al, 2015).

In a hallmark cell biology paper, Lundgaard and colleagues (2013) found that GluN3A in OPCs is regulated by activity, much like in neurons (**Figure 13**). In cocultures of rat DRG neurons and mouse OPCs, NRG1 and BDNF increased NMDAR currents in oligodendroglial cells by 6-fold. The effect was larger in OPCs when compared to differentiated OLs, likely because a dynamic switch in modes of OPC differentiation and myelination from an activity-independent to activity-dependent. Myelination was increased in presence of NRG1, but NMDAR block reduced myelination to far below its level without NRG1 (**Figure 13A and 13B**). The increase in NMDA responses reflected a change in subunit composition, with 40% down-regulation of GluN3A levels when NRG1 was added to OPC-neuron co-cultures (**Figure 13C**). NRG1 similarly down-regulated GluN3A by 33% in pure OPC cultures, but only when glutamate was added to mimic glutamate release from DRG axons (see **Figure 13D**).

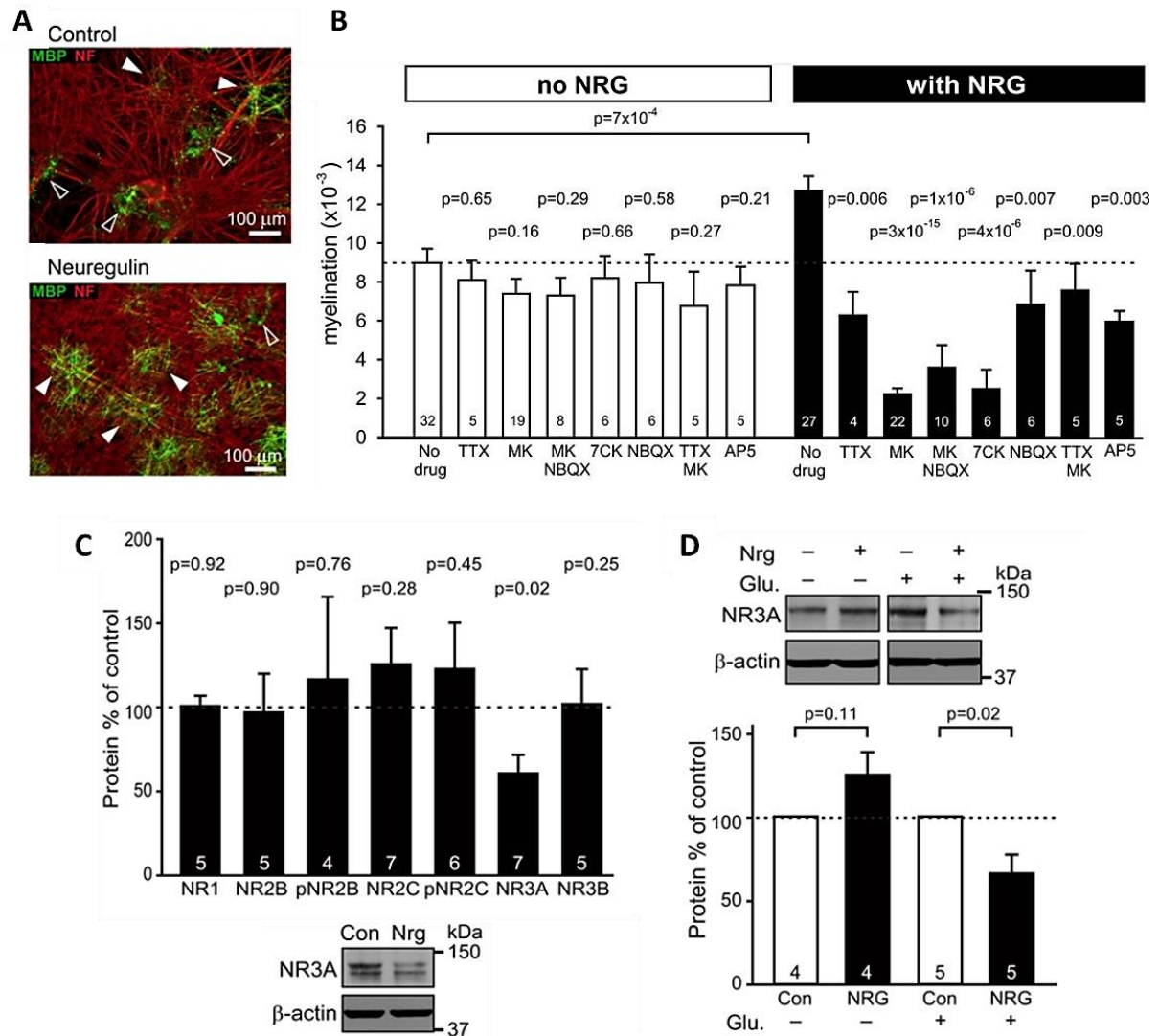


Figure 13. Activity-dependent GluN3A downregulation. (a) Western blots and densitometric quantification of NMDAR subunits detected in control and NRG-treated cocultures (NR1, NR2B and its phosphorylated form pNR2B, NR2C and its phosphorylated form pNR2C, NR3A and NR3B, while NR2A and NR2D levels were undetectable); β -actin acts as a loading control throughout. Only GluN3A was significantly downregulated upon activity stimulation. (c) Western blot for NR1 and NR3A of control (Con) and NRG-treated (for 6 d) pure OPC cultures, treated (+) or not treated (-) with 20 min glutamate (Glu, 100 μ M) stimulation every day, with densitometric quantification of subunit protein levels (normalized to β -actin and then to control). Adapted from Lundgaard et al., 2013.

4.4. Demyelination and remyelination in aging and disease

4.4.1 Demyelination and remyelination processes

Demyelination refers to the loss of myelin sheaths around nerves (**Figure 14A** and **14B**) and is a feature of many CNS disorders. Inflammation and direct targeting of myelin is the most common cause of myelin damage. Following demyelination, OPCs are activated and recruited to the damage area, where upon migration they proliferate and differentiate to form new myelin wraps around denuded axons (**Figure 14C**). This spontaneous regenerative response is called remyelination and while highly efficient in young people, is prone to failure especially in the context of aging or in the kind of persistent inflammatory environment that occurs in some disease states.

4.4.2 Multiple sclerosis (MS) and experimental animal models

MS is the most common primary demyelinating disease of the CNS. It affects 2.9 million people world-wide (National Multiple Sclerosis Society, updated Atlas of MS 2023) and is a main cause of disability among the adult and aged population. It is caused by an immune-mediated attack of the myelin sheath or the OLs that form it, which leads to inflammation, myelin loss and ultimately injury of the nerve fibers it surrounds. MS presents in various forms: with individual relapses (relapsing-remitting MS), or with gradual progression (progressive MS) and no periods of remission. Most patients present relapsing-remitting MS that with time and age converts into progressive MS in most cases, while around 10% of the patients present a progressive form of disease with no relapses from the onset, known as primary progressive MS (Coles and Compston, 2008). Significant progress has been made in developing immunomodulatory treatments that limit immune-mediated attacks and thus, control relapses, with very limited success in the progressive forms of the disease. This is, at least in part, because there are no therapies that promote remyelination or functional recovery and prevent axonal damage and accumulation of disability in progressive MS stages, when remyelination fails. Remyelination failure is thought to be a major contributor to disease progression, and thus developing strategies for regenerating myelin is now a top priority.

Unfortunately no specific mouse model recapitulates the diverse features of the disease, but multiple models covering specific pathophysiological aspects have been developed. These animal models (reviewed in Torre-Fuentes et al., 2020) may be classified into 3 categories:

- Immune-mediated and/or inflammatory models, such as EAE that is triggered by injection of myelin antigens like PLP, MOG and MBP together with complete Freud adjuvant.
- Genetic mutant models of myelin deficiency that specifically replicate the pathological loss of myelin, such as the shiverer mice (in which the gene coding for MBP is duplicated and inverted), rumpshaker mice (mutation in the gene coding for PLP), or jimpy mice (74 base deletion in the gene coding for PLP).
- Models of focal acute or chronic demyelination, including models of chemical lesions induced with cuprizone (CPZ) or lysolecithin (Lysophosphatidylcholine, LPC), which are crucial to better understand the remyelination process. CPZ is a chelating agent that is widely used due to its ability to induce demyelination of specific CNS regions like corpus callosum and hippocampus upon systemic administration (Praet et al., 2014; Vega-Riquer et al., 2019), with limited blood brain barrier disturbance and infiltration of peripheral immune cells. It causes acute demyelinating lesions that may become chronic if administration is prolonged. This model has the advantage that discontinuing administration triggers spontaneous remyelination, enabling the study of both processes. However, although CPZ-induced OL loss has been historically attributed solely to primary OL death, we now know that CNS inflammation with microglia and astrocyte activation either causes or aggravates demyelination (Zirngibl et al., 2022). On another side, direct injection of LPC into the WM causes focal demyelinating plaques, as the toxin damages the myelin sheath and triggers an inflammatory response. As with other toxin-induced models of demyelination, the myelin damage stage is quickly followed by remyelination, although the speed and degree of remyelination are age-dependent (Gingele et al., 2020).

4.4.3 Myelin loss in other neurodegenerative diseases

Apart from MS, OL dysfunction and WM loss has been observed in a variety of neurodegenerative diseases like Alzheimer's disease (AD, Mitew et al., 2010; Ihara et al., 2010), amyotrophic lateral sclerosis (ALS, Kang et al., 2013; Philips et al., 2013; Ferraiuolo et al., 2016), Parkinson's disease (PD, Dean et al., 2016; Bryois et al., 2020), early stages of Huntington's disease (Bourbon-Teles et al., 2019; Ferrari Bardile et al., 2019; Sun et al., 2022), schizophrenia and bipolar disorders (Bartzokis et al., 2012; Valdés-Tovar et al., 2022). It is also a feature of aging that is correlated with cognitive decline (Bartzokis et al., 2012; Li et al., 2023). Whether OL dysfunction is a consequence of chronic neuronal damage and inflammation or a primary feature present from early disease stages remains an open question. However, several studies support the latter hypothesis. For instance, AD mouse models exhibit alterations of myelin morphology and OL development before the formation of amyloid and tau deposits (Araque Caballero et al., 2018; Desai et al., 2009; Depp et al., 2023), and a disease-associated OL signature shared among multiple CNS pathologies has been described (Kenigsbuch et al., 2022). Besides, genetically or pharmacologically enhancing myelin renewal, by oligodendroglial deletion of the muscarinic M1 receptor or systemic administration of the pro-myelinating drug clemastine, improved the performance of a mouse model of AD in memory-related tasks and increased hippocampal sharp wave ripples (Chen et al., 2021).

4.4.4 Why does remyelination fail in MS? Intrinsic and extrinsic factors

Despite the unfavorable regenerative environment of the CNS, and in contrast to the limited capacity for neuronal/axonal regeneration, remyelination is highly efficient in relapsing-remitting MS, giving rise to so-called shadow plaques--sharply demarcated areas characterized by more sparsely myelinated axonal fibers with thinner myelin sheaths. Remyelinated axons are not only observed in established lesions but also in the earliest stages of acute demyelination. Remyelination varies between patients but seems to be more active at early stages of the disease and declines with age and disease progression (Prineas et al., 1993; Patrikios et al., 2006; Patani et al., 2007; Bramow et al., 2010). This failure becomes a major reason for the inexorable disease progression (Shields et al., 1999; Goldschmidt et al., 2009; Frischer et al., 2015). The major lesion type found at autopsy

are chronic demyelinated lesions (Frischer et al., 2015); however, it remains unknown why such lesions fail to regenerate. The presence of OPCs in chronic lesions (Wolswijk, 2002; Rodriguez et al., 2014; Boyd et al., 2013) has led to the notion that a differentiation block underlies the remyelination failure (Kuhlmann et al., 2008; Franklin and Ffrench-Constant, 2017). Hence identifying and targeting the mechanisms that promote (or interfere with) OPC differentiation and myelination of appropriate axons is critical to develop effective therapeutic interventions.

With **aging**, each step of remyelination becomes slower (Shields et al., 1999; study on rats). The last phase in which recruited progenitors differentiate is rate-limiting, since increasing OPC numbers after demyelination in aged animals does not increase the efficiency of remyelination (Woodruff et al., 2004). In fact, even in healthy brains aged OPCs fail to respond to pro-differentiation signals and acquire hallmarks of cell aging, including decreased metabolic functions and increased DNA damage (Neumann et al., 2019).

A number of recent studies have started to identify **intrinsic** or **extrinsic** factors within the **stem cell niche** and intense work is directed towards developing ways to modulate them and restore the lost myelination ability.

- ***Intrinsic factors:*** Young and aged OPCs are transcriptional different (Spitzer et al., 2019; Neumann et al., 2019). Aged OPCs have reduced expression of OPC-specific genes and increased expression of genes involved in mitochondrial dysfunction, unfolded protein response, autophagy, DNA damage, cellular senescence, inflammasome signaling and mTOR activity. Restoring normal mTOR signaling with **fasting** or treatment with **metformin** reverse these changes and **rejuvenate aged OPCs**, bringing back their regenerative capacity and improving remyelination in aged animals following focal demyelination with LPC (Neumann et al., 2019). Dysregulation of Gpr17 is another hallmark of aging OPCs (Rivera et al., 2021). Interestingly, Gpr17 is specifically expressed in a subset of OPCs responsible for rapid reactions to damage (Viganò et al., 2016). It has recently been shown that **transcriptional heterogeneity** also exists between oligodendroglial cells during MS and may contribute to disease progression (Jakel et al., 2019). OPCs become “stalled” and fail to differentiate into mOLs, contributing to

demyelination and axonal damage within lesions and leading to neurodegeneration (Chang et al., 2002; Boyd et al., 2013; Gruchot et al., 2019; Franklin, 2022). scRNA-seq studies have identified unique cell states among oligodendroglial cells in MS, including OPCs with some characteristics of immune cells (Jakel et al., 2019).

- **Extrinsic factors:** Remyelination is ultimately mediated by adult OPCs, but there are many cell types and local cues present within lesions that contribute to creating an inhibitory environment for remyelination. A pivotal study by Segel and colleagues (2020) showed that the **OPC microenvironment stiffens** with age and the phenomenon is sufficient to cause age-related OPC loss of function. In fact, isolated aged OPCs cultured on synthetic scaffolds that mimic the stiffness of young brains exhibited molecular and functional rejuvenation. Saraswat and colleagues (2021) identified sulfatase 2 (Sulf2), an **extracellular matrix** component, as a factor actively secreted by mouse and human OPCs during demyelination and enriched in MS lesions. Sulf2 potentiates the inhibitory microenvironment by promoting bone morphogenetic protein (BMP) and wingless (WNT) signaling in OPCs, impairing progenitor recruitment and subsequent generation of postmitotic OL, thereby limiting remyelination. Finally, **inflammation** represents a key factor in the suppression of OPC differentiation in aging and disease, as differential expression of surface receptors allows OPCs to have a very broad and diverse response to cytokine stimulation (Schmitz and Chew, 2008; Moore et al., 2015), making them primed to modulate immune functions and inducing cytotoxicity contributing to inflammation and neurodegeneration.

An under-explored way to facilitate remyelination is targeting activity-dependent myelin plasticity. Enhanced neuronal activity in the healthy brain can induce *de novo* myelination and behavioral changes (see 4.1.4). In mice, remyelination can be improved with **physical exercise** and **motor learning** (see 4.1.4.1 and 4.1.4.2). From a mechanistic point of view, Gautier and colleagues (2015) showed that neuronal activity regulates remyelination via glutamate-mediated signaling between axons and OPCs in mice. Additionally, Lundgaard and colleagues (2013) demonstrated

that remyelination after WM damage is NMDAR-dependent and, as in development (Mensch et al. 2015), remyelination targets small diameter axons which is known to depend on neuronal activity and glutamate. Larger caliber axons still become myelinated when vesicular release of neurotransmitters is blocked (Mensch et al. 2015) and are also remyelinated even when activity or synaptic signaling are blocked (Gautier et al. 2015). Both in mice and humans, neuronal activity can be modulated in invasive ways such as **deep brain stimulation** or non-invasive, such as **repetitive transcranial magnetic stimulation** or **transcranial ultrasound stimulation** and **aerobic exercise** (Darmiani et al., 2022), with reported benefits on promoting OL survival, remyelination (**Figure 14C**) and cognitive recovery in demyelinated brains (Cullen et al., 2019; Wang et al., 2021; Zhao et al., 2019; Yang et al., 2022, Feinstein et al., 2023). Preclinical studies in rats and MS patients (reviewed in Maas and Angulo, 2021) indicate that non-invasive stimulation of neuronal activity in demyelinated lesions indeed has the potential to improve remyelination and that the stimulation paradigm is an important determinant of success. Drug discovery studies have recently identified compounds that promote OPC differentiation and remyelination which modulate neurotransmitter signaling in OPCs such as the Food and Drug Administration Agency (FDA)-approved drugs like solifenacin and benztropine, which act as direct muscarinic receptor antagonists (Abiraman et al., 2015; Deshmukh et al., 2013; Mei et al., 2016), miconazole and clobetasol, which exert their effects through mitogen-activated protein kinase and glucocorticoid receptor signalling, respectively (Wang et al., 2011; Najm et al. 2015), and the anti-histaminic and anti-cholinergic compound clemastine (Chen et al., 2022; Du et al., 2022). These studies suggests that enhancing **activity-dependent myelination** can represent a novel alternative approach. Yet lack of information on molecular and cellular mechanisms whereby OPCs sense and integrate neural activity to execute myelin formation, has prevented the identification of therapeutic targets targeting myelin plasticity. In this context, GluN3A-NMDARs and their demonstrated role in maintaining plasticity in young brains (see 4.3.1) and their hypothesized role in activity-dependent OL responses (see **Results**) can represent a potential target for interventions.

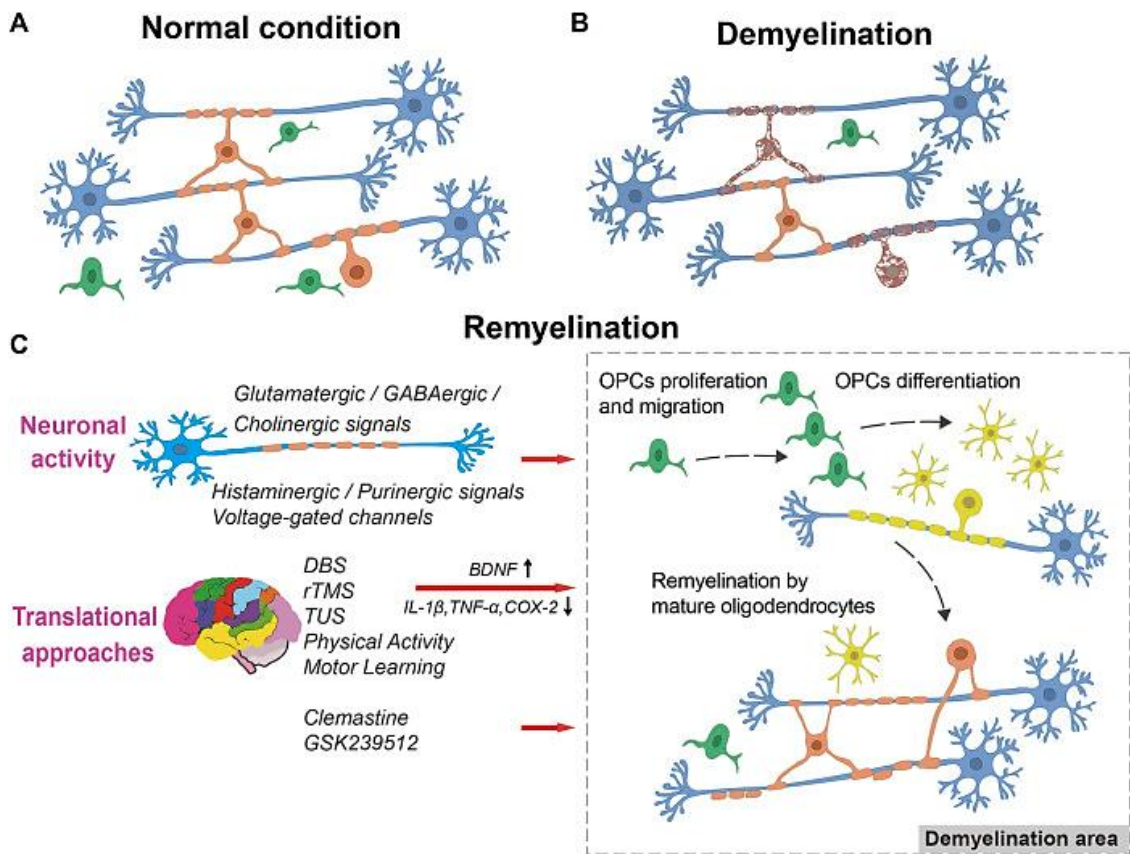


Figure 14. The process of remyelination. A cartoon illustrating myelination in normal condition (A), demyelination (B), and remyelination (C), showing OPC proliferation, migration into the lesion, differentiation into myelinating OLs and remyelination of naked axons that can also be promote by neuronal activity or stimulation by other translational approaches (from Zhou and Zhang, 2023).

A microscopic image of neurons. The cell bodies (soma) are stained blue, and the branching processes (dendrites and axons) are stained red. The background is black, making the stained structures stand out. The text '5. OBJECTIVES' is overlaid in the top right corner.

5. OBJECTIVES

Author: *Alice Staffa*

Classically seen as a stable insulator that forms at postnatal stages and is maintained through life, work in the last decade has revealed that myelination is enormously dynamic and responds to axonal activity and experience. The phenomenon, known as “myelin plasticity” or “activity-dependent myelination”, operates into adulthood to adapt neural circuits to changes in life experience (de Faria et al., 2021). This mechanism is driven by OPCs and relies on their unique properties. OPCs are widespread in the young and adult CNS, where they make 3-9% of the cell population (Dawson et al., 2003), and provide an unmatched progenitor niche. Their proliferation, differentiation into myelinating OLs, as well as appropriate myelin production and wrapping of unmyelinated axons or parts of axons, can be activated by neuronal signals (see **Introduction 4.1**) through synaptic-like contacts (Bergles and Jahr, 2000) or non-synaptic mechanisms. However, lack of information on the molecular and cellular mechanisms whereby OPCs sense and integrate neural activity to execute myelin formation, has prevented the identification of therapeutic targets.

The work presented in this thesis builds on the discovery that neuronal non-conventional NMDA receptors containing GluN3A subunits (GluN3A-NMDARs) are key modulators of synaptic plasticity. GluN3A-NMDARs are prevalent during critical periods of postnatal development, when they work as gate-keepers of synaptic modifications, preventing premature or inappropriate maturation and stabilization of synaptic circuits (Pérez-Otaño et al, 2016). While most studies to date have focused on the impact of neuronal GluN3A on coupling activity to the remodeling of excitatory synapses, growing electrophysiological and transcriptomic evidence demonstrate expression of GluN3A subunits in selected non-neuronal populations, most prominently OPCs (Karadottir et al., 2005; Salter and Fern, 2005; Burzomato et al., 2010; Zhang et al., 2014; Marques et al., 2016). The findings prompted our quest to investigate the roles of GluN3A within this non-electrically active cell type and the search for commonalities between neuronal and non-neuronal functions in setting plasticity states.

We hypothesized that GluN3A expression operates to control myelin plasticity, and mediates responses of OPCs to neuronal activity and experience to ensure the myelination of appropriate axons. To test this hypothesis, the objectives of the present study are:

Specific Aim 1: To confirm GluN3A expression in postnatal and young adult OPCs

Specific Aim 2: To evaluate the effects of GluN3A deletion on the proliferation and differentiation of OPCs, and the wrapping of axons by myelin sheaths during postnatal periods of developmental myelination

Specific Aim 3: To characterize GluN3A roles in activity-dependent OPC differentiation and myelination in juvenile and adult constitutive and OPC-specific knockout mice

Specific Aim 4: To provide insights into the molecular properties underlying GluN3A actions in OPCs

Specific Aim 5: To provide preliminary insights into the impact of GluN3A in remyelination

The background of the page is an abstract, textured composition. It features a dense network of fine, green, thread-like or fibrous structures that appear to be layered or woven. Interspersed among these green fibers are small, irregular, reddish-orange spots and patches. The overall color palette is dominated by a deep, dark blue or indigo, which serves as the base for the other colors. The texture is highly detailed and organic, resembling perhaps a microscopic view of a material or a complex, natural structure like a forest canopy or a neural network.

6. MATERIALS AND METHODS

Author: *Alice Staffa*

6.1. Experimental animals

Animals were maintained under standard ILAR type III and 3 R's-based housing and environmental conditions in the animal facility of the Institute of Neuroscience of Alicante (IN, CSIC-UMH). They were housed two to five per cage with *ad libitum* access to food and water, and maintained in an environment with HEPA (high-efficiency particulate) - filtered air with a rate of 16-20 changes per hour, 12 hours' dark/light cycle and regulated temperature of $22 \pm 2^\circ\text{C}$ and relative humidity of $55 \pm 10\%$. Colony founders were obtained from Charles River Europe or other laboratories and bred and raised at the IN animal facility. Mice of both sexes were used for the experiments unless indicated. All experimental procedures were conducted in accordance with the European and Spanish regulations (2010/63/UE; RD 53/2013) and were approved by the Ethical Committee of the Generalitat Valenciana and the animal welfare committee at the Universidad Miguel Hernández according to biosafety and bioethical guidelines and authorized by the Spanish government.

6.1.1 Mouse lines

Constitutive Grin3a knockout mice: B6;129X1-*Grin3a*^{tm1Nnk/J} (JAX:029974) mice (hereafter *Grin3a*^{-/-}), is an established mouse line in our laboratory derived from founders provided by Nobuki Nakanishi and Stuart Lipton (Sanford-Burnham Medical Research Institute, USA; Das et al, 1998). Founders were bred for >10 generations into a C57BL/6J background, and kept in homozygosis with periodic backcrossing into a C57BL/6J background. C57BL/6J mice JAXTM were used as wild-type controls.

Grin3a-floxed mice: *Grin3a*^{tm1a(EUCOMM)Hmgu} mice (hereafter *Grin3a*^{fl/fl}) were bred for >12 generations into a C57BL/6J background and kept in homozygosis with periodic backcrossing. The floxed line was generated by inserting the L1L2_Bact_P cassette at position 49793582 of chromosome 4 upstream the critical exons. This cassette is composed of a flipase recognition target (FRT) site followed by a lacZ sequence and a loxP site. This first loxP site is followed by a neomycin resistance gene under the control of the human beta-actin promoter, SV40 poly-A, a second FRT site and a second lox-P site. A third loxP site is inserted downstream of the targeted axon. The critical axon

is thus flanked by loxP sites that subsequent expression of the Cre recombinase (by crossing with Cre-driven mouse lines) leads to specific knockout.

Selective ablation of Grin3a from oligodendroglial cells: To knockout *Grin3a* specifically in oligodendrocyte lineage cells, *Grin3a^{fl/fl}* mice were crossed with a *Sox10*-Cre (line 22–7) (Matsuoka et al, 2005; Kougiumtzidou et al., 2017; provided by Dr. Richardson, UCL London; MGI:3586900) that express Cre under *Sox10* transcriptional control in a phage artificial chromosome (PAC). For experiments, female Cre carriers were crossed with *Grin3a^{fl/fl}* males yielding to *Sox10*-Cre^{-/-};*Grin3a^{fl/fl}* (used as a controls) and *Sox10*-Cre^{+/-};*Grin3a^{fl/fl}* mice. To knockout *Grin3a* only from differentiated OLs we also tested a mouse line expressing Cre recombinase under control of the endogenous Cnp regulatory sequences, *CNP*-Cre (Lappe-Siefke et al., 2003) mice. Finally, to conditionally knockout *Grin3a* specifically from OPCs, *Grin3a^{fl/fl}* were crossed with *PDGFRα*-CreER^{T2} mice (Rivers et al., 2008; provided by Dr. Richardson, University College London).

All the Cre-driver mouse lines were maintained as a heterozygous (He) breeding colony and backcrossed with C57BL/6J mice for >10 generations in our animal facility.

Reporter tdTomato-floxed mice: To test for Cre-driven recombination efficiency and specificity, a tdTomato^{fl/fl} mouse line, in which a targeted mutation of the Gt(ROSA)26Sor locus with a loxP-flanked STOP cassette prevents transcription of a CAG promoter-driven red fluorescent protein variant (tdTomato), was crossed with *Sox10*-Cre, *CNP*-Cre and *PDGFRα*-CreER^{T2} lines (see **Figure 15**). The recombined cells can be detected as Tomato⁺ and Cre⁺ (see **Results**). To induce recombination in *PDGFRα*-CreER^{T2} mice, tamoxifen (TMX; Sigma-Aldrich T5680) was injected into the stomach at P1-P2-P3 (1mg/ml), as previously described (Lizen et al., 2015), and mouse were perfused at P12.

We tested and characterized all the Cre-driver mouse lines but for the experiment described in this thesis only *Sox10*-Cre mice crossed with our *Grin3a^{fl/fl}* have been used.

mClover3-GluN3A knockin mice: a mouse line recently generated by Dr. O. Crawley in our laboratory by inserting the mClover3 fluorophore sequence before *Grin3a* exon1 in chromosome 4 using CRISPR technology. mClover3-GluN3A mice allow visualization of endogenous GluN3A

with a simple immunofluorescence staining upon mClover3 signal amplification with GFP antibody.

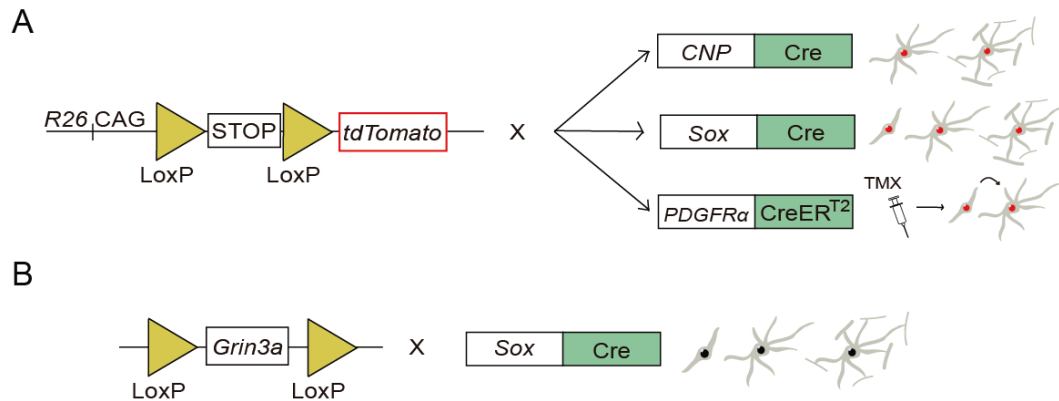


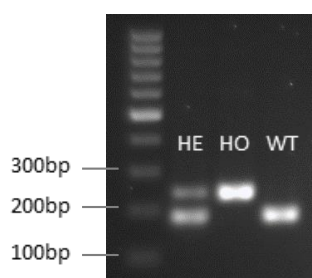
Figure 15. Breeding scheme for Cre-driver mouse line characterization and GluN3A knockout in oligodendroglial cell lineage. (A) A tdTomato^{fl/fl} mouse line, with a loxP-flanked STOP cassette prevents transcription of a R26-CAG promoter-driven red fluorescent protein variant (tdTomato), was crossed with *CNP*-Cre, *Sox10*-Cre, and *PDGFRα*-CreER^{T2} lines to specifically activate Cre and tdTomato expression in differentiated OLs, in all oligodendroglial cells including OPCs or (conditionally) in OPCs and their progeny, respectively. (B) *Sox10*-Cre mouse line was selected for the experiments presented in this thesis and crossed with *Grin3a*^{fl/fl} to remove GluN3A specifically from oligodendroglial cells.

6.1.2 Mouse genotyping

DNA for genotyping was extracted from ear or tail snips. DNA (100 ng/μl) was amplified using the polymerase chain reaction (PCR) on a thermocycler (Bio-Rad, CA, USA) following this protocol: 3 min, 95°C for the initial denaturation; 32 or 35 cycles of 15 s, 94°C for the denaturation, 20 s, 60°C for the annealing; 30 s, 72°C for the elongation; 10 min, 72°C for the final extension.

The following primers were used:

Constitutive Grin3a^{-/-}:



Wt allele:

MAT 21mod: 5' GGTCCACCCGGCTCCCGCAAG 3'

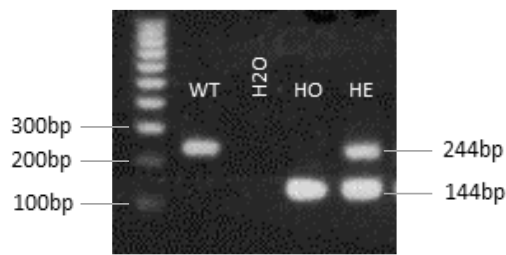
MAT 2 AN4blast: 5' AAAGGCATAAGTGGCAGGTC 3'

Ko allele:

MAT 23: 5' GCCTGAAGGAACGAGATCAGC 3'

MAT 2 AN4blast: 5' AAAGGCATAAGTGGCAGGTC 3'

Grin3a-floxed:



Forward common:

5arm-WTF: 5'GCAAGAGCTCAAAATCAAACA3'

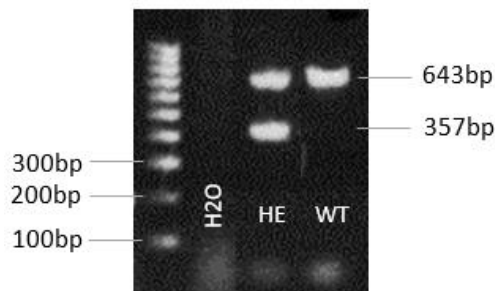
Reverse Wt:

Crit-WTR: 5'CATTTCACCTCAGGAGAATAATTGG3'

Reverse Mutant:

5mut-R1: 5'GAACTTCGGAATAGGAACTTCG3'

CNP-Cre:



Wt forward:

CNP-E3s 5'GCCTTCAAACGTCCATCTC3'

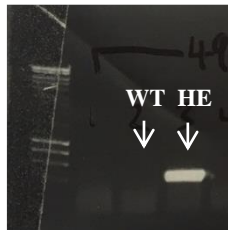
Wt reverse:

CNP-E3a 5'CCCAGCCCTTTTATTACCAC3'

Mutant forward:

Puro3 5'CATAGCCTGAAGAACGAGA3'

Sox10-Cre and PDGFRa-CreER^{T2}:



Cre1: 5' - TCGATGCAACGAGTGATGAG - Forward

Cre2: 3' - TTCGGCTATACGTAACAGGG - Reverse

A sample is He when a band of 480 base pair is amplified.

A sample is Wt when no band is amplified.

6.2. Transcriptomic analysis

In silico analysis of *Grin3a* expression was performed in collaboration with Dr. Parras (Paris Brain Institute, ICM) using scRNA-seq data from Marques et al., 2016, 2018, following the method used in Merour et al., 2022. Briefly, counts per gene were downloaded from GEO datasets GSE75330 and GSE95194, and processed in R (4.0) using the following packages: Seurat (3.0) for data processing, sctransform for normalization, and ggplot2 for graphical plots. Seurat objects were first generated for each dataset independently using CreateSeuratObject function (min.cells = 5, min.features = 100). Cell neighbors and clusters were found using FindNeighbors (dims =

1:30) and FindClusters (resolution = 0.4) functions. Clusters were manually annotated based on the top 50 markers obtained by the FindAllMarkers, adopting mainly the nomenclature from Marques et al., 2016. Using the subset function, we selected only the clusters containing neural progenitors and oligodendroglia cells. Using the merge function, we combined both oligodendroglial datasets into a single Seurat object (OLgliaDevP) containing 5516 cells. The new object was subjected to NormalizeData, FindVariableFeatures, ScaleData, RunPCA, and RunUMAP functions with default parameters. Different OPC clusters were fused into a single one keeping apart the cycling OPC cluster. For DimPlots and Dotplots, clusters were ordered by stages of oligodendrogenesis from neural stem cells to myelinating OLs.

Bulk whole-genome transcriptional profiling messenger RNA - strand specific (mRNA-seq) was performed in tissue samples from the somatosensory cortex of P11 and P18 Wt and *Grin3a*^{-/-} mice. Briefly, mice were sacrificed by decapitation, the skin and the cranium were removed, and somatosensory cortices were dissected out. The tissues were weighed and homogenized in QIAzol using a tissue disruptor and RNA isolated using the RNeasy® mini kit (QIAGEN® 74104) following the manufacturer's protocol. RNA concentration and purity were assessed with Nanodrop™. RNA quality was determined by the RNA Integrity Number (RIN) algorithm using the Agilent® 2100 Bioanalyzer. Each sample has a score from 1 to 10, being 10 the least degraded; only samples with RIN > 9 has been considered for the experiments. Whole-genome mRNA-seq was performed using the RNAseq Illumina HiSeq2500. The preparation of the polyA sequencing library, library's quality control and quantification, sequencing run and base calling data were carried out by the Genomics Core Facility of the Centre for Genomic Regulation (CRG, Barcelona). The analysis was performed in collaboration with Dr. J. P. Lopez-Atalaya at the IN. Briefly, quality of raw data was evaluated with FastQC (Andrews, 2010), and mapping was done using HISAT2 (Kim et al., 2019) onto mm10 reference genome. Differential expression analysis were conducted using DESeq2 (Love et al., 2014), and enrichment analysis using ShinyGO (Ge et al., 2020). Genes were considered significantly differentially regulated when log2FC > 0.35 and adjusted p-value < 0.05.

Bulk mRNA-seq was also performed on purified OPCs to specifically assess intrinsic transcriptional changes in absence of GluN3A. OPCs were isolated from P7 Wt and *Grin3a*^{-/-} mice based on PDGFRα expression. Briefly, forebrain was dissected and dissociated using the Neuronal

Tissue Dissociation Kit (Miltenyi, 130-092-628) followed by filtration through a 70 μm cell strainer (Smartstainer; Miltenyi Biotec, 130-098-462). The cell suspension was centrifuged at 300xg for 10 minutes and the supernatant completely aspirated. The pellet was resuspended and incubated with MicroBeads conjugated to monoclonal CD140a (PDGFR α) antibody (Miltenyi kit, 130-101-502), following the manufacturer's instructions provided in the kit. Unbound bead-coupled antibodies were washed away by centrifugation, leaving bound cells which were loaded into LS columns containing ferromagnetic spheres and sorted using a magneticQuadroMACS™ Separator (Miltenyi Biotec; 130-098-637) and a MACS MultiStand (Miltenyi Biotec; 130-042-303). RNA was then extracted using NucleoSpin® RNA (Mini) (Macherey-Nagel; 677497) according to instructions of the provider. The RNA-seq libraries were prepared using the NEBNext Ultra II Directional RNA Library Prep Kit (NEB) and sequenced with the Novaseq 6000 Illumina platform. Quality of raw data was evaluated with FastQC and mapping was done using Illumina DRAGEN bio-IT Platform (v3.6.3) onto mm10 reference genome. Following analysis were conducted using EdgeR. Genes were presented as counts per million (cpm) and considered regulated when $\log_2\text{FC} > 0.26$ and $p\text{-value} < 0.05$.

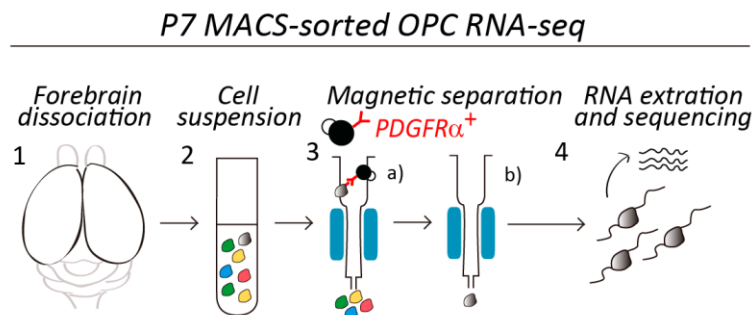


Figure 16. Magnetic cell sorting followed by RNA extraction and sequencing. P7 mouse forebrains were dissected and dissociated (1) obtaining a cell suspension (2). The cells were then incubated with magnetic beads coated with a PDGFR α -antibody and loaded into a column containing ferromagnetic spheres that will bind the magnetic beads (PDGFR α^+ cells) and flow through the unlabeled cells (3a). The labeled cells were finally eluted (3a) and their RNA extracted for sequencing (4).

6.3. Histological analysis

For in situ hybridization and immunohistochemistry, mice were perfused transcardially with 4% paraformaldehyde (PFA) in phosphate-buffered saline (PBS, 1X) using a peristaltic pump, and their brains were removed and post-fixed in the same fixative overnight.

6.3.1 Fluorescent In-Situ Hybridization (FISH)

P8 brains were embedded in 4% agarose, sectioned coronally in 80 µm-thick slices with a vibrating microtome and stored in PBS at 4°C. Free-floating sections were permeabilized with detergent mix (1% NP-40, 1% SDS, 0.5% sodium deoxycholate, 50 mM Tris pH 8.0, 1 mM EDTA, and 150 mM NaCl) for 1 h at room temperature, and incubated with *Grin3a* digoxigenin-labeled riboprobes (Murillo et al., 2021) at 63°C in hybridization buffer (50% formamide; 2x saline-sodium citrate pH 5.3; 50 µg/mL heparin; 50 µg/mL tRNA; 50 µg/mL salmon sperm DNA; 0.1% Tween-20) overnight. Hybridized probes were detected using an peroxidase-conjugated antidigoxigenin antibody (Roche 11 207 733 910) in blocking solution (2% Roche blocking reagent and 20% sheep serum in MABT buffer) overnight at 4°C. A TSA plus fluorescence kit was used for signal amplification and detection according to the manufacturer protocol (Thermo Fisher, NEL744001KT). To avoid nonspecific signal, endogenous peroxidases were inactivated by incubation with MABT buffer (500 mM maleic acid, 750 mM NaCl, 0.95 M NaOH, and 0.1% Tween-20, pH 7.5) - 1% H₂O₂ for 1 h in the dark. Sense probes used as control yielded no signal.

After the FISH procedure, free-floating brain sections were incubated with primary antibody in 1% Bovine Albumin Serum (BSA), 0.1% Triton X-100, and 1% normal serum in PBS overnight at 4°C. The following primary antibodies were used: rabbit anti-PDGFR α (Synaptic systems 132 002, 1:500) and mouse anti-Olig2 (Sigma, MABN50, 1:500). After washing with PBS, sections were incubated with fluorophore-conjugated secondary antibody in 1% BSA, 0.1% Triton X-100 in PBS for 1 h at room temperature. The following secondary antibodies were used: anti-rabbit-Cy3 (Jackson ImmunoResearch 111 165 003, 1:500) and anti-mouse-Alexa647 (Invitrogen A32728, 1:500). After several washes in PBS, sections were counterstained with 4',6-diamidino-2-phenylindole (DAPI), mounted onto Superfrost Plus slides, air-dried, and coverslipped with fluorescence mounting medium (DAKO).

6.3.2 Immunofluorescence (IF)

Brains were cryoprotected with 30% sucrose, stored in cryoprotectant solution at -20° C and coronally cut into 30-40 µm thick slices, with an automated cryotome (Leica). Free-floating sections were permeabilized for 2 hours in blocking solution (PBS 0.3% Triton-X 100 + 4%

Normal Goat Serum + 1% BSA) and incubated overnight at 4° C with primary antibodies (Table 2) diluted in the same solution. Slices were then incubated for 2 hours in the dark with fluorescence-conjugated secondary antibodies (Table 3) diluted in PBS 0.1% Triton-X + 1% BSA followed by DAPI for 10 min (3 washes of 10 minutes between steps). To unmask Opalin signal and enhance the ability of the primary antibody to bind the epitope in the fixed tissue, an antigen retrieval treatment was applied before IF. Briefly, slices were incubated in Buffer Citrate (10mM Citric Acid, 0.05% Tween 20, pH 6.0) pre-heated at 95° C for 10 min.

Antigen	Host	Supplier	Catalog number	Working concentration
Olig2	Mouse	Millipore Sigma	MABN50	1:500
Olig2	Rabbit	Millipore Sigma	AB9610	1:500
PDGFR α	Rabbit	Cell Signaling Technology	3164S	1:500
CC1 (APC)	Mouse	Calbiochem	OP80	1:500
MBP	Rat	Bio-Rad	MCA409S	1:500
Opalin	Mouse	Santa Cruz Biotechnology	Sc-374490	1:500
Bcas1	Rabbit	Synaptic Systems	445 003	1:1000
Olig1	Mouse	Neuromab	75-180	1:500
Caspr	Rabbit	Gift of J. A. Girault	-	1:500
C-Fos	Rabbit	Synaptic Systems	226 008	1:700
m-Cherry (RFP)	Rat	ChromoTek	5f8-100	1:500
m-Cherry (RFP)	Guinea Pig	Synaptic Systems	390 004	1:500
BrdU	Rat	Abcam	Ab6326	1:1000
Cre	Rabbit	Synaptic Systems	257 003	1:500
Iba1	Rabbit	Wako	019-19741	1:500
GFP	Chicken	Aves Labs	1020	1:1000

Table 2. Primary antibodies used for IF.

Antibody	Host	Supplier	Catalog number	Working conc.
Cy3 Affinity Pure anti-Mouse IgG (H+L)	Goat	Jackson ImmunoResearch	115-165-003	1:500
Cy3 Affinity Pure anti-Rabbit IgG (H+L)	Goat	Jackson ImmunoResearch	111-165-003	1:500
Cy3 Affinity Pure anti-Guinea Pig IgG (H+L)	Goat	Jackson ImmunoResearch	106-166-003	1:500
Cy5 Affinity Pure anti-Mouse IgG (H+L)	Goat	Jackson ImmunoResearch	115-175-166	1:500
Cy5 Affinity Pure anti-Rabbit IgG (H+L)	Goat	Jackson ImmunoResearch	111-175-144	1:500
Alexa Fluor 488 anti-Mouse IgG (H+L)	Goat	Invitrogen	A11029	1:500
Alexa Fluor 488 anti-Rabbit IgG (H+L)	Goat	Invitrogen	A11008	1:500
Alexa Fluor 568 anti-Rat IgG (H+L)	Goat	Invitrogen	A11077	1:500
Alexa Fluor 555 anti-Rat IgG (H+L)	Goat	Invitrogen	A21434	1:500
Alexa Fluor 594 anti-Mouse IgG2a	Goat	Invitrogen	A21135	1:500
Alexa Fluor 488 anti-Mouse IgG2b	Goat	Invitrogen	A21141	1:500
Alexa Fluor 647 anti-Mouse IgG1	Goat	Invitrogen	A21240	1:500

Table 3. Secondary antibodies used for IF. IgG: immunoglobulin G; H+L: heavy and light chain.

6.4. Electron microscopy (EM)

EM was performed in collaboration with Dr. C. Matute (Achucarro Basque Center for Neuroscience, Spain) to analyse myelin ultrastructure in P11-P18 wild-type and GluN3A knockout mice; and for immunogold or immunoperoxidase analysis of GluN3A expression. Mice were transcardially perfused with saline solution (0.9% NaCl; pH 7.4) followed by a fixative solution containing 4% paraformaldehyde (PFA) and 2.5% glutaraldehyde in 0.1 M phosphate buffer (PB; pH 7.4) or 4% PFA, 0.1% glutaraldehyde and 0.3% picric acid in 0.1 M PB (pH 7.4),

respectively. Brains were removed, postfixed overnight at 4°C and stored in 1% PFA in PB at 4°C or in PBS-Azide 0.02% at 4°C., respectively. Then, 50-micrometer thick coronal sections were cut using vibratome.

Pre-embedding immunogold: Slices were treated with 1% hydrogen peroxide (H₂O₂), followed by blocking in a solution containing 10% BSA, 0.1% sodium azide, and 0.02% saponin. The slices were then incubated with a primary anti-GluN3A antibody (Rabbit, 1:100; 07-356, Millipore Sigma) for 2 days at 4°C. After washing, sections were treated with goat anti-rabbit IgG conjugated to 10 nm colloidal gold particles (Nanoprobes). Slices were then treated with silver-intensified with a HQ Silver kit (Nanoprobes) in the dark for 12 min. The specificity of the anti-GluN3A antibody was previously assessed by the absence of signal in samples from GluN3A knockout mice.

Immunoperoxidase: Slices were treated with 1% hydrogen peroxide (H₂O₂), followed by blocking in a solution containing 10% BSA, 0.1% sodium azide, and 0.02% saponin. The slices were then incubated with a primary anti-GluN3A antibody (Rabbit, 1:100; 07-356, Millipore Sigma) for 2 days at 4°C. After washing, sections were treated with goat anti-rabbit IgG conjugated and the immunoperoxidase was developed using 3'-diaminobenzidine (DAB) as a chromogen (Roche Diagnostics).

Sections were osmicated 30 minutes, dehydrated, and embedded in epoxy resin (Sigma-Aldrich). Ultrathin sections (50–60 nm) were cut for electron microscopy, stained with 4% uranyl acetate for 30 min and 10 min with 2.5% lead citrate for visualization with a Jeol JEM 1400 Plus electron microscope at the Service of Analytical and High-Resolution Microscopy in Biomedicine of University of the Basque Country.

Analysis of myelin ultrastructure: The g-ratio of myelinated axons was calculated as the ratio of the inner to the outer radius of the myelin sheath using ×8,000 magnification images from at least 100–150 axons from 60 images per animal. The number of myelinated axons was quantified using ×1,000 magnification images.

6.5. Western blotting

Mice were sacrificed by decapitation, then the skin and the skull were removed and forebrains were dissected. Dissected tissue was immediately snap-frozen by immersion in liquid nitrogen and stored at -80°C until protein isolation. Tissues were homogenized in 10-15 (w/v) of modified ice-cold RIPA buffer (50 mM Tris-HCl pH 7.5, 150 mM NaCl, 1% NP40, 0.5% Deoxycholate, 0.1% SDS, 0.1 mM PMSF) supplemented with protease and phosphatase inhibitors, using 12 strokes of a motor-driven glass-teflon homogenizer (Heidolph RZR-1, 600-800 rpm). The mechanical lysis was performed by 2 round of sonication with 20 pulses in a Branson tip-sonicator (duty cycle 20, 15% amplitude), interleaved with a nutation stage at 4°C for 15 minutes. The suspension was centrifuged for 20 minutes at 16200 x g at 4°C and protein content was estimated using a Pierce BCA Assay kit (ThermoFisher). Then, proteins were resolved using SDS-PAGE electrophoresis and gels transferred onto 0.45 µm PDVF membranes (GE Healthcare®, 10600023) in Transfer Buffer (10 mM glycine, 10 mM Tris-HCl, 5% methanol) in a Criterion Blotter set at constant 300 mA for 2 hours at 4°C. After staining with 0.1% (w/v) Ponceau S solution (Sigma-Aldrich P3509) in 5% acetic acid for 10 minutes, membranes were blocked for 1 hour at room temperature with 5% BSA or dry milk (for MBP) in Tris-buffer saline (TBS) - Tween 0.05% and then incubated overnight at 4°C with the following primary antibodies: MBP BioRad MCA409S; CNP Sigma-Aldrich C5922; MOG Millipore Sigma MAB5680; OSP Abcam ab53041 (1:500, 1% BSA or dry milk). The following day, the blot was washed and incubated with horseradish secondary antibodies in (1:10000, 2% BSA or dry milk) for 1 hour at room temperature. Finally, proteins were visualized using an enhanced chemiluminescence (ECL) western blotting detection reagent (GE Healthcare® RPN2209) and scanned with a high-sensitive digital blot chemiluminescence imager (Amersham™ Imager 680). Individual bands were quantified after background subtraction using Image Studio™ Lite (LI_COR Biosciences) software.

6.6. Paradigms for stimulation of activity-dependent plasticity

6.6.1 Chemogenetic stimulation of neuronal activity *in vivo* (DREADDs)

We utilized the DREADD (designer receptor exclusively activated by designer drug) system to modulate neuronal activity in callosal axons. Expression of the activating DREADD hM3Dg (Gq) causes depolarization of neurons in response to the synthetic ligand clozapine-N-oxide (CNO) engaging the Gq signaling pathway that induce intracellular calcium release (Alexander et al., 2009). For chemogenetic stimulation, we unilaterally electroporated 1 µg/µl of plasmids expressing hM3Dg fused to mCherry (pCAGS1-hM3Dg-mCherry; 7300 base pair), or mCherry alone (pCAGS-mCherry; 5449 base pair) as control (kindly provided by Professors Akihiro Yamanaka, Nagoya University and Kazunori Nakajima, Keio University School of Medicine, Tokyo), into the right cortical neuroepithelium in utero at embryonic day (E) 15.5. Briefly, pregnant females were deeply anaesthetized with isoflurane to perform laparotomies. The embryos were exposed and the plasmids were injected into the right cortical neuroepithelium at the level of somatosensory cortex with a capillary. For electroporation, the negative and positive palettes were placed near the head of the embryo, and 5 square electric pulses of 45 V and 50 ms were delivered through the uterus at 950 ms intervals using a square pulse electroporator (CUIY21 Edit: NepaGene Co., Japan). The surgical incision was then closed and embryos were allowed to develop until postnatal stages. CNO was daily intraperitoneally (i.p.) administered (1mg/kg, Tocris 4936) at different postnatal stages as indicated.

6.6.2 Chronic physical exercise (Treadmill)

The treadmill exercise protocol was adapted from the described in Chen et al., 2018; 2019 and Adamovich et al, 2021. Mice were trained in a five-channel treadmill apparatus (Panlab, LE8710MTS) (Figure 17) at a speed of 9-12 m/min for one hour daily. Control mice, or non-runners, were placed on the stationary treadmill device for 15 minutes in the same environmental conditions. To ensure compliance and encourage continued movement on the treadmill, a grid was positioned at the end of the apparatus. A minimal shock intensity of 0.4 mA was applied to the mice upon reaching the grid, which prompted them to re-enter the treadmill belt. The exercise

routine involved a 2-day habituation period, with mice exposed to the treadmill for 15 minutes each day, followed by 5 days of exercise per week for 3 consecutive weeks. Weekends were designated as rest days.

During the initial habituation phase, mice were allowed to freely explore the treadmill for a duration of 1-3 minutes and/or received at least one shock from the grid. The treadmill was then activated, and the speed was gradually increased up to 3.0 m/min. Careful monitoring ensured that all mice initiated walking for few minutes, and the velocity was slowly and constantly increased until reaching the designated speed of 9-12 m/min to be maintained throughout the exercise period. Similar precautions were taken at the conclusion of each training session, gradually reducing the speed to zero, which ensured a smooth transition to prevent abrupt stops and potential distress. To assess fatigue levels and exclude mice exhibiting signs of exhaustion, a specific criterion was applied: mice spending more than 5 accumulative seconds in contact with the grid within a 30-minute window during the 1-hour run were excluded from the analysis.



Figure 17. Treadmill apparatus for mouse running. Five-line treadmill device was used to train the mice daily for 3 weeks. Mice run at a speed of 9-12 m/min and received a mild shock (0.4 mA) when arriving at the end of the belt to motivate to keep running.

6.6.3 Motor learning (Erasmus Ladder)

Briefly, the main component of the Erasmus Ladder (Noldus, Wageningen, Netherlands) consists of a horizontal ladder with alternate high (H) and low (L) rungs equipped with touch-sensitive sensors that detect the position of the mouse on the ladder, flanked by two goal boxes. The ladder is made of 2 x 37 rungs (L, 6 mm; H, 12 mm) spaced 15 mm apart from each other and positioned in a left-right alternating pattern with 30 mm gaps. Rungs can be moved individually to generate various levels of difficulty, that is, creating an obstacle (raising the high rungs by 18 mm) (Figure

18). A trial is defined as one run on the ladder between the starting and ending goal boxes. At the beginning of the session, a mouse is placed in one of the starting boxes; after a set time of 15 ± 5 s ("resting" state), motivational cues are applied: a light cue (max. 3 s) followed by an air cue (max. 45 s) that generate a constant tailwind until the mouse completely crosses the ladder, to increase consistency and skip the need for experimenter intervention which is a major source of variability. A headwind from the opposite direction is applied when a mouse attempts to leave the goal box before the scheduled resting time making the mouse return to the original goal box. Coupled with an automated recording system (Erasmus Ladder software designed by Erasmus MC, Rotterdam, The Netherlands) and associating modifications of the rung pattern with sensory stimuli, the Erasmus ladder tests for fine motor learning and adaptation of motor performance in response to environmental challenges (appearance of a higher rung to simulate an obstacle, an unconditioned stimulus [US]) or association with sensory stimuli (a tone, a conditioned stimulus [CS]). Testing involves two distinct phases, each assessing improvement in motor performance over 4 days, during which mice undergo a session of 42 consecutive trials per day (Cupido, 2009). In the initial phase, mice are trained to navigate the ladder to assess "fine" or "skilled" motor learning. The second phase consists of interleaved trials where an obstacle in the form of a higher rung is presented in the path of the moving animal. The perturbation can be unexpected to assess "challenged" motor learning (US-only trials) or announced by an auditory tone to assess "associative" motor learning (Paired trials) (see **Results**).

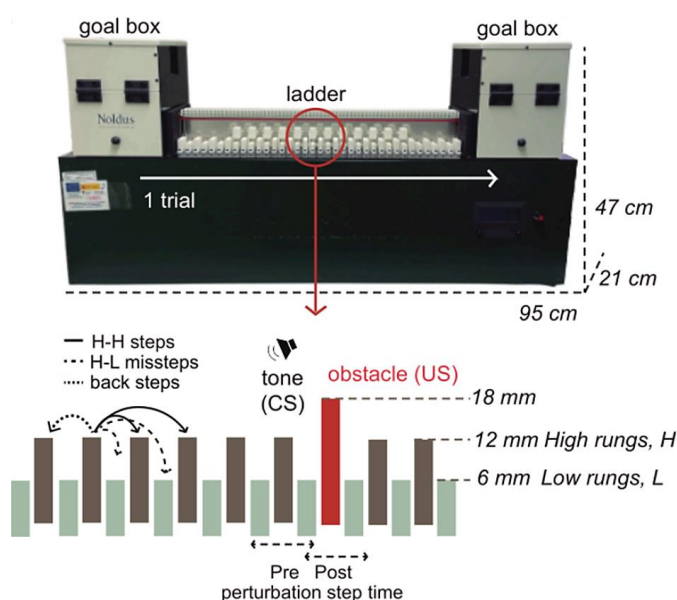


Figure 18. Erasmus Ladder device to automatically monitor mouse motor skill learning and associative learning. The Erasmus Ladder consists of a ladder with high (H) and low (L) rungs flanked by 2 goal boxes. One trial is defined by one run on the ladder from starting and ending goal box. An higher rung can be introduce as an obstacle (US) that can be anticipated or not by an auditory tone (CS). The different stepping pattern (H-H normal steps, H-L missteps aor backsteps), response to cues, trial duration and step times (including pre and post perturbation) are automatically recorded.

6.7. Cell proliferation assay

To label proliferating cells and fate map newly-formed OLs, control and trained mice received single i.p. injections of BrdU (Sigma, B5002) at 50 mg/kg body weight (10 mg/mL stock, dissolved in 0.9% saline) during the last 4-5 days of the protocols (Treadmill and Erasmus Ladder, respectively). 3-4 days later animals were perfused and stained as follow. For BrdU detection, on the second day of IF, slices were fixed for 50 min with 4% PFA in PBS at room temperature, hydrolyzed with 2N HCl for 30 min at 37° C and neutralized with Borate Buffer (0.1M pH 8.6) 10 min for 3 times, followed by a second incubation with blocking solution for 2 hours and rat anti-BrdU primary antibody (Abcam, 1:1000). On the third day, slices were incubated with the goat anti-rat Alexa 555 (Invitrogen; 1:500) and mounted.

6.8. Lysolecithin-induced focal demyelination

To induce demyelination, young adult (2-3 months) mice were anesthetized with a single intraperitoneal injection of Ketamine (50mg/kg) and Xylazine (10 mg/kg) and analgesized with a subcutaneous injection of Buprenorfin (0,1 mg/kg) before starting the surgery, to prevent post-surgery pain. Next, we gently removed the hairs of the top of the skull with razor blade, applied Ocry-gel on the mouse's eyes and cut the skin through the medial line within the shaved area. Once the animal was well positioned under the stereotaxic device (putting Xylocaine on the end of the earbars before insert them into the ear holes to immobilize the head), Bregma (Br.) coordinates were set up at -1 mm lateral, +1.3 mm anterior, -1.7 mm deep to inject in the anterior corpus callosum (based on C57BL6 mouse brain). Lysolecithin (LPC 1%) was charged with a Hamilton syringe connected to a thin plastic tube to a capillary made of glass pulled. Positioning the capillary on top of the determined injection site, we marked the position on the skull with a needle and drilled the skull to create a hole that allowed the introduction of the capillary at the previously calculate depth and the injection of 1 µl of LPC, pushing the Hamilton syringe. We wait at least 1 minute after inserting the capillary into the brain before injecting to let the tissue expand and at least 2 minutes after the injection to avoid any undesirable leakage of liquid. After suturing the skin, we placed the mouse in a warm wake-up chamber for recovery. Mice were

perfused at two time points: 7 days' post-injection (dpi), marking the peak of OPC migration and proliferation, and 14 dpi, marking the peak of OPC differentiation and the onset of active remyelination. Brains were cut in 40 μ m thick coronal slices. Before staining for OPCs and mOLs, we verified the accuracy of the injection site. The lesion exhibited distinct characteristics, including high cellularity (visualized with DAPI staining), microglia activation (identified by Iba1 staining), a demyelinated core (lacking MBP), and remyelinated borders (showing intense MBP staining), spanning from Br. +1.5 to Br. +0.6 mm (**Figure 19**). Only slices with a well defined lesion were considered for the analysis (**Figure 19**, bottom panels).

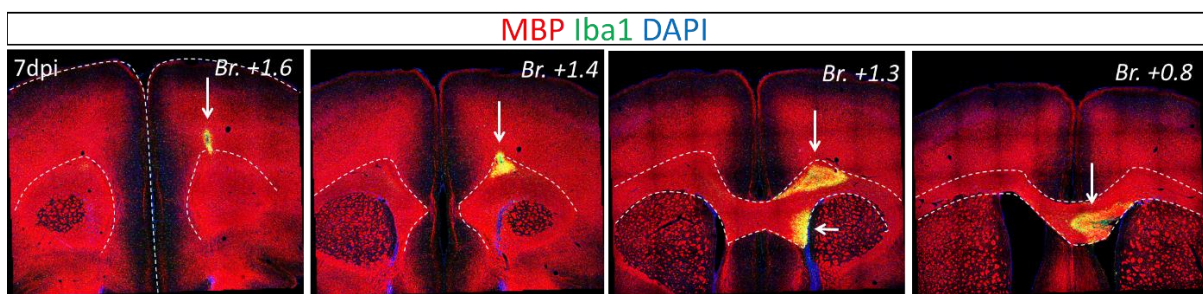


Figure 19. Characterization of the lesion site after LPC injection. Sequential frontal cortex containing slices have been stained for MBP (marker of myelin), Iba1 (marker of microglia) and DAPI. Representative images showing that the lesion, characterized by cell proliferation, myelin loss and regeneration, spans from bregma +1.6 to > +0.8.

6.9. Electrophysiology

In collaboration with Dr. T. Karadottir (University of Cambridge), we performed whole-cell patch-clamped of OPCs from knockin mice expressing Enhanced Yellow Fluorescent Protein (EYFP) under the endogenous NG2 promoter (NG2-EYFP mice). Corpus callosum EYFP⁺ OPCs were dye-filled with Lucifer Yellow during recording and post-hoc labelled for EYFP and Olig2. Patch-clamp recordings were performed as described in Spitzer et al., 2019. NMDA (60 μ M; Tocris) plus glycine (100 μ M) or glycine plus CGP-78608 (CGP 500nM; Tocris 1493) – a blocker of GluN1/GluN3A desensitization - were bath applied to record NMDAR-evoked and GluN3A-mediate glycine-evoked currents.

6.10. Image acquisition, processing and analysis

Immunofluorescence images were captured with a vertical confocal (Leica TCS-SPEII; DM 5500 Q) or an inverted widefield Thunder microscope (Leica DMI8) using the appropriate objectives and uniform acquisition settings through the same experiment. Cell densities have been manually quantified on maximum projection images (30 μm depth, 3 μm step, unless indicated) in the corresponding regions of interests using ImageJ software. For the analysis of c-Fos, cell signal was segmented from the background by smoothing and thresholding and positive cells (min. 58, max. 255) and automatically counted using the 'Analyse Particles' tool with a 10 μm^2 minimum size cut-off. The integrated density of the C-Fos⁺ nuclei were measured and expressed as Arbitrary Units (AU). The resulting C-Fos⁺ masks were then overlaid onto the mCherry channel image for colocalization analysis.

Imaris software was utilized for 3D-cell reconstruction using a semi-automatic filament tracer tool, based on 40X z-stack (40 μm depth, 1 μm step) confocal images containing individual Opalin⁺ OLs. The process involved several custom settings, including a gaussian filter (0.179 μm) for image smoothing and enhanced detection, thresholding Background subtraction (Local Contrast), and specifications for nucleus diameter (max. 15 μm), process diameter (min. 0.4 μm) and filament diameter (max. 5 μm) thresholds. Manual removal of unspecific detections was performed, and only cells with nuclei completely within the section thickness were included for analysis. Fused processes from 2 separate OLs that were falsely recognized as one entity by the software were manually separated using the cut function. Caspr1⁺ paranodes per OL reconstruction was conducted on the same images using the semi-automatic Imaris spot segmentation tool. Internode number and length analysis were performed using post-processing tools within Leica Application Suite X (LAS X).

6.11. Statistical analyses

Statistical analyses and graph generation were conducted with GraphPad Prism software. Sample size "n" refers to the number of mice, unless indicated. In datasets following a normal distribution comparison of one variable between two groups were performed using two-tailed unpaired t-test

and comparison between groups that have two independent variables using two-way analysis of variance (ANOVA) test followed by a post-hoc Tukey's multiple comparison corrections. Data showing non-Gaussian distributions were analyzed using the Mann–Whitney U test and the Kruskal–Wallis test followed by Dunn's multiple comparison test. Frequency and cumulative distribution analysis were performed using Kolmogorov-Smirnov test. P values are reported in the figure legends according to the following star symbols: * $P < 0.05$, ** $P < 0.01$, *** $P < 0.001$; ns for 'not significant'. All data are presented as mean \pm standard error of the mean (SEM), unless indicated.



7. RESULTS

Author: *Alice Staffa*

7.1. GluN3A is expressed in postnatal and young adult OPCs

Neuronal GluN3A roles have been extensively investigated in the context of activity-dependent synaptic plasticity but less is known about their expression and function in other non-neuronal cell types. Almost two decades ago, a series of studies suggested that oligodendroglia express NMDARs with biophysical properties consistent with the presence of GluN3A subunits (Karadottir et al., 2005; Salter and Fern, 2005; Micu et al., 2006; Burzomato et al., 2010) (see **Introduction**), but the findings and potential roles of GluN3A have been controversial since for researchers in the myelin field. To address this, we started by evaluating new evidence from RNA-seq studies and confirming the presence of GluN3A across the oligodendroglial lineage using histological methods.

7.1.1 Transcriptomic analyses demonstrate *Grin3a* mRNA expression in OPCs

We searched recently available scRNA-seq databases of gene expression in oligodendroglial cells for *Grin3a* mRNA expression (Marques et al., 2016, 2018). Pooling cells from juvenile (P21-30) and adult (P60) brain, these studies were able to identify 12 distinct oligodendroglial populations which represent a continuum from *Pdgfra*⁺ OPCs to myelinating mOLs (**Figure 20A**). Our analysis found *Grin3a* to be among the top 50 highly-expressed genes in OPCs relative to other OL subpopulations. Expression seemed to be a feature of a subset of cycling OPCs and OPCs committed to differentiate (COPs, also referred to as immature OL-type1, iOL1, according to Marques et al., 2016 nomenclature) (**Figure 20B**). High *Grin3a* mRNA levels were found in around 40% of OPCs and cycling OPCs, while around 20% of COPs exhibited lower to mid-level expression (**Figure 20C**). By contrast, *Grin3a* mRNA was practically undetectable in newly-formed pre-myelinating OLs (NFOLs, also referred to as immature OL-type2, iOL2, according to Marques et al., 2016 nomenclature) and myelin-forming and mature OLs (MFOLs, MOLs) (**Figure 20**). However, OPCs in these databases come from different regions so we cannot rule out a contribution of region-specificity in *Grin3a* expression.

To confirm the presence of *Grin3a* in OPCs we performed a bulk RNA-seq analysis of gene expression in OPCs isolated from forebrains of P7 wild-type (Wt) mice using PDGFR α -antibody coated magnetic beads. Isolated OPCs exhibited high *Pdgfra* mRNA levels, while *Myrf*, *Gfap*,

Cx3cr1 and *Rbfox3* (*NeuN*) were nearly undetectable, indicating absence of mOLs, astrocytes, microglia and neurons and validating the purity and efficiency of our protocol (Figure 21A). We additionally confirmed the expression of general markers of the oligodendroglial lineage, such as *Olig2* and *Sox10*, and OPC-specific markers including *Cspg4*, *Olig1*, and *Gpr17*. Markers of differentiating NFOs and mOLs, such as *Bcas1*, *Tcf4*, *Cc1*, *Mbp*, and *Mog*, showed much lower expression levels (Figure 21B).

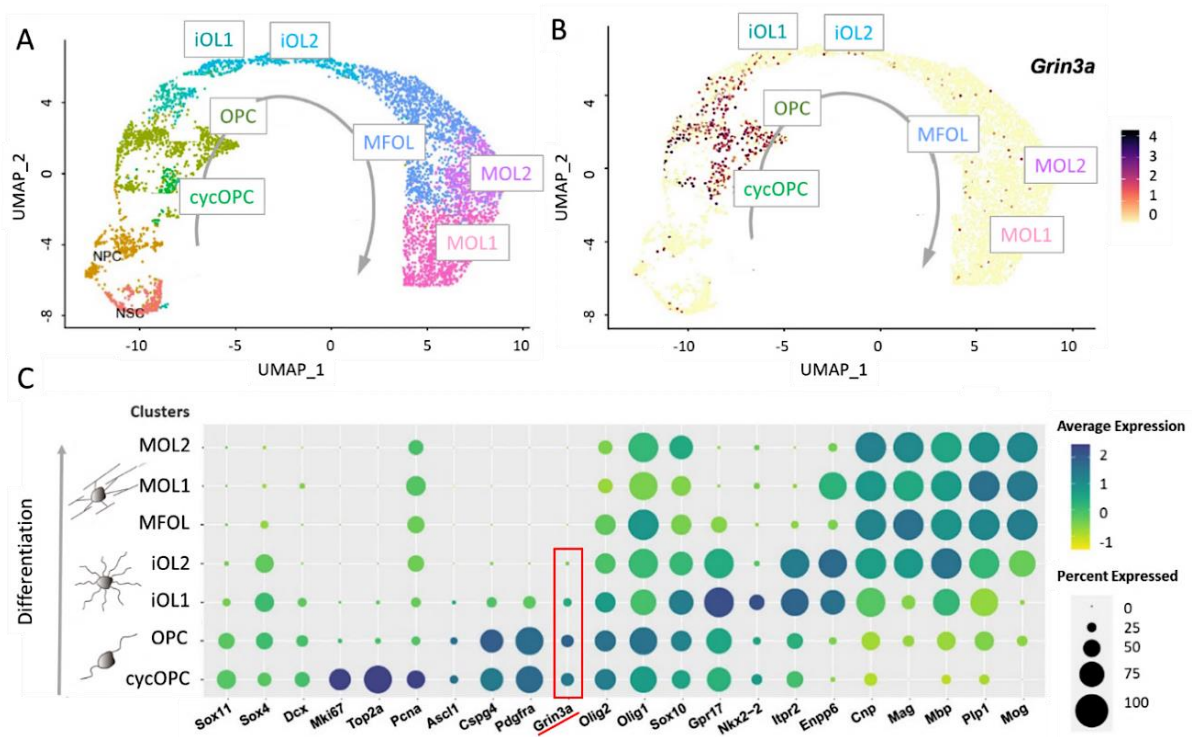


Figure 20. *In silico* analysis of *Grin3a* mRNA expression. Analysis from scRNA-seq databases in Marques et al., 2016, 2018. Clusters from the two datasets containing oligodendroglia cells were manually annotated based on the top 50 markers and merged into a single Seurat object (OLgliaDevP) containing 5516 cells (Merour et al., 2022). (A) Dimensionality reduction of the distinct populations of the oligodendroglial lineage using the UMAP (Uniform Manifold Approximation and Projection) algorithm. (B) *Grin3a* mRNA expression is high in OPCs and in COPs (iOL1) but absent from mature OLs. (C) Graph showing the percentage of cells within specific clusters that express *Grin3a* and average expression levels as well as control genes used to identify different OPC and OL subpopulations.

In the context of glutamate receptor subunits, postnatal OPCs expressed several of the NMDAR subunits, with highest levels of *Grin3a* followed by *Grin1*, *Grin2d* and *Grin2c* (Figure 21C). OPCs also expressed the AMPA receptor subunits *Gria2*, *Gria3*, *Gria4*, but low levels of *Gria1* (Figure 21D) in line with previous findings (Karadottir et al., 2005; Kougioumtzidou et al., 2017).

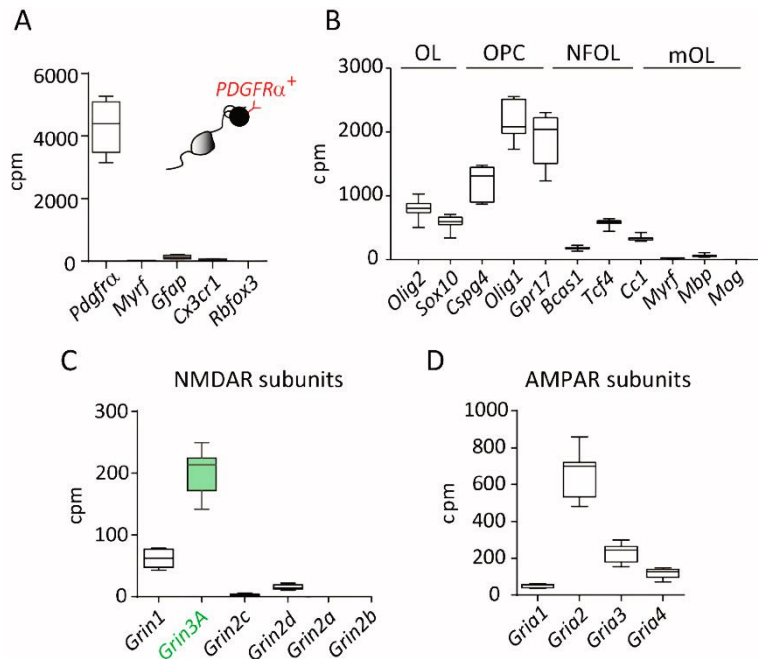


Figure 21. *Grin3a* mRNA in isolated OPCs revealed by RNA-seq. (A) OPCs were isolated from forebrains of P7 Wt mice with magnetic beads coated with PDGFR α antibody followed by mRNA extraction and RNA-seq. Purity of isolated cells was confirmed by high *pdgfra* level, but minimal to undetectable expression of markers of other cell types. (B) Markers for differentiated NFOLs and mOLs were expressed at low levels. Expression of NMDAR (C) and AMPA (D) receptor subunits in isolated OPCs (n=7 mice). Cpm: counts per millions.

Analysis of datasets from two additional studies indicated that *Grin3a* mRNA expression in OPCs is regulated across the rodent lifespan. Bulk RNA-seq of mouse OPCs isolated from whole brain showed highest *Grin3a* mRNA levels at postnatal developmental stages (P12) with significant decline in aged mice (P310) (Spitzer et al., 2019) (Figure 22A). RNA-seq analysis of OPCs isolated from young adult (2-3 months) and aged (20-24 months) rat telencephalon and cerebellum revealed a similar age-related decline. Of note, *Grin3a* was one of the top-10 genes differentially expressed in the aged rat brain (Neumann et al., 2019) (Figure 22B).

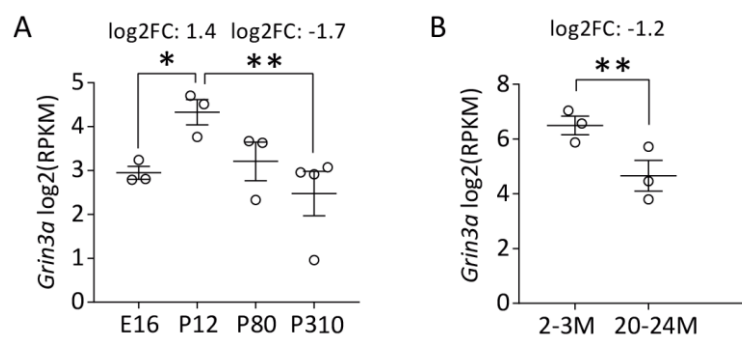


Figure 22. *In silico* analysis of temporal *Grin3a* expression. (A) OPCs isolated from mouse brains with magnetic beads coated with PDGFR α antibody (Spitzer et al., 2019) display a postnatal peak of expression (P12 vs E16: log2FC = 1.4, padj = 0,015 *) with decreasing expression into adulthood and aging (P80 vs P12: log2FC = -1.05, padj = 0,28; P310 vs P12: log2FC = -1.7, padj = 0.005 **). (B) Age-decline in *Grin3a* expression in OPCs isolated from young (2-3 months) and aged (20-24 months) rat brains with magnetic beads coated with the AB25 OPC-specific antibody (Neumann et al., 2019) (log2FC = -1.2, p = 0,002 **).

7.1.2 Localization of *Grin3a* mRNA and GluN3A protein in OPCs

Fluorescent in situ hybridization (FISH) combined with immunostaining for PDGFR α and Olig2 provided independent evidence for *Grin3a* expression in OPCs. The experiments were conducted around P12, when GluN3A expression is high (see **Figure 22A**). On initial observation, *Grin3a* expression in WM regions was much lesser compared to GM, for instance relative to layers (L) 2/3 or layer 5 cortical neurons. Closer examination allowed us to detect *Grin3a* mRNA in PDGFR α ⁺ OPCs (**Figure 23A**), with mRNA granules often located in OPC processes (**Figure 23B**, arrowheads).

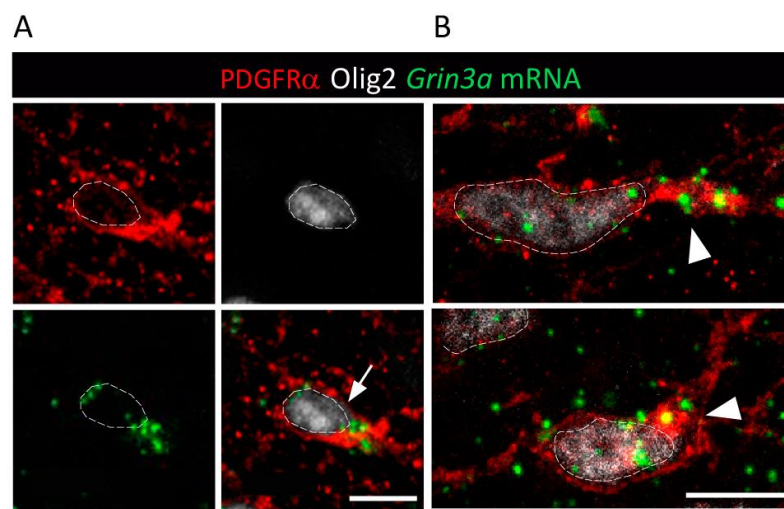


Figure 23. *Grin3a* mRNA in postnatal OPC processes revealed by FISH. (A) Representative high-magnification images of the subcortical WM of a P8 Wt mouse brain showing an OPC (arrow) labelled by FISH with *Grin3a* mRNA probes and stained with PDGFR α and Olig2 antibodies. (B) *Grin3a* mRNA granules are often visible along OPC processes (arrowheads). DAPI nuclear stain is outlines as a reference to identify cells. Scale bars: 10 μ m.

Next, we took advantage of an mClover-GluN3A knock-in mouse line generated in our laboratory that allowed us to overcome limitations in the availability of specific GluN3A antibodies for immunohistochemistry. mClover3-GluN3A protein was detected in a subset of PDGFR α ⁺ OPCs (**Figure 24A**), with no signal in littermate control mice. As with FISH, GluN3A protein was observed in OPC processes (**Figure 24B**, arrowheads), suggesting a role in sensing axonal signals that we further assessed with electron microscopy (see below).

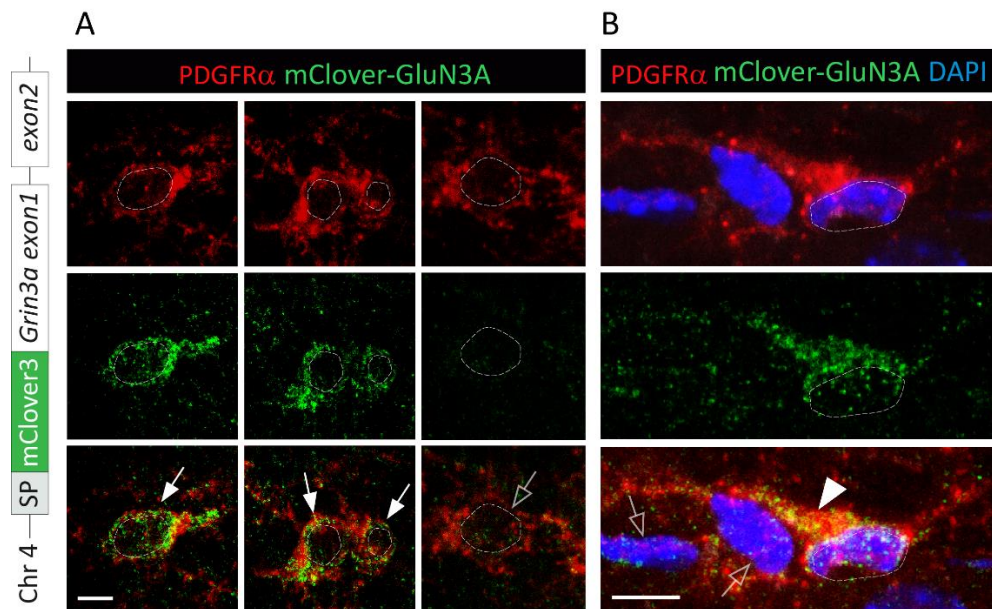


Figure 24. GluN3A protein expression in postnatal OPCs of mClover-GluN3A knock-in mice. Experiments were conducted in a mouse line generated by inserting the mClover3 fluorophore sequence before *Grin3a* exon1 in chromosome 4 (cartoon on the left) using CRISPR technology. mClover3-GluN3A mice allow visualization of endogenous GluN3A upon amplification of mClover3 signal with a GFP antibody (green). (A) Representative images of PDGFR α ⁺ OPCs (red) in the scWM of P12 mice; GluN3A was detected in some OPCs (arrows) but not others (empty arrows). (B) High magnification image showing GluN3A expression in the cytoplasm and processes of an OPC (arrowhead). DAPI stain was used to identify individual cell nuclei and is outlined as a reference. Scale bars: 5 μ m.

7.1.3 Electron microscopy confirms the localization of GluN3A protein in OPC processes that surround unmyelinated axons

To map the subcellular localization of GluN3A at the ultrastructural level, we used immunoperoxidase and preembedding immunogold electron microscopy (EM). Intense peroxidase deposits (**Figure 25A**) and immunogold particles (**Figure 25B**) demonstrated GluN3A immunoreactivity in OPC processes (green shaded cells) that surround unmyelinated axons within the scWM, in line with our FISH and immunostaining data.

Together these results demonstrate that GluN3A subunit complexes are restricted to OPCs, well placed to sense axonal signals and, perhaps in concert with other trophic factors such as BDNF or NRG1, instruct OPCs to stop proliferating and start differentiation and myelination.

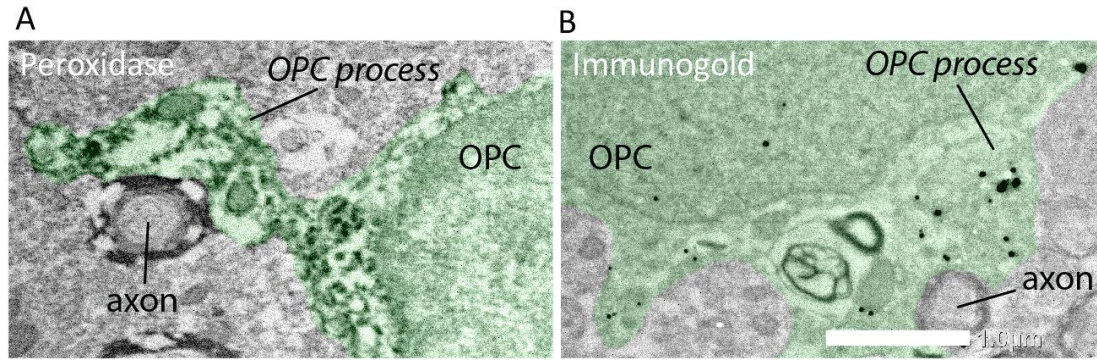


Figure 25. GluN3A subcellular localization in OPC processes visualized by peroxidase and immunogold EM. Oligodendroglial cells (shaded in green) were morphologically identified as cells with a dense nucleus and a thin cytoplasm typically positioned in close proximity to axons in the WM. (A) Intense GluN3A peroxidase deposits and (B) immunogold particles were detected in processes of OPCs that contact unmyelinated axons in P11 scWM. Scale bars: 1 μ m.

7.1.4 Electrophysiological evidence for functional GluN3A receptors in OPCs

We finally performed electrophysiological recordings to look for functional evidence for GluN3A expression and identify the type of GluN3A complexes formed in OPCs. This work was done in collaboration with Dr. Thora Karadottir at the University of Cambridge. Whole-cell patch-clamp recordings of fluorescently-labeled OPCs were conducted in the corpus callosum of NG2-EYFP mice (see **Figure 26A**). NMDA plus glycine was applied to activate GluN1/2/3A triheteromeric receptors; and glycine in the presence of CGP-78608 to unmask GluN1/3 excitatory glycine receptors. Glycine binding to GluN1 subunits causes a rapid desensitization of GluN1/3 channels which can be prevented by preapplication of CGP-78608, a selective antagonist of the GluN1 glycine-binding site.

Our current data demonstrate the existence of GluN3A-mediated glycine currents (**Figure 26B**) in a subset of P7 OPCs (**Figure 26C**), in line with transcriptomic and histological data that not all OPCs express GluN3A. All OPCs that displayed excitatory glycine currents mediated by GluN1/3A receptors also displayed NMDA-evoked currents of small conductance, consistent with the presence of GluN1/2/3A triheteromeric receptors (**Figure 26D**). Overall, 53% of OPCs recorded in P7-P40 corpus callosum expressed both types of known GluN3A-containing configurations. 23% express only conventional NMDA receptors while NMDAR currents were

undetectable in the remaining fraction. Further experiments are being conducted in Cambridge to increase the number of OPCs recorded both from WM and GM areas in postnatal, adult and aged brains.

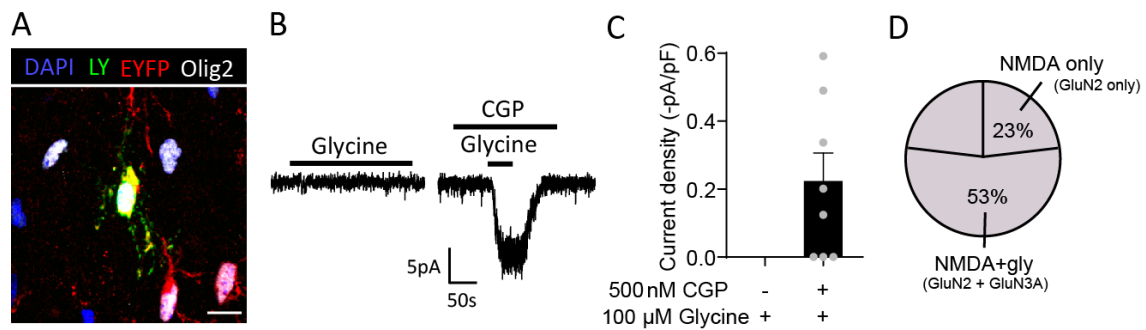


Figure 26. Whole-cell patch-clamped OPCs reveals GluN3A-mediated current. (A) OPCs from the corpus callosum of P7 to P40 NG2-EYFP mice were whole-cell patch-clamped of mice dye-filled with Lucifer Yellow (LY) during the recording, and post-hoc labelled for EYFP (red) and Olig2 (white). (B) 100 μ M glycine-evoked current in the absence (left) and presence (right) of 500 nM CGP-78608. (C) In the presence of CGP, glycine application evoked currents in 5 out of 8 recorded P7 OPCs. (D) Glycine/CGP evoked currents were detected in 53% of newly recorded OPCs in the corpus callosum of P7/P40 mice, along with NMDAR currents of small conductance. Scale bar: 10 μ m.

7.2. Accelerated expression of markers of OPC differentiation and myelination in postnatal *Grin3a*^{-/-} mice

A pilot screening of gene expression changes in the forebrain of early postnatal (P8) *Grin3a*^{-/-} mice using DNA microarray technologies (Figure 27A) revealed a major - but unexpected in our neuronal-centred view - upregulation of markers of OPC differentiation and subsequent myelination stages (Figure 27B, C). For instance, we observed a large upregulation of *Enpp6*, marker of NFOLs, of myelin constituents such as *Mbp*, and of proteins involved in axon-glia signalling such as *Mag* that is a ligand for the axonal Nogo receptor.

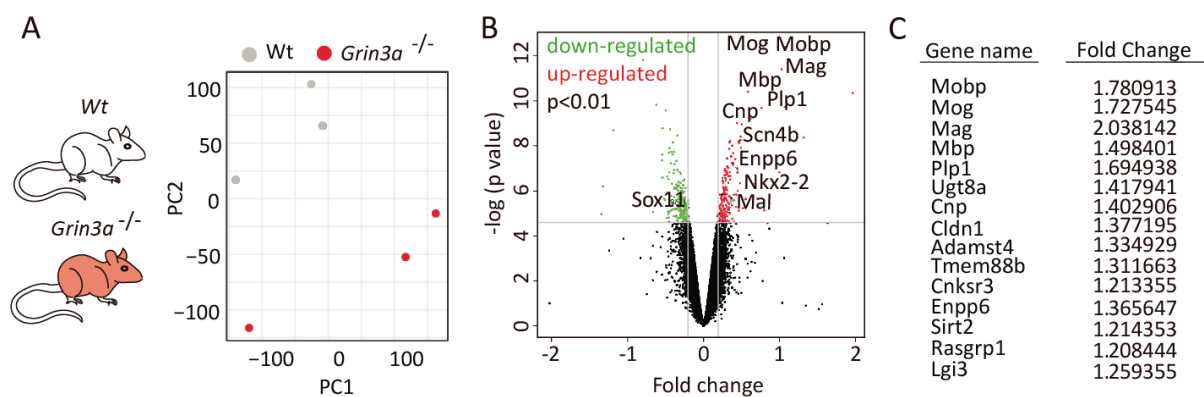


Figure 27. DNA microarray screening revealed enhanced expression of myelin-related genes in the forebrain of P8 *Grin3a*^{-/-} mice relative to Wt counterparts. (A) Principal component analysis (PCA) shows a clear separation between Wt and *Grin3a*^{-/-} samples. (B) Volcano plot of the significantly differently expressed genes (p<0.01) illustrating upregulation of numerous genes associated to OPC differentiation and myelination. (C) A list of the most prominently upregulated genes alongside their respective fold change values (n=3 mice per group).

7.2.1 Markers of OPC differentiation and myelination are upregulated in *Grin3a*^{-/-} mice during a critical window of postnatal development

To validate and extend our analysis of molecular changes in myelination in *Grin3a*^{-/-} mice and narrow down the temporal window, we conducted a bulk RNA-seq of mRNA extracted from the somatosensory cortex (SS1) of wild-type and constitutive *Grin3a*^{-/-} mice at two different ages, P11 and P18. The areas and ages were chosen to match the temporal time-course of myelination, which varies across brain regions matching the different timings of neuronal and circuit maturation. In SS1, P11 is an early time point when intracortical myelination is just beginning, and is equivalent to P18 in primary visual cortex (V1) when myelination starts later (McGee et al., 2005).

Applying a threshold for fold change (\log_2FC) > 0.35 and pvalue (p-adjusted, p_{adj}) < 0.05, we found 485 differentially expressed genes (DEGs) at P11 and only 55 at P18. Among the DEGs, 304 were upregulated genes at P11 and 35 at P18. A PCA component analysis showed a clear separation between genotypes at P11 but not at P18 (**Figure 28A**). Using gene ontology analysis, the main cell biological processes driven by DEGs in GluN3 knockout cortex were CNS myelination and axon ensheathment as well as oligodendroglial development, surpassing changes in functions related to transmembrane protein transfer, synaptic transmission, and cell-cell signaling (**Figure 28B**). A finer analysis showed that a long list of genes involved in OPC differentiation, maturation and myelin deposition were upregulated at P11. The list included classical markers of newly-formed and pre-myelinating OLs such as *Ennp6*, *Tcf7l2* (*Tcf4*), *Bcas1*, *Nkx6.2*, *Cnp*, *9630013A20Rik* (*lncOL1*), *Cnksr3*, *Tns3*, as well as of mature myelinating OLs such as *Myrf*, *Tmem10* (*Opalin*), *Mal*, *Mag*, *Mobp*, *Mog*, *Plp1*, *Mbp*, *Ugt8a*, *Cldn11* (*Osp*), *Ermn* (**Figure 28C**). OPC-specific genes such as *Pdgfra*, *Cspg4*, *Gpr17* and *Ptzpr1* were not differently expressed. The hypermyelination phenotype was not apparent at P18. A heatmap of genes associated to specific oligodendroglial maturation stages illustrates the acceleration of myelination in absence of GluN3A, with the transcriptional profile of P11 *Grin3a*^{-/-} mice becoming closer to P18 Wt mice (**Figure 28D**). In sum, the transcriptomic analysis demonstrated that GluN3A deletion favours OPC differentiation into OLs during a critical postnatal period, culminating in enhanced myelination that can be detected at premature stages. It is also possible that a later-stage phenotype was not detected due to the massive developmental enhancement in myelin gene expression (compare P11 Wt to P18 Wt, **Figure 28D**).

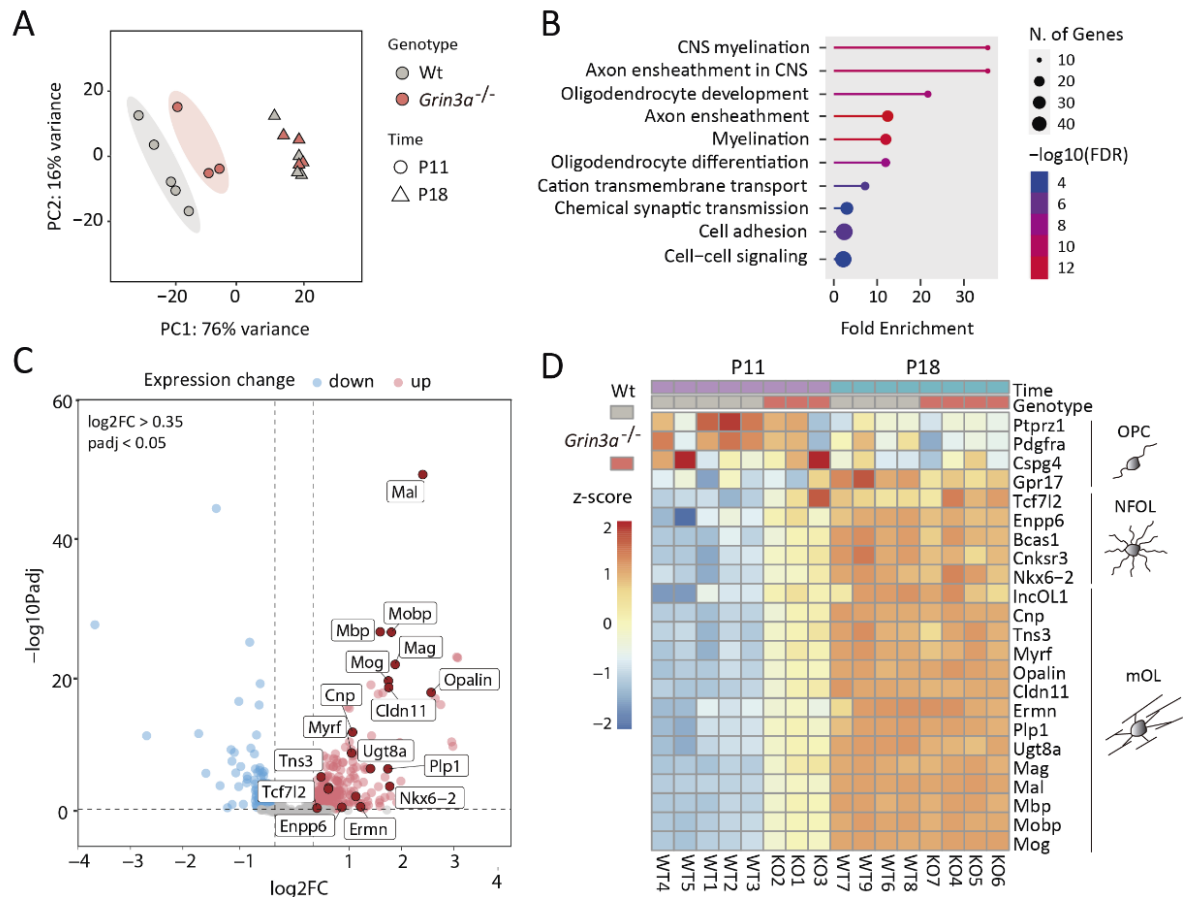


Figure 28. Upregulation of myelin-related genes in *Grin3a*^{-/-} SS1 at P11 detected by RNAseq. (A) PCA component analysis of Bulk RNAseq data from Wt and *Grin3a*^{-/-} SS1 samples at P11 and P18. (B) Gene Ontology (GO) analysis of log₂FC > 0.35 and padj < 0.05 upregulated genes at P11 shows myelination and OL differentiation as main upregulated biological functions in *Grin3a*^{-/-} SS1. (C) Volcano plot of significantly DEGs highlights upregulation of genes associated to OPC differentiation and myelination. (D) Heatmap of genes associated to different oligodendroglial maturation stages reveals no differences in OPC markers, while genes associated to OPC differentiation and myelination are increased in P11 *Grin3a*^{-/-} mice, approaching levels of P18 Wt. Z-score (calculated by subtracting the mean from the data point and dividing the difference by the standard deviation) instead of fold change is used (n=3-5 mice per group).

RNA-seq results were validated by quantitative western blot analysis. A large (2 to 4-fold) increase in levels of the myelin proteins MBP, CNP, MOG and OSP was observed in P11 *Grin3a*^{-/-} forebrains relative to wild-type mice (Figure 29A, B). Differences were detectable but much lesser by P18, suggesting the existence of a subtler, later-stage phenotype (Figure 29B).

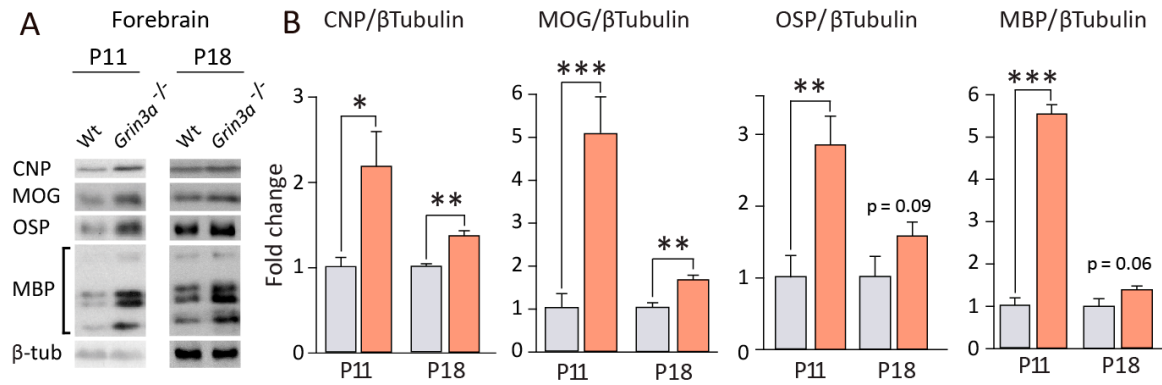


Figure 29. Upregulation of myelin-related protein expression in P11 and P18 forebrain of *Grin3a*^{-/-} mice. (A) Representative western blot of P11 and P18 mouse forebrain of Wt controls and *Grin3a*^{-/-} mice. (B) Quantification of the protein levels of MBP, CNP, MOG and OSP. Protein expression was normalized to β-tubulin and expressed as fold-change of corresponding age-matched Wt values (n=4 mice per group; two-tailed unpaired t-test, *p<0.05, **p<0.01, ***p<0.001).

7.2.2 Accelerated OPC differentiation and myelination in *Grin3a*^{-/-} mice

A limitation of RNA-seq and immunoblot analyses is that selective expression changes across brain areas, cortical modalities, or cortical layers with diverse temporal courses of myelination might be obscured. To evaluate potential region-specific differences in the hypermyelination phenotype, we conducted an immunohistochemical analysis for the classical myelin marker MBP. **Figures 30 and 31** show that MBP immunofluorescence was higher in P11 *Grin3a*^{-/-} mice relative to Wt controls across brain regions, irrespective of differences in the timing of postnatal myelination. At this age, MBP expression in Wt mice was restricted to inner cortical layers of SS1, mostly layer 6, while in *Grin3a*^{-/-} mice myelin sheaths reached layer 4 and covered a significant larger area of layers 6, 5 and 4/2 (**Figure 30A, B**). Heightened MBP expression was observed in other brain regions of P11 *Grin3a*^{-/-} mice such as the secondary motor cortex (M2), both in the GM and scWM, corpus callosum (**Figure 30C, D**), and notably, the primary visual cortex (V1) (**Figure 31A, B**). This is noteworthy because cortical myelination in V1 at P11 is still in its early stages, as visual stimuli only reach the cortex upon eye opening around P15-P17. No differences were found in V1 at P18 (**Figure 31C, D**). The results demonstrate an early and general acceleration of myelin formation that is independent of the timing of arrival of neuronal activity inputs.

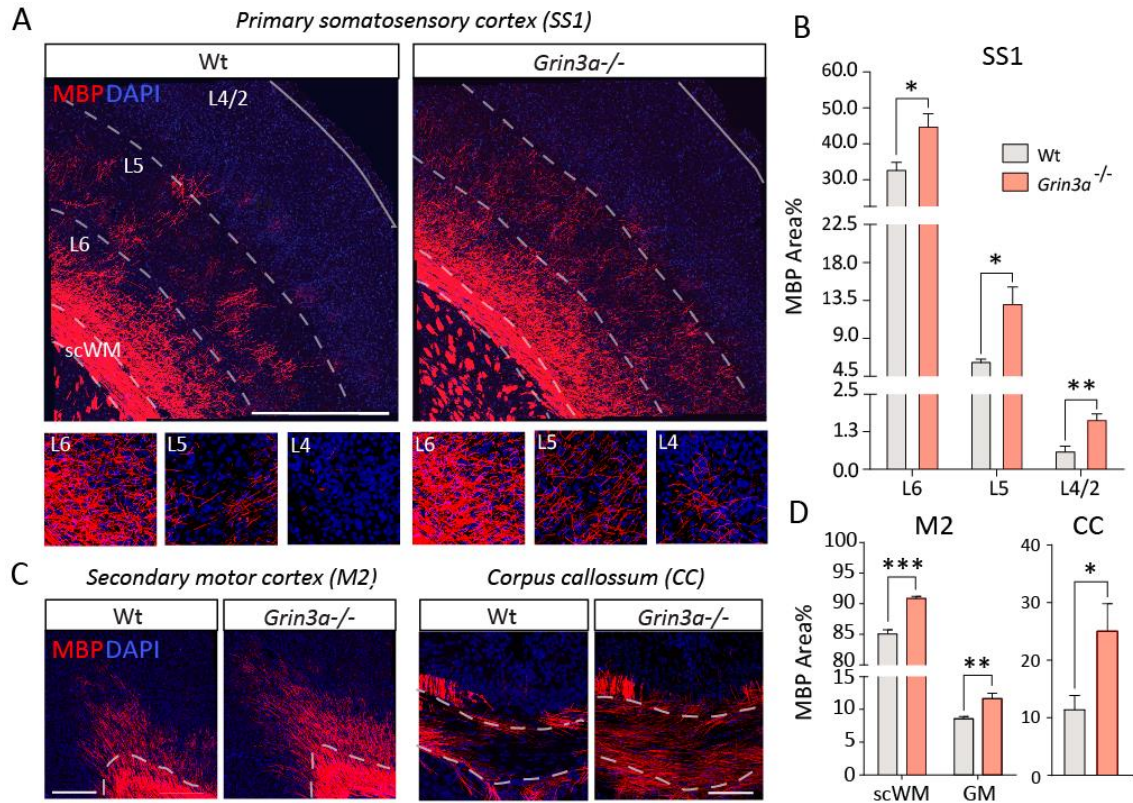


Figure 30. Increased MBP expression in P11 *Grin3a*^{-/-} brains. (A) Representative images of MBP immunostaining across SS1 cortical layers in coronal brain sections of P11 Wt and *Grin3a*^{-/-} mice. (B) Quantification of MBP⁺ area as percentage of cortical layer area. (C) Representative images and (D) quantification of MBP⁺ area in M2 scWM and GM, and CC (n=4; two-tailed unpaired t-test, *p<0.05, **p<0.01, ***p<0.001). Scale bars: 600 μ m (A), 300 μ m (C, M2) and 200 μ m (C, CC). L: layer.

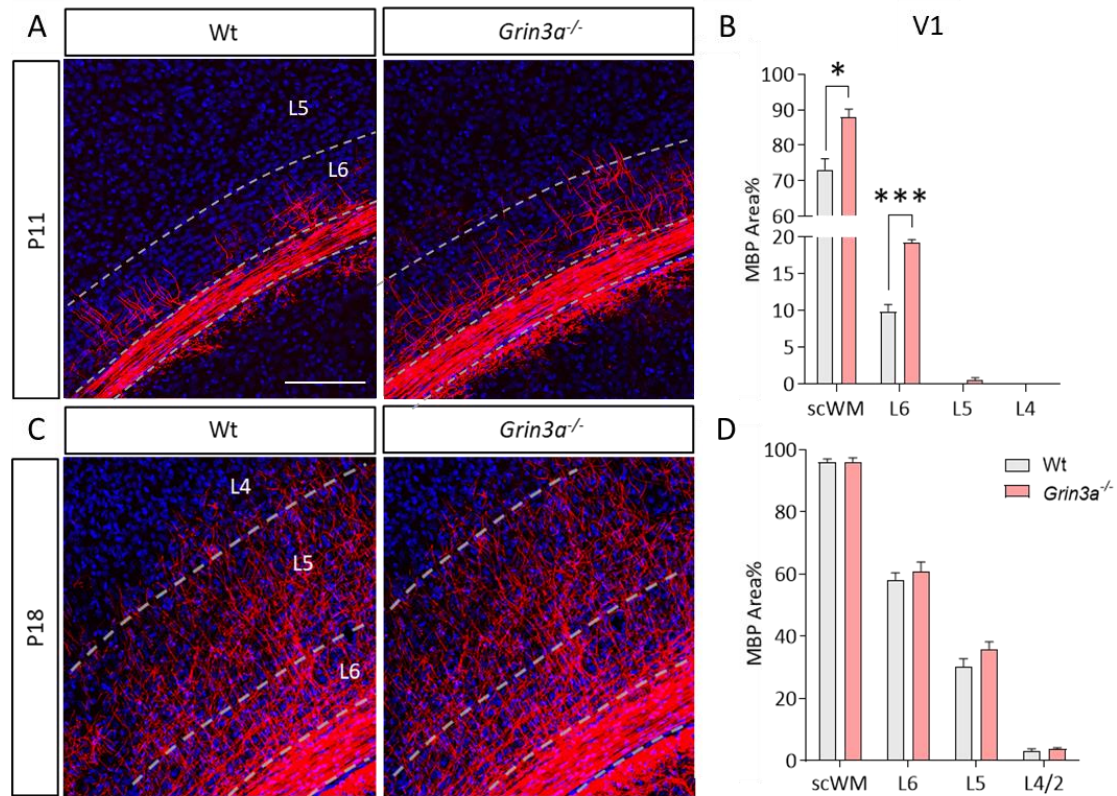


Figure 31. Increased MBP expression in V1 of *Grin3a*^{-/-} mice prior to eye opening. (A) Representative images and (B) quantification show how at P11, MBP is only detectable in L6 in both Wt and *Grin3a*^{-/-} mice with increased MBP signal in scWM and L6 in *Grin3a*^{-/-} mice. C, D) At P18 MBP reaches L5/4 with no apparent differences between genotypes (n=3; two-tailed unpaired t-test, *p<0.05, **p<0.01, ***p<0.001). Scale bar: 100 μ m.

To determine if the accelerated myelination was due to enhanced OPC differentiation, we quantified the numbers and differentiation state of oligodendroglial cells across cortical layers using stage-specific markers: Olig2 that labels all oligodendroglial lineage, and CC1 and PDGFR α to label differentiated OLs and progenitor cells, respectively. In line with MBP regulation, an increase in the density of differentiated OLs (CC1⁺/Olig2⁺) was observed in all SS1 layers of *Grin3a*^{-/-} mice at P11 (**Figure 32A, B**). Enhanced differentiation was accompanied by a slight decrease in OPC density (PDGFR α ⁺/Olig2⁺) in upper layers (**Figure 32D, E**). No significant differences were found in the overall oligodendroglial population (Olig2⁺ cells) (**Figure 32C**). Note that as with MBP and cortical maturation, OPC differentiation follows an inside-out temporal pattern (scWM>L6>L5>L2/4).

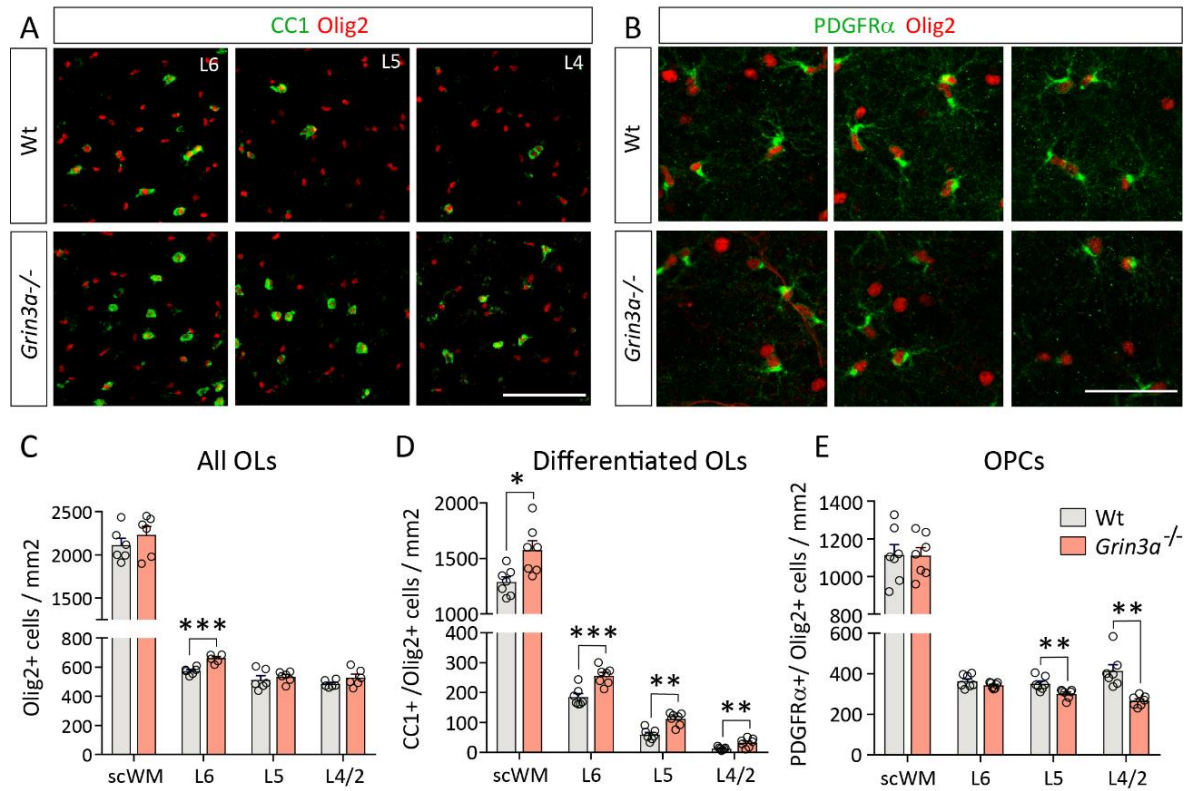


Figure 32. Increased OPC differentiation in P11 *Grin3a*^{-/-} mice. Representative images of differentiated OLs (A) stained with CC1 (green) and Olig2 (red) and OPCs (B) stained with PDGFRα (green) and Olig2 (red) in SS1 cortical layers of Wt and *Grin3a*^{-/-} mice. (C-E) Quantification of total Olig2⁺ cell density (C) differentiated OLs CC1⁺/Olig2⁺ (D) and OPCs PDGFRα⁺/Olig2⁺ (n=7 mice per groups; two-tailed unpaired t-test, *p<0.05, **p<0.01, ***p<0.001). Scale bars: 100 μm (A) and 50 μm (B).

We conducted an additional analysis to determine if GluN3A deletion affected a specific state of differentiation. For this, we used triple staining with Olig1, Olig2 and CC1 that allows to discriminate between immature stages of OL maturation (Merour et al., 2022) (**Figure 33A**). Increased numbers of both CC1^{high}/Olig2^{high}/Olig1⁻ type-1 immature cells and CC1⁺/Olig2^{high}/Olig1^{high} type-2 immature to CC1⁺/Olig2^{low}/Olig1^{low} mature cells were found in P11 SS1 cortical layers of *Grin3a*^{-/-} mice (**Figure 33B, C**), confirming that postnatal OPCs are primed to differentiate earlier in absence of GluN3A or respond better to environment signals. The results suggested that GluN3A controls the dynamics of OPC proliferation and differentiation, with GluN3A-lacking OPCs adopting a “fast-forward mode” that accelerates progression from early to late differentiation stages.

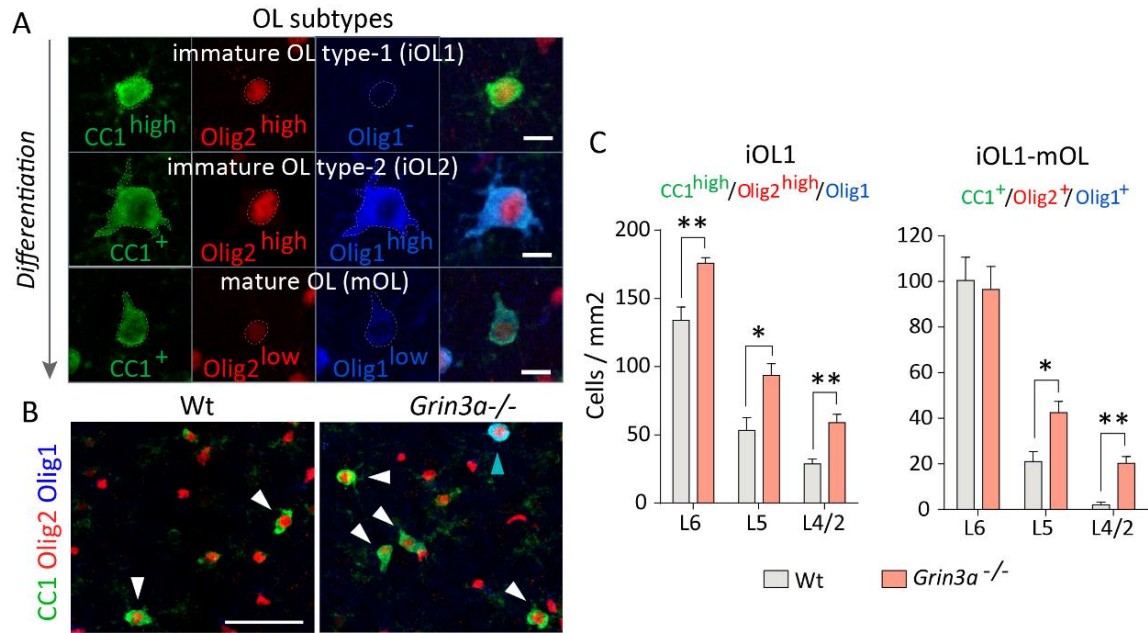


Figure 33. Increased transition from OPC to immature and then to mature OLs in *Grin3a*^{-/-} P11 brains. (A) Labeling of different stages: Olig1 displays nuclear localization in OPCs (not shown), is downregulated in iOL1 and re-expressed in the cytoplasm of iOL2 (high level) and mOL (low level). Colocalization of Olig1, CC1 and Olig2 antibodies allows to differentiate: iOL1, small green cells with high CC1 (green), high nuclear Olig2 (red) and no Olig1; iOL2, bigger blue cells with CC1, Olig2 and high level of Olig1 (blue); and mOL, smaller cells with CC1, lower Olig2 and Olig1. (B) Representative images of triple staining in P11 SS1 of Wt and *Grin3a*^{-/-} mice. (C) Quantification of iOL1 and iOL2-mOL numbers across SS1 cortical layers (n=4 mice per group; two-tailed unpaired t-test, *p<0.05. **p<0.01). Scale bars: 50 μ m (A) and 10 μ m (B).

By P18 the enhanced myelination was less apparent (Figures 28D, 29 and 31), but individual myelinating OLs in upper SS1 layers still exhibited a larger morphological complexity (Figure 34). For this structural analysis, we used a combination of antibodies against Opalin, a marker of mature OLs that fills processes and myelin sheaths, and Caspr1, a marker of paranodal segments flanking nodes of Ranvier gaps (Figure 34A, B). Plotting Opalin⁺ cells 3D-reconstructed with Imaris revealed a clear separation of OLs from Wt and *Grin3a*^{-/-} into two distinct clusters. *Grin3a*^{-/-} OLs displayed had larger size (Figure 34B, C) and a more complex morphology, with increased number of intersections between 20 and 50 μ m from the soma (Figure 34D). A significant increase in Caspr1⁺ paranodal segments was also found along Opalin⁺ myelin sheaths of *Grin3a*^{-/-} OLs relative to Wt (Figure 34E, F). Another indicator of myelination potential is the number and length of myelin sheaths, or internodes when referring to the axonal segment surrounded by the myelin

sheath. On average, *Grin3a*^{-/-} cells generated a higher number of myelin sheaths, with no discernible differences in their length (Figure 34G).

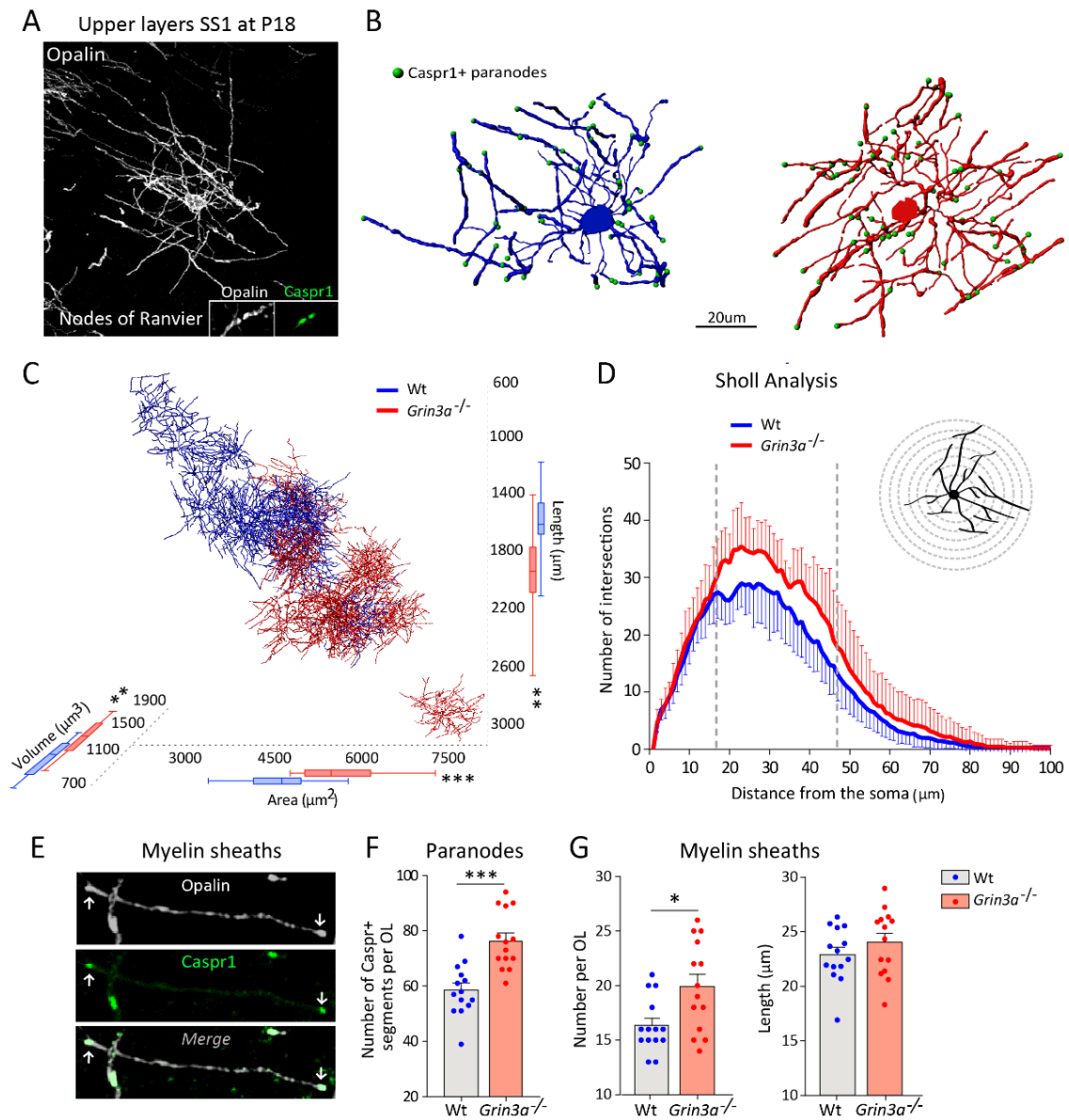


Figure 34. Morphological analysis of myelinating OLs in P18 *Grin3a*^{-/-} SS1. (A) Individual Opalin⁺ myelinating OL in upper SS1 layers of SS1 at P18. Caspr1 paranode stain (green) allowed identification of nodes of Ranvier between myelin sheaths. (B) Representative Wt and *Grin3a*^{-/-} 3D-reconstructed cell based on Opalin and Caspr1 staining (Imaris filament tracing and spot algorithm). (C) Multi-axis representation of reconstructed cells (x = Area; y = Length; z = Volume). (D) Analysis of cell complexity using Sholl-analysis of intersections of Opalin⁺ processes (1 µm distance concentric circles). (E) High magnification image of a Opalin⁺ myelin sheath flanked by Caspr1⁺ paranodal segments. (F) Quantification of number of Caspr1⁺ paranodal segments (F) and myelin sheaths (G) per OL (n=14 cells from n=3 mice per group; two-tailed unpaired t-test, *p<0.05, **p<0.01, ***p<0.001).

7.2.3 Preferential myelination of large caliber axons in *Grin3a*^{-/-} mice

Ultrastructural analyses of myelin using electron microscopy revealed a small but significant increase in the number of myelinated axons in the deeper layers of SS1 at P11 (**Figure 35B, D**) that was in-line with the enhanced myelination phenotype. Intriguingly, we noticed a remarkable shift towards myelination of axons of larger diameter in the SS1 of GluN3A knockout mice (**Figure 16E**) that pointed towards differences in modes of myelination between phenotypes. As discussed in the **Introduction**, activity-dependent myelination targets small axons (Gautier et al., 2015). Thus, we reasoned that the preference to myelinate larger axons in absence of GluN3A could result from uncoupling of OL differentiation from axonal signals distinct from axon caliber. Further evidence for preferred myelination of large diameter axons came from measurements of the G-ratios (**Figure 35C**). G-ratios for larger axons were smaller in both SS1 (**Figure 35F**) and corpus callosum of P11 *Grin3a*^{-/-} mice (**Figure 35G**). Conversely, G-ratios for smaller axons were larger, indicative of thicker myelin sheaths and possibly deficient myelination in response to activity in absence of GluN3A.

Together, the data presented in **Chapters 1&2** showed that GluN3A deletion drives a general enhancement in myelin formation that is likely independent of neuronal activity, with axonal selection responding instead to physical cues such as axonal diameter. One possibility is that GluN3A is a required factor to enable activity-dependent myelination. In its absence, OL differentiation switch to an activity-independent mode that alters the appropriate selection of axons to be myelinated. In **Chapter 3**, I describe a series of experiments that were designed to test this idea.

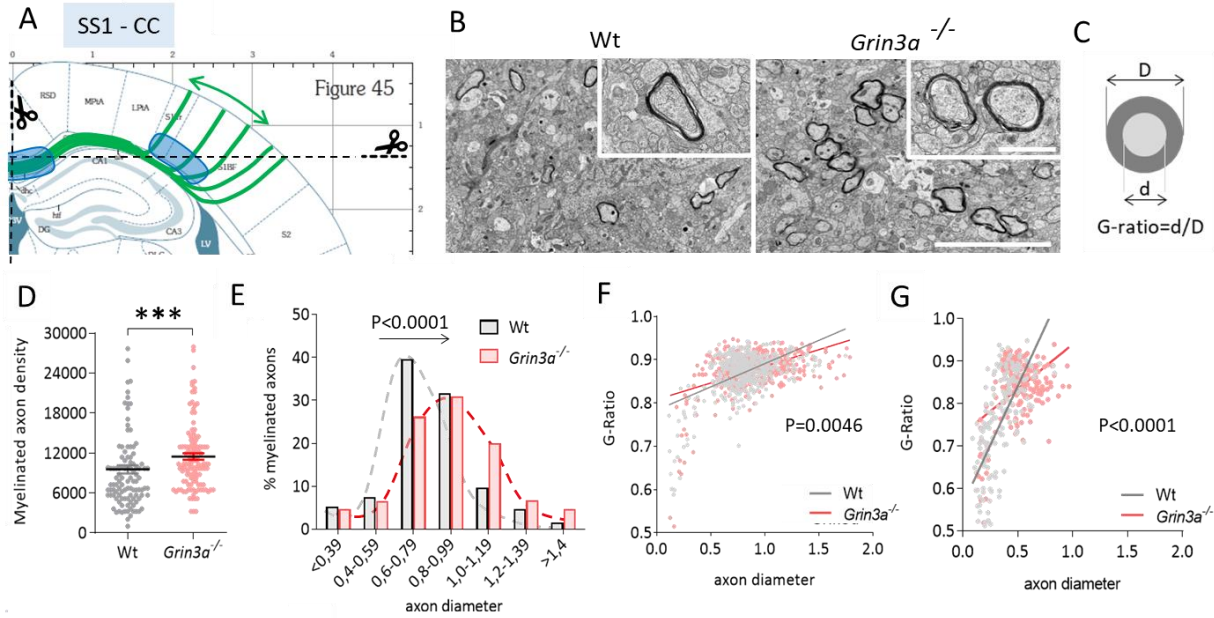


Figure 35. EM analysis of myelin ultrastructure in SS1 and CC at P11. (A) Areas of analysis are shaded in blue and callosal axons are indicated in green. Brains were cut horizontally at the levels of L5/6 for the SS1 analysis and sagittally across the central part for the CC analysis. (B) Representative images of layers 6/5 SS1 axons in Wt and *Grin3a*^{-/-} mice. (C) Cartoon of G-ratio calculated as the inner diameter of the axon (d) divided by the fiber diameter (D), including myelin. (D) Quantification of myelinated axon density (mm²) in P11 Wt and *Grin3a*^{-/-} mice (Mann-Whitney test, ***p<0.001). (E) Frequency distribution of myelinated axons relative to axon diameter (Kolmogorov-Smirnov test, ****p<0.0001). (F) Scatter plot showing the correlation between axon diameter and G-ratio in the SS1 (Linear regression Wt $R^2=0.259$; *Grin3a*^{-/-} $R^2=0.216$; slopes difference **p=0.0046). For a fixed axon diameter, a smaller g-ratio indicates greater myelin thickness. (G) Correlation between axon diameter and G-ratio in the CC (Linear regression Wt $R^2=0.451$; *Grin3a*^{-/-} $R^2=0.179$; slopes difference ****p<0.0001) ((n=495 and n=443 axons from n=3 mice per group). Scale bars: 50 μ m and 1 μ m high magnification.

7.3. Loss of activity-dependent OPC plasticity in *Grin3a*^{-/-} mice

To evaluate differences in activity-dependent myelination in absence of GluN3A, we compared the responses of OPCs from Wt and *Grin3a*^{-/-} mice to chemogenetic stimulation of callosal axon activity using DREADDs. We utilized the hM3Dg(q) DREADD, which triggers depolarization of neurons in response to the synthetic ligand clozapine-N-oxide (CNO). Specifically, we *in utero* electroporated hM3Dg-mCherry (or mCherry as control) plasmid into the right neuroepithelium of E15.5 embryos (Figure 36A). IUE yielded extensive and highly reproducible labelling of layer 2/3 SS1 pyramidal neurons along with their axonal projections, which extend into ipsilateral layer 5 and traverse the corpus callosum to reach their contralateral targets in SS1 (Figure 36B). As expected, mCherry and mCherry-hM3Dg displayed different subcellular localization and expression intensity (Figure 36C), but the number of mCherry⁺ somas (electroporated neurons) was identical between control and stimulated Wt and *Grin3a*^{-/-} mice (Figure 36D).

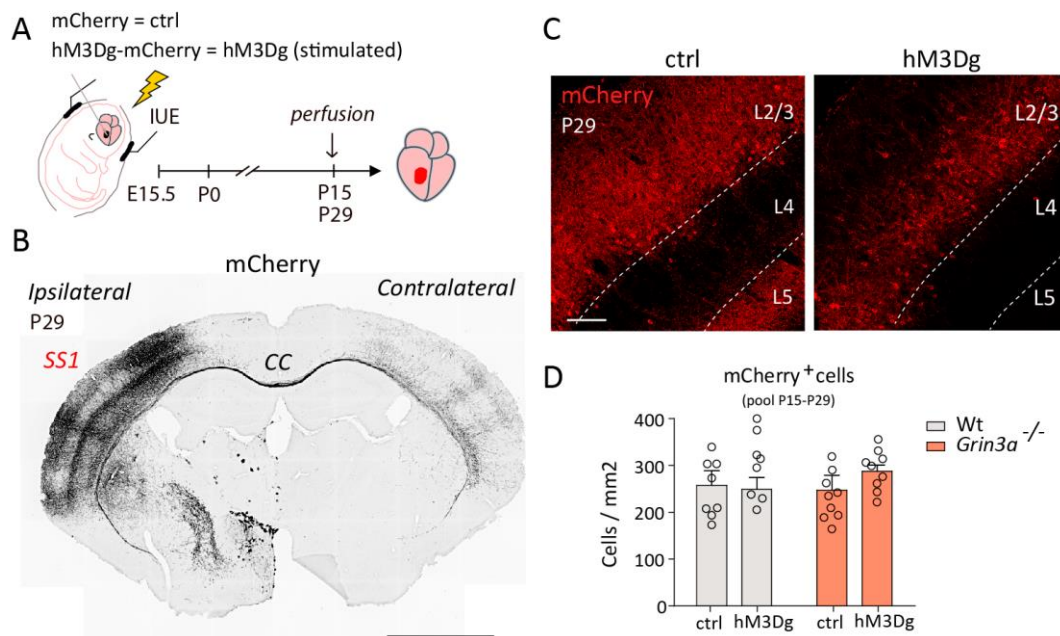


Figure 36. *In utero* electroporation of mCherry and hM3Dg-mCherry into SS1 layer 2/3 neurons. (A) Timing of mCherry (ctrl) and hM3Dg-mCherry (hM3Dg) IUE and mice perfusion at P15 or P29. (B) Confocal image of mCherry⁺ expression in SS1 L2/3 neurons, ipsilateral axonal projections in L5, CC and contralateral SS1 in a P29 mouse. (C) In control mice, there are filled somas and dendrites, whereas in hM3Dg mice, only cell bodies are intensely stained. (D) Quantification of mCherry⁺ layer 2/3 neurons in ctrl and hM3Dg both in Wt and *Grin3a*^{-/-} mice (n= 8-9 mice, pool of P15 and P29 mice; two-way ANOVA with Tukey's multiple comparison test). Scale bars: 2 mm (B) and 100 μ m (C).

To stimulate neuronal activity in the electroporated neurons, we administered CNO (1 mg/kg, i.p.) daily from P11-P15 or P22-29 (**Figure 37A**) and perfused mice immediately after the last injection. To confirm activity-stimulation by CNO, we measured the expression of the immediate early gene c-Fos, a established marker of neuronal activation. Both the number of c-Fos positive cells and c-Fos intensity were increased in L2/3 neurons electroporated with hM3Dg-mCherry but not with mCherry (**Figure 37C**). No differences in the number of c-Fos⁺ cells or c-Fos intensity per cell were observed between genotypes (**Figure 37D**).

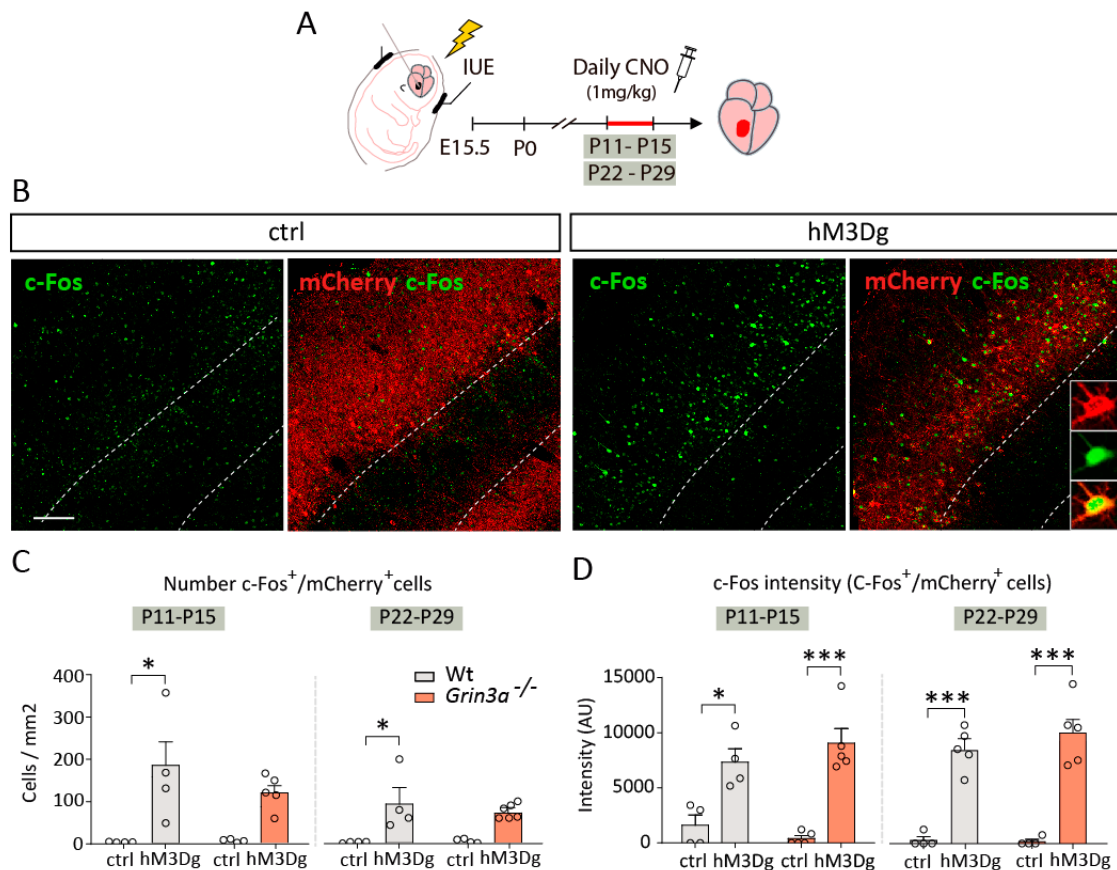


Figure 37. CNO administration turns on c-Fos expression in mCherry⁺ electroporated neurons. (A) Cartoons of CNO injection protocols, applied from P11 to P15 or from P22 to P29. (B) Representative images of P29 brains with increased c-Fos expression in mice electroporated with hM3Dg plasmids compared to ctrls. (C) C-Fos⁺/mCherry⁺ cell density (C) and C-Fos intensity (Integrated Density, measured with Arbitrary Unit, AU) in c-Fos⁺/mCherry⁺ cells (after applying a threshold to remove the background and low intensity cells) were significantly higher in hM3Dg electroporated brains compared to ctrls in both Wt and *Grin3a*^{-/-} mice (P11-P15 protocol)(n=4/5 mice per group; two-way ANOVA with Tukey's multiple comparison test, *p<0.05, ***p<0.001). Scale bar: 100 μ m.

We then tested the effects of chemogenetic stimulation in OPC proliferation and differentiation at the level of the corpus callosum where SS1-activated axons are located (**Figure 38A**).

In Wt mice, we observed a significant increase after stimulation in the number of OPCs as well as in their differentiation status at both P15 (**Figure 38B**) and P29 (**Figure 38C**), recapitulating previous findings (Mitew et al., 2018). Strikingly both OPC proliferation and differentiation in response to activity were impaired in *Grin3a*^{-/-} mice, with no differences in the density of OPCs and differentiated OLs in stimulated brains compared to controls. The data suggested that GluN3A-lacking OPCs may not be able to properly sense and respond to neuronal activity. Yet, this first set of experiments were conducted in constitutive GluN3A knockout mice that lack GluN3A in all cell populations, brain regions and ages, and we could not rule out contributions of GluN3A expression in other cell types.

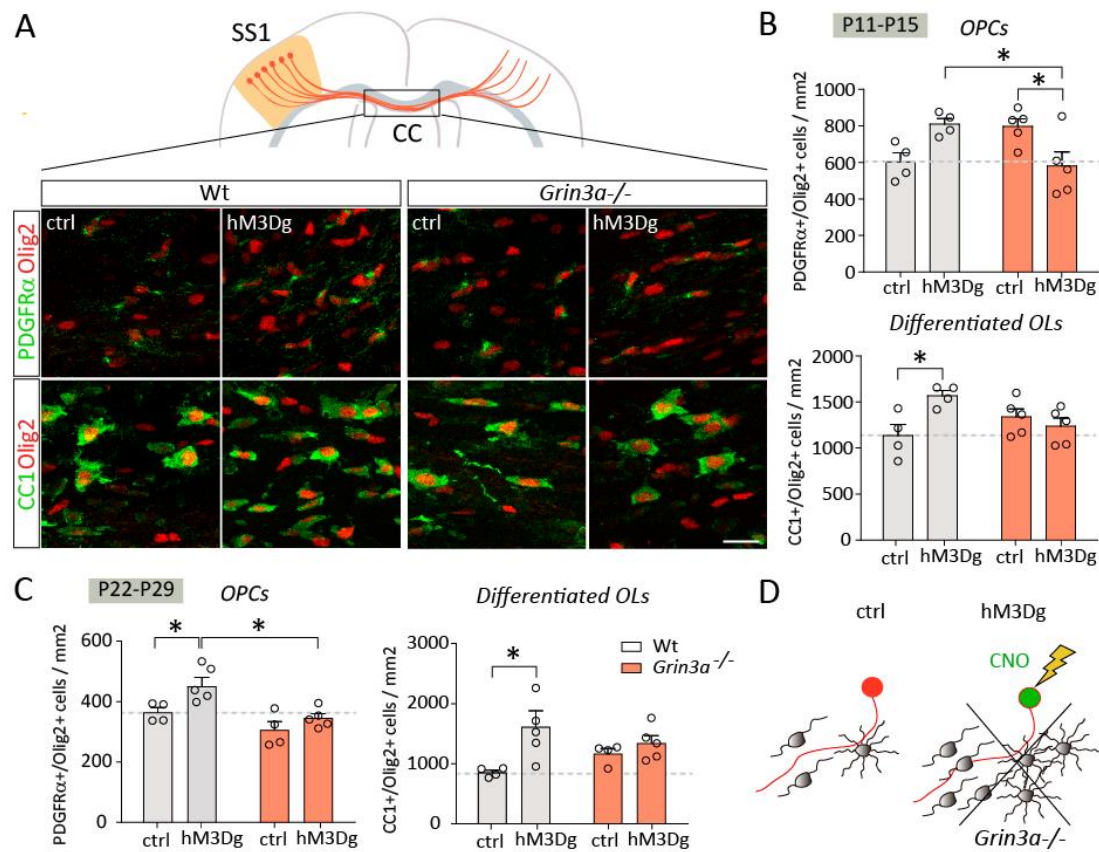


Figure 38. Loss of OPC proliferation and differentiation in response to chemogenetic stimulation of callosal axons in *Grin3a*^{-/-} mice. (A) Number of PDGFRα⁺ OPCs and CC1⁺ OLs was quantified in the CC where SS1-activated axons are located. Cell density quantifications after CNO injection from P11 to P15 (B) and from P22 to P29 (C) in Wt and *Grin3a*^{-/-} mice. (D) Cartoon showing the physiological response of OPCs upon activity stimulation prevented by GluN3A deletion (n=4/5 mice per group; two-way ANOVA with Tukey's multiple comparison test, *p<0.05). Scale bar: 20 μm.

7.4. Characterization of Cre-driver mouse lines for specific GluN3A deletion in oligodendroglial cells

To determine if the lost myelin plasticity was due to cell-autonomous GluN3A deletion from OPCs, we deleted GluN3A selectively from this cell population by crossing *Grin3a*^{fl/fl} mice with oligodendroglial-specific Cre-deleter lines. To choose the appropriate mouse line for our experiments, we began by characterizing Cre expression in 3 different mouse lines using a R26-tdTomato^{fl/fl} reporter line: *CNP*-Cre and *Sox10*-Cre, that target all the oligodendroglial cells, including OPCs, although *CNP*-Cre seems to be prevalent in differentiating OLs (see below); and *PDGFRα*-CreER^{T2}, that target newly-formed OPCs and their progeny at desired time points by induction with tamoxifen (TMX).

In P11-12 *CNP*-Cre mice, tdTomato was found in the majority of Olig2⁺/CC1⁺ OLs and some PDGFRα⁺-OPCs both in WM and GM (**Figure 39A**, upper and lower panels respectively). However, recombination was not specific as we found tdTomato also in non-oligodendroglial cells such as NeuN⁺ neurons (Tognatta et al., 2017). In P11-12 *Sox10*-Cre mice, tdTomato was found in a majority of Olig2⁺ cells (> 90% of cells in the regions analysed, **Figure 39B**). Colocalization with CC1 or PDGFRα in cortex and CC demonstrated specific targeting of entire OL lineage. Using an antibody against Cre, we confirmed Cre recombinase expression in OLs. In *PDGFRα*-CreER^{T2} mice, tdTomato expression was driven by perinatal TMX injection and appeared in PDGFRα⁺ cells and CC1⁺ cells that differentiated from the recombined OPCs (**Figure 39C**). In the WM tdTomato was mainly in CC1⁺ OPC-progeny while in the GM mainly in OPCs that still express PDGFRα⁺, as expected given different differentiation rates between WM and GM (Dimou et al., 2008; Vigano et al., 2013). While this mouse line is not presented in the current thesis, we have already generated *PDGFRα*-CreER^{T2} mice crossed with *Grin3a*^{fl/fl} mice that are in the process of being tested in the context of activity-dependent plasticity to establish unequivocally that GluN3A is involved in adult stages. Nevertheless, for the experiments described in this thesis we used *Sox10*-Cre mice crossed with our *Grin3a*^{fl/fl} mice to investigate the impact of GluN3A absence in oligodendroglial cells and discriminate their contribution to the myelination phenotype observed in the constitutive GluN3A knockouts.

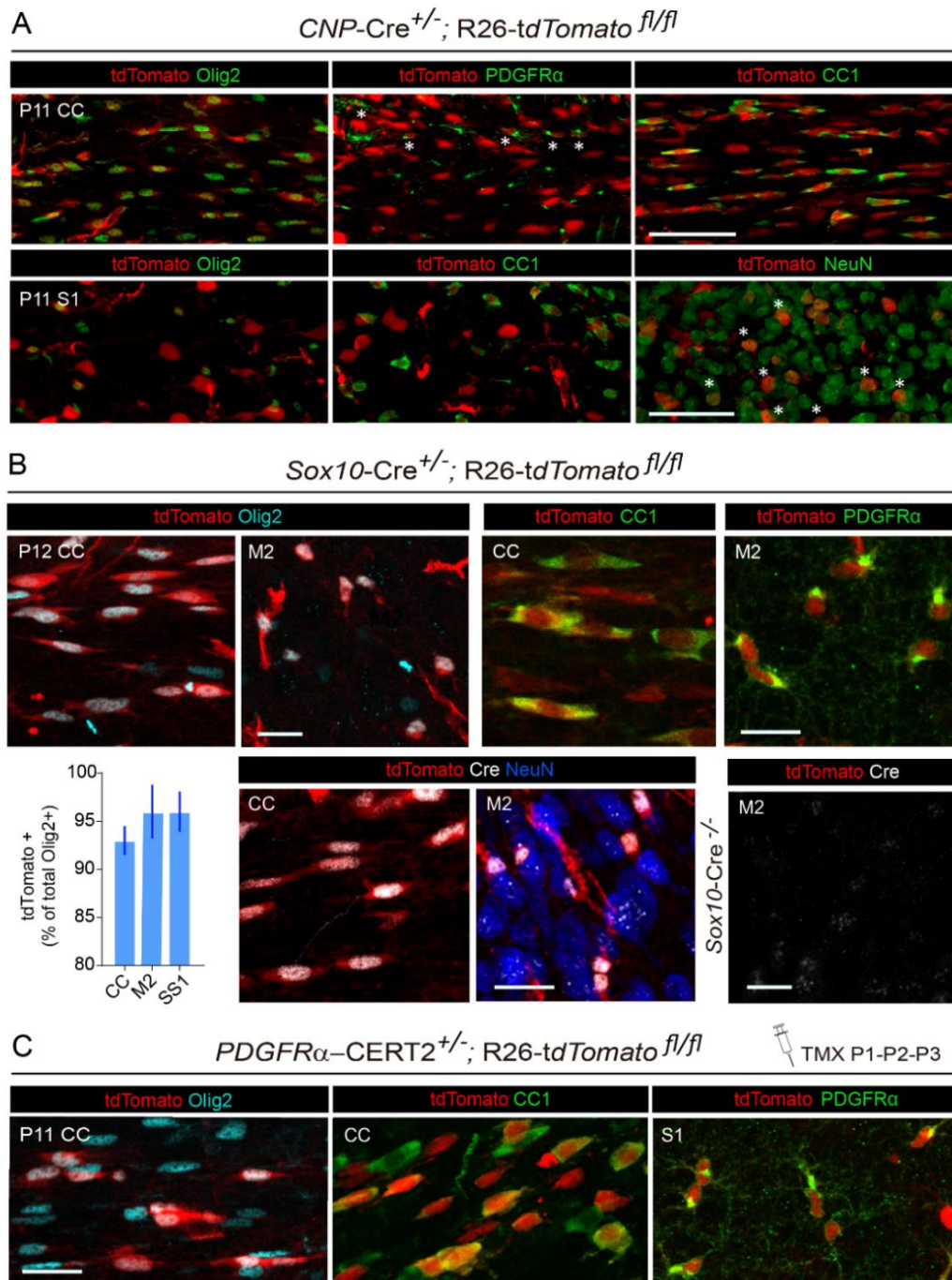


Figure 39. Characterization of Cre-driven mouse lines. (A) Analysis of tdTomato expression in *CNP-Cre* mice crossed with the R26-tdTomato reporter line, we found tdTomato expression in the oligodendroglial lineage. Unspecific recombination was detected in NeuN⁺ cortical neurons (bottom right panel). (B) In *Sox10-Cre* mice crossed with the R26-tdTomato reporter, tdTomato and Cre were selectively expressed by oligodendroglial cells and the recombination efficiency reached >90% both in WM and GM (bottom left graph). *Sox10-Cre^{-/-}* control littermate mice showed no expression of Cre. (C) Upon perinatal TMX injections, *PDGFRα-Cre^{ERT2}* mice showed selective recombination in Olig2⁺ cells, mainly CC1⁺ OPC-progeny in the WM and still PDGFRα⁺ in the GM. Scale bars: 60 μm (A) and 20 μm (B, C).

7.5. Loss of activity-dependent OPC plasticity in *Sox10-Cre^{+/-};Grin3a^{fl/fl}* mice

To investigate whether the block of OPC plastic responses upon stimulation in the constitutive knockout was due to the absence of GluN3A in OPCs, we conducted the DREADDs stimulation experiment in *Sox10-Cre^{+/-};Grin3a^{fl/fl}* mice. Additionally, we broadened our investigation by exploring alternative methods to stimulate neuronal activity and boost myelin plasticity, including physical exercise or motor skill learning paradigms.

7.5.1 Loss of OPC plasticity in response to chemogenetic activation of callosal axons activity in *Sox10-Cre^{+/-};Grin3a^{fl/fl}* mice

We electroporated mCherry and mCherry-hM3Dg plasmids in the neuroepithelium of E15.5 embryos of *Sox10-Cre^{+/-};Grin3a^{fl/fl}* and *Sox10-Cre^{+/-};Grin3a^{fl/fl}*. CNO was administered from P11 to P15 (**Figure 40A**), as previously described. Using c-Fos expression, we confirmed neuronal stimulation of SS1 cortical L2/3 neurons in both *Sox10-Cre^{+/-};Grin3a^{fl/fl}* mice and *Sox10-Cre^{+/-};Grin3a^{fl/fl}* littermates, which served as control (**Figure 40B**). We then assessed the effects of chemogenetic stimulation on OPC proliferation and differentiation in the corpus callosum (**Figure 40C**). As expected, control mice exhibited a significant increase in the number of OPCs and differentiated OLs following stimulation. However, this response was not observed in *Sox10-Cre^{+/-};Grin3a^{fl/fl}* mice (**Figure 40D, E**) demonstrating that cell-autonomous GluN3A expression is responsible for the loss of activity-dependent OPC plasticity.

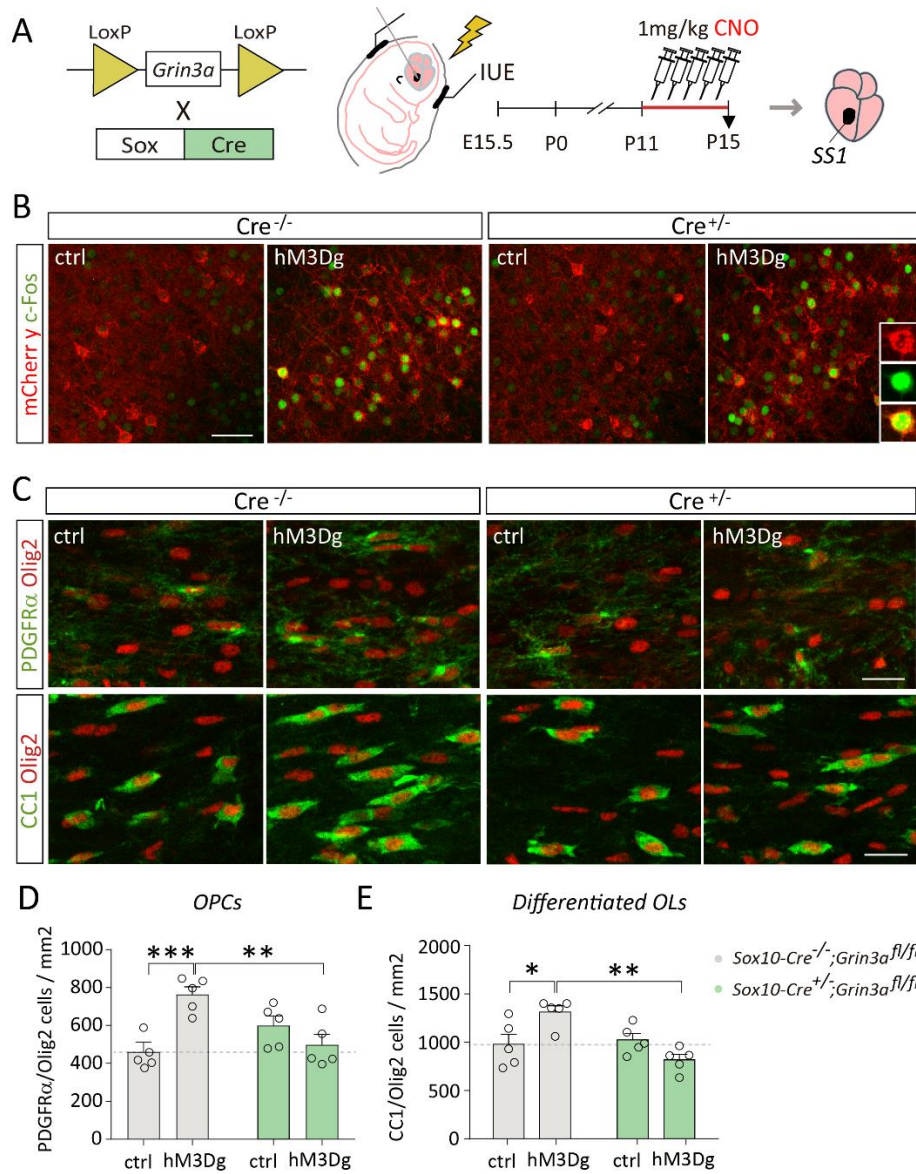


Figure 40. Loss of OPC proliferation and differentiation in response to chemogenetic stimulation of callosal axons upon OPC-specific GluN3A deletion. A) *Sox10-Cre^{+/-};Grin3a^{fl/fl}* mouse line used to specifically remove GluN3A from OPCs. CNO was injected from P11 to P15 and mouse perfused the next day. (B) Representative images of c-Fos activation in L2/3 neurons of hM3Dg electroporated brains in both Cre^{-/-} controls and Cre^{+/-} mice. (C) Representative images of OPCs (top) and differentiated OLs (bottom) in ctrl and stimulated corpus callosum of Cre^{-/-} and Cre^{+/-} mice. (D) Quantification of OPC (D) and differentiated OLs (E) density after stimulation (n=5 mice per group; two-way ANOVA with Tukey's multiple comparison test, *p<0.05, **p<0.01, ***p<0.001). Scale bars: 50 μ m (A) and 20 μ m (B).

7.5.2 Loss of OPC plasticity in response to natural stimulation of neuronal activity with chronic physical exercise in *Sox10-Cre^{+/-};Grin3a^{fl/fl}* mice

We next asked whether the outcome observed with DREADD stimulation of neuronal activity was recapitulated using natural paradigms that induce myelin plasticity. We first chose the treadmill as a chronic physical exercise protocol documented to enhance motor circuit-related myelin plasticity (Chen et al., 2019), and explored the response of OPCs lacking GluN3A.

We designed a variation of the protocol used by Chen and colleagues (2019) consisting of 5 days of exercise per week for 3 consecutive weeks, to minimize the contribution of factors such as mouse fatigue or refusal to run (Figure 41A). Every day the mice run on the treadmill for one hour at an average speed of 10 m/min. Here, rather than measuring the entire population of OPCs and OLs, we conducted fate-mapping of newly-formed OLs by injecting BrdU (50mg/kg daily) during the last 5 days of the protocol. Mice were perfused 4 days later to enable the differentiation of proliferating OPCs. Mice performance was tracked by monitoring the number and total time of mild shocks each mouse received to complete the entire running program. This parameter served as an indicator of learning at the beginning and of fatigue at the end of the protocol. Similar trends of shock increase across the experimental weeks were observed in *Sox10-Cre^{+/-};Grin3a^{fl/fl}* mice and *Sox10-Cre^{-/-};Grin3a^{fl/fl}* controls, with *Sox10-Cre^{+/-};Grin3a^{fl/fl}* mice exhibiting overall worse performance with higher shock scores across time (Figure 41B). However, our results show that treadmill performance cannot be considered a fine or accurate parameter of motor behavior and we have designed specific protocols to assess the motor phenotype of *Sox10-Cre^{+/-};Grin3a^{fl/fl}* mice (see 5.3).

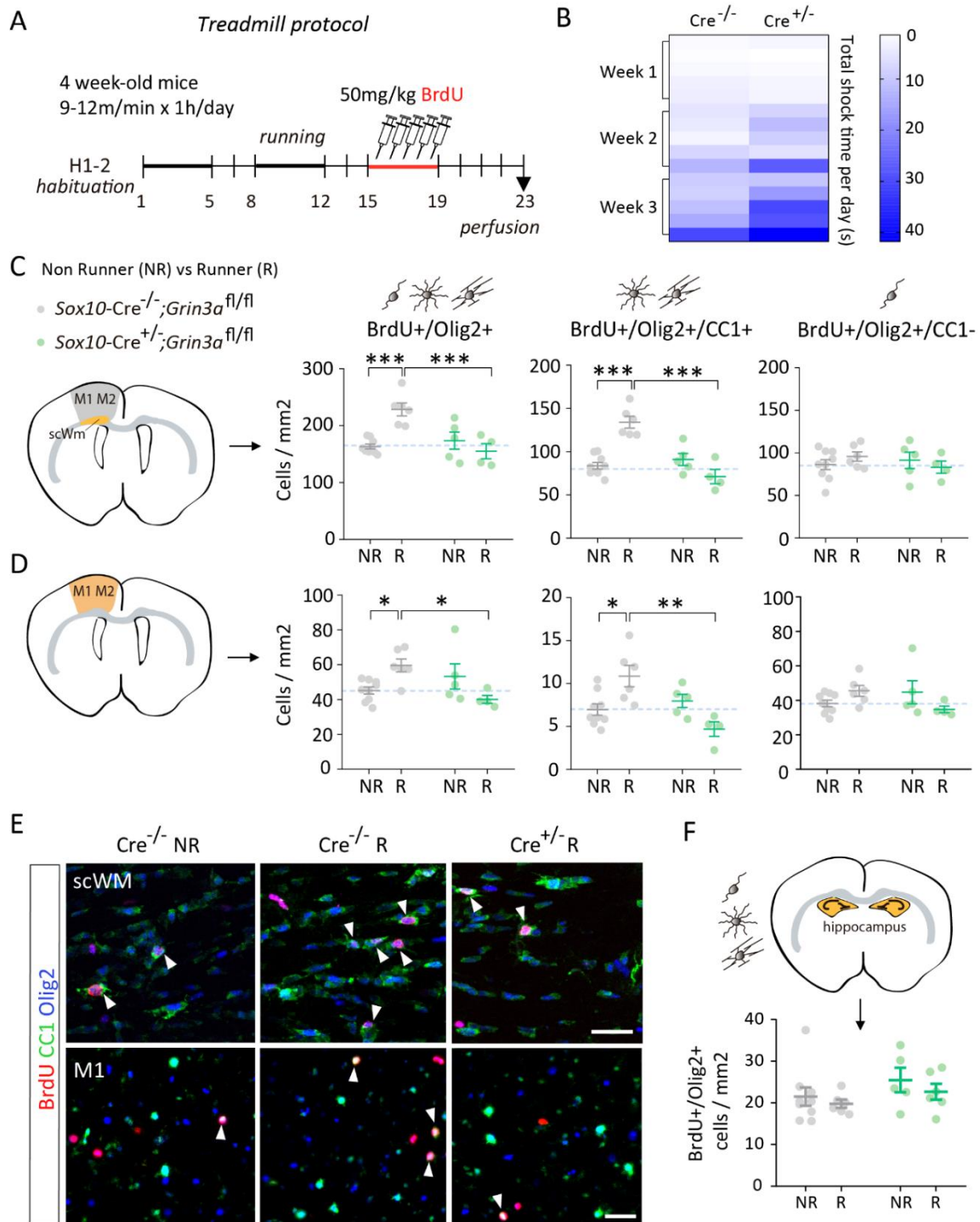


Figure 41. Loss of OPC plasticity in response to physical exercise in OPC-selective GluN3A knockout mice. (A) Chronic treadmill exercise protocol; BrdU was injected during the last 5 days. (B) Mice performance measured as the total time of shocks (s) received per day to continue running over the 3 weeks of training. Quantifications of newly-formed OLs (BrdU⁺) and differentiation state in scWM (C) and M1/M2 cortical areas (D) of non-runners and runners (NR and R) of the indicated genotypes. (E) Representative images of newly-formed OLs in the scWM and M1 of NR and R mice, acquired with a confocal and thunder microscope respectively. (F) Quantification of newly-formed OLs in the hippocampus (n=4/9 mice per group; two-way ANOVA with Tukey's multiple comparison test, *p<0.05, **p<0.01, ***p<0.001). Scale bars: 30 and 50 μ m.

To investigate the effect of treadmill running on oligodendrogenesis, we quantified the number of newly-formed OPCs (BrdU⁺/Olig2⁺) and their differentiation rate (BrdU⁺/Olig2⁺/CC1⁺) in the scWM under motor cortices as well as in primary and associative motor cortex (M1/M2) (Figure 41C, D). The absolute densities of newly-formed oligodendroglial cells were higher in WM compared to GM in both *Sox10-Cre^{+/+};Grin3a^{fl/fl}* mice and *Sox10-Cre^{-/-};Grin3a^{fl/fl}* controls non-runners. Differentiation rates also differed. In the scWM of non-runner control mice ~50% of BrdU⁺/Olig2⁺ cells became CC1⁺, while in M1/M2 only ~7% of BrdU⁺/Olig2⁺ were CC1⁺ in line with different differentiation rates between WM and GM. Running increased both OPC proliferation and differentiation in both regions of control *Sox10-Cre^{-/-};Grin3a^{fl/fl}* mice. In non-runner control mice, we counted an average of 180 BrdU⁺/Olig2⁺ cells/mm² of in the scWM, which significantly increased to 240 cells/mm² in runners. In M1/M2 the average count was 45 cells/mm², which increased to 60 cells/mm² in runners. In both regions, the ~35% increase in BrdU⁺/Olig2⁺ cell number after treadmill running culminated in increased differentiation by 4 days (~60 increase in the number of BrdU⁺/Olig2⁺/CC1⁺ mOLs relative to non-runners). No significant differences were found in CC1⁻ cells of runners compared to non-runners in both controls and *Sox10-Cre^{+/+};Grin3a^{fl/fl}*. No differences in newly-formed OLs were detected in non-motor areas such as the hippocampus (Figure 41F).

Together, our findings confirm that OPCs lose their ability to proliferate and differentiate in response to activity in the absence of GluN3A. We are conducting investigations at the level of light and electron microscopy to examine whether these cellular dynamics alterations result in changes in myelination.

7.5.3 A novel paradigm to study myelin plasticity and different aspects of motor learning using the Erasmus Ladder

Our treadmill experiments identified a need for paradigms that allow simultaneously studying myelin plasticity and behaviour. To address this, we have implemented a less explored paradigm, the Erasmus Ladder, based on skilled motor training in the Erasmus ladder (**Figure 42**, Staffa et al., 2023). This paradigm provides several advantages: it is shorter (8 days) and thus allows a finer dissection of time-courses of OPC differentiation and proliferation during fine motor skill learning, and has the capability for simultaneous and automated assessment of different aspects of motor performance and learning.

Briefly, the Erasmus Ladder consists of a horizontal ladder built of alternate high and low rungs equipped with touch-sensitive sensors, flanked by two goal boxes. The paradigm requires a finer motor ability than the treadmill or rotarod normally used for motor assessment. Some rungs can be randomly elevated to create an obstacle (unconditioned stimulus, US) that increases the difficulty of the motor task. A tone (conditioned stimulus, CS) can be applied prior to the obstacle for association studies (see **Material and Methods**). The test involves two phases: an initial phase where mice are trained to navigate the horizontal ladder ("fine motor learning"), and a second phase where an obstacle is presented in the path of the moving animal. The obstacle or perturbation can be unexpected ("challenged motor learning") or preceded by an auditory tone ("associative motor learning"). The protocol consists of four undisturbed and four challenge sessions (42 trials each, one session per day) (**Figure 42A**). During the protocol set-up, we screened a variety of read-outs (**Figure 42B**) to assess motor performance and learning in Wt mice during the first days as well as challenge motor learning and associative learning during the last 4 days. Time on ladder, % of trials with missteps, and step time were chosen based on reproducibility and information obtained.

Figure 32C shows how measurements of the time to cross the ladder yielded a significant learning curve from days 1 to 4 that could be fitted with a power regression curve ($R = 0.50$, $*p = 0.047$). A key parameter that determines the time taken to cross the ladder is the occurrence of missteps, defined as a high to low rung step. In line with the shortening of times on the ladder, the number of trials where mice made missteps (**Figure 42E**) decreased over undisturbed sessions as mice

learned to walk on the upper rungs and avoid the lower ones as a more efficient pattern to cross the ladder ($R = 0.90$, $***p < 0.0001$). Over the 4-day initial phase, Wt mice master the skill and cross the ladder by learning to adopt the most efficient running pattern and missteps occur rarely by day 4. With the beginning of challenge sessions on day 5, animals required more time to cross the ladder (**Figure 42D**) during US-only trials because of the unpredicted introduction of the obstacle day 4: 5.01 s; day 5: 7.84 s; paired t-test, $*p < 0.039$). Mouse performance improved from days 5 to 8, yielding a significant learning curve across US-only sessions ($R = 0.50$, $*p = 0.045$, orange). In associative learning trials, where the obstacle was paired with a tone, animals completed the daily sessions significantly faster relative to US-only trials ($R = 0.63$, purple; two-way repeated measure -RM- ANOVA, $*p = 0.028$). Finally, in control trials when the tone was presented alone (CS-only), a significant learning curve that resembled undisturbed sessions was reported ($R = 0.82$, $***p < 0.001$, blue).

Analysis of step patterns provided additional confirmation and enhanced sensitivity in detecting differences between US-only and associative trials. **Figure 42F** shows how the percentage of trials with missteps remained constant throughout US-only trials ($R = 0.01$, $p = 0.90$, orange), while a significant decrease in trials with missteps was observed during paired sessions ($R = 0.61$, $*p = 0.01$, purple). **Figure 42H** shows a significant difference between pre and post perturbation step times in US-only trials (two-way RM ANOVA, $*p = 0.05$) but not in paired trials where mice learned faster to overcome the obstacle. Control step times during undisturbed sessions are reported in **Figure 42G**.

Next, we compared the robustness of this protocol relative to the treadmill to induce OPC plasticity by injecting BrdU during the last 4 days of challenge sessions (**Figure 42A**) and quantifying newly-formed oligodendroglial cells and their differentiation in the scWM under motor areas two days later (**Figure 43A**). Preliminary quantifications in Wt revealed that Erasmus ladder training is a stronger inducer of oligodendrogenesis relative to chronic treadmill exercise: $\sim 33\%$ increase of total BrdU⁺/Olig2⁺ and $\sim 62\%$ increase of BrdU⁺/Olig2⁺/CC1⁺ cells in treadmill runners relative to non-runners vs $\sim 78\%$ increase in total BrdU⁺/Olig2⁺ and 225% increase of BrdU⁺/Olig2⁺/CC1⁺ cells in Erasmus Ladder trained mice relative to home cage (**Figure 43B, C**).

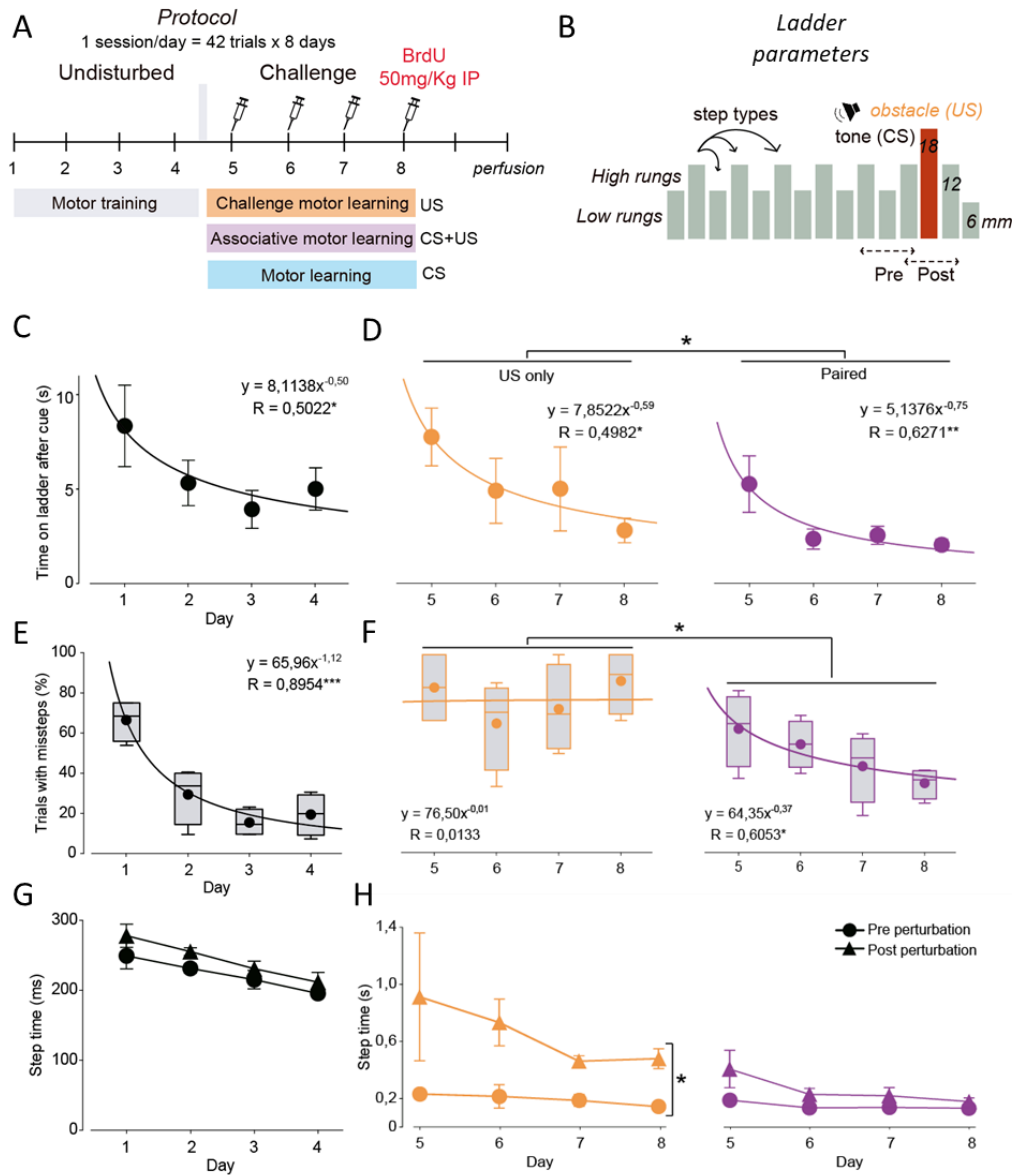


Figure 42. Monitoring fine and associative motor learning in mice using the Erasmus Ladder. (A) Erasmus ladder protocol. (B) Cartoon of the ladder and parameters. (C) Time on ladder during undisturbed session on days 1 to 4 and (D) during challenge sessions on days 5 to 8 (US-only in orange, paired in purple). Percentage of trials with missteps during days 1 to 4 (E) and 5 to 8 (F). Pre and post perturbation step time during days 1 to 4 (G) and 5 to 8 (H) (n=4 Wt mice; power non-linear regression analysis of the learning curves [C: *p = 0.047; D: *p = 0.047 and **p = 0.0093, US-only and Paired, respectively; E: ***p < 0.001; F: ns and *p = 0.013, US-only and Paired, respectively] and two-way RM ANOVA between trial types and pre and post-perturbation step times within the same session (D: *p = 0.028; F: *p = 0.032; H: *p < 0.05 and ns (US-only and Paired, respectively)).

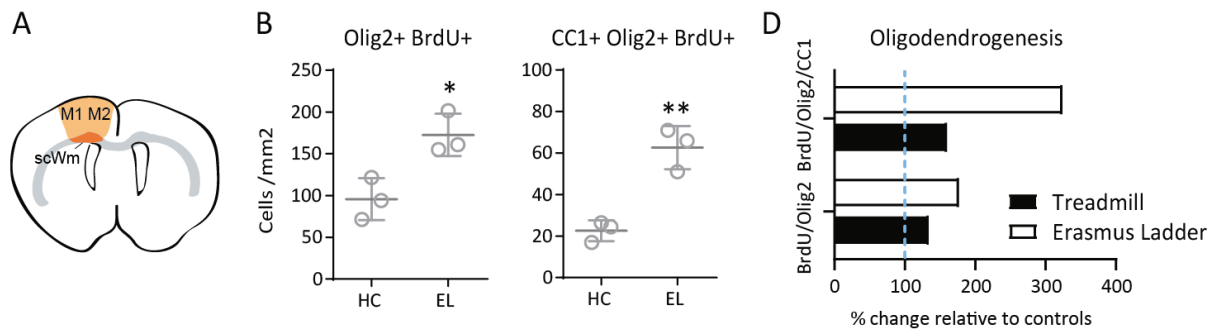


Figure 43. Erasmus Ladder is a strong inducer of oligodendrogenesis. (A) Cartoon of the area of the analysis in the scWM under motor cortices. (B) Quantifications of total newly-formed and differentiated OL cell densities in Erasmus Ladder (EL) trained vs home cage (HC) mice. Comparison between treadmill and Erasmus Ladder ability to induce oligodendrogenesis, expressed as % change (relative to Wt controls, NR and HC, respectively) in BrdU⁺/Olig2⁺ and BrdU⁺/Olig2⁺/CC1⁺ cells (n=3 mice; two-tailed unpaired t-test, *p<0.05. **p<0.01).

7.6. Molecular properties of plastic GluN3A-expressing OPCs

Next, we asked what is different in GluN3A-lacking OPCs that contributes to plasticity loss. For this, we compared the transcriptome of OPCs isolated from P7 Wt (**Figure 21**) and *Grin3a*^{-/-} forebrains using RNA-seq (**Figure 44**). Postnatal GluN3A-lacking OPCs exhibited signatures of aged OPCs compared to control OPCs. Among the 360 upregulated genes with a log2FC > 0.26 and a pvalue < 0.05, we found elevated levels of a set of immune-related genes and inflammatory networks (**Figure 44A**; *GO: Response to interferon-β*, 18 genes with FDR: 3.4E-15 and fold enrichment: 20.3; *GO: innate immune response*, 48 genes with FDR: 4.8E-13 and fold enrichment: 3.8; *GO: Response to cytokine*, 55 genes with FDR: 2.1E-14 and fold enrichment: 3.7). The gene expression pattern resembles transitions to immune-competent states in OPCs in old mice (Spitzer et al., 2019) and confers susceptibility to EAE in mice (Falcao et al., 2019) and MS in humans (Meijer et al., 2022) (**Figure 44B**). Considering that one of the most prominent molecular alterations in aged OPCs is down-regulation of GluN3A expression (Spitzer et al., 2019, Neumann et al., 2019, see **Figure 22**) and that aged OPCs become unresponsive to pro-differentiation signals with a lower regenerative capacity, our result that postnatal OPCs shown signals of aging or disease open up possibilities for research and interventions.

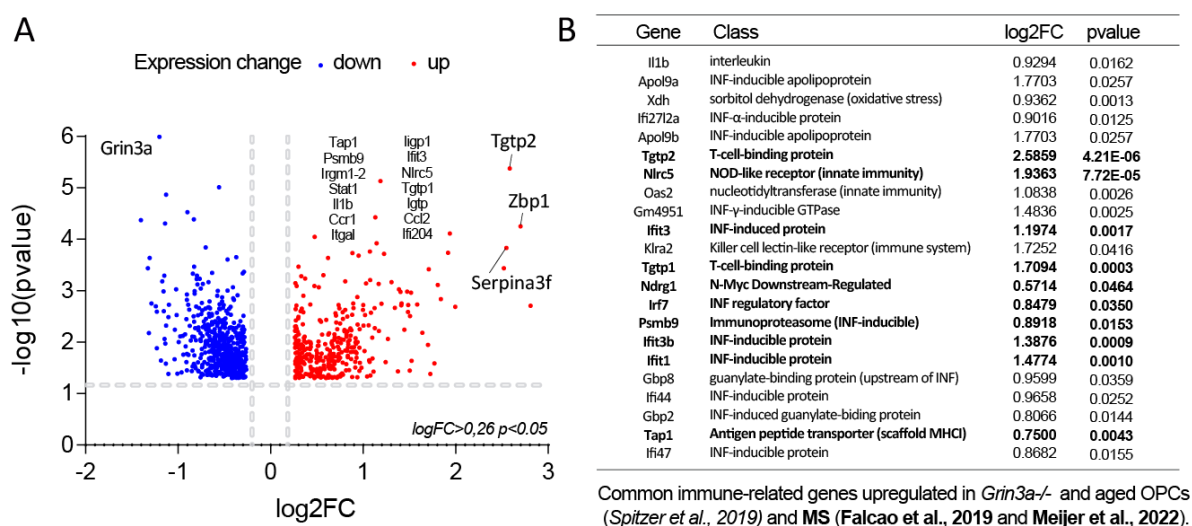


Figure 44. The transcriptome of GluN3A-lacking OPCs mirrors that of aged and diseased OPCs. (A) Volcano plot of downregulated (blue) and upregulated (red) genes in MACs isolated OPCs from P7 *Grin3a*^{-/-} forebrains relative to Wt (threshold: log2FC > 0,26 and pvalue < 0.05). Note *Grin3a* among the highest downregulated genes as control. (B) Table of common immune-related genes upregulated both in GluN3A-lacking OPCs and aged OPCs (Spitzer et al., 2019) as well as EAE-OPCs (Falcao et al., 2019) and human MS-OPCs (Meijer et al., 2022) (bold).

7.7. Preliminary insights into GluN3A role in remyelination

The natural regenerative process following demyelination, known as remyelination, is typically robust in younger individuals but becomes increasingly prone to failure with age or in persistent inflammatory condition associated with myelin-related diseases. Our discovery that the myelin plasticity impairment in OPC-lacking GluN3A mice mirrors characteristics seen in aging or disease states prompted us to investigate remyelination in this context. We used a toxin-induced demyelination model by injection of lysolecithin (LPC). Compared to other demyelination models, stereotaxic LPC injection has the advantage of making demyelinating lesion in specific regions leaving unaffected the surrounding tissue. Moreover, the LPC-induced demyelination model elicits a synchronized and successive response of OPC across days' post-injections (dpi) in adult mice: first a phase of OPC migration and proliferation in the lesion site, by 7 dpi, followed by differentiation and (re)-myelination, by 14 dpi. A pilot analysis demonstrated that the remyelination of focal lesions induced by injection of LPC in the anterior corpus callosum (**Figure 45A, B**) was impaired in adult *Sox10-Cre^{+/-};Grin3a^{fl/fl}* mice compared to controls. No main differences were found in the number of OPCs recruited and proliferated in the lesion area at 7dpi (end of the proliferation phase), with a similar reduction in OPC numbers by 14dpi. However, the number of differentiated OLs became significantly lower in GluN3A-lacking mice from 7dpi to 14 dpi (phase of OPC maturation) (**Figure 45C, D**).

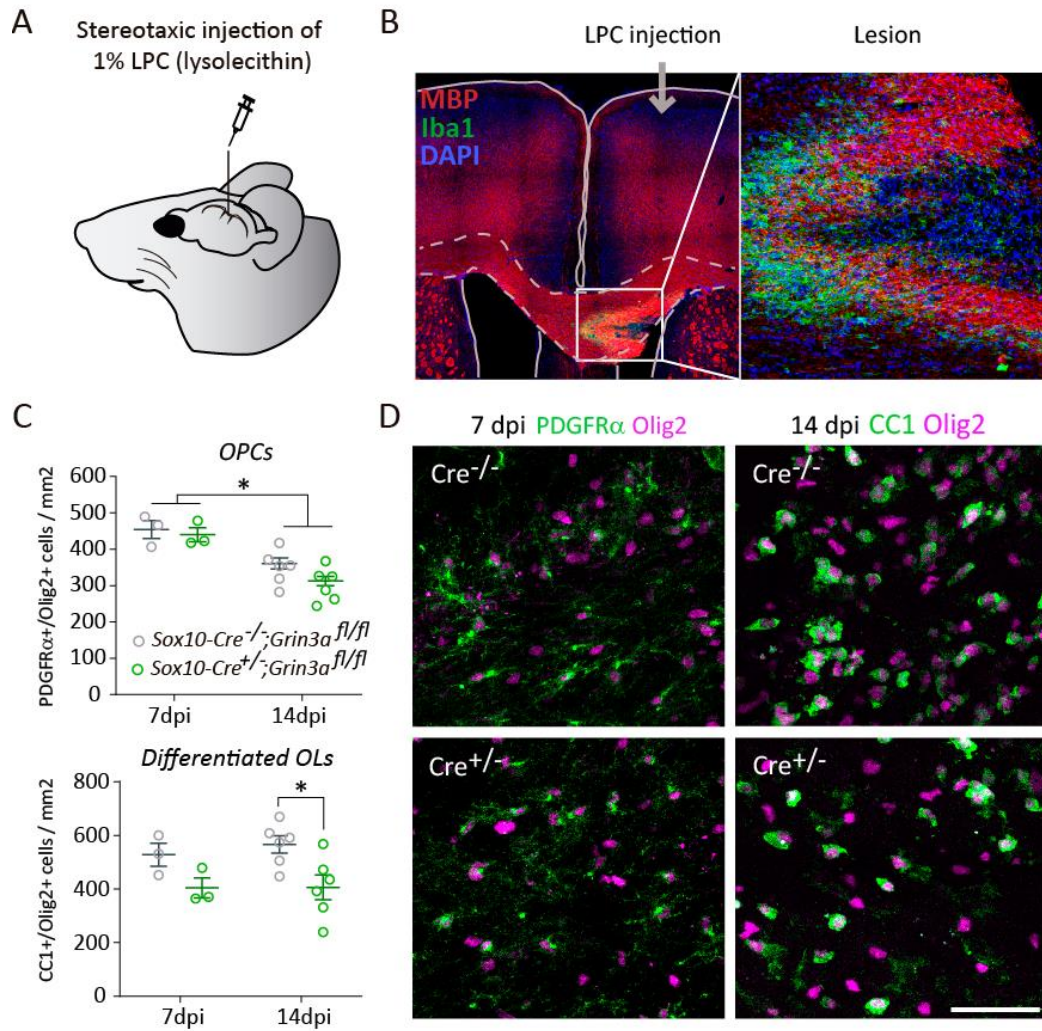


Figure 45. OPC responses after lysolecithin-induced focal demyelination in the anterior corpus callosum. (A) LPC was injected in the anterior corpus callosum under anaesthesia with a stereotaxic apparatus (coordinates respect to bregma: -1 mm lateral, +1.3 mm anterior, -1.7 mm deep). (B) Coronal slices stained with MBP and Iba1 to identify the lesion site: the demyelinated area lacks MBP and the remyelinated area is characterized by microglia proliferation (green) and intense MBP (high magnification). (C) Quantification of OPC and differentiated OL densities in the lesion at 7 and 14 dpi. (D) Representative images of OPCs at 7 dpi and mOLs at 14 dpi, in control and OPC-lacking mice (n=3/6 mice per group, two-way ANOVA with Tukey's multiple comparison test, *p<0.05.). Scale bar: 50 μ m.

8. DISCUSSION

Author: *Alice Staffa*

Work in the last decade has revealed that not only neurons but other brain cells are capable of plasticity. A pre-eminent example is myelin that was previously seen as a stable insulator but is now recognized as enormously dynamic and regulated by neuronal activity and environmental experience to adapt neural circuits to changes in life experience (de Faria et al., 2021). Beyond the interest of a basic biological understanding, myelin plasticity has become an area of intense study as a point of entry to foster myelination to enhance learning or restore lost myelin in pathological conditions. Two lines of evidence support this idea. First, human studies where learning of cognitive or motor skills such as juggling or piano playing induces WM changes in task-related regions (Bengtsson et al., 2005; Scholz et al., 2009). Second, observations that neuronal activity modulate OPC proliferation and differentiation in pathological settings (Gautier et al., 2015; Ortiz et al., 2019; Geraghty et al., 2019), and pilot studies supporting interventions like aerobic exercise and motor/cognitive rehabilitation to alleviate MS symptoms (Feinstein et al., 2023).

The discovery that glutamatergic axons form synapse-like contacts with OPCs revealed a route for OPCs to “listen” and respond to neuronal activity and axonal signals (Bergles and Jahr, 2000) and opened a path to harness myelin plasticity and identify targets that foster myelination. The idea was that signaling via axon-OPC synapses regulates OPC differentiation to favour the myelination of electrically active axons (de Biase et al., 2010; Karadottir et al., 2008). But while OPCs express a variety of ionotropic and metabotropic glutamate receptors which make them able to sense glutamate released by axons, attempts to link AMPA- or NMDA-type receptors to OPC differentiation and myelination have been disappointing - with only moderate and controversial effects of deleting specific receptor subunits (de Biase et al., 2011; Kouioumtzidou et al., 2017).

A breakthrough was the discovery that OPCs express NMDARs of unusual composition - including the non-conventional GluN3A subunit (Karadottir et al., 2005; Salter and Fern, 2005; Burzomato et al., 2010). Neuronal GluN3A-NMDARs (Perez-Otaño et al., 2001) play essential roles in maintaining plasticity niches in young brains by modulating glutamate signaling (Perez-Otaño et al., 2016; Conde-Dusman et al., 2021). My Thesis work demonstrates a more general role of GluN3A in plasticity control in OPCs, with commonalities to known roles in neuronal synapses. Below we summarize and discuss our main findings and propose a working model that stemmed from our results.

GluN3A is expressed in OPCs

Initial reports described GluN3A expression in oligodendroglial cells and correlated the low Mg^{2+} block of NMDA currents recorded in oligodendroglial cells with the kinetic and pharmacological properties of recombinant receptors expressing GluN1, GluN2C and GluN3A (Karadottir et al., 2005; Burzomato et al., 2010). Using our or published bulk and single cell transcriptomic resources, we now confirm that GluN3A (encoded by the *Grin3a* gene in rodents, *GRIN3A* in humans) is expressed in oligodendroglia. Within the OL lineage, GluN3A mRNA is restricted to a subset of postnatal and adult OPCs and OPCs committed to differentiate. Expression is downregulated with cell maturation (**Figure 20, 21**) and declines during brain aging (**Figure 22**). Histological analysis of young mouse brains using FISH combined with OPC immunolabeling and electron microscopy showed that *Grin3a* mRNA and GluN3A protein are located in OPC processes surrounding axons and thus well placed to sense axonal signals (**Figure 23-25**).

OPCs populate the CNS early on and remain through life, but how activity couples their differentiation with the preferential myelination of selected axons is largely unknown. After division and cell cycle exit, OPCs in the postnatal brain “pause” in a “dormant” state that lasts 3-8 days (Hill et al., 2014). A similar transient suppression of OPC proliferation and differentiation into mOLs has been observed during the first stages of learning (Bacmeister et al., 2020). This intermediate state is poorly defined but creates a window of opportunity where OPC fate can be modulated by changes in the environment to ensure myelination of appropriate axons, and could be the point of divergence between intrinsic activity-independent and activity-dependent OPC differentiation programs. In line with this, GluN3A expression seems to be a property of a subset of OPCs (**Figure 20C**); with estimates varying across studies, ages and potentially regions. Our pilot study using electrophysiological recordings of fluorescently labeled OPCs confirms this heterogeneity and shows that about 53% of OPCs in postnatal-young brains (between P7 and P40) had GluN3A-mediated currents (**Figure 26**). Future works should address the key question related to the nature of the receptor that sustains OPC plasticity: tri-heteromeric GluN1/2/3A NMDARs that respond to glutamate or di-heteromeric GluN1/3A receptors that respond to glycine or a mixture of receptors? Both are expressed by OPCs, and the recent development of

pharmacological tools, including positive allosteric modulators (PAMs) and negative allosteric modulators (NAMs) (Hansen et al., 2018) with selectivity for GluN3A containing receptors, like the NAM EU1180-438 (Zhu et al., 2020) will help address this issue.

Constitutive GluN3A deletion induces premature neuronal circuit myelination

During critical periods of postnatal development, a regulated switch from juvenile (containing GluN2B or GluN3A) to mature (containing GluN2A) NMDAR subtypes gates the selective maturation and stabilization of excitatory synapses to allow the formation of precise neural circuits (Paoletti et al., 2013; Perez-Otaño et al., 2016). Work from our laboratory highlighted a crucial modulatory role of non-conventional NMDARs containing GluN3A subunits (GluN3A-NMDARs), that limit juvenile plasticity and guide this type of experience-dependent synapse selection (reviewed in Perez-Otaño et al., 2016). The current idea is that GluN3A-NMDARs fulfill a dual role as: 1) “synapse brake”, by maintaining synapses in an immature state until the arrival of sensory experience; 2) “synapse selector” with GluN3A removal gating the emergence of local mechanisms for maturation of active synapses.

My Thesis work show that GluN3A in OPCs plays an additional role as a regulated brake to control the timing and coupling to activity of postnatal myelination. Using transcriptomics (Figure 27, 28) and histological analysis (Figure 30-34), we find that OPC differentiation and myelination are accelerated in WM and GM regions of P11 *Grin3a*^{-/-} brains compared to age-matched wild-type controls. Differences are less apparent at P18, indicating either a transient defect with compensatory mechanisms taking place or a finer later-stage phenotype that is undetectable with our methods due to the massive developmental enhancement in myelin gene expression (Figure 28D). The latter explanation is supported by western blot data (Figure 29) showing that myelin-related proteins are still expressed at higher levels in *Grin3a*^{-/-} forebrains at P18 (even if to a lesser extent compared to differences observed at P11). Additionally, 3D-cell reconstruction reveals that myelinating OLs in the upper layers of SS1 exhibited a more complex morphology with higher numbers of processes and myelin sheaths at P18 (Figure 34).

While the accelerated or increased myelination observed could potentially be attributed to enhanced OPC responses to neuronal activity, several observations led us to discard this

hypothesis. First, the increased myelin deposition was generally observed across brain areas, independent of the timing of arrival of neuronal activity. This was particularly evident in V1, where the phenotype was observed at P11, prior to eye opening, but not at P18 (**Figure 31B**). Second, the preferential myelination of large caliber axons in *Grin3a*^{-/-} mice (**Figure 35E**) suggested uncoupling of OPC differentiation from axonal signals distinct from axon caliber. Taken together, these findings pointed towards a predominance of activity-independent myelination programs in the absence of GluN3A that continue beyond its typical time window, with OPCs only responding to physical cues like axon caliber in detriment of adaptation to neuronal signals. The acceleration phenotype is further consistent with a loss of the OPC dynamic pause state in absence of GluN3A and the adoption of a “fast-forward” differentiation mode that does not respond to activity signals.

GluN3A support activity-dependent plasticity capabilities of OPCs

Taken our results together with GluN3A neuronal roles in maintaining dynamic plasticity niches (Pérez-Otaño et al, 2016), we proposed that GluN3A keeps OPCs in the paused plastic state, “waiting” for the appropriate axonal trigger to initiate differentiation and directed myelin production (**Figure 46**).

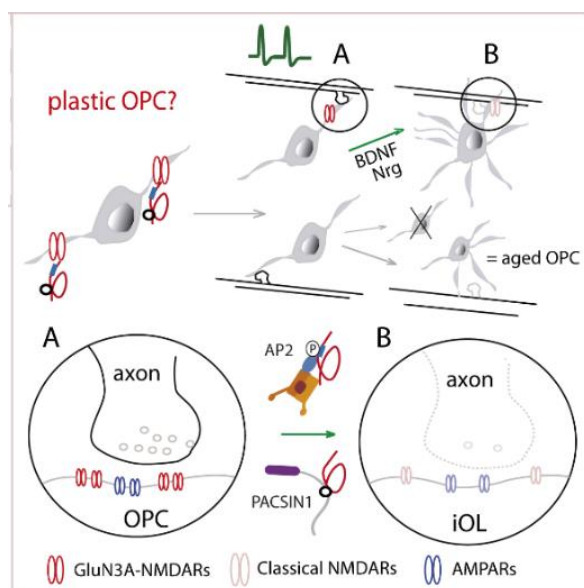


Figure 46. Working model for GluN3A roles in modulating activity-dependent myelination. Putative intermediate stage between OPCs and iOLs: a plastic OPC lineage cell that express GluN3A and senses neuronal activity or signals released by active axons (i.e. BDNF, Nrg1) that would trigger GluN3A down-regulation and OPC differentiation. By contrast, GluN3A-lacking OPCs in GluN3A knockout mice or aged brains fail to sense axonal signals and proceed via an intrinsic myelination program, with preference for larger axons and independent of axonal activity that prefers small caliber axons (Gautier et al., 2015). (A) Axon-OPC synapse of a plastic, GluN3A expressing OPC. (B) GluN3A down-regulation by activity-dependent signals within the GluN3A C-terminal tail and disassembly of the receptive machinery after OPC differentiation in response to signals.

In this model, GluN3A would be down-regulated by activity signals that unleashed OPC maturation and myelination of appropriate axons. If so: the plastic OPC state would be missing in absence of GluN3A; and differentiation would be insensitive to axonal signals and instead respond to intrinsic cues. To directly assess the status of activity-dependent myelination, we directly stimulated neuronal activity with DREADDs and studied OPC responses in absence of GluN3A. First evidence came from constitutive GluN3A knockout mice, and was later validated by generating a mouse line where GluN3A was specifically deleted in oligodendroglial cells (*Sox10-Cre^{+/+};Grin3a^{fl/fl}* mice). Our results demonstrated that OPCs-lacking GluN3A fail to differentiate in response to chemogenetic stimulation of callosal axons (**Figure 38, 40**). This results further support our hypothesis that in postnatal *Grin3a^{-/-}* mice OPCs adopt a “fast-forward” differentiation mode that does not respond to activity signals.

We went one step further and explored the ability of natural paradigms that induce myelin plasticity, starting with a simple chronic physical exercise protocol based on the work of Chen et al., 2019. Here it was necessary to carefully titrate the time, speed and frequency of running as mice tended to abandon the task. Again we found that the physiological increase in OPC proliferation and/or differentiation after neuronal activity stimulation in the treadmill observed in wild-type mice was abrogated in *Sox10-Cre^{+/+};Grin3a^{fl/fl}* mice (**Figure 41**). We additionally set up a new paradigm of motor skill learning, the Erasmus ladder and tested its ability to stimulate myelin plasticity (**Figure 42**). This paradigm provided several advantages: it has a short duration (8 days) allowing finer dissection of time-courses of OPC differentiation and proliferation; it allows simultaneous and automated assessment of different aspects of motor learning; it does not induce fatigue unlike other motor tests such as the rotarod or treadmill; and it is a stronger inducer of OPC proliferation and differentiation in wild-type mice (**Figure 43**). The stronger myelin plasticity induction is in-line with findings previously obtained using complex wheel paradigms (McKenzie et al., 2014; Xiao et al., 2016). This holds significant translational relevance, as it opens doors for future investigations into a synergistic approach involving genetic restoration of GluN3A to restore activity-dependent OPC plasticity alongside behavioral rehabilitative interventions, increasing feasibility and efficacy in clinical settings.

Lundgaard and colleagues (2013) shed light on signals involved in GluN3A removal. For instance, GluN3A is down-regulated by glutamate and pro-differentiation axonal signals like NRG1 and BDNF that induce a switch to NMDAR-dependent myelination. BDNF signaling is involved in intracellular NMDAR trafficking (Caldeira et al., 2007), is one of the molecules to date implicated in activity-dependent myelination (Geraghty et al., 2019), and could be a key GluN3A upstream factor. These data support the idea of GluN3A as a regulated switch that senses activity and signals OPC exit from the paused plastic state, analogous to neurons where built-in activity-dependent signals target GluN3A for removal and prime synapses for maturation (Perez-Otaño et al., 2016).

GluN3A declines with age and deletion confers aging features to OPCs

The regenerative capacity of the widespread OPC population deteriorates and eventually fails in the aging or diseased CNS. Aged OPCs become unresponsive to pro-differentiation signals (Neumann et al., 2019), posing intrinsic constraints in therapeutics aimed at enhancing OPC differentiation. One of the most prominent molecular alterations in aged OPCs is down-regulation of GluN3A expression (**Figure 22**; from datasets in Spitzer et al., 2019, Neumann et al., 2019) that we demonstrated to be an important factor for OPC plasticity in response to activity.

We found that OPCs isolated from GluN3A knockout forebrain exhibit signatures of aged OPCs. This include elevated levels of a set of immune-related genes and inflammatory networks (**Figure 44**) such as: T-cell binding genes (*Tgtp1-2*), serine peptidase inhibitors (*Serpina3f*), z-DNA-binding proteins (*Zbp1*), NOD-like receptors (*Nlrc5*), interleukins (*Il1b*), interferon-response genes (*Psmb9*, *Irf7*, *Ifit1-3*, *Ifi44-47-209*, *Stat1*) and major histocompatibility (MHC-I and II) genes (*Psmb9*, *Tap1*). The gene expression pattern resembles OPCs in old (Spitzer et al., 2019) and EAE mice (Meijer et al., 2022). scRNAseq analysis from Falcao and colleagues (2018) further suggests that a disease-associated subpopulation of OPCs with reduced GluN3A expression, distinct from the OPC population found in healthy mice, emerges in the spinal cord of adult EAE mice, model of MS. Future analysis will be needed to investigate the ability of GluN3A-lacking OPCs to respond to pro-differentiation signals and their similarities with the behavior of aged OPCs *in vitro*. It will be necessary as well to assess GluN3A expression in human samples of MS patients to determine if it declines not only with age but also disease factors.

Relevance for fostering remyelination in disease states

Much of advanced MS results from disrupted communication between the axons and the myelin sheath, which deprives nude axons of crucial metabolic support. Thus a path to devise neuro-restoration therapies is to promote myelin repair and regenerate the functional axon-myelin unit. A main obstacle is that remyelination, the spontaneous response to focal demyelinating lesions, is very efficient in young people but becomes slower and eventually fails with aging - as is the case for most regenerative processes. This age-dependent decline in myelination capacity is thought to be a major contributor to irreversible, progressive MS often lasting several decades but the reasons are poorly understood. Intriguingly, postmortem studies of demyelinated plaques from MS patients show limited remyelination despite available OPCs. This led to the notion that the age-dependent myelination failure stem from a decrease in the differentiation potential of OPCs. A challenge has been to find ways to enhance their responses and sustain their capacity to produce myelin throughout life by identifying and overcoming the aging factors that limit their function. And identifying and targeting the mechanisms that promote (or interfere with) OPC differentiation and myelination of appropriate axons has been identified as critical to devise effective therapeutic interventions. While this information had been missing, recent discoveries implicate intrinsic (e.g. disrupted mTOR signaling, Neumann et al., 2019) or extrinsic (e.g. niche stiffness, Segel et al., 2019) age factors.

Along with driving experience-dependent myelination, neuronal activity modulates OPC proliferation and differentiation in pathological settings (Gautier et al., 2015; Ortiz et al., 2019). This suggested that fostering activity-dependent myelination by targeting GluN3A might be a novel therapeutic opportunity to restore myelination capabilities in aged brains or disease states.

Thus we tested whether OPC-specific *Grin3a* loss of function modifies OPC differentiation and remyelination in response to focal demyelinating lesions. Our pilot analysis demonstrated defects in the remyelination process of focal LPC lesions (**Figure 45**) in adult *Sox10-Cre^{+/+};Grin3a^{fl/fl}* mice compared to controls. Electron microscopy will be additionally required to directly test whether GluN3A deletion impedes effective remyelination.

Perspectives

Of the glutamate receptors expressed by OPCs, GluN3A-NMDARs are the first to be linked to activity-dependent myelin plasticity, with their down-regulation a culprit of the inefficient capacity to regenerate myelin in aged brains. Quiescence is essential for maintaining cell populations in reserve for tissue regeneration and repair, and restoring the population of GluN3A-expressing OPCs offers a promising avenue for therapeutic intervention. Ongoing and future work will aim at providing a mechanistic understanding of the molecular sensors, cell biological, transcriptomic and signaling pathways that mediate activity-dependent OL differentiation and myelination, as well as of the heterogeneity and state transitions of OPCs and how they determine their plasticity properties and dynamics.

9. CONCLUSIONS / CONCLUSIONES

1. GluN3A is expressed in a subset of postnatal and young adult OPCs, where it localizes to OPC processes contacting axons to be myelinated.
2. Genetic GluN3A deletion accelerates postnatal OPC differentiation and myelination independently of the timing of arrival of neuronal activity inputs, suggesting predominance of activity-independent myelination events.
3. OPC proliferation and differentiation responses to chemogenetic axonal stimulation or chronic physical exercise is prevented in constitutive and in OPC-selective GluN3A knockout mice.
4. The capacity to induce OPC plasticity can be modulated by refining behavioral interventions.
5. OPC-lacking GluN3A display gene expression signatures characteristic of aging and disease-associated OPCs, in line with their loss plasticity properties.
6. GluN3A expression is required for OPC differentiation responses aimed to repair adult demyelinated lesions.

1. GluN3A se expresa en una parte de OPC postnatales y adultos, y se localiza en los procesos de OPC que contactan con los axones que tienen que ser mielinizados.
2. La ablación genética de GluN3A acelera la diferenciación postnatal de OPC y la mielinización independientemente del momento de llegada de la actividad neuronal, lo que sugiere un predominio de eventos de mielinización independientes de la actividad.
3. Las respuestas de proliferación y diferenciación de OPC a la estimulación quimiogénica de los axones o al ejercicio físico crónico se previenen en ratones knockout para GluN3A constitutivos y selectivos para OPC.
4. La capacidad de inducir la plasticidad de OPC se puede modular refinando las intervenciones conductuales.
5. Los OPC posnatales que carecen de GluN3A muestran características de envejecimiento y enfermedad, de acuerdo con su pérdida de propiedades de plasticidad.
6. La expresión de GluN3A es necesaria para las respuestas de diferenciación de OPC destinadas a reparar lesiones desmielinizadas en adultos.

The background of the entire page is a high-magnification fluorescence micrograph of cells. The cells are stained with three different fluorescent dyes: red, green, and blue. The red signal is the most prominent, appearing as numerous bright red spots and elongated structures, particularly concentrated in the lower-left quadrant. Green fluorescence highlights the cell membranes and some internal organelles, appearing as green outlines and patches. Blue fluorescence, likely from a nuclear stain like DAPI, highlights the nuclei of the cells as bright blue or cyan spots. The overall effect is a dense field of multi-colored cellular structures against a dark, almost black background.

10. BIBLIOGRAPHY

Author: *Alice Staffa*

- Abiraman, K., Pol, S. U., O'Bara, M. A., Chen, G. D., Khaku, Z. M., Wang, J., Thorn, D., Vedia, B. H., Ekwegbalu, E. C., Li, J. X., Salvi, R. J., & Sim, F. J. (2015). Anti-muscarinic adjunct therapy accelerates functional human oligodendrocyte repair. *The Journal of neuroscience : the official journal of the Society for Neuroscience*, 35(8), 3676–3688.
- Alexander, G. M., Rogan, S. C., Abbas, A. I., Armbruster, B. N., Pei, Y., Allen, J. A., Nonneman, R. J., Hartmann, J., Moy, S. S., Nicolelis, M. A., McNamara, J. O., & Roth, B. L. (2009). Remote control of neuronal activity in transgenic mice expressing evolved G protein-coupled receptors. *Neuron*, 63(1), 27–39.
- Almeida R. G. (2018). The Rules of Attraction in Central Nervous System Myelination. *Frontiers in cellular neuroscience*, 12, 367.
- Almeida, R. G., Williamson, J. M., Madden, M. E., Early, J. J., Voas, M. G., Talbot, W. S., Bianco, I. H., & Lyons, D. A. (2021). Myelination induces axonal hotspots of synaptic vesicle fusion that promote sheath growth. *Current biology : CB*, 31(17), 3743–3754.e5.
- Alvarez-Saavedra, M., De Repentigny, Y., Yang, D., O'Meara, R. W., Yan, K., Hashem, L. E., Racacho, L., Ioshikhes, I., Bulman, D. E., Parks, R. J., Kothary, R., & Picketts, D. J. (2016). Voluntary Running Triggers VGF-Mediated Oligodendrogenesis to Prolong the Lifespan of Snf2h-Null Ataxic Mice. *Cell reports*, 17(3), 862–875.
- Arancibia-Cárcamo, I. L., Ford, M. C., Cossell, L., Ishida, K., Tohyama, K., & Attwell, D. (2017). Node of Ranvier length as a potential regulator of myelinated axon conduction speed. *eLife*, 6, e23329.
- Araque Caballero, M. Á., Suárez-Calvet, M., Duering, M., Franzmeier, N., Benzinger, T., Fagan, A. M., Bateman, R. J., Jack, C. R., Levin, J., Dichgans, M., Jucker, M., Karch, C., Masters, C. L., Morris, J. C., Weiner, M., Rossor, M., Fox, N. C., Lee, J. H., Salloway, S., Danek, A., ... Ewers, M. (2018). White matter diffusion alterations precede symptom onset in autosomal dominant Alzheimer's disease. *Brain : a journal of neurology*, 141(10), 3065–3080.
- Auguste, Y. S. S., Ferro, A., Kahng, J. A., Xavier, A. M., Dixon, J. R., Vrudhula, U., Nichitiu, A. S., Rosado, D., Wee, T. L., Pedmale, U. V., & Cheadle, L. (2022). Publisher Correction: Oligodendrocyte precursor cells engulf synapses during circuit remodeling in mice. *Nature neuroscience*, 25(12), 1735.
- Bacmeister, C. M., Barr, H. J., McClain, C. R., Thornton, M. A., Nettles, D., Welle, C. G., & Hughes, E. G. (2020). Motor learning promotes remyelination via new and surviving oligodendrocytes. *Nature neuroscience*, 23(7), 819–831.
- Bacmeister, C. M., Huang, R., Osso, L. A., Thornton, M. A., Conant, L., Chavez, A. R., Poleg-Polsky, A., & Hughes, E. G. (2022). Motor learning drives dynamic patterns of intermittent myelination on learning-activated axons. *Nature neuroscience*, 25(10), 1300–1313.
- Barrera, K., Chu, P., Abramowitz, J., Steger, R., Ramos, R. L., & Brumberg, J. C. (2013). Organization of myelin in the mouse somatosensory barrel cortex and the effects of sensory deprivation. *Developmental neurobiology*, 73(4), 297–314.
- Barres, B. A., Hart, I. K., Coles, H. S., Burne, J. F., Voyvodic, J. T., Richardson, W. D., & Raff, M. C. (1992). Cell death and control of cell survival in the oligodendrocyte lineage. *Cell*, 70(1), 31–46.
- Barres, B. A., Schmid, R., Sendtner, M., & Raff, M. C. (1993). Multiple extracellular signals are required for long-term oligodendrocyte survival. *Development (Cambridge, England)*, 118(1), 283–295.

- Barres, B. A., & Raff, M. C. (1999). Axonal control of oligodendrocyte development. *The Journal of cell biology*, 147(6), 1123–1128.
- Bartzokis, G., Lu, P. H., Raven, E. P., Amar, C. P., Detore, N. R., Couvrette, A. J., Mintz, J., Ventura, J., Casaus, L. R., Luo, J. S., Subotnik, K. L., & Nuechterlein, K. H. (2012). Impact on intracortical myelination trajectory of long acting injection versus oral risperidone in first-episode schizophrenia. *Schizophrenia research*, 140(1-3), 122–128.
- Bechler, M. E., Byrne, L., & Ffrench-Constant, C. (2015). CNS Myelin Sheath Lengths Are an Intrinsic Property of Oligodendrocytes. *Current biology : CB*, 25(18), 2411–2416.
- Beiter, R. M., Rivet-Noor, C., Merchak, A. R., Bai, R., Johanson, D. M., Slogar, E., Sol-Church, K., Overall, C. C., & Gaultier, A. (2022). Evidence for oligodendrocyte progenitor cell heterogeneity in the adult mouse brain. *Scientific reports*, 12(1), 12921.
- Ben Geren B. (1954). The formation from the Schwann cell surface of myelin in the peripheral nerves of chick embryos. *Experimental cell research*, 7(2), 558–562.
- Bengtsson, S. L., Nagy, Z., Skare, S., Forsman, L., Forssberg, H., & Ullén, F. (2005). Extensive piano practicing has regionally specific effects on white matter development. *Nature neuroscience*, 8(9), 1148–1150.
- Bergles, D. E., Roberts, J. D., Somogyi, P., & Jahr, C. E. (2000). Glutamatergic synapses on oligodendrocyte precursor cells in the hippocampus. *Nature*, 405(6783), 187–191.
- Bergles, D. E., Jabs, R., & Steinhäuser, C. (2010). Neuron-glia synapses in the brain. *Brain research reviews*, 63(1-2), 130–137.
- Bernardes, D., Oliveira-Lima, O. C., Silva, T. V., Faraco, C. C., Leite, H. R., Juliano, M. A., Santos, D. M., Bethea, J. R., Brambilla, R., Orian, J. M., Arantes, R. M., & Carvalho-Tavares, J. (2013). Differential brain and spinal cord cytokine and BDNF levels in experimental autoimmune encephalomyelitis are modulated by prior and regular exercise. *Journal of neuroimmunology*, 264(1-2), 24–34.
- Boda, E., Di Maria, S., Rosa, P., Taylor, V., Abbracchio, M. P., & Buffo, A. (2015). Early phenotypic asymmetry of sister oligodendrocyte progenitor cells after mitosis and its modulation by aging and extrinsic factors. *Glia*, 63(2), 271–286.
- Boda, E., Lorenzati, M., Parolisi, R., Harding, B., Pallavicini, G., Bonfanti, L., Moccia, A., Bielas, S., Di Cunto, F., & Buffo, A. (2022). Molecular and functional heterogeneity in dorsal and ventral oligodendrocyte progenitor cells of the mouse forebrain in response to DNA damage. *Nature communications*, 13(1), 2331.
- Bossi, S., Dhanasobhon, D., Ellis-Davies, G. C. R., Frontera, J., de Brito Van Velze, M., Lourenço, J., Murillo, A., Luján, R., Casado, M., Perez-Otaño, I., Bacci, A., Popa, D., Paoletti, P., & Rebola, N. (2022). GluN3A excitatory glycine receptors control adult cortical and amygdalar circuits. *Neuron*, 110(15), 2438–2454.e8.
- Bourbon-Teles, J., Bells, S., Jones, D. K., Coulthard, E., Rosser, A., & Metzler-Baddeley, C. (2019). Myelin Breakdown in Human Huntington's Disease: Multi-Modal Evidence from Diffusion MRI and Quantitative Magnetization Transfer. *Neuroscience*, 403, 79–92.

- Boyd, A., Zhang, H., & Williams, A. (2013). Insufficient OPC migration into demyelinated lesions is a cause of poor remyelination in MS and mouse models. *Acta neuropathologica*, 125(6), 841–859.
- Bradbury, E. J., & Burnside, E. R. (2019). Moving beyond the glial scar for spinal cord repair. *Nature communications*, 10(1), 3879.
- Bramow, S., Frischer, J. M., Lassmann, H., Koch-Henriksen, N., Lucchinetti, C. F., Sørensen, P. S., & Laursen, H. (2010). Demyelination versus remyelination in progressive multiple sclerosis. *Brain : a journal of neurology*, 133(10), 2983–2998.
- Bryois, J., Skene, N. G., Hansen, T. F., Kogelman, L. J. A., Watson, H. J., Liu, Z., Eating Disorders Working Group of the Psychiatric Genomics Consortium, International Headache Genetics Consortium, 23andMe Research Team, Brueggeman, L., Breen, G., Bulik, C. M., Arenas, E., Hjerling-Leffler, J., & Sullivan, P. F. (2020). Genetic identification of cell types underlying brain complex traits yields insights into the etiology of Parkinson's disease. *Nature genetics*, 52(5), 482–493.
- Buchanan, J., Elabbady, L., Collman, F., Jorstad, N. L., Bakken, T. E., Ott, C., Glatzer, J., Bleckert, A. A., Bodor, A. L., Brittain, D., Bumbarger, D. J., Mahalingam, G., Seshamani, S., Schneider-Mizell, C., Takeno, M. M., Torres, R., Yin, W., Hodge, R. D., Castro, M., Dorkenwald, S., ... da Costa, N. M. (2022). Oligodendrocyte precursor cells ingest axons in the mouse neocortex. *Proceedings of the National Academy of Sciences of the United States of America*, 119(48), e2202580119.
- Bunge, M. B., Bunge, R. P., & Pappas, G. D. (1962). Electron microscopic demonstration of connections between glia and myelin sheaths in the developing mammalian central nervous system. *The Journal of cell biology*, 12, 448–453.
- Burzomato, V., Frugier, G., Pérez-Otaño, I., Kittler, J. T., & Attwell, D. (2010). The receptor subunits generating NMDA receptor mediated currents in oligodendrocytes. *The Journal of physiology*, 588(Pt 18), 3403–3414.
- Cahoy, J. D., Emery, B., Kaushal, A., Foo, L. C., Zamanian, J. L., Christopherson, K. S., Xing, Y., Lubischer, J. L., Krieg, P. A., Krupenko, S. A., Thompson, W. J., & Barres, B. A. (2008). A transcriptome database for astrocytes, neurons, and oligodendrocytes: a new resource for understanding brain development and function. *The Journal of neuroscience : the official journal of the Society for Neuroscience*, 28(1), 264–278.
- Caldeira, M. V., Melo, C. V., Pereira, D. B., Carvalho, R. F., Carvalho, A. L., & Duarte, C. B. (2007). BDNF regulates the expression and traffic of NMDA receptors in cultured hippocampal neurons. *Molecular and cellular neurosciences*, 35(2), 208–219.
- Carreiras, M., Seghier, M. L., Baquero, S., Estévez, A., Lozano, A., Devlin, J. T., & Price, C. J. (2009). An anatomical signature for literacy. *Nature*, 461(7266), 983–986.
- Chamling, X., Kallman, A., Fang, W., Berlinicke, C. A., Mertz, J. L., Devkota, P., Pantoja, I. E. M., Smith, M. D., Ji, Z., Chang, C., Kaushik, A., Chen, L., Whartenby, K. A., Calabresi, P. A., Mao, H. Q., Ji, H., Wang, T. H., & Zack, D. J. (2021). Single-cell transcriptomic reveals molecular diversity and developmental heterogeneity of human stem cell-derived oligodendrocyte lineage cells. *Nature communications*, 12(1), 652.
- Chang, A., Tourtellotte, W. W., Rudick, R., & Trapp, B. D. (2002). Premyelinating oligodendrocytes in chronic lesions of multiple sclerosis. *The New England journal of medicine*, 346(3), 165–173.

- Chatterton, J. E., Awobuluyi, M., Premkumar, L. S., Takahashi, H., Talantova, M., Shin, Y., Cui, J., Tu, S., Sevarino, K. A., Nakanishi, N., Tong, G., Lipton, S. A., & Zhang, D. (2002). Excitatory glycine receptors containing the NR3 family of NMDA receptor subunits. *Nature*, 415(6873), 793–798.
- Chavali, M., Ulloa-Navas, M. J., Pérez-Borredá, P., Garcia-Verdugo, J. M., McQuillen, P. S., Huang, E. J., & Rowitch, D. H. (2020). Wnt-Dependent Oligodendroglial-Endothelial Interactions Regulate White Matter Vascularization and Attenuate Injury. *Neuron*, 108(6), 1130–1145.e5.
- Chen, K., Zheng, Y., Wei, J. A., Ouyang, H., Huang, X., Zhang, F., Lai, C. S. W., Ren, C., So, K. F., & Zhang, L. (2019). Exercise training improves motor skill learning via selective activation of mTOR. *Science advances*, 5(7), eaaw1888.
- Chen, J. F., Liu, K., Hu, B., Li, R. R., Xin, W., Chen, H., Wang, F., Chen, L., Li, R. X., Ren, S. Y., Xiao, L., Chan, J. R., & Mei, F. (2021). Enhancing myelin renewal reverses cognitive dysfunction in a murine model of Alzheimer's disease. *Neuron*, 109(14), 2292–2307.e5.
- Chen, Y., Sheng, J., Tang, X., Zhao, Y., Zhu, S., & Liu, Q. (2022). Clemastine Rescues Chemotherapy-Induced Cognitive Impairment by Improving White Matter Integrity. *Neuroscience*, 484, 66–79.
- Chittajallu, R., Aguirre, A., & Gallo, V. (2004). NG2-positive cells in the mouse white and grey matter display distinct physiological properties. *The Journal of physiology*, 561(Pt 1), 109–122.
- Chugani, H. T., Behen, M. E., Muzik, O., Juhász, C., Nagy, F., & Chugani, D. C. (2001). Local brain functional activity following early deprivation: a study of postinstitutionalized Romanian orphans. *NeuroImage*, 14(6), 1290–1301.
- Compston, A., & Coles, A. (2008). Multiple sclerosis. *Lancet (London, England)*, 372(9648), 1502–1517.
- Conde-Dusman, M. J., Dey, P. N., Elía-Zudaire, Ó., Rabaneda, L. G., García-Lira, C., Grand, T., Briz, V., Velasco, E. R., Andero, R., Niñerola, S., Barco, A., Paoletti, P., Wesseling, J. F., Gardoni, F., Tavalin, S. J., & Perez-Otaño, I. (2021). Control of protein synthesis and memory by GluN3A-NMDA receptors through inhibition of GIT1/mTORC1 assembly. *eLife*, 10, e71575.
- Crawford, A. H., Tripathi, R. B., Richardson, W. D., & Franklin, R. J. M. (2016). Developmental Origin of Oligodendrocyte Lineage Cells Determines Response to Demyelination and Susceptibility to Age-Associated Functional Decline. *Cell reports*, 15(4), 761–773.
- Cullen, C. L., Senesi, M., Tang, A. D., Clutterbuck, M. T., Auderset, L., O'Rourke, M. E., Rodger, J., & Young, K. M. (2019). Low-intensity transcranial magnetic stimulation promotes the survival and maturation of newborn oligodendrocytes in the adult mouse brain. *Glia*, 67(8), 1462–1477.
- Das, S., Sasaki, Y. F., Rothe, T., Premkumar, L. S., Takasu, M., Crandall, J. E., Dikkes, P., Conner, D. A., Rayudu, P. V., Cheung, W., Chen, H. S., Lipton, S. A., & Nakanishi, N. (1998). Increased NMDA current and spine density in mice lacking the NMDA receptor subunit NR3A. *Nature*, 393(6683), 377–381.
- Dawson, M. R., Polito, A., Levine, J. M., & Reynolds, R. (2003). NG2-expressing glial progenitor cells: an abundant and widespread population of cycling cells in the adult rat CNS. *Molecular and cellular neurosciences*, 24(2), 476–488.

- De Biase, L. M., Kang, S. H., Baxi, E. G., Fukaya, M., Pucak, M. L., Mishina, M., Calabresi, P. A., & Bergles, D. E. (2011). NMDA receptor signaling in oligodendrocyte progenitors is not required for oligodendrogenesis and myelination. *The Journal of neuroscience : the official journal of the Society for Neuroscience*, 31(35), 12650–12662.
- De la Fuente, A. G., Queiroz, R. M. L., Ghosh, T., McMurrin, C. E., Cubillos, J. F., Bergles, D. E., Fitzgerald, D. C., Jones, C. A., Lilley, K. S., Glover, C. P., & Franklin, R. J. M. (2020). Changes in the Oligodendrocyte Progenitor Cell Proteome with Ageing. *Molecular & cellular proteomics : MCP*, 19(8), 1281–1302.
- Dean, D. C., 3rd, Sojkova, J., Hurley, S., Kecskemeti, S., Okonkwo, O., Bendlin, B. B., Theisen, F., Johnson, S. C., Alexander, A. L., & Gallagher, C. L. (2016). Alterations of Myelin Content in Parkinson's Disease: A Cross-Sectional Neuroimaging Study. *PloS one*, 11(10), e0163774.
- Del Río-Hortega P. (1921). La glía de escasas radiaciones (oligodendroglía). *Bol. Real Soc. Esp. Hist. Nat.* 21, 63–92.
- Del Río-Hortega P. (1928). Tercera aportación al conocimiento morfológico e interpretación funcional de la oligodendroglía. *Mem. Real Soc. Esp. Hist. Nat.* 14, 5–122.
- Demerens, C., Stankoff, B., Logak, M., Anglade, P., Allinquant, B., Couraud, F., Zalc, B., & Lubetzki, C. (1996). Induction of myelination in the central nervous system by electrical activity. *Proceedings of the National Academy of Sciences of the United States of America*, 93(18), 9887–9892.
- Depp, C., Sun, T., Sasmita, A. O., Spieth, L., Berghoff, S. A., Nazarenko, T., Overhoff, K., Steixner-Kumar, A. A., Subramanian, S., Arinrad, S., Ruhwedel, T., Möbius, W., Göbbels, S., Saher, G., Werner, H. B., Damkou, A., Zampar, S., Wirths, O., Thalmann, M., Simons, M., ... Nave, K. A. (2023). Myelin dysfunction drives amyloid- β deposition in models of Alzheimer's disease. *Nature*, 618(7964), 349–357.
- Desai, M. K., Sudol, K. L., Janelins, M. C., Mastrangelo, M. A., Frazer, M. E., & Bowers, W. J. (2009). Triple-transgenic Alzheimer's disease mice exhibit region-specific abnormalities in brain myelination patterns prior to appearance of amyloid and tau pathology. *Glia*, 57(1), 54–65.
- Deshmukh, V. A., Tardif, V., Lyssiotis, C. A., Green, C. C., Kerman, B., Kim, H. J., Padmanabhan, K., Swoboda, J. G., Ahmad, I., Kondo, T., Gage, F. H., Theofilopoulos, A. N., Lawson, B. R., Schultz, P. G., & Lairson, L. L. (2013). A regenerative approach to the treatment of multiple sclerosis. *Nature*, 502(7471), 327–332.
- Dimou, L., Simon, C., Kirchhoff, F., Takebayashi, H., & Götz, M. (2008). Progeny of Olig2-expressing progenitors in the gray and white matter of the adult mouse cerebral cortex. *The Journal of neuroscience : the official journal of the Society for Neuroscience*, 28(41), 10434–10442.
- Doyle, S., Hansen, D. B., Vella, J., Bond, P., Harper, G., Zammit, C., Valentino, M., & Fern, R. (2018). Vesicular glutamate release from central axons contributes to myelin damage. *Nature communications*, 9(1), 1032.
- Du, W., Deng, Y., Jiang, R., Tong, L., Li, R., & Jiang, X. (2022). Clemastine Enhances Myelination, Delays Axonal Loss and Promotes Functional Recovery in Spinal Cord Injury. *Neurochemical research*, 47(2), 503–515.
- Einstein, O., Fainstein, N., Touloumi, O., Lagoudaki, R., Hanya, E., Grigoriadis, N., Katz, A., & Ben-Hur, T. (2018). Exercise training attenuates experimental autoimmune encephalomyelitis by peripheral immunomodulation rather than direct neuroprotection. *Experimental neurology*, 299(Pt A), 56–64.

- Eluvathingal, T. J., Chugani, H. T., Behen, M. E., Juhász, C., Muzik, O., Maqbool, M., Chugani, D. C., & Makki, M. (2006). Abnormal brain connectivity in children after early severe socioemotional deprivation: a diffusion tensor imaging study. *Pediatrics*, 117(6), 2093–2100.
- Emery, B., Agalliu, D., Cahoy, J. D., Watkins, T. A., Dugas, J. C., Mulinyawe, S. B., Ibrahim, A., Ligon, K. L., Rowitch, D. H., & Barres, B. A. (2009). Myelin gene regulatory factor is a critical transcriptional regulator required for CNS myelination. *Cell*, 138(1), 172–185.
- Emery, B., & Lu, Q. R. (2015). Transcriptional and Epigenetic Regulation of Oligodendrocyte Development and Myelination in the Central Nervous System. *Cold Spring Harbor perspectives in biology*, 7(9), a020461.
- Etxeberria, A., Mangin, J. M., Aguirre, A., & Gallo, V. (2010). Adult-born SVZ progenitors receive transient synapses during remyelination in corpus callosum. *Nature neuroscience*, 13(3), 287–289.
- Etxeberria, A., Hokanson, K. C., Dao, D. Q., Mayoral, S. R., Mei, F., Redmond, S. A., Ullian, E. M., & Chan, J. R. (2016). Dynamic Modulation of Myelination in Response to Visual Stimuli Alters Optic Nerve Conduction Velocity. *The Journal of neuroscience : the official journal of the Society for Neuroscience*, 36(26), 6937–6948.
- Eugenin von Bernhardt, J., & Dimou, L. (2022). Oligodendrogenesis is a key process for cognitive performance improvement induced by voluntary physical activity. *Glia*, 70(6), 1052–1067.
- Falcão, A. M., van Bruggen, D., Marques, S., Meijer, M., Jäkel, S., Agirre, E., Samudiyata, Floriddia, E. M., Vanichkina, D. P., Ffrench-Constant, C., Williams, A., Guerreiro-Cacais, A. O., & Castelo-Branco, G. (2018). Disease-specific oligodendrocyte lineage cells arise in multiple sclerosis. *Nature medicine*, 24(12), 1837–1844.
- Feinstein, A., Amato, M. P., Brichetto, G., Chataway, J., Chiaravalloti, N. D., Cutter, G., Dalgas, U., DeLuca, J., Farrell, R., Feys, P., Filippi, M., Freeman, J., Inglese, M., Meza, C., Motl, R. W., Rocca, M. A., Sandroff, B. M., Salter, A., & CogEx Research Team (2023). Cognitive rehabilitation and aerobic exercise for cognitive impairment in people with progressive multiple sclerosis (CogEx): a randomised, blinded, sham-controlled trial. *The Lancet. Neurology*, 22(10), 912–924.
- Ferraiuolo, L., Meyer, K., Sherwood, T. W., Vick, J., Likhite, S., Frakes, A., Miranda, C. J., Braun, L., Heath, P. R., Pineda, R., Beattie, C. E., Shaw, P. J., Askwith, C. C., McTigue, D., & Kaspar, B. K. (2016). Oligodendrocytes contribute to motor neuron death in ALS via SOD1-dependent mechanism. *Proceedings of the National Academy of Sciences of the United States of America*, 113(42), E6496–E6505.
- Ferrari Bardile, C., Garcia-Miralles, M., Caron, N. S., Rayan, N. A., Langley, S. R., Harmston, N., Rondelli, A. M., Teo, R. T. Y., Walzl, S., Anderson, L. M., Bae, H. G., Jung, S., Williams, A., Prabhakar, S., Petretto, E., Hayden, M. R., & Pouladi, M. A. (2019). Intrinsic mutant HTT-mediated defects in oligodendroglia cause myelination deficits and behavioral abnormalities in Huntington disease. *Proceedings of the National Academy of Sciences of the United States of America*, 116(19), 9622–9627.
- Fiuza, M., González-González, I., & Pérez-Otaño, I. (2013). GluN3A expression restricts spine maturation via inhibition of GIT1/Rac1 signaling. *Proceedings of the National Academy of Sciences of the United States of America*, 110(51), 20807–20812.

- Franklin, R. J. M., & Ffrench-Constant, C. (2017). Regenerating CNS myelin - from mechanisms to experimental medicines. *Nature reviews. Neuroscience*, 18(12), 753–769.
- Franklin, R. J. M., & Simons, M. (2022). CNS remyelination and inflammation: From basic mechanisms to therapeutic opportunities. *Neuron*, 110(21), 3549–3565.
- Frischer, J. M., Weigand, S. D., Guo, Y., Kale, N., Parisi, J. E., Pirko, I., Mandrekar, J., Bramow, S., Metz, I., Brück, W., Lassmann, H., & Lucchinetti, C. F. (2015). Clinical and pathological insights into the dynamic nature of the white matter multiple sclerosis plaque. *Annals of neurology*, 78(5), 710–721.
- Fu, Y., Sun, W., Shi, Y., Shi, R., & Cheng, J. X. (2009). Glutamate excitotoxicity inflicts paranodal myelin splitting and retraction. *PloS one*, 4(8), e6705.
- Fulcher, B. D., Murray, J. D., Zerbi, V., & Wang, X. J. (2019). Multimodal gradients across mouse cortex. *Proceedings of the National Academy of Sciences of the United States of America*, 116(10), 4689–4695.
- Fünfschilling, U., Supplie, L. M., Mahad, D., Boretius, S., Saab, A. S., Edgar, J., Brinkmann, B. G., Kassmann, C. M., Tzvetanova, I. D., Möbius, W., Diaz, F., Meijer, D., Suter, U., Hamprecht, B., Sereda, M. W., Moraes, C. T., Frahm, J., Goebbels, S., & Nave, K. A. (2012). Glycolytic oligodendrocytes maintain myelin and long-term axonal integrity. *Nature*, 485(7399), 517–521.
- Gary, D. S., Malone, M., Capestany, P., Houdayer, T., & McDonald, J. W. (2012). Electrical stimulation promotes the survival of oligodendrocytes in mixed cortical cultures. *Journal of neuroscience research*, 90(1), 72–83.
- Ge, S. X., Jung, D., & Yao, R. (2020). ShinyGO: a graphical gene-set enrichment tool for animals and plants. *Bioinformatics (Oxford, England)*, 36(8), 2628–2629.
- Geraghty, A. C., Gibson, E. M., Ghanem, R. A., Greene, J. J., Ocampo, A., Goldstein, A. K., Ni, L., Yang, T., Marton, R. M., Pasca, S. P., Greenberg, M. E., Longo, F. M., & Monje, M. (2019). Loss of Adaptive Myelination Contributes to Methotrexate Chemotherapy-Related Cognitive Impairment. *Neuron*, 103(2), 250–265.e8.
- Gibson, E. M., Purger, D., Mount, C. W., Goldstein, A. K., Lin, G. L., Wood, L. S., Inema, I., Miller, S. E., Bieri, G., Zuchero, J. B., Barres, B. A., Woo, P. J., Vogel, H., & Monje, M. (2014). Neuronal activity promotes oligodendrogenesis and adaptive myelination in the mammalian brain. *Science (New York, N.Y.)*, 344(6183), 1252304.
- Gibson, E. M., Nagaraja, S., Ocampo, A., Tam, L. T., Wood, L. S., Pallegar, P. N., Greene, J. J., Geraghty, A. C., Goldstein, A. K., Ni, L., Woo, P. J., Barres, B. A., Liddel, S., Vogel, H., & Monje, M. (2019). Methotrexate Chemotherapy Induces Persistent Tri-glial Dysregulation that Underlies Chemotherapy-Related Cognitive Impairment. *Cell*, 176(1-2), 43–55.e13.
- Gingele, S., Henkel, F., Heckers, S., Moellenkamp, T. M., Hümmert, M. W., Skripuletz, T., Stangel, M., & Gudi, V. (2020). Delayed Demyelination and Impaired Remyelination in Aged Mice in the Cuprizone Model. *Cells*, 9(4), 945.
- Goldschmidt, T., Antel, J., König, F. B., Brück, W., & Kuhlmann, T. (2009). Remyelination capacity of the MS brain decreases with disease chronicity. *Neurology*, 72(22), 1914–1921.

- Goldstein, E. Z., Pertsovskaya, V., Forbes, T. A., Dupree, J. L., & Gallo, V. (2021). Prolonged Environmental Enrichment Promotes Developmental Myelination. *Frontiers in cell and developmental biology*, 9, 665409.
- Grand, T., Abi Gerges, S., David, M., & Paoletti, P. (2018). Unmasking GluN1/GluN3A excitatory glycine NMDA receptors. *Nature Communications* 9, 4769.
- Griffiths, I., Klugmann, M., Anderson, T., Yool, D., Thomson, C., Schwab, M. H., Schneider, A., Zimmermann, F., McCulloch, M., Nadon, N., & Nave, K. A. (1998). Axonal swellings and degeneration in mice lacking the major proteolipid of myelin. *Science (New York, N.Y.)*, 280(5369), 1610–1613.
- Gruchot, J., Weyers, V., Göttle, P., Förster, M., Hartung, H. P., Küry, P., & Kremer, D. (2019). The Molecular Basis for Remyelination Failure in Multiple Sclerosis. *Cells*, 8(8), 825.
- Guo, F., Maeda, Y., Ko, E. M., Delgado, M., Horiuchi, M., Soulika, A., Miers, L., Burns, T., Itoh, T., Shen, H., Lee, E., Sohn, J., & Pleasure, D. (2012). Disruption of NMDA receptors in oligodendroglial lineage cells does not alter their susceptibility to experimental autoimmune encephalomyelitis or their normal development. *The Journal of neuroscience : the official journal of the Society for Neuroscience*, 32(2), 639–645.
- Gyllenstein, L., & Malmfors, T. (1963). Myelination of the optic nerve and its dependence on visual function--a quantitative investigation in mice. *Journal of embryology and experimental morphology*, 11, 255–266.
- Hansen, K. B., Yi, F., Perszyk, R. E., Menniti, F. S., & Traynelis, S. F. (2017). NMDA Receptors in the Central Nervous System. *Methods in molecular biology (Clifton, N.J.)*, 1677, 1–80.
- Hansen, K. B., Yi, F., Perszyk, R. E., Furukawa, H., Wollmuth, L. P., Gibb, A. J., & Traynelis, S. F. (2018). Structure, function, and allosteric modulation of NMDA receptors. *The Journal of general physiology*, 150(8), 1081–1105.
- Henson, M. A., Larsen, R. S., Lawson, S. N., Pérez-Otaño, I., Nakanishi, N., Lipton, S. A., & Philpot, B. D. (2012). Genetic deletion of NR3A accelerates glutamatergic synapse maturation. *PloS one*, 7(8), e42327.
- Henson, M. A., Roberts, A. C., Pérez-Otaño, I., & Philpot, B. D. (2010). Influence of the NR3A subunit on NMDA receptor functions. *Progress in neurobiology*, 91(1), 23–37.
- Hill, R. A., Patel, K. D., Goncalves, C. M., Grutzendler, J., & Nishiyama, A. (2014). Modulation of oligodendrocyte generation during a critical temporal window after NG2 cell division. *Nature neuroscience*, 17(11), 1518–1527.
- Hill, R. A., Li, A. M., & Grutzendler, J. (2018). Lifelong cortical myelin plasticity and age-related degeneration in the live mammalian brain. *Nature neuroscience*, 21(5), 683–695.
- Hilscher, M. M., Langseth, C. M., Kukanja, P., Yokota, C., Nilsson, M., & Castelo-Branco, G. (2022). Spatial and temporal heterogeneity in the lineage progression of fine oligodendrocyte subtypes. *BMC biology*, 20(1), 122.
- Hines, J. H., Ravanelli, A. M., Schwindt, R., Scott, E. K., & Appel, B. (2015). Neuronal activity biases axon selection for myelination in vivo. *Nature neuroscience*, 18(5), 683–689.
- Hinman, J. D., Peters, A., Cabral, H., Rosene, D. L., Hollander, W., Rasband, M. N., & Abraham, C. R. (2006). Age-related molecular reorganization at the node of Ranvier. *The Journal of comparative neurology*, 495(4), 351–362.

- Howell, O. W., Palser, A., Polito, A., Melrose, S., Zonta, B., Scheiermann, C., Vora, A. J., Brophy, P. J., & Reynolds, R. (2006). Disruption of neurofascin localization reveals early changes preceding demyelination and remyelination in multiple sclerosis. *Brain : a journal of neurology*, 129(Pt 12), 3173–3185.
- Hughes, E. G., Kang, S. H., Fukaya, M., & Bergles, D. E. (2013). Oligodendrocyte progenitors balance growth with self-repulsion to achieve homeostasis in the adult brain. *Nature neuroscience*, 16(6), 668–676.
- Hughes, E. G., Orthmann-Murphy, J. L., Langseth, A. J., & Bergles, D. E. (2018). Myelin remodeling through experience-dependent oligodendrogenesis in the adult somatosensory cortex. *Nature neuroscience*, 21(5), 696–706.
- Hughes, A. N., & Appel, B. (2019). Oligodendrocytes express synaptic proteins that modulate myelin sheath formation. *Nature communications*, 10(1), 4125.
- Huxley, A. F., & Stampfli, R. (1949). Evidence for saltatory conduction in peripheral myelinated nerve fibres. *The Journal of physiology*, 108(3), 315–339.
- Ihara, M., Polvikoski, T. M., Hall, R., Slade, J. Y., Perry, R. H., Oakley, A. E., Englund, E., O'Brien, J. T., Ince, P. G., & Kalara, R. N. (2010). Quantification of myelin loss in frontal lobe white matter in vascular dementia, Alzheimer's disease, and dementia with Lewy bodies. *Acta neuropathologica*, 119(5), 579–589.
- Jäkel, S., Agirre, E., Mendanha Falcão, A., van Bruggen, D., Lee, K. W., Knuesel, I., Malhotra, D., Ffrench-Constant, C., Williams, A., & Castelo-Branco, G. (2019). Altered human oligodendrocyte heterogeneity in multiple sclerosis. *Nature*, 566(7745), 543–547.
- Jakovcevski, I., & Zecevic, N. (2005). Sequence of oligodendrocyte development in the human fetal telencephalon. *Glia*, 49(4), 480–491.
- James, O. G., Selvaraj, B. T., Magnani, D., Burr, K., Connick, P., Barton, S. K., Vasistha, N. A., Hampton, D. W., Story, D., Smigiel, R., Ploski, R., Brophy, P. J., Ffrench-Constant, C., Lyons, D. A., & Chandran, S. (2021). iPSC-derived myelinoids to study myelin biology of humans. *Developmental cell*, 56(9), 1346–1358.e6.
- Jantzie, L. L., Talos, D. M., Jackson, M. C., Park, H. K., Graham, D. A., Lechpammer, M., Folkerth, R. D., Volpe, J. J., & Jensen, F. E. (2015). Developmental expression of N-methyl-D-aspartate (NMDA) receptor subunits in human white and gray matter: potential mechanism of increased vulnerability in the immature brain. *Cerebral cortex (New York, N.Y. : 1991)*, 25(2), 482–495.
- Jensen, S. K., Michaels, N. J., Ilyntskyy, S., Keough, M. B., Kovalchuk, O., & Yong, V. W. (2018). Multimodal Enhancement of Remyelination by Exercise with a Pivotal Role for Oligodendroglial PGC1 α . *Cell reports*, 24(12), 3167–3179.
- Kaller, M. S., Lazari, A., Blanco-Duque, C., Sampaio-Baptista, C., & Johansen-Berg, H. (2017). Myelin plasticity and behaviour-connecting the dots. *Current opinion in neurobiology*, 47, 86–92.
- Kang, S. H., Li, Y., Fukaya, M., Lorenzini, I., Cleveland, D. W., Ostrow, L. W., Rothstein, J. D., & Bergles, D. E. (2013). Degeneration and impaired regeneration of gray matter oligodendrocytes in amyotrophic lateral sclerosis. *Nature neuroscience*, 16(5), 571–579.

- Káradóttir, R., Cavelier, P., Bergersen, L. H., & Attwell, D. (2005). NMDA receptors are expressed in oligodendrocytes and activated in ischaemia. *Nature*, 438(7071), 1162–1166.
- Káradóttir, R., Hamilton, N. B., Bakiri, Y., & Attwell, D. (2008). Spiking and nonspiking classes of oligodendrocyte precursor glia in CNS white matter. *Nature neuroscience*, 11(4), 450–456.
- Kehoe, L. A., Bellone, C., De Roo, M., Zanduetta, A., Dey, P. N., Pérez-Otaño, I., & Muller, D. (2014). GluN3A promotes dendritic spine pruning and destabilization during postnatal development. *The Journal of neuroscience : the official journal of the Society for Neuroscience*, 34(28), 9213–9221.
- Kenigsbuch, M., Bost, P., Halevi, S., Chang, Y., Chen, S., Ma, Q., Hajbi, R., Schwikowski, B., Bodenmiller, B., Fu, H., Schwartz, M., & Amit, I. (2022). A shared disease-associated oligodendrocyte signature among multiple CNS pathologies. *Nature neuroscience*, 25(7), 876–886.
- Kessaris, N., Fogarty, M., Iannarelli, P., Grist, M., Wegner, M., & Richardson, W. D. (2006). Competing waves of oligodendrocytes in the forebrain and postnatal elimination of an embryonic lineage. *Nature neuroscience*, 9(2), 173–179.
- Kim, D., Paggi, J. M., Park, C., Bennett, C., & Salzberg, S. L. (2019). Graph-based genome alignment and genotyping with HISAT2 and HISAT-genotype. *Nature biotechnology*, 37(8), 907–915.
- Kirby, L., Jin, J., Cardona, J. G., Smith, M. D., Martin, K. A., Wang, J., Strasburger, H., Herbst, L., Alexis, M., Karnell, J., Davidson, T., Dutta, R., Goverman, J., Bergles, D., & Calabresi, P. A. (2019). Oligodendrocyte precursor cells present antigen and are cytotoxic targets in inflammatory demyelination. *Nature communications*, 10(1), 3887.
- Klaren, R. E., Sebastiao, E., Chiu, C. Y., Kinnett-Hopkins, D., McAuley, E., & Motl, R. W. (2016). Levels and Rates of Physical Activity in Older Adults with Multiple Sclerosis. *Aging and disease*, 7(3), 278–284.
- Knowles, J. K., Xu, H., Soane, C., Batra, A., Saucedo, T., Frost, E., Tam, L. T., Fraga, D., Ni, L., Villar, K., Talmi, S., Huguenard, J. R., & Monje, M. (2022). Maladaptive myelination promotes generalized epilepsy progression. *Nature neuroscience*, 25(5), 596–606.
- Kole, M. H., & Stuart, G. J. (2012). Signal processing in the axon initial segment. *Neuron*, 73(2), 235–247.
- Koskinen, M. K., Laine, M., Abdollahzadeh, A., Gigliotta, A., Mazzini, G., Journée, S., Alenius, V., Tronetti, K., Tohka, J., Hyytiä, P., Sierra, A., & Hovatta, I. (2023). Node of Ranvier remodeling in chronic psychosocial stress and anxiety. *Neuropsychopharmacology : official publication of the American College of Neuropsychopharmacology*, 48(10), 1532–1540.
- Kougioumtzidou, E., Shimizu, T., Hamilton, N. B., Tohyama, K., Sprengel, R., Monyer, H., Attwell, D., & Richardson, W. D. (2017). Signalling through AMPA receptors on oligodendrocyte precursors promotes myelination by enhancing oligodendrocyte survival. *eLife*, 6, e28080.
- Kuhlmann, T., Miron, V., Cui, Q., Wegner, C., Antel, J., & Brück, W. (2008). Differentiation block of oligodendroglial progenitor cells as a cause for remyelination failure in chronic multiple sclerosis. *Brain : a journal of neurology*, 131(Pt 7), 1749–1758.

- Kujawa, M. J., Marcinkowska, A. B., Grzywińska, M., Waśkow, M., Romanowski, A., Szurowska, E., Winklewski, P. J., & Szarmach, A. (2023). Physical activity and the brain myelin content in humans. *Frontiers in cellular neuroscience*, 17, 1198657.
- Kukley, M., Capetillo-Zarate, E., & Dietrich, D. (2007). Vesicular glutamate release from axons in white matter. *Nature neuroscience*, 10(3), 311–320.
- Kukley, M., Nishiyama, A., & Dietrich, D. (2010). The fate of synaptic input to NG2 glial cells: neurons specifically downregulate transmitter release onto differentiating oligodendroglial cells. *The Journal of neuroscience : the official journal of the Society for Neuroscience*, 30(24), 8320–8331.
- La Manno, G., Gyllborg, D., Codeluppi, S., Nishimura, K., Salto, C., Zeisel, A., Borm, L. E., Stott, S. R. W., Toledo, E. M., Villaescusa, J. C., Lönnerberg, P., Ryge, J., Barker, R. A., Arenas, E., & Linnarsson, S. (2016). Molecular Diversity of Midbrain Development in Mouse, Human, and Stem Cells. *Cell*, 167(2), 566–580.e19.
- Larsen, R. S., Smith, I. T., Miriyala, J., Han, J. E., Corlew, R. J., Smith, S. L., & Philpot, B. D. (2014). Synapse-specific control of experience-dependent plasticity by presynaptic NMDA receptors. *Neuron*, 83(4), 879–893.
- Lau, C. G., & Zukin, R. S. (2007). NMDA receptor trafficking in synaptic plasticity and neuropsychiatric disorders. *Nature reviews. Neuroscience*, 8(6), 413–426.
- Lee, S., Leach, M. K., Redmond, S. A., Chong, S. Y., Mellon, S. H., Tuck, S. J., Feng, Z. Q., Corey, J. M., & Chan, J. R. (2012). A culture system to study oligodendrocyte myelination processes using engineered nanofibers. *Nature methods*, 9(9), 917–922.
- Li, C., Xiao, L., Liu, X., Yang, W., Shen, W., Hu, C., Yang, G., & He, C. (2013). A functional role of NMDA receptor in regulating the differentiation of oligodendrocyte precursor cells and remyelination. *Glia*, 61(5), 732–749.
- Li, M., Gao, Y., Lawless, R. D., Xu, L., Zhao, Y., Schilling, K. G., Ding, Z., Anderson, A. W., Landman, B. A., & Gore, J. C. (2023). Changes in white matter functional networks across late adulthood. *Frontiers in aging neuroscience*, 15, 1204301.
- Li, J., Miramontes, T. G., Czopka, T., & Monk, K. R. (2024). Synaptic input and Ca²⁺ activity in zebrafish oligodendrocyte precursor cells contribute to myelin sheath formation. *Nature neuroscience*, 27(2), 219–231.
- Lin, S. C., & Bergles, D. E. (2004). Synaptic signaling between GABAergic interneurons and oligodendrocyte precursor cells in the hippocampus. *Nature neuroscience*, 7(1), 24–32.
- Lin, S. C., Huck, J. H., Roberts, J. D., Macklin, W. B., Somogyi, P., & Bergles, D. E. (2005). Climbing fiber innervation of NG2-expressing glia in the mammalian cerebellum. *Neuron*, 46(5), 773–785.
- Liu, J., Dietz, K., DeLoyht, J. M., Pedre, X., Kelkar, D., Kaur, J., Vialou, V., Lobo, M. K., Dietz, D. M., Nestler, E. J., Dupree, J., & Casaccia, P. (2012). Impaired adult myelination in the prefrontal cortex of socially isolated mice. *Nature neuroscience*, 15(12), 1621–1623.
- Love, M. I., Huber, W., & Anders, S. (2014). Moderated estimation of fold change and dispersion for RNA-seq data with DESeq2. *Genome biology*, 15(12), 550.

- Lundgaard, I., Luzhynskaya, A., Stockley, J. H., Wang, Z., Evans, K. A., Swire, M., Volbracht, K., Gautier, H. O., Franklin, R. J., Charles Ffrench-Constant, Attwell, D., & Káradóttir, R. T. (2013). Neuregulin and BDNF induce a switch to NMDA receptor-dependent myelination by oligodendrocytes. *PLoS biology*, *11*(12), e1001743.
- Maas, D. A., & Angulo, M. C. (2021). Can Enhancing Neuronal Activity Improve Myelin Repair in Multiple Sclerosis?. *Frontiers in cellular neuroscience*, *15*, 645240.
- Makinodan, M., Rosen, K. M., Ito, S., & Corfas, G. (2012). A critical period for social experience-dependent oligodendrocyte maturation and myelination. *Science (New York, N.Y.)*, *337*(6100), 1357–1360.
- Mandolesi, G., Bullitta, S., Fresegna, D., De Vito, F., Rizzo, F. R., Musella, A., Guadalupi, L., Vanni, V., Stampanoni Bassi, M., Buttari, F., Viscomi, M. T., Centonze, D., & Gentile, A. (2019). Voluntary running wheel attenuates motor deterioration and brain damage in cuprizone-induced demyelination. *Neurobiology of disease*, *129*, 102–117.
- Mangin, J. M., Kunze, A., Chittajallu, R., & Gallo, V. (2008). Satellite NG2 progenitor cells share common glutamatergic inputs with associated interneurons in the mouse dentate gyrus. *The Journal of neuroscience : the official journal of the Society for Neuroscience*, *28*(30), 7610–7623.
- Mangin, J. M., Li, P., Scafidi, J., & Gallo, V. (2012). Experience-dependent regulation of NG2 progenitors in the developing barrel cortex. *Nature neuroscience*, *15*(9), 1192–1194.
- Marques, S., Zeisel, A., Codeluppi, S., van Bruggen, D., Mendenha Falcão, A., Xiao, L., Li, H., Häring, M., Hochgerner, H., Romanov, R. A., Gyllborg, D., Muñoz Manchado, A., La Manno, G., Lönnerberg, P., Floriddia, E. M., Rezayee, F., Ernfors, P., Arenas, E., Hjerling-Leffler, J., Harkany, T., ... Castelo-Branco, G. (2016). Oligodendrocyte heterogeneity in the mouse juvenile and adult central nervous system. *Science (New York, N.Y.)*, *352*(6291), 1326–1329.
- Marques, S., van Bruggen, D., Vanichkina, D. P., Floriddia, E. M., Munguba, H., Våremo, L., Giacomello, S., Falcão, A. M., Meijer, M., Björklund, Å. K., Hjerling-Leffler, J., Taft, R. J., & Castelo-Branco, G. (2018). Transcriptional Convergence of Oligodendrocyte Lineage Progenitors during Development. *Developmental cell*, *46*(4), 504–517.e7.
- Matsuoka, T., Ahlberg, P. E., Kessaris, N., Iannarelli, P., Dennehy, U., Richardson, W. D., McMahon, A. P., & Koentges, G. (2005). Neural crest origins of the neck and shoulder. *Nature*, *436*(7049), 347–355.
- McKenzie, I. A., Ohayon, D., Li, H., de Faria, J. P., Emery, B., Tohyama, K., & Richardson, W. D. (2014). Motor skill learning requires active central myelination. *Science (New York, N.Y.)*, *346*(6207), 318–322.
- Mei, F., Lehmann-Horn, K., Shen, Y. A., Rankin, K. A., Stebbins, K. J., Lorrain, D. S., Pekarek, K., A Sagan, S., Xiao, L., Teuscher, C., von Büdingen, H. C., Wess, J., Lawrence, J. J., Green, A. J., Fancy, S. P., Zamvil, S. S., & Chan, J. R. (2016). Accelerated remyelination during inflammatory demyelination prevents axonal loss and improves functional recovery. *eLife*, *5*, e18246.
- Mendez Colmenares, A., Voss, M. W., Fanning, J., Salerno, E. A., Gothe, N. P., Thomas, M. L., McAuley, E., Kramer, A. F., & Burzynska, A. Z. (2021). White matter plasticity in healthy older adults: The effects of aerobic exercise. *NeuroImage*, *239*, 118305.

- Mensch, S., Baraban, M., Almeida, R., Czopka, T., Ausborn, J., El Manira, A., & Lyons, D. A. (2015). Synaptic vesicle release regulates myelin sheath number of individual oligodendrocytes in vivo. *Nature neuroscience*, 18(5), 628–630.
- Merour, E., Hmidan, H., Marie, C., Helou, P. H., Lu, H., Potel, A., Hure, J. B., Clavairolly, A., Shih, Y. P., Goudarzi, S., Dussaud, S., Ravassard, P., Hafizi, S., Lo, S. H., Hassan, B. A., & Parras, C. (2022). Transient regulation of focal adhesion via Tensin3 is required for nascent oligodendrocyte differentiation. *eLife*, 11, e80273.
- Michailov, G. V., Sereda, M. W., Brinkmann, B. G., Fischer, T. M., Haug, B., Birchmeier, C., Role, L., Lai, C., Schwab, M. H., & Nave, K. A. (2004). Axonal neuregulin-1 regulates myelin sheath thickness. *Science (New York, N.Y.)*, 304(5671), 700–703.
- Micheva, K. D., Wolman, D., Mensh, B. D., Pax, E., Buchanan, J., Smith, S. J., & Bock, D. D. (2016). A large fraction of neocortical myelin ensheathes axons of local inhibitory neurons. *eLife*, 5, e15784.
- Micu, I., Jiang, Q., Coderre, E., Ridsdale, A., Zhang, L., Woulfe, J., Yin, X., Trapp, B. D., McRory, J. E., Rehak, R., Zamponi, G. W., Wang, W., & Stys, P. K. (2006). NMDA receptors mediate calcium accumulation in myelin during chemical ischaemia. *Nature*, 439(7079), 988–992.
- Micu, I., Plemel, J. R., Lachance, C., Proft, J., Jansen, A. J., Cummins, K., van Minnen, J., & Stys, P. K. (2016). The molecular physiology of the axo-myelinic synapse. *Experimental neurology*, 276, 41–50.
- Miller R. H. (1996). Oligodendrocyte origins. *Trends in neurosciences*, 19(3), 92–96.
- Mitew, S., Kirkcaldie, M. T., Halliday, G. M., Shepherd, C. E., Vickers, J. C., & Dickson, T. C. (2010). Focal demyelination in Alzheimer's disease and transgenic mouse models. *Acta neuropathologica*, 119(5), 567–577.
- Mitew, S., Gobius, I., Fenlon, L. R., McDougall, S. J., Hawkes, D., Xing, Y. L., Bujalka, H., Gundlach, A. L., Richards, L. J., Kilpatrick, T. J., Merson, T. D., & Emery, B. (2018). Pharmacogenetic stimulation of neuronal activity increases myelination in an axon-specific manner. *Nature communications*, 9(1), 306.
- Monyer, H., Sprengel, R., Schoepfer, R., Herb, A., Higuchi, M., Lomeli, H., Burnashev, N., Sakmann, B., & Seeburg, P. H. (1992). Heteromeric NMDA receptors: molecular and functional distinction of subtypes. *Science (New York, N.Y.)*, 256(5060), 1217–1221.
- Monyer, H., Burnashev, N., Laurie, D. J., Sakmann, B., & Seeburg, P. H. (1994). Developmental and regional expression in the rat brain and functional properties of four NMDA receptors. *Neuron*, 12(3), 529–540.
- Moore, C. S., Cui, Q. L., Warsi, N. M., Durafour, B. A., Zorko, N., Owen, D. R., Antel, J. P., & Bar-Or, A. (2015). Direct and indirect effects of immune and central nervous system-resident cells on human oligodendrocyte progenitor cell differentiation. *Journal of immunology (Baltimore, Md. : 1950)*, 194(2), 761–772.
- Müller, J., Reyes-Haro, D., Pivneva, T., Nolte, C., Schaette, R., Lübke, J., & Kettenmann, H. (2009). The principal neurons of the medial nucleus of the trapezoid body and NG2(+) glial cells receive coordinated excitatory synaptic input. *The Journal of general physiology*, 134(2), 115–127.
- Munyeshyaka, M., & Fields, R. D. (2022). Oligodendroglia are emerging players in several forms of learning and memory. *Communications biology*, 5(1), 1148.

- Murillo, A., Navarro, A. I., Puellas, E., Zhang, Y., Petros, T. J., & Pérez-Otaño, I. (2021). Temporal Dynamics and Neuronal Specificity of Grin3a Expression in the Mouse Forebrain. *Cerebral cortex (New York, N.Y. : 1991)*, 31(4), 1914–1926.
- Murphy, K. M., Mancini, S. J., Clayworth, K. V., Arbabi, K., & Beshara, S. (2020). Experience-Dependent Changes in Myelin Basic Protein Expression in Adult Visual and Somatosensory Cortex. *Frontiers in cellular neuroscience*, 14, 56.
- Najm, F. J., Madhavan, M., Zaremba, A., Shick, E., Karl, R. T., Factor, D. C., Miller, T. E., Nevin, Z. S., Kantor, C., Sargent, A., Quick, K. L., Schlatzer, D. M., Tang, H., Papoian, R., Brimacombe, K. R., Shen, M., Boxer, M. B., Jadhav, A., Robinson, A. P., Podojil, J. R., ... Tesar, P. J. (2015). Drug-based modulation of endogenous stem cells promotes functional remyelination in vivo. *Nature*, 522(7555), 216–220.
- Neumann, B., Baror, R., Zhao, C., Segel, M., Dietmann, S., Rawji, K. S., Foerster, S., McClain, C. R., Chalut, K., van Wijngaarden, P., & Franklin, R. J. M. (2019). Metformin Restores CNS Remyelination Capacity by Rejuvenating Aged Stem Cells. *Cell stem cell*, 25(4), 473–485.e8.
- Nicholson, M., Wood, R. J., Gonsalvez, D. G., Hannan, A. J., Fletcher, J. L., Xiao, J., & Murray, S. S. (2022). Remodelling of myelinated axons and oligodendrocyte differentiation is stimulated by environmental enrichment in the young adult brain. *The European journal of neuroscience*, 56(12), 6099–6114.
- Nikić, I., Merkler, D., Sorbara, C., Brinkoetter, M., Kreutzfeldt, M., Bareyre, F. M., Brück, W., Bishop, D., Misgeld, T., & Kerschensteiner, M. (2011). A reversible form of axon damage in experimental autoimmune encephalomyelitis and multiple sclerosis. *Nature medicine*, 17(4), 495–499.
- Oka, A., Belliveau, M. J., Rosenberg, P. A., & Volpe, J. J. (1993). Vulnerability of oligodendroglia to glutamate: pharmacology, mechanisms, and prevention. *The Journal of neuroscience : the official journal of the Society for Neuroscience*, 13(4), 1441–1453.
- Orduz, D., Benamer, N., Ortolani, D., Coppola, E., Vigier, L., Pierani, A., & Angulo, M. C. (2019). Developmental cell death regulates lineage-related interneuron-oligodendroglia functional clusters and oligodendrocyte homeostasis. *Nature communications*, 10(1), 4249.
- Ortiz, F. C., Habermacher, C., Graciarena, M., Houry, P. Y., Nishiyama, A., Nait Oumesmar, B., & Angulo, M. C. (2019). Neuronal activity in vivo enhances functional myelin repair. *JCI insight*, 5(9), e123434.
- Osorio, N., Martineau, M., Fortea, M., Rouget, C., Penalba, V., Lee, C. J., Boesmans, W., Rolli-Derkinderen, M., Patel, A. V., Mondielli, G., Conrod, S., Labat-Gest, V., Papin, A., Sasabe, J., Sweedler, J. V., Vanden Berghe, P., Delmas, P., & Mothet, J. P. (2023). d-Serine agonism of GluN1-GluN3 NMDA receptors regulates the activity of enteric neurons and coordinates gut motility. *bioRxiv : the preprint server for biology*, 2023.04.19.537136.
- Osso, L. A., Rankin, K. A., & Chan, J. R. (2021). Experience-dependent myelination following stress is mediated by the neuropeptide dynorphin. *Neuron*, 109(22), 3619–3632.e5.

- Otsu, Y., Darcq, E., Pietrajtis, K., Mátyás, F., Schwartz, E., Bessaih, T., Abi Gerges, S., Rousseau, C. V., Grand, T., Dieudonné, S., Paoletti, P., Acsády, L., Agulhon, C., Kieffer, B. L., & Diana, M. A. (2019). Control of aversion by glycine-gated GluN1/GluN3A NMDA receptors in the adult medial habenula. *Science (New York, N.Y.)*, 366(6462), 250–254.
- Pachernegg, S., Strutz-Seebohm, N., & Hollmann, M. (2012). GluN3 subunit-containing NMDA receptors: not just one-trick ponies. *Trends in neurosciences*, 35(4), 240–249.
- Pan, S., Mayoral, S. R., Choi, H. S., Chan, J. R., & Kheirbek, M. A. (2020). Preservation of a remote fear memory requires new myelin formation. *Nature neuroscience*, 23(4), 487–499.
- Paoletti, P., Bellone, C., & Zhou, Q. (2013). NMDA receptor subunit diversity: impact on receptor properties, synaptic plasticity and disease. *Nature reviews. Neuroscience*, 14(6), 383–400.
- Patani, R., Balaratnam, M., Vora, A., & Reynolds, R. (2007). Remyelination can be extensive in multiple sclerosis despite a long disease course. *Neuropathology and applied neurobiology*, 33(3), 277–287.
- Patrikios, P., Stadelmann, C., Kutzelnigg, A., Rauschka, H., Schmidbauer, M., Laursen, H., Sorensen, P. S., Brück, W., Lucchinetti, C., & Lassmann, H. (2006). Remyelination is extensive in a subset of multiple sclerosis patients. *Brain : a journal of neurology*, 129(Pt 12), 3165–3172.
- Pérez-Cerdá, F., Sánchez-Gómez, M. V., & Matute, C. (2015). Pío del Río Hortega and the discovery of the oligodendrocytes. *Frontiers in neuroanatomy*, 9, 92.
- Perez-Otano, I., Schulteis, C. T., Contractor, A., Lipton, S. A., Trimmer, J. S., Sucher, N. J., & Heinemann, S. F. (2001). Assembly with the NR1 subunit is required for surface expression of NR3A-containing NMDA receptors. *The Journal of neuroscience : the official journal of the Society for Neuroscience*, 21(4), 1228–1237.
- Pérez-Otaño, I., Luján, R., Tavalin, S. J., Plomann, M., Modregger, J., Liu, X. B., Jones, E. G., Heinemann, S. F., Lo, D. C., & Ehlers, M. D. (2006). Endocytosis and synaptic removal of NR3A-containing NMDA receptors by PACSIN1/syndapin1. *Nature neuroscience*, 9(5), 611–621.
- Pérez-Otaño, I., Larsen, R. S., & Wesseling, J. F. (2016). Emerging roles of GluN3-containing NMDA receptors in the CNS. *Nature reviews. Neuroscience*, 17(10), 623–635.
- Peters, A., Proskauer, C.C., and Kaiserman-Abramof, I.R. (1968). The small pyramidal neuron of the rat cerebral cortex. The axon hillock and initial segment. *Journal of Cell Biology* 39, 604–619.
- Pfeffer, C., Xue, M., He, M., Huang, Z. J., & Scanziani, M. (2013). Inhibition of inhibition in visual cortex: the logic of connections between molecularly distinct interneurons. *Nature Neuroscience* 16, 1068–1076.
- Philips, T., Bento-Abreu, A., Nonneman, A., Haeck, W., Staats, K., Geelen, V., Hersmus, N., Küsters, B., Van Den Bosch, L., Van Damme, P., Richardson, W. D., & Robberecht, W. (2013). Oligodendrocyte dysfunction in the pathogenesis of amyotrophic lateral sclerosis. *Brain : a journal of neurology*, 136(Pt 2), 471–482.

- Piña-Crespo, J. C., Talantova, M., Micu, I., States, B., Chen, H. S., Tu, S., Nakanishi, N., Tong, G., Zhang, D., Heinemann, S. F., Zamponi, G. W., Stys, P. K., & Lipton, S. A. (2010). Excitatory glycine responses of CNS myelin mediated by NR1/NR3 "NMDA" receptor subunits. *The Journal of neuroscience : the official journal of the Society for Neuroscience*, 30(34), 11501–11505.
- Poggi, G., Albiez, J., & Pryce, C. R. (2022). Effects of chronic social stress on oligodendrocyte proliferation-maturation and myelin status in prefrontal cortex and amygdala in adult mice. *Neurobiology of stress*, 18, 100451.
- Praet, J., Guglielmetti, C., Berneman, Z., Van der Linden, A., & Ponsaerts, P. (2014). Cellular and molecular neuropathology of the cuprizone mouse model: clinical relevance for multiple sclerosis. *Neuroscience and biobehavioral reviews*, 47, 485–505.
- Prineas, J. W., Barnard, R. O., Kwon, E. E., Sharer, L. R., & Cho, E. S. (1993). Multiple sclerosis: remyelination of nascent lesions. *Annals of neurology*, 33(2), 137–151.
- Pryor, W. M., Freeman, K. G., Larson, R. D., Edwards, G. L., & White, L. J. (2015). Chronic exercise confers neuroprotection in experimental autoimmune encephalomyelitis. *Journal of neuroscience research*, 93(5), 697–706.
- Psachoulia, K., Jamen, F., Young, K. M., & Richardson, W. D. (2009). Cell cycle dynamics of NG2 cells in the postnatal and ageing brain. *Neuron glia biology*, 5(3-4), 57–67.
- Ranvier L. Contributions à l'histologie et à la physiologie des nerfs périphériques. *C R Acad Sci*. 1871;73:1168–1171.
- Rasband, M. N., & Peles, E. (2015). The Nodes of Ranvier: Molecular Assembly and Maintenance. *Cold Spring Harbor perspectives in biology*, 8(3), a020495.
- Redmond, S. A., Mei, F., Eshed-Eisenbach, Y., Osso, L. A., Leshkowitz, D., Shen, Y. A., Kay, J. N., Aurrand-Lions, M., Lyons, D. A., Peles, E., & Chan, J. R. (2016). Somatodendritic Expression of JAM2 Inhibits Oligodendrocyte Myelination. *Neuron*, 91(4), 824–836.
- Rivera, A. D., Pieropan, F., Chacon-De-La-Rocha, I., Lecca, D., Abbracchio, M. P., Azim, K., & Butt, A. M. (2021). Functional genomic analyses highlight a shift in Gpr17-regulated cellular processes in oligodendrocyte progenitor cells and underlying myelin dysregulation in the aged mouse cerebrum. *Aging cell*, 20(4), e13335.
- Rivers, L. E., Young, K. M., Rizzi, M., Jamen, F., Psachoulia, K., Wade, A., Kessaris, N., & Richardson, W. D. (2008). PDGFRA/NG2 glia generate myelinating oligodendrocytes and piriform projection neurons in adult mice. *Nature neuroscience*, 11(12), 1392–1401.
- Roberts, A. C., Díez-García, J., Rodríguez, R. M., López, I. P., Luján, R., Martínez-Turrillas, R., Picó, E., Henson, M. A., Bernardo, D. R., Jarrett, T. M., Clendeninn, D. J., López-Mascaraque, L., Feng, G., Lo, D. C., Wesseling, J. F., Wetsel, W. C., Philpot, B. D., & Pérez-Otaño, I. (2009). Downregulation of NR3A-containing NMDARs is required for synapse maturation and memory consolidation. *Neuron*, 63(3), 342–356.
- Robertson W. F. (1899). On a new method of obtaining a black reaction in certain tissue-elements of central nervous system (platinum method). *Scottish Med. Surg* 4, 23–30.

- Rodriguez, E. G., Wegner, C., Kreutzfeldt, M., Neid, K., Thal, D. R., Jürgens, T., Brück, W., Stadelmann, C., & Merkler, D. (2014). Oligodendroglia in cortical multiple sclerosis lesions decrease with disease progression, but regenerate after repeated experimental demyelination. *Acta neuropathologica*, 128(2), 231–246.
- Rowitch, D. H., & Kriegstein, A. R. (2010). Developmental genetics of vertebrate glial-cell specification. *Nature*, 468(7321), 214–222.
- Roy, K., Murtie, J. C., El-Khodori, B. F., Edgar, N., Sardi, S. P., Hooks, B. M., Benoit-Marand, M., Chen, C., Moore, H., O'Donnell, P., Brunner, D., & Corfas, G. (2007). Loss of erbB signaling in oligodendrocytes alters myelin and dopaminergic function, a potential mechanism for neuropsychiatric disorders. *Proceedings of the National Academy of Sciences of the United States of America*, 104(19), 8131–8136.
- Saab, A. S., Tzvetavona, I. D., Trevisiol, A., Baltan, S., Dibaj, P., Kusch, K., Möbius, W., Goetze, B., Jahn, H. M., Huang, W., Steffens, H., Schomburg, E. D., Pérez-Samartín, A., Pérez-Cerdá, F., Bakhtiari, D., Matute, C., Löwel, S., Griesinger, C., Hirrlinger, J., Kirchhoff, F., ... Nave, K. A. (2016). Oligodendroglial NMDA Receptors Regulate Glucose Import and Axonal Energy Metabolism. *Neuron*, 91(1), 119–132.
- Salter, M. G., & Fern, R. (2005). NMDA receptors are expressed in developing oligodendrocyte processes and mediate injury. *Nature*, 438(7071), 1167–1171.
- Sampaio-Baptista, C., Khrapitchev, A. A., Foxley, S., Schlagheck, T., Scholz, J., Jbabdi, S., DeLuca, G. C., Miller, K. L., Taylor, A., Thomas, N., Kleim, J., Sibson, N. R., Bannerman, D., & Johansen-Berg, H. (2013). Motor skill learning induces changes in white matter microstructure and myelination. *The Journal of neuroscience : the official journal of the Society for Neuroscience*, 33(50), 19499–19503.
- Saraswat, D., Shayya, H. J., Polanco, J. J., Tripathi, A., Welliver, R. R., Pol, S. U., Seidman, R. A., Broome, J. E., O'Bara, M. A., van Kuppervelt, T. H., Phillips, J. J., Dutta, R., & Sim, F. J. (2021). Overcoming the inhibitory microenvironment surrounding oligodendrocyte progenitor cells following experimental demyelination. *Nature communications*, 12(1), 1923.
- Sasaki, Y. F., Rothe, T., Premkumar, L. S., Das, S., Cui, J., Talantova, M. V., Wong, H. K., Gong, X., Chan, S. F., Zhang, D., Nakanishi, N., Sucher, N. J., & Lipton, S. A. (2002). Characterization and comparison of the NR3A subunit of the NMDA receptor in recombinant systems and primary cortical neurons. *Journal of neurophysiology*, 87(4), 2052–2063.
- Savtchouk, I., Di Castro, M. A., Ali, R., Stubbe, H., Luján, R., & Volterra, A. (2019). Circuit-specific control of the medial entorhinal inputs to the dentate gyrus by atypical presynaptic NMDARs activated by astrocytes. *Proceedings of the National Academy of Sciences of the United States of America*, 116(27), 13602–13610.
- Schlegel, A. A., Rudelson, J. J., & Tse, P. U. (2012). White matter structure changes as adults learn a second language. *Journal of cognitive neuroscience*, 24(8), 1664–1670.
- Schmitz, T., & Chew, L. J. (2008). Cytokines and myelination in the central nervous system. *TheScientificWorldJournal*, 8, 1119–1147.
- Scholz, J., Klein, M. C., Behrens, T. E., & Johansen-Berg, H. (2009). Training induces changes in white-matter architecture. *Nature neuroscience*, 12(11), 1370–1371.

- Schorge, S., & Colquhoun, D. (2003). Studies of NMDA receptor function and stoichiometry with truncated and tandem subunits. *The Journal of neuroscience : the official journal of the Society for Neuroscience*, 23(4), 1151–1158.
- Seeker, L. A., Bestard-Cuche, N., Jäkel, S., Kazakou, N. L., Bøstrand, S. M. K., Wagstaff, L. J., Cholewa-Waclaw, J., Kilpatrick, A. M., Van Bruggen, D., Kabbe, M., Baldivia Pohl, F., Moslehi, Z., Henderson, N. C., Vallejos, C. A., La Manno, G., Castelo-Branco, G., & Williams, A. (2023). Brain matters: unveiling the distinct contributions of region, age, and sex to glia diversity and CNS function. *Acta neuropathologica communications*, 11(1), 84.
- Segel, M., Neumann, B., Hill, M. F. E., Weber, I. P., Viscomi, C., Zhao, C., Young, A., Agle, C. C., Thompson, A. J., Gonzalez, G. A., Sharma, A., Holmqvist, S., Rowitch, D. H., Franze, K., Franklin, R. J. M., & Chalut, K. J. (2019). Niche stiffness underlies the ageing of central nervous system progenitor cells. *Nature*, 573(7772), 130–134.
- Shaker, M. R., Pietrogrande, G., Martin, S., Lee, J. H., Sun, W., & Wolvetang, E. J. (2021). Rapid and Efficient Generation of Myelinating Human Oligodendrocytes in Organoids. *Frontiers in cellular neuroscience*, 15, 631548.
- Shields, S. A., Gilson, J. M., Blakemore, W. F., & Franklin, R. J. (1999). Remyelination occurs as extensively but more slowly in old rats compared to young rats following gliotoxin-induced CNS demyelination. *Glia*, 28(1), 77–83.
- Shimizu, T., Nayar, S. G., Swire, M., Jiang, Y., Grist, M., Kaller, M., Sampaio Baptista, C., Bannerman, D. M., Johansen-Berg, H., Ogasawara, K., Tohyama, K., Li, H., & Richardson, W. D. (2023). Oligodendrocyte dynamics dictate cognitive performance outcomes of working memory training in mice. *Nature communications*, 14(1), 6499.
- Shin, H., & Kawai, H. D. (2021). Sensitive timing of undifferentiation in oligodendrocyte progenitor cells and their enhanced maturation in primary visual cortex of binocularly enucleated mice. *PloS one*, 16(9), e0257395.
- Simon, C., Götz, M., & Dimou, L. (2011). Progenitors in the adult cerebral cortex: cell cycle properties and regulation by physiological stimuli and injury. *Glia*, 59(6), 869–881.
- Souza, P. S., Gonçalves, E. D., Pedroso, G. S., Farias, H. R., Junqueira, S. C., Marcon, R., Tuon, T., Cola, M., Silveira, P. C. L., Santos, A. R., Calixto, J. B., Souza, C. T., de Pinho, R. A., & Dutra, R. C. (2017). Physical Exercise Attenuates Experimental Autoimmune Encephalomyelitis by Inhibiting Peripheral Immune Response and Blood-Brain Barrier Disruption. *Molecular neurobiology*, 54(6), 4723–4737.
- Spitzer, S. O., Sitnikov, S., Kamen, Y., Evans, K. A., Kronenberg-Versteeg, D., Dietmann, S., de Faria, O., Jr, Agathou, S., & Káradóttir, R. T. (2019). Oligodendrocyte Progenitor Cells Become Regionally Diverse and Heterogeneous with Age. *Neuron*, 101(3), 459–471.e5.
- Staffa, A., Chatterjee, M., Diaz-Tahoces, A., Leroy, F., & Perez-Otaño, I. (2023). Monitoring Fine and Associative Motor Learning in Mice Using the Erasmus Ladder. *Journal of visualized experiments : JoVE*, (202), 10.3791/65958.
- Steadman, P. E., Xia, F., Ahmed, M., Mocle, A. J., Penning, A. R. A., Geraghty, A. C., Steenland, H. W., Monje, M., Josselyn, S. A., & Frankland, P. W. (2020). Disruption of Oligodendrogenesis Impairs Memory Consolidation in Adult Mice. *Neuron*, 105(1), 150–164.e6.
- Sun, L. O., Mulinyawe, S. B., Collins, H. Y., Ibrahim, A., Li, Q., Simon, D. J., Tessier-Lavigne, M., & Barres, B. A. (2018). Spatiotemporal Control of CNS Myelination by Oligodendrocyte Programmed Cell Death through the TFEB-PUMA Axis. *Cell*, 175(7), 1811–1826.e21.

- Sun, Y., Tong, H., Yang, T., Liu, L., Li, X. J., & Li, S. (2022). Insights into White Matter Defect in Huntington's Disease. *Cells*, 11(21), 3381.
- Susuki K. (2013). Node of Ranvier disruption as a cause of neurological diseases. *ASN neuro*, 5(3), 209–219.
- Susuki, K., Chang, K. J., Zollinger, D. R., Liu, Y., Ogawa, Y., Eshed-Eisenbach, Y., Dours-Zimmermann, M. T., Osés-Prieto, J. A., Burlingame, A. L., Seidenbecher, C. I., Zimmermann, D. R., Oohashi, T., Peles, E., & Rasband, M. N. (2013). Three mechanisms assemble central nervous system nodes of Ranvier. *Neuron*, 78(3), 469–482.
- Swire, M., Kotelevtsev, Y., Webb, D. J., Lyons, D. A., & Ffrench-Constant, C. (2019). Endothelin signalling mediates experience-dependent myelination in the CNS. *eLife*, 8, e49493.
- Takeuchi, H., Sekiguchi, A., Taki, Y., Yokoyama, S., Yomogida, Y., Komuro, N., Yamanouchi, T., Suzuki, S., & Kawashima, R. (2010). Training of working memory impacts structural connectivity. *The Journal of neuroscience : the official journal of the Society for Neuroscience*, 30(9), 3297–3303.
- Tang, J., Liang, X., Dou, X., Qi, Y., Yang, C., Luo, Y., Chao, F., Zhang, L., Xiao, Q., Jiang, L., Zhou, C., & Tang, Y. (2021). Exercise rather than fluoxetine promotes oligodendrocyte differentiation and myelination in the hippocampus in a male mouse model of depression. *Translational psychiatry*, 11(1), 622.
- Tauber, H., Waehneldt, T. V., & Neuhoﬀ, V. (1980). Myelination in rabbit optic nerves is accelerated by artificial eye opening. *Neuroscience letters*, 16(3), 235–238.
- Taveggia, C., Zanazzi, G., Petrylak, A., Yano, H., Rosenbluth, J., Einheber, S., Xu, X., Esper, R. M., Loeb, J. A., Shrager, P., Chao, M. V., Falls, D. L., Role, L., & Salzer, J. L. (2005). Neuregulin-1 type III determines the ensheathment fate of axons. *Neuron*, 47(5), 681–694.
- Tiane, A., Schepers, M., Rombaut, B., Hupperts, R., Prickaerts, J., Hellings, N., van den Hove, D., & Vanmierlo, T. (2019). From OPC to Oligodendrocyte: An Epigenetic Journey. *Cells*, 8(10), 1236.
- Tomassy, G. S., Berger, D. R., Chen, H. H., Kasthuri, N., Hayworth, K. J., Vercelli, A., Seung, H. S., Lichtman, J. W., & Arlotta, P. (2014). Distinct profiles of myelin distribution along single axons of pyramidal neurons in the neocortex. *Science (New York, N.Y.)*, 344(6181), 319–324.
- Tong, G., Takahashi, H., Tu, S., Shin, Y., Talantova, M., Zago, W., Xia, P., Nie, Z., Goetz, T., Zhang, D., Lipton, S. A., & Nakanishi, N. (2008). Modulation of NMDA receptor properties and synaptic transmission by the NR3A subunit in mouse hippocampal and cerebrocortical neurons. *Journal of neurophysiology*, 99(1), 122–132.
- Torre-Fuentes, L., Moreno-Jiménez, L., Pytel, V., Matías-Guiu, J. A., Gómez-Pinedo, U., & Matías-Guiu, J. (2020). Experimental models of demyelination and remyelination. Modelos experimentales de desmielinización-remielinización. *Neurologia*, 35(1), 32–39.
- Trapp, B. D., Nishiyama, A., Cheng, D., & Macklin, W. (1997). Differentiation and death of premyelinating oligodendrocytes in developing rodent brain. *The Journal of cell biology*, 137(2), 459–468.
- Tripathi, R. B., Jackiewicz, M., McKenzie, I. A., Kougioumtzidou, E., Grist, M., & Richardson, W. D. (2017). Remarkable Stability of Myelinating Oligodendrocytes in Mice. *Cell reports*, 21(2), 316–323.

- Valdés-Tovar, M., Rodríguez-Ramírez, A. M., Rodríguez-Cárdenas, L., Sotelo-Ramírez, C. E., Camarena, B., Sanabrais-Jiménez, M. A., Solís-Chagoyán, H., Argueta, J., & López-Riquelme, G. O. (2022). Insights into myelin dysfunction in schizophrenia and bipolar disorder. *World journal of psychiatry*, 12(2), 264–285.
- Van Leeuwenhoek A. *Delft, Adrianum Beman*. 1719. Epistola XXXII. Epistolae Physiologicae Super Compluribus Naturae Arcanis; pp. 309–317.
- Van Tilborg, E., de Theije, C. G. M., van Hal, M., Wagenaar, N., de Vries, L. S., Benders, M. J., Rowitch, D. H., & Nijboer, C. H. (2018). Origin and dynamics of oligodendrocytes in the developing brain: Implications for perinatal white matter injury. *Glia*, 66(2), 221–238.
- Vega-Riquer, J. M., Mendez-Victoriano, G., Morales-Luckie, R. A., & Gonzalez-Perez, O. (2019). Five Decades of Cuprizone, an Updated Model to Replicate Demyelinating Diseases. *Current neuropharmacology*, 17(2), 129–141.
- Velasco, S., Kedaigle, A. J., Simmons, S. K., Nash, A., Rocha, M., Quadrato, G., Paulsen, B., Nguyen, L., Adiconis, X., Regev, A., Levin, J. Z., & Arlotta, P. (2019). Individual brain organoids reproducibly form cell diversity of the human cerebral cortex. *Nature*, 570(7762), 523–527.
- Vesalius A. *De Humani Corporis Fabrica Libri Septem*. 1543.
- Vestergaard, M., Madsen, K. S., Baaré, W. F., Skimminge, A., Ejersbo, L. R., Ramsøy, T. Z., Gerlach, C., Akesson, P., Paulson, O. B., & Jernigan, T. L. (2011). White matter microstructure in superior longitudinal fasciculus associated with spatial working memory performance in children. *Journal of cognitive neuroscience*, 23(9), 2135–2146.
- Viganò, F., Möbius, W., Götz, M., & Dimou, L. (2013). Transplantation reveals regional differences in oligodendrocyte differentiation in the adult brain. *Nature neuroscience*, 16(10), 1370–1372.
- Viganò, F., Schneider, S., Cimino, M., Bonfanti, E., Gelosa, P., Sironi, L., Abbracchio, M. P., & Dimou, L. (2016). GPR17 expressing NG2-Glia: Oligodendrocyte progenitors serving as a reserve pool after injury. *Glia*, 64(2), 287–299.
- Vondran, M. W., Clinton-Luke, P., Honeywell, J. Z., & Dreyfus, C. F. (2010). BDNF+/- mice exhibit deficits in oligodendrocyte lineage cells of the basal forebrain. *Glia*, 58(7), 848–856.
- Wake, H., Lee, P. R., & Fields, R. D. (2011). Control of local protein synthesis and initial events in myelination by action potentials. *Science (New York, N.Y.)*, 333(6049), 1647–1651.
- Wang, H. Y., Crupi, D., Liu, J., Stucky, A., Cruciata, G., Di Rocco, A., Friedman, E., Quartarone, A., & Ghilardi, M. F. (2011). Repetitive transcranial magnetic stimulation enhances BDNF-TrkB signaling in both brain and lymphocyte. *The Journal of neuroscience : the official journal of the Society for Neuroscience*, 31(30), 11044–11054.
- Wang, S., Bates, J., Li, X., Schanz, S., Chandler-Militello, D., Levine, C., Maherali, N., Studer, L., Hochedlinger, K., Windrem, M., & Goldman, S. A. (2013). Human iPSC-derived oligodendrocyte progenitor cells can myelinate and rescue a mouse model of congenital hypomyelination. *Cell stem cell*, 12(2), 252–264.
- Wang, Z., Baharani, A., Wei, Z., Truong, D., Bi, X., Wang, F., Li, X. M., Verge, V. M. K., & Zhang, Y. (2021). Low field magnetic stimulation promotes myelin repair and cognitive recovery in chronic cuprizone mouse model. *Clinical and experimental pharmacology & physiology*, 48(8), 1090–1102.

- Warf, B. C., Fok-Seang, J., & Miller, R. H. (1991). Evidence for the ventral origin of oligodendrocyte precursors in the rat spinal cord. *The Journal of neuroscience : the official journal of the Society for Neuroscience*, 11(8), 2477–2488.
- Wolswijk G. (2002). Oligodendrocyte precursor cells in the demyelinated multiple sclerosis spinal cord. *Brain : a journal of neurology*, 125(Pt 2), 338–349.
- Wong, R. W., Setou, M., Teng, J., Takei, Y., & Hirokawa, N. (2002). Overexpression of motor protein KIF17 enhances spatial and working memory in transgenic mice. *Proceedings of the National Academy of Sciences of the United States of America*, 99(22), 14500–14505.
- Wong, A. W., Xiao, J., Kemper, D., Kilpatrick, T. J., & Murray, S. S. (2013). Oligodendroglial expression of TrkB independently regulates myelination and progenitor cell proliferation. *The Journal of neuroscience : the official journal of the Society for Neuroscience*, 33(11), 4947–4957.
- Woodruff, R. H., Fruttiger, M., Richardson, W. D., & Franklin, R. J. (2004). Platelet-derived growth factor regulates oligodendrocyte progenitor numbers in adult CNS and their response following CNS demyelination. *Molecular and cellular neurosciences*, 25(2), 252–262.
- Xiao, L., Ohayon, D., McKenzie, I. A., Sinclair-Wilson, A., Wright, J. L., Fudge, A. D., Emery, B., Li, H., & Richardson, W. D. (2016). Rapid production of new oligodendrocytes is required in the earliest stages of motor-skill learning. *Nature neuroscience*, 19(9), 1210–1217.
- Xiao, Y., Petrucco, L., Hoodless, L. J., Portugues, R., & Czopka, T. (2022). Oligodendrocyte precursor cells sculpt the visual system by regulating axonal remodeling. *Nature neuroscience*, 25(3), 280–284.
- Xie, Y., Li, Z., Wang, Y., Xue, X., Ma, W., Zhang, Y., & Wang, J. (2019). Effects of moderate- versus high- intensity swimming training on inflammatory and CD4⁺ T cell subset profiles in experimental autoimmune encephalomyelitis mice. *Journal of neuroimmunology*, 328, 60–67.
- Xu, T., Yu, X., Perlik, A. J., Tobin, W. F., Zweig, J. A., Tennant, K., Jones, T., & Zuo, Y. (2009). Rapid formation and selective stabilization of synapses for enduring motor memories. *Nature*, 462(7275), 915–919.
- Yalçın, B., & Monje, M. (2021). Microenvironmental interactions of oligodendroglial cells. *Developmental cell*, 56(13), 1821–1832.
- Yan, L., Wang, M., Yang, F., Wang, Y., Wang, S., So, K. F., & Zhang, L. (2023). Physical exercise mediates a cortical FMRP-mTOR pathway to improve resilience against chronic stress in adolescent mice. *Translational psychiatry*, 13(1), 16.
- Yang, S. M., Michel, K., Jokhi, V., Nedivi, E., & Arlotta, P. (2020). Neuron class-specific responses govern adaptive myelin remodeling in the neocortex. *Science (New York, N.Y.)*, 370(6523), eabd2109.
- Yang, F. Y., Huang, L. H., Wu, M. T., & Pan, Z. Y. (2022). Ultrasound Neuromodulation Reduces Demyelination in a Rat Model of Multiple Sclerosis. *International journal of molecular sciences*, 23(17), 10034.
- Yeung, M. S., Zdunek, S., Bergmann, O., Bernard, S., Salehpour, M., Alkass, K., Perl, S., Tisdale, J., Possnert, G., Brundin, L., Druid, H., & Frisén, J. (2014). Dynamics of oligodendrocyte generation and myelination in the human brain. *Cell*, 159(4), 766–774.

- Young, K. M., Psachoulia, K., Tripathi, R. B., Dunn, S. J., Cossell, L., Attwell, D., Tohyama, K., & Richardson, W. D. (2013). Oligodendrocyte dynamics in the healthy adult CNS: evidence for myelin remodeling. *Neuron*, 77(5), 873–885.
- Yuen, T. J., Silbereis, J. C., Griveau, A., Chang, S. M., Daneman, R., Fancy, S. P. J., Zahed, H., Maltepe, E., & Rowitch, D. H. (2014). Oligodendrocyte-encoded HIF function couples postnatal myelination and white matter angiogenesis. *Cell*, 158(2), 383–396.
- Zhang, Y., Chen, K., Sloan, S. A., Bennett, M. L., Scholze, A. R., O'Keeffe, S., Phatnani, H. P., Guarnieri, P., Caneda, C., Ruderisch, N., Deng, S., Liddelow, S. A., Zhang, C., Daneman, R., Maniatis, T., Barres, B. A., & Wu, J. Q. (2014). An RNA-sequencing transcriptome and splicing database of glia, neurons, and vascular cells of the cerebral cortex. *The Journal of neuroscience : the official journal of the Society for Neuroscience*, 34(36), 11929–11947.
- Zhao, X., Li, Y., Tian, Q., Zhu, B., & Zhao, Z. (2019). Repetitive transcranial magnetic stimulation increases serum brain-derived neurotrophic factor and decreases interleukin-1 β and tumor necrosis factor- α in elderly patients with refractory depression. *The Journal of international medical research*, 47(5), 1848–1855.
- Zheng, J., Sun, X., Ma, C., Li, B. M., & Luo, F. (2019). Voluntary wheel running promotes myelination in the motor cortex through Wnt signaling in mice. *Molecular brain*, 12(1), 85.
- Zhou, Y., & Zhang, J. (2023). Neuronal activity and remyelination: new insights into the molecular mechanisms and therapeutic advancements. *Frontiers in cell and developmental biology*, 11, 1221890.
- Zhu, X., Hill, R. A., Dietrich, D., Komitova, M., Suzuki, R., & Nishiyama, A. (2011). Age-dependent fate and lineage restriction of single NG2 cells. *Development (Cambridge, England)*, 138(4), 745–753.
- Zhu, Z., Yi, F., Epplin, M. P., Liu, D., Summer, S. L., Mizu, R., Shaulsky, G., XiangWei, W., Tang, W., Burger, P. B., Menaldino, D. S., Myers, S. J., Liotta, D. C., Hansen, K. B., Yuan, H., & Traynelis, S. F. (2020). Negative allosteric modulation of GluN1/GluN3 NMDA receptors. *Neuropharmacology*, 176, 108117.
- Zirngibl, M., Assinck, P., Sizov, A., Caprariello, A. V., & Plemel, J. R. (2022). Oligodendrocyte death and myelin loss in the cuprizone model: an updated overview of the intrinsic and extrinsic causes of cuprizone demyelination. *Molecular neurodegeneration*, 17(1), 34.
- Zonouzi, M., Berger, D., Jokhi, V., Kedaigle, A., Lichtman, J., & Arlotta, P. (2019). Individual Oligodendrocytes Show Bias for Inhibitory Axons in the Neocortex. *Cell reports*, 27(10), 2799–2808.e3.



11. ANNEX

Author: *Alice Staffa*

Monitoring Fine and Associative Motor Learning in Mice Using the Erasmus Ladder

Alice Staffa^{*1}, Moumita Chatterjee^{*1}, Ariadna Diaz-Tahoces^{*1}, Felix Leroy¹, Isabel Perez-Otaño¹

¹ Instituto de Neurociencias, Sant Joan d'Alacant, Spain - Consejo Superior de Investigaciones Científicas and Universidad Miguel Hernández

^{*}These authors contributed equally

Corresponding Author

Alice Staffa
astaffa@umh.es

Citation

Staffa, A., Chatterjee, M., Diaz-Tahoces, A., Leroy, F., Perez-Otaño, I. Monitoring Fine and Associative Motor Learning in Mice Using the Erasmus Ladder. *J. Vis. Exp.* (2022), e65958, doi:10.3791/65958 (2023).

Date Published

December 15, 2023

DOI

10.3791/65958

URL

jove.com/video/65958

Abstract

Behavior is shaped by actions, and actions necessitate motor skills such as strength, coordination, and learning. None of the behaviors essential for sustaining life would be possible without the ability to transition from one position to another. Unfortunately, motor skills can be compromised in a wide array of diseases. Therefore, investigating the mechanisms of motor functions at the cellular, molecular, and circuit levels, as well as understanding the symptoms, causes, and progression of motor disorders, is crucial for developing effective treatments. Mouse models are frequently employed for this purpose.

This article describes a protocol that allows the monitoring of various aspects of motor performance and learning in mice using an automated tool called the Erasmus Ladder. The assay involves two phases: an initial phase where mice are trained to navigate a horizontal ladder built of irregular rungs ("fine motor learning"), and a second phase where an obstacle is presented in the path of the moving animal. The perturbation can be unexpected ("challenged motor learning") or preceded by an auditory tone ("associative motor learning"). The task is easy to conduct and is fully supported by automated software.

This report shows how different readouts from the test, when analyzed with sensitive statistical methods, allow fine monitoring of mouse motor skills using a small cohort of mice. We propose that the method will be highly sensitive to evaluate motor adaptations driven by environmental modifications as well as early-stage subtle motor deficits in mutant mice with compromised motor functions.

Introduction

A variety of tests have been developed to assess motor phenotypes in mice. Each test gives information on a specific aspect of motor behavior¹. For example, the open field test informs on general locomotion and anxiety state; the rotarod and walking beam tests on coordination and balance; footprint analysis is about gait; the treadmill or running wheel on forced or voluntary physical exercise; and the complex wheel is about motor skill learning. To analyze mouse motor phenotypes, investigators must perform these tests sequentially, which involves a lot of time and effort and often several animal cohorts. If there is information at the cellular or circuitry level, the investigator normally opts for a test that monitors a related aspect and follows from there. However, paradigms that discriminate different aspects of motor behavior in an automated way are lacking.

This article describes a protocol to use the Erasmus Ladder^{2,3}, a system that allows comprehensive assessment of a variety of motor learning features in mice. The main advantages are the reproducibility and sensitivity of the method, along with the ability to titrate motor difficulty and to separate deficits in motor performance from impaired associative motor learning. The main component consists of a horizontal ladder with alternate high (H) and low (L) rungs equipped with touch-sensitive sensors that detect the position of the mouse on the ladder. The ladder is made of 2 x 37 rungs (L, 6 mm; H, 12 mm) spaced 15 mm apart from each other and positioned in a left-right alternating pattern with 30 mm gaps (**Figure 1A**). Rungs can be moved individually to generate various levels of difficulty, that is, creating an obstacle (raising the high rungs by 18 mm). Coupled with an automated recording system and associating modifications of the rung pattern with sensory stimuli, the

Erasmus ladder tests for fine motor learning and adaptation of motor performance in response to environmental challenges (appearance of a higher rung to simulate an obstacle, an unconditioned stimulus [US]) or association with sensory stimuli (a tone, a conditioned stimulus [CS]). Testing involves two distinct phases, each assessing improvement in motor performance over 4 days, during which mice undergo a session of 42 consecutive trials per day. In the initial phase, mice are trained to navigate the ladder to assess "fine" or "skilled" motor learning. The second phase consists of interleaved trials where an obstacle in the form of a higher rung is presented in the path of the moving animal. The perturbation can be unexpected to assess "challenged" motor learning (US-only trials) or announced by an auditory tone to assess "associative" motor learning (Paired trials).

The Erasmus ladder has been developed relatively recently^{2,3}. It has not been extensively used because setting up and optimizing the protocol required focused effort and was specifically designed to assess cerebellar-dependent associative learning without exploring in detail its potential to reveal other motor deficits. To date, it has been validated for its ability to unveil subtle motor impairments linked to cerebellar dysfunction in mice^{3,4,5,6,7,8}. For instance, *connexin36* (Cx36) knockout mice, where gap junctions are impaired in olivary neurons, display firing deficits due to lack of electrotonic coupling but the motor phenotype had been hard to pinpoint. Testing using the Erasmus ladder suggested that the role of inferior olivary neurons in a cerebellar motor learning task is to encode precise temporal coding of stimuli and facilitate learning-dependent responses to unexpected events^{3,4}. *Fragile X Messenger Ribonucleoprotein 1* (*Fmr1*) knockout mouse, a model for Fragile-X-Syndrome (FXS),

exhibits a well-known cognitive impairment along with milder defects in procedural memory formation. *Fmr1* knockouts showed no significant differences in step times, missteps per trial, or motor performance improvement over sessions in the Erasmus Ladder but failed to adjust their walking pattern to the suddenly appearing obstacle compared to their wild-type (WT) littermates, confirming specific procedural and associative memory deficits^{3,5}. Furthermore, cell-specific mouse mutant lines with defects in cerebellar function, including impaired Purkinje cell output, potentiation, and molecular layer interneuron or granule cell outputs, exhibited problems in motor coordination with altered acquisition of efficient step patterns and in the number of steps taken to cross the ladder⁶. Neonatal brain injury causes cerebellar learning deficits and Purkinje cell dysfunction that could also be detected with the Erasmus Ladder^{7,8}.

In this video, we present a comprehensive step-by-step guide, which details the setup of the behavioral room, the behavioral test protocol, and subsequent data analysis. This report is crafted to be accessible and user-friendly and is designed specifically to assist newcomers. This protocol provides insight into different phases of motor training and expected motor patterns that mice adopt. Finally, the article proposes a systematic workflow for data analysis using a powerful non-linear regression approach, complete with valuable recommendations and suggestions for adapting and applying the protocol in other research contexts.

Protocol

In the current study, adult (2-3 months old) C57BL/6J mice of both sexes were used. Animals were housed two to five per cage with *ad libitum* access to food and water in an animal unit under observation and maintained in a temperature-controlled environment on a 12 h dark/light

cycle. All procedures were conducted in accordance with the European and Spanish regulations (2010/63/UE; RD 53/2013) and were approved by the Ethical Committee of the Generalitat Valenciana and the animal welfare committee of the Universidad Miguel Hernández.

1. Behavioral room setup

1. Reserve the behavioral testing room every day at the same time and establish the list and order of mice to be used, as well as arrangements for their hosting.
2. Keep the experimental mice outside the testing room so they do not hear the sounds of the air compressor and Erasmus Ladder tones when not being tested.
3. Check that all components of the Erasmus Ladder system are in order and ready to use: the network router, the computer with the software (see **Table of Materials**), the air compressor, two goal boxes, and the ladder with the rungs properly positioned.
4. Extensively clean the goal boxes, ladder, and rungs with water after each animal and with water and 70% ethanol at the end of each training day.

2. Behavioral test protocol

1. Create an experiment and enter the protocol into the software (**Supplementary Figure S1**).
 1. Turn on the software.
 2. To create an experiment, choose **File | New experiment | New or Set up | Experiment protocol**.

NOTE: The default protocol, used in this study, is named EMC and was designed at Erasmus University Medical Center, Rotterdam.

3. Give the experiment a name and click **OK**.
 4. Check that the default EMC protocol selected consists of **4 days of undisturbed sessions (42 undisturbed trials per day)** and **4 days of challenge sessions (42 daily mixed trials: undisturbed, CS-only (tone), US-only (obstacle), Paired (obstacle announced by tone)** (see **Figure 1B**). In the right side panel, also check the light cue (3 s maximum duration), air cue (45 s maximum duration), and tailwind (**Yes** in all the trial types), used to encourage the mouse to cross the ladder, and the tone (250 ms, **Yes** only in **CS-only** and **Paired trials**).
 5. To create a different protocol, choose **Set up | Experiment protocol | New | From scratch** or **Copy from the EMC protocol** and simply modify it, editing the table lines related to **number of sessions (days of experiment)** and **number and type of trials per day**.
NOTE: Resting time, cues type and activation, duration, intensity, and interval can also be adapted according to the experimental questions.
 6. To open the session list and name the subjects, choose **Setup | Session List**.
 7. Click on **Add Subjects and Variables**.
 8. Enter each specific **Mouse Identifier, Birth Date, Sex, Genotype**, and relevant categories, following the ordered list of mice.
2. Start the session (**Supplementary Figure S2**).
 1. Before starting, check that the software is open, then turn on the Ladder.
 2. Check that the air compressor is connected and switched on.
 3. To open the **Acquisition window**, open the Experiment created.
 4. Choose **Acquisition | Open Acquisition**.
 5. Place the mouse with the identifier indicated by the software in the starting goal box (right side of the ladder).
 6. Select the **mouse identifier** to acquire in the first session.
 7. Click on **Start Acquisition**.
 8. Press the **red ladder menu knob** 3x. Check that the session starts and automatically controls and records mouse movements until the end of the last trial of the session.
 3. End the session.
 1. Check that at the end of the 42nd trial, the display shows the messages **Sending Data** and **Acquired**.
 2. Return the mouse to the home cage.
 3. Clean the ladder and the goal boxes.
 4. Place the next mouse and repeat from step 2.2.6 onwards.
 4. Perform the selected type of session every day until the end of the protocol. Repeat steps 2.2 and 2.3 every day according to the selected protocol.
 5. Export the data (**Supplementary Figure S2**).
 1. To visualize the recorded data, choose from the **Analysis** menu, **Trial Statistics**, **Session statistics**, and **Group Statistic & Charts**.
NOTE: Data can be downloaded as a spreadsheet with data for individual trials and the means of the

same trial types within a session. Sessions can also be filtered by variables chosen for specific analysis.

2. Click on the **Export** button at the top-right corner choosing the file format (spreadsheet) and folder location.
3. Right-click on the automatically generated charts and select **Save to File** as *.jpg.

3. Data analysis

NOTE: A list of parameters is automatically measured by the Erasmus Ladder based on the instantaneous recording of the activities of the touch-sensitive sensors. For analysis, output parameters selected by the user are organized and processed in the spreadsheets. Along with the software-generated graphs, users can generate graphs using the graphing software of choice to visualize specific changes in different parameters over sessions.

1. Choose specific parameters to analyze basal motivation or anxiety states, sensory responses, motor performance, and fine motor learning over the first 4 days.

1. Select and plot **control parameters**, including **resting time in the goal box** and **time to exit the goal box after the resting period** in response to **light and air cues (Figure 2A)**.

NOTE: Resting times or response to cues are relatively constant in WT mice. Other parameters such as frequency of exits are basically negligible in WT mice-the animals rarely leave the rest box without the cues or come back once in the ladder, resulting in frequencies of exit equal to 1 per trial. If an animal goes out before cues are applied, an airflow gets activated forcing the mouse to return to

the goal box; this is not counted as a trial by the software.

2. Select and plot the **time on ladder after cues**, measured as the **time spent crossing the ladder once the mouse leaves the goal box (Figure 2B)**.

NOTE: A power non-linear regression is a robust method for evaluating learning. The Pearson or Spearman coefficients (R) will provide a measure of whether the data fitting is good (R values close to one when the animals learn/improve over sessions; R values close to 0 imply that the data are constant and mice do not learn).

3. Select and plot **stepping pattern parameters** such as the **percentage of trials with missteps** as a sensitive learning parameter (**Figure 2C**).

1. Define a correct step as a step from a high rung to another high rung (H-H), irrespective of the length of the step. Consider step types that involve a lower rung as missteps.
2. Divide correct steps and missteps into short and long steps, backsteps, and jumps depending on the length and directionality of the step between the rungs pressed (see **Figure 1A**).

2. Select and plot specific parameters to evaluate challenged motor learning (US-only trials) and associative learning (paired trials) over the last 4 days.

1. Select and plot the **time on ladder after cues (Figure 3)**.
2. Select and plot the **percentage of trials with missteps (Figure 4A)**.
3. Select and plot the **pre and post perturbation step times**, defined as a ms precision difference between

rung activation just before (control step) and after the obstacle (adapted step) on the same side of the ladder (**Figure 4B**).

NOTE: Pre vs post-perturbation step times analysis should be performed to compare data inside each type of session. The parameter measures the ability of the mice to predict and overcome the obstacles during associative learning.

3. Analyze the data with dedicated statistical software (e.g., SigmaPlot). Perform a power non-linear regression analysis of data collected from the same trial type across sessions to describe the learning process more efficiently and use Two-Way Repeated Measures (RM) ANOVA to compare between trial types.

Representative Results

The Erasmus Ladder device, setup, and protocol applied are presented in **Figure 1**. The protocol consists of four undisturbed and four challenge sessions (42 trials each). Each trial is one run on the ladder between the starting and ending goal boxes. At the beginning of the session, a mouse is placed in one of the starting boxes. After a set time of 15 ± 5 s ("resting" state), the light is turned on (cue 1, for a maximum of 3 s). A light air cue (cue 2, 45 s maximum) is then applied to encourage the mice to leave the box and walk to the opposite end. The time to respond to the air cue can vary between mice and sessions and can be used as a parameter to compare motivation or anxiety states between groups. A new trial is immediately started after the mouse reaches the ending goal box.

No differences in resting time and time to respond to the light cue were observed in WT mice across days 1-4, but the time to respond to the air cue decreased slightly between days 1 and 2 (**Figure 2A**). Measurements of the time to cross the

ladder yielded a significant learning curve from days 1 to 4 that could be fitted with a power regression curve ($R = 0.50$, $*p = 0.047$, **Figure 2B**). A key parameter that determines the time taken to cross the ladder is the occurrence of missteps. In line with the shortening of times on the ladder, the number of trials where mice made missteps decreased over undisturbed sessions as mice learned to walk on the upper rungs (H-H steps) and avoid the lower ones as a more efficient pattern to cross the ladder ($R = 0.90$, $***p < 0.0001$, **Figure 2C**).

From days 5 to 8, the mice were subjected to challenge sessions where an unexpected obstacle (US) was introduced (one rung is randomly raised by 18 mm above the stepping surface). In some trials, a tone (CS, 90 dB, 15 kHz tone lasting 250 ms) is presented 250 ms before the US perturbation (see **Figure 1B**).

With the beginning of challenge sessions on day 5, animals required more time to cross the ladder during US-only trials because of the unpredicted introduction of the obstacle (day 4: 5.01 s; **Figure 2B**; day 5: 7.84 s; **Figure 3**; paired t -test, $*p < 0.039$). Mouse performance improved from days 5 to 8, yielding a significant learning curve across US-only sessions ($R = 0.50$, $*p = 0.045$, **Figure 3**, orange). In associative learning trials, where the obstacle was paired with a tone, animals completed the daily sessions significantly faster relative to US-only trials ($R = 0.63$, **Figure 3**, purple; two-way RM ANOVA, $*p = 0.028$). Finally, in control trials when the tone was presented alone (CS-only), a significant learning curve that resembled undisturbed sessions was reported ($R = 0.82$, $***p < 0.001$, **Figure 3**, blue).

Analysis of the step patterns provided additional confirmation and enhanced sensitivity in detecting differences between US-only and associative trials. **Figure 4A** shows how the percentage of trials with missteps remained constant

throughout US-only trials ($R = 0.01$, $p = 0.90$, orange), while a significant decrease in trials with missteps was observed during paired sessions ($R = 0.61$, $*p = 0.01$, purple).

Figure 4B shows a significant difference between pre and post perturbation step times in US-only trials (two-way RM

ANOVA, $*p = 0.05$) but not in paired trials where mice learned faster to overcome the obstacle. All the variables studied and the statistical tests applied are reported in **Supplementary Table S1**.

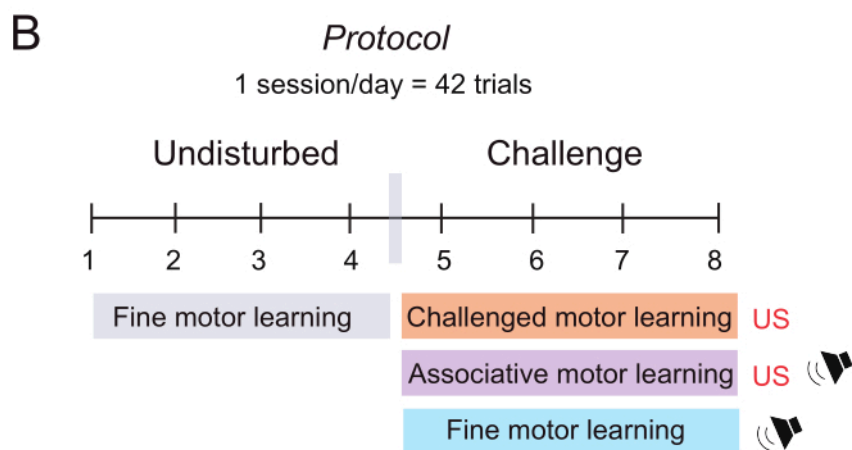
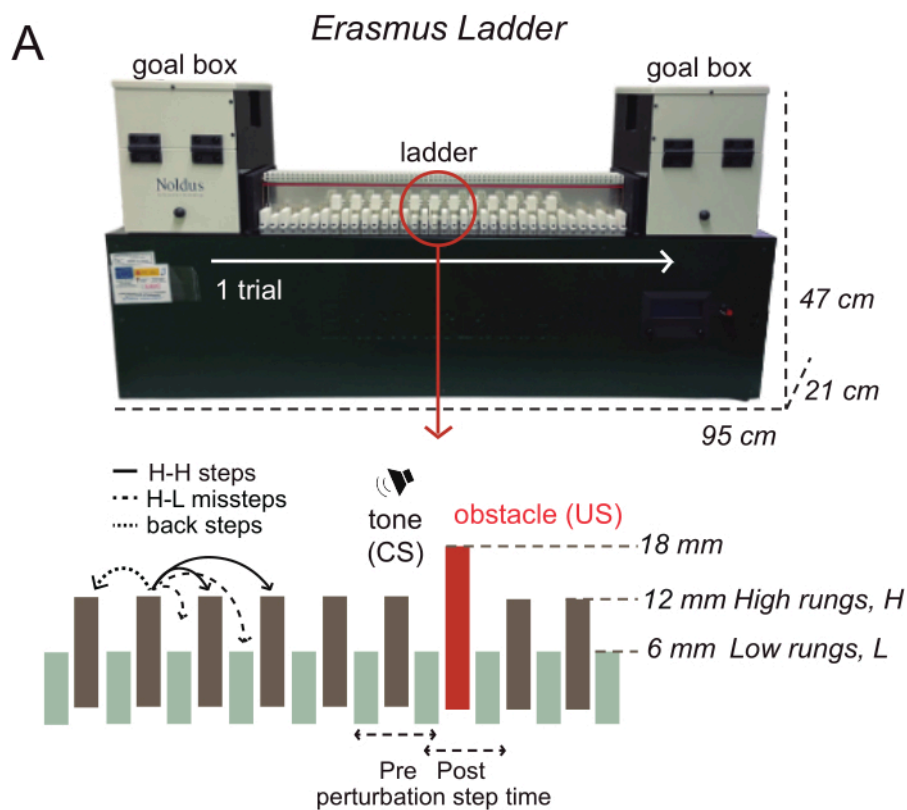


Figure 1: System, protocol, and parameters. (A) The Erasmus Ladder consists of a horizontal ladder flanked by two goal boxes. The cartoon represents the ladder with alternated high and low rungs and the main parameters recorded, including step types (normal steps, filled line; or missteps, dashed line) and pre and post perturbation step time defined as the time that the mouse needs to overcome an obstacle (unconditioned stimulus; higher rung) announced or not by a tone (conditioned stimulus). (B) The protocol consists of four undisturbed and four challenge sessions (one session/day, 42 trials/session) that allow for separately analyzing fine motor learning (undisturbed and CS-only in blue), challenged motor learning (US-only, in orange), and associative motor learning (paired CS + US, in purple). Abbreviations: H = high; L = low; CS = conditioned stimulus; US = unconditioned stimulus. [Please click here to view a larger version of this figure.](#)

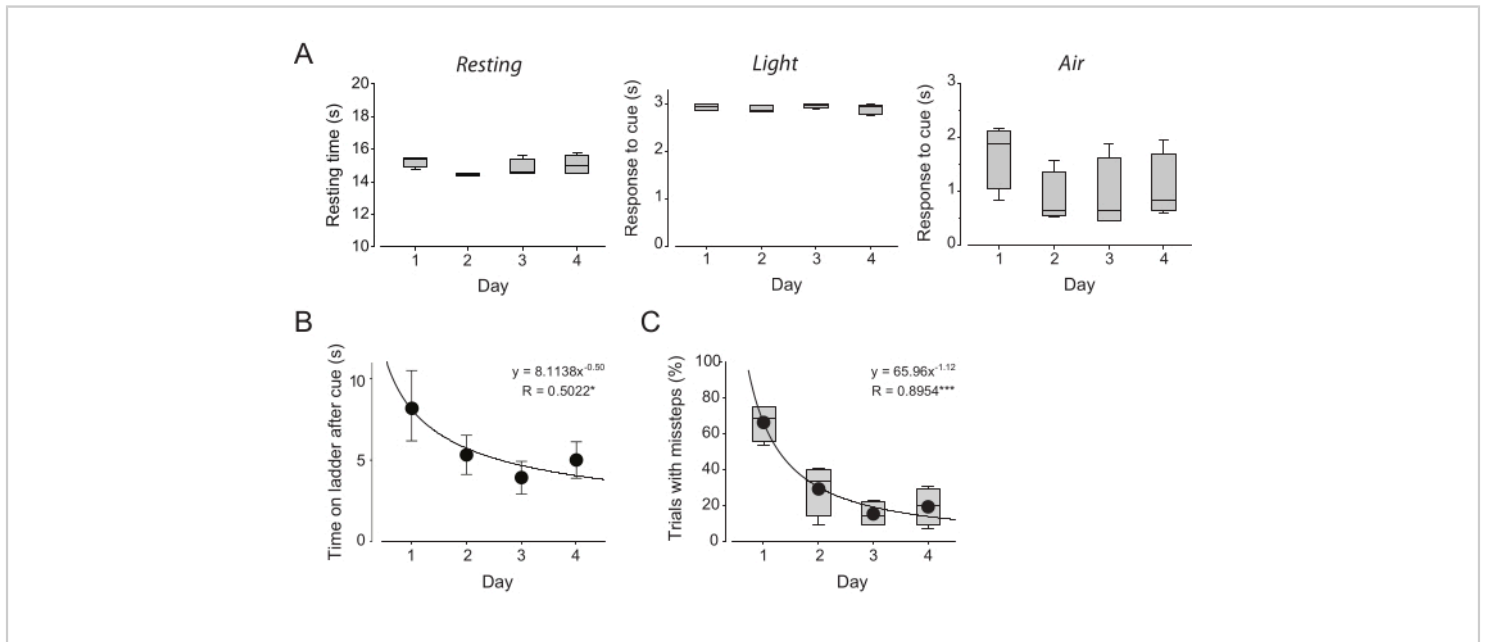


Figure 2: Motor performance of WT mice during undisturbed sessions. (A) Resting time in the goal box (constant, 15 s), time to respond to cues: light (constant, 3 s) and air (variable); over days 1-4 of undisturbed sessions. (B) Time to cross the ladder after cue (light and air) during undisturbed sessions. (C) Percentage of trials in each undisturbed session where the animal missed a step. A power regression analysis was used to study the learning progress ($R = 0.50$: $*p = 0.047$, $R = 0.90$ $^{***}p < 0.0001$, respectively, $n = 4$ mice). Abbreviation: WT = wild type. [Please click here to view a larger version of this figure.](#)

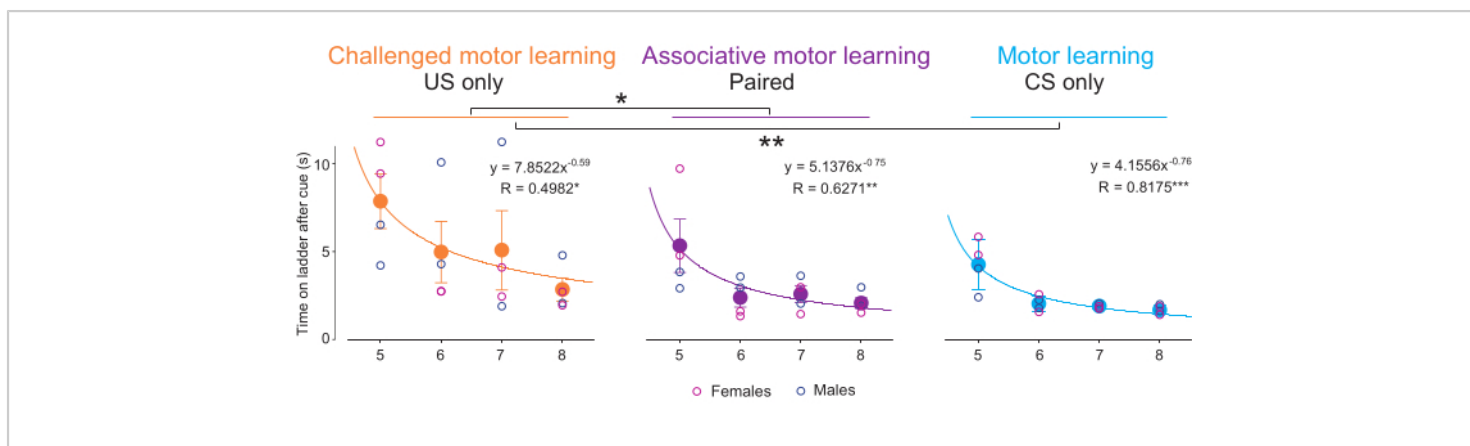


Figure 3: Performance of WT mice during challenge sessions. Average time on the ladder after cues during days 5-8 for US-only (orange), paired (purple), and CS-only (light blue) trials. A power non-linear regression analysis was used to study the learning progress (* $p = 0.047$, ** $p = 0.0093$, *** $p < 0.001$, $n=4$ mice). Two-way RM ANOVA to compare trial types (* $p = 0.028$, ** $p = 0.008$, $n=4$ mice, two males and two females, mean \pm SEM). Abbreviations: CS = conditioned stimulus; US = unconditioned stimulus. [Please click here to view a larger version of this figure.](#)

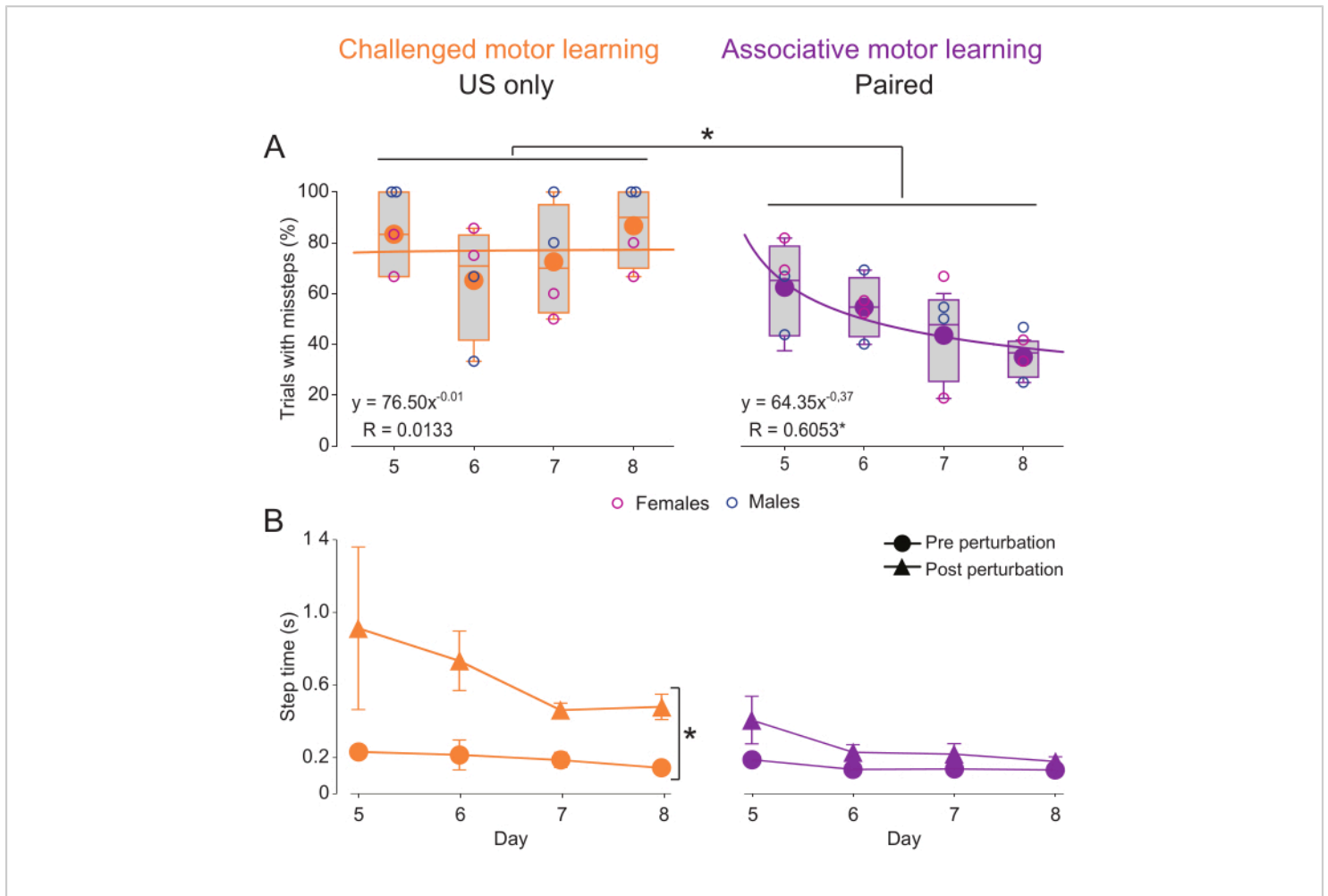


Figure 4: Changes in mouse step patterns over challenge sessions. (A) Percentage of trials per session where the animal missed a step during US-only and paired sessions. A power regression analysis was used to study the learning process (* $p = 0.013$) and a Two-way RM ANOVA for comparison between trial types (* $p = 0.032$, $n = 4$ mice). **(B)** Pre and post-perturbation step time (s) in US-only and paired sessions throughout the sessions. Two-way Repeated Measures ANOVA, * $p < 0.05$, $n = 4$ mice, two males and two females, mean \pm SEM. [Please click here to view a larger version of this figure.](#)

Supplementary Figure S1: Software interface: how to create an experiment and select a protocol. Screenshots from the software illustrating the workflow described in protocol step 2.1, covering steps 2.1.4 to 2.1.8. [Please click here to download this File.](#)

Supplementary Figure S2: Software interface: how to start the session and export the data. Screenshots from the software illustrating the workflow described in protocol steps 2.2 and 2.5, covering steps 2.2.4 to 2.2.7 and 2.5.1 to 2.5.3. [Please click here to download this File.](#)

Supplementary Table S1: Statistical table. Description of all the variables studied and the statistical tests applied, reported in **Figure 2B,C**, **Figure 3**, and **Figure 4A,B**. [Please click here to download this File.](#)

Discussion

The Erasmus Ladder presents major advantages for motor phenotype assessment beyond current approaches. Testing is easy to conduct, automated, reproducible, and allows researchers to assess various aspects of motor behavior separately using a single mouse cohort. In the current study, reproducibility allowed the generation of robust data with a small number of WT mice taking advantage of the features of the device, experimental design, and analysis methods. For instance, when compared to traditional beam-walk assays, the addition of motivational cues (air and light) to enter the ladder path and the tailwind to complete the trial increases consistency and skips the need for experimenter intervention which is a major source of variability.

An air compressor system is required to generate an airflow that can be adjusted to the direction and position of the mouse. The airflow creates a 30 km/h headwind from the opposite direction when a mouse attempts to leave the goal box before the scheduled trial initiation, making the mice return to the goal box. It also generates a constant tailwind (1 to 16 km/h) during the trial until the mouse completely crosses the ladder and enters the opposite goal box. Without the pressurized air as an incentive to cross the ladder, mice frequently pause on the rungs and reverse directions at a leisurely pace, which introduces an exploratory variable counterproductive for the analysis.

The standard protocol described here provides measurements of basic fine motor coordination and learning (undisturbed sessions), as well as of adaptation to challenges

and associative motor learning (challenge sessions) over a time span of 8 days. The task is easy for WT mouse strains typically used for neuroscience studies such as the C57Bl6J mice used here, and is safe, with no injuries observed in any of the testing sessions. In addition, we did not detect signs of fatigue when compared to other motor tests such as the rotarod or treadmill.

Over the 4 day initial phase, WT mice master the skill and cross the ladder by learning to adopt the most efficient running pattern (H-H steps) and missteps occur rarely by day 4 (**Figure 2B,C**). On day 5 of the second phase, mice are slower when they first encounter the obstacle but quickly adapt (**Figure 3**, US-only). Coupling the obstacle with a conditioning stimulus (tone) facilitates learning to the extent that trial duration equals trials where the obstacle is not presented (**Figure 3**, paired). Of note, the number of trials with missteps remained constant throughout US-only trials (**Figure 4A**), while a significant decrease was observed in paired sessions (**Figure 4A**), confirming the effectiveness of the associative learning process.

We propose a workflow for the analysis of representative parameters provided by the Erasmus Ladder software. The power regression analysis allowed us to register significant learning curves and detect differences in challenged versus associative learning using four WT mice. Based on additional literature and pilot experiments, experimental designs involving mutant or treated mice might require increasing mouse numbers to 7-10 mice^{4,5,6}. In our hands, 42 trials per session was an optimal number to obtain robust data with a small mouse cohort because averaging several trials decreases variability. While the number might appear high, each 42 trial session takes between 15 min and 35 min, and 12-16 mice can be reasonably tested per day. Trial duration

(including the resting time and response to cues plus time to traverse the ladder) varies between 20 s and 50s, depending on the training day and type of trial.

Nevertheless, the versatility of the system will allow researchers to design customized protocols by adjusting various settings, including the number of sessions and trials per day, the intensity and duration of cues and CS, as well as the nature of the US. For example, our data showed a rapid learning curve in WT mice, particularly between day 1 and day 2 after performance reaches a plateau (**Figures 2B,C**). This suggested that the additional 2 days might not be strictly necessary for testing basic motor learning in undisturbed sessions, and modifications to the standard protocol can be implemented by reducing the training duration to just 2 days. Yet this adaptation might not be suitable for the second phase of the protocol, which incorporates interleaved undisturbed, US-only, CS-only, and paired trials. The stimuli are presented randomly and unexpectedly to assess specific behaviors, and the need to divide experimental trials into these four categories makes 42 a suitable number of trials required for statistical power. Thus, a reorganization of the protocol would need to assess the feasibility of reducing the number of undisturbed trials or increasing specific challenge trials. The inter-stimulus interval (ISI) between CS (90 dB, 15 kHz tone) and US, here set at 250 ms, can also be varied to study the stimulus-response association. This kind of adjustment would allow researchers to titrate the level of difficulty or focus on different behaviors according to the scientific question.

To date, the Erasmus ladder has been mostly used to detect subtle defects in motor coordination of cerebellar origin. For instance, missteps are a measure of whole-body locomotor coordination. In this study, young adult mice were used but mice as young as P23 have been used by

others to study the maturation of locomotor functions^{7,8}. Ipsilateral pathologies of central origin could be studied through discriminative analysis of the position of the mouse's right and left paws. Finally, mastering motor skills in the Erasmus ladder likely engages other motor control circuits, involving the basal ganglia, motor cortex, and connecting pathways, including the corpus callosum. Combining this behavioral paradigm with cellular, molecular, and circuit techniques will be useful to investigate circuit mechanisms that mediate motor adaptation and can be harnessed to boost motor learning. One such example would be to study the influence on axonal myelination, which is highly sensitive to the acquisition of fine motor skills in mouse models of demyelination^{9,10}.

Disclosures

The authors have no conflicts of interest to disclose.

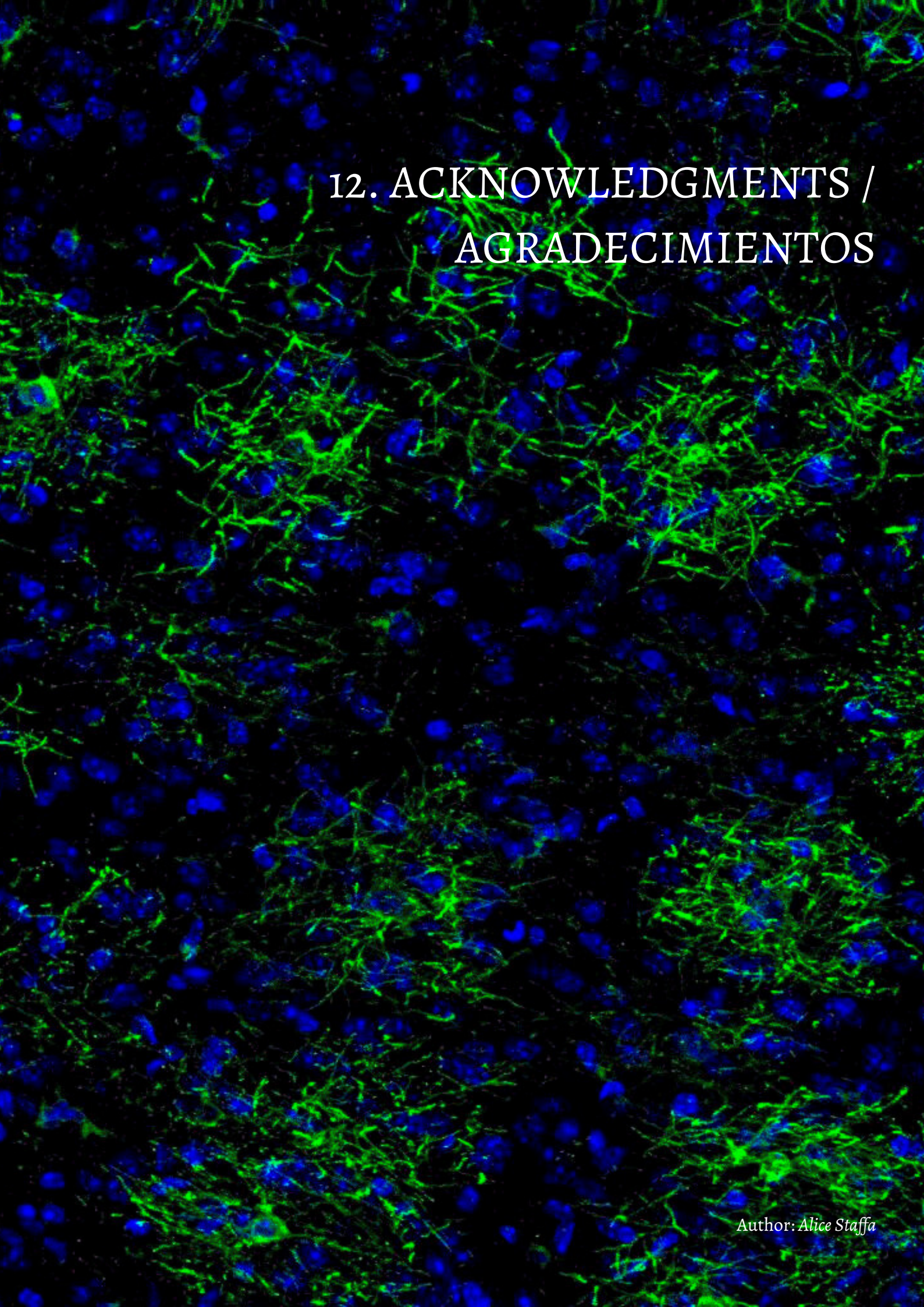
Acknowledgments

We acknowledge the audiovisual technician and video producer Rebeca De las Heras Ponce as well as the head veterinarian Gonzalo Moreno del Val, for the supervision of good practice during mouse experimentation. Work was funded by grants from the GVA Excellence Program (2022/8) and the Spanish Research Agency (PID2022143237OB-I00) to Isabel Pérez-Otaño.

References

1. Brooks, S. P., Dunnett, S. B. Tests to assess motor phenotype in mice: a user's guide. *Nat. Rev. Neurosci.* **10** (7), 519-529 (2009).
2. *Noldus*. <https://www.noldus.com/erasmusladder> (2023).

3. Cupido, A. et al. *Detecting cerebellar phenotypes with the Erasmus ladder*. Erasmus University Rotterdam PhD dissertation (2009).
4. Van Der Giessen, R. S. et al. Role of olivary electrical coupling in cerebellar motor learning. *Neuron*. **58** (4), 599-612 (2008).
5. Vinueza Veloz, M. F. et al. The effect of an mGluR5 inhibitor on procedural memory and avoidance discrimination impairments in Fmr1 KO mice. *Genes Brain Behav.* **11** (3), 325-331 (2012).
6. Vinueza Veloz, M. F. et al. Cerebellar control of gait and interlimb coordination. *Brain Struct. Funct.* **220** (6), 3513-3536 (2015).
7. Sathyanesan, A., Kundu, S., Abbah, J., Gallo, V. Neonatal brain injury causes cerebellar learning deficits and Purkinje cell dysfunction. *Nat. Commun.* **9** (1), 3235 (2018).
8. Sathyanesan, A. and Gallo, V. Cerebellar contribution to locomotor behavior: A neurodevelopmental perspective. *Neurobiol. Learn Mem.* **165**, 106861 (2019).
9. McKenzie, I. A. et al. Motor skill learning requires active central myelination. *Science*. **346**(6207), 318-322 (2014).
10. Xiao, L. et al. Rapid production of new oligodendrocytes is required in the earliest stages of motor-skill learning. *Nat. Neurosci.* **19** (9), 1210-1217 (2016).



12. ACKNOWLEDGMENTS / AGRADECIMIENTOS

Author: *Alice Staffa*

Este largo viaje ha marcado la etapa más bonita de mi vida, y a la vez la más desafiante. He tenido que volver a empezar de cero en otro país, alejada de mi familia y de mis amigos de toda la vida. Sin embargo, siempre estaré orgullosa de mi decisión y de mi dedicación, porque gracias a este doctorado he crecido mucho tanto profesional como personalmente.

Gracias a Isabel, mi directora de tesis, por creer en mí, darme la oportunidad de explorar el mundo de la investigación y desarrollar habilidades que me acompañarán siempre y serán fundamentales en mi futuro.

Gracias a José y Miriam, por el apoyo con los análisis de RNA-seq.

Gracias a Carlos y Juan Carlos, por el apoyo con la microscopia electrónica.

Thank you to Carlos y Corentine, for the help with the RNA-seq on OPCs and the LPC lesions, for your travels to Alicante and the good moments passed working hours and hours together in the animal facility.

Thank you to Thora, for her generosity, enthusiasm for the project and invaluable help with the electrophysiology, key for future directions.

Gracias a Ariadna y Moumita, por su grande apoyo en poner a punto el Erasmus Ladder. Gracias a Felix y Rebeca por participar en el desarrollo del artículo y video de Jove.

Gracias a Alerie, por enseñarme los fundamentos de los cultivos de OPC y por su apoyo e inspiración constante tanto a nivel científico como personal.

Gracias a todos mis compañeros, increíbles personas que me han acompañado en este camino, compartiendo sonrisas y lágrimas, satisfacciones y frustraciones:

Gracias al alcalde Álvaro, por su amabilidad y compañerismo cuando aún era una novata.

Gracias a Noelia, la japonesa de Elche, por seguir a nuestro lado desde la distancia.

Gracias a Sergio, alias Carlos Alcaraz, por empezar y terminar juntos este viaje.

Gracias a María José, fan nº1 de Harry Potter, por su alegría y por los confetis que aún seguirán a día de hoy debajo del sofá.

Gracias a Ana, mi referencia en la organización, por su experiencia y apoyo.

Gracias a Diana, por su ayuda y tenacidad.

Thank you to Oliver, for helping me in practicing English and for being my go-to person for challenging scientific questions.

Gracias a Remy, por su alegría, singularidad y habilidad para mezclar idiomas.

Gracias al pequeño Padawan (ahora maestro Jedi) Óscar, por existir.

Gracias a Juanjo, por su extroversión y sus comidas en la terraza.

Gracias a Carmen, por su ternura y energía positiva.

Thank you to Moumita, my little apprentice, for sharing with me these past few years, through experiments, troubleshooting, tears and smiles.

Gracias a Bárbara, mi hermanita inseparable, psicóloga personal de los últimos años, por su forma de ser y su paciencia conmigo.

Gracias a todos los que no he mencionado detenidamente, pero con los cuales he tenido el placer de colaborar o compartir momentos, los recuerdos todos con cariño: Doris, Pablo, Sonia, Juan Ramón, Mónica, Adriana, Ismael, Federica, Noelia, Ana, Sara, Gloria, Roberto (y Selene), Chiara, Sergio, Ramón, Juan, John, Cruz, Silvia, Hugo, Niki, Sandra, Pili, Patri, Quique, Selene, Alicia, Marta, Martina, Leonor, Isabel, Adrián, Antonio, Gonzalo, Verona y Giovanna (en honor a las miles de horas pasadas en microscopía) y Trini (el sol del instituto).

Gracias a Marialinda y Joaquín, con los cuales compartí el primer año loco en Alicante.

Gracias a María, Juanjo, Kine, Alex, Ruben y Clara por conseguir sacarme fuera del laboratorio y compartir momentos de diversión, así como por formar parte de mi familia plogging como muchos más que no puedo nombrar todos aquí. Gracias a Pedro, por creer en mi potencial.

Gracias a mis amigas de siempre, que aún en la distancia, siempre están ahí:

Grazie a Carmen, mia amica dalla culla, per essere speciale e differente. Non tutti possono dire di avere una amicizia così.

Grazie a Giulia e Veronica, le mie amiche nerd del liceo, per le nostre rimpatriate e videochiamate che ci riportano indietro nel tempo, a quei giorni spensierati e magici.

Grazie a Sara, Lucía e Marilena, per tutti i momenti condivisi e per aver avuto la fortuna di vederci crescere in questi anni, passo dopo passo, e per quello che ci riserva il futuro.

Grazie anche alle amicizie che non sono sopravvisute alla distanza e al cambiamento. Saranno sempre parte di me.

Por último, lo más importante. Gracias a mi familia:

Grazie a papà e nonna, i miei pilastri, la mia roccia. Grazie per avermi permesso di vivere e fare le mie esperienze senza mai farmi pesare la mia assenza o distanza. Per il vostro aiuto economico, morale. Grazie per tutto.

Grazie ai miei zii Piero, Giulia e Gianfranco, per appoggiarmi sempre.

Grazie ai miei cugini pazzi, Andrea, Simona, Stefania e Davide.

Y:

Gracias a David, mi compañero de vida, mi hogar, el regalo más grande que Alicante tenía reservado para mí. Gracias por apoyarme siempre, por hacerme reír tanto, por hacerme sentir especial, por poder mostrarme contigo exactamente como soy, por ser tan diferente a mí y a la vez tan similar. Gracias a sus padres, Manuel y Nieves, su abuela y sus tíos, su hermana Sheila, Alex y el pequeño Mateo. Mi nueva familia.

En recuerdo de mi madre, mis abuelos y mi tía que ya no están conmigo, pero sí en mi corazón.

In memoria della mia mamma, dei miei nonni e di mia zia, che non sono più fisicamente accanto a me ma vivono sempre nel mio cuore.

Alice